# MRS Workshop 2022
## Overcoming the Barriers to Clinical Use
### DISCONNECT 2 RECONNECT

22-24 August 2022 @ EPFL, Lausanne, Switzerland

IT'S TIME

# MRS Workshop 2022
## Overcoming the Barriers to Clinical Use
### DISCONNECT 2 RECONNECT
22-24 August 2022 @ EPFL, Lausanne, Switzerland

IT'S TIME

## Supported by



CIBM
Center for Biomedical Imaging

EPFL

Swiss National Science Foundation

## GOLD SPONSOR

Nestlé HealthScience

## BRONZE SPONSORS

Neusoft Medical Systems

Mendes S.A.

## Donators

BRUKER

RAPID Biomedical

## Endorsed by

ENDORSED ISMRM ENDORSED

# MRS Workshop 2022

Proceedings of the

**The International Magnetic Resonance Spectroscopy Workshop**

**"MRS 2022: Overcoming the Barriers to Clinical Use"**

22 - 24 August 2022

Swiss Federal Institute of Technology in Lausanne, EPFL

Switzerland

# Contents

**MRS Workshop 2022**
Overcoming the Barriers to Clinical Use
DISCONNECT 2 RECONNECT
22-24 August 2022 @ EPFL, Lausanne, Switzerland

1

# 1   Welcome message



Cristina R. Cudalbu
CIBM MRI EPFL, Lausanne

Jannie P. Wijnen
UMCU, Utrecht

In harmony with our past traditions it is our great pleasure to welcome you in person at the International Magnetic Resonance Workshop: "MRS 2022: Overcoming the Barriers to Clinical Use" that will take place at EPFL in Lausanne, Switzerland between the 22nd and the 24th of August 2022.

The main aim of the MRS workshop 2022 is to unite the international MRS community in an on-site event, educate young scientists and provide ample opportunities for students to meet and share their exciting work with the MRS experts in-person. In addition to the latest state-of-the-art results and advancements in the field of MRS and MRSI this workshop will cover the latest frontiers in clinical applications and will allow in depth discussions on MRS community achievements during the last 10 – 15 years.

The program of the workshop is spread over 3 days and contains 9 scientific sessions. The sessions cover educational invited topics from the basics to the recent advancements in the field and proffered oral presentations based on submitted abstracts by PhD students or senior scientists describing the latest advancements in the field. In addition, poster sessions (42 on-site posters and 8 online posters), lunches, breaks, 2 panel discussions and a dinner at the Olympic museum are organized to facilitate and provide ample opportunity for students to meet and share their exciting work with their peers and MRS experts in-person. Given the lack of in-person events over the last two years due to COVID-19, we feel it is of high value and importance for researchers that just entered the field to have informal discussions with each other and the more senior scientists.

**Educational objectives:**
* Present the current MRS/ MRSI data acquisition methodology: sequences, artifacts, corrections and quality control.
* Describe the current MRS/ MRSI data processing, reconstruction and quantification methods.
* Summarize advanced MRS/ MRSI methods and applications used in clinical and basic research together with vendor harmonization, validation, and reproducibility requirements.
* Discuss the latest preclinical and clinical applications together with the main role of detected metabolites.

Welcome to MRS Workshop 2022 and enjoy Lausanne, Switzerland !

Cristina and Jannie
Co-chairs of the workshop

MRS Workshop 2022
Overcoming the Barriers to Clinical Use
DISCONNECT 2 RECONNECT
22-24 August 2022 @ EPFL, Lausanne, Switzerland

2

# 2 Organizing committees

## 2.1 Scientific organizing committee

Cristina Cudalbu, Ph.D., (chair)
CIBM MRI EPFL
Lausanne, Switzerland

Jannie P. Wijnen, Ph.D., (co-chair)
UMCU
Utrecht, Netherlands

Wolfgang Bogner, Ph.D.
Medical University Vienna
Vienna, Austria

Christoph Juchem, Ph.D.
Columbia University
New York, USA

Dinesh K. Deelchand, Ph.D.
CMRR, University of Minnesota
Minnesota, USA

Dunja Simicic, M.Sc.
CIBM MRI EPFL
Lausanne, Switzerland

George Bouzalis
Ygeia Ptolemaidas diagnostic center, MR Department
Kozani, Greece

Alexander P. Lin, Ph.D.
Brigham and Women's Hospital, Harvard Medical School
Boston, USA

Roland Kreis, Ph.D.
University of Bern
Bern, Switzerland

Dimitri Van De Ville, Ph.D.
CIBM MRI EPFL
Lausanne, Switzerland

## 2.2 Local organizing committee

Bernard Lanz, Ph.D., (co-chair)
CIBM MRI EPFL
Lausanne, Switzerland

Sarah Junod, (co-chair)
CIBM GE
Lausanne, Switzerland

Brayan Alves, M.Sc.
CIBM MRI EPFL
Lausanne, Switzerland

Jan Luxemburg, M.Sc.
CIBM MRI EPFL
Lausanne, Switzerland

Jessie Mosso, M.Sc.
CIBM MRI EPFL
Lausanne, Switzerland

Katarzyna Pierzchala, Ph.D.
CIBM MRI EPFL
Lausanne, Switzerland

Daniel Wenz, Ph.D.
CIBM MRI EPFL
Lausanne, Switzerland

Lijing Xin, Ph.D.
CIBM MRI EPFL
Lausanne, Switzerland

Antoine Klauser, Ph.D.
CIBM MRI HUG-UNIGE
Geneva, Switzerland

Hélène Lajous, Ph.D.
CIBM SP CHUV-UNIL
Lausanne, Switzerland

# MRS Workshop 2022
## Overcoming the Barriers to Clinical Use
### DISCONNECT 2 RECONNECT
22-24 August 2022 @ EPFL, Lausanne, Switzerland

3

# 3 General information

In between the scientific sessions there will be breaks with drinks and snacks as well as on-site lunches. The food and drinks are included in the registration fees.

In case you need to do a COVID test, please, find all the necessary information "HERE"

## 3.1 Workshop venue

The workshop is hosted by CIBM Center for Biomedical Imaging located on the EPFL campus. The event room is the Auditorium SG1 at the EPFL.

**WiFi network for a free internet access on site of the MRS Workshop** (and all other EPFL premises): freewifi-epfl Detailed instructions can be found "HERE".

## 3.2 Transportation

The event room is the Auditorium SG1 at the EPFL. Below, two route options are explained. First, by public transport. Second, by car.

### 3.2.1 By public transport

To get to the Auditorium SG1 you need to get off the metro at the station EPFL. Then, follow the red route on the map below.

### 3.2.2 By car

You can park your car in an underground parking lot under the Rolex Learning Center. **Use only the white parking spots and, please, do not forget to pay the parking fee at the automat**. Then, follow the blue route on the map below.
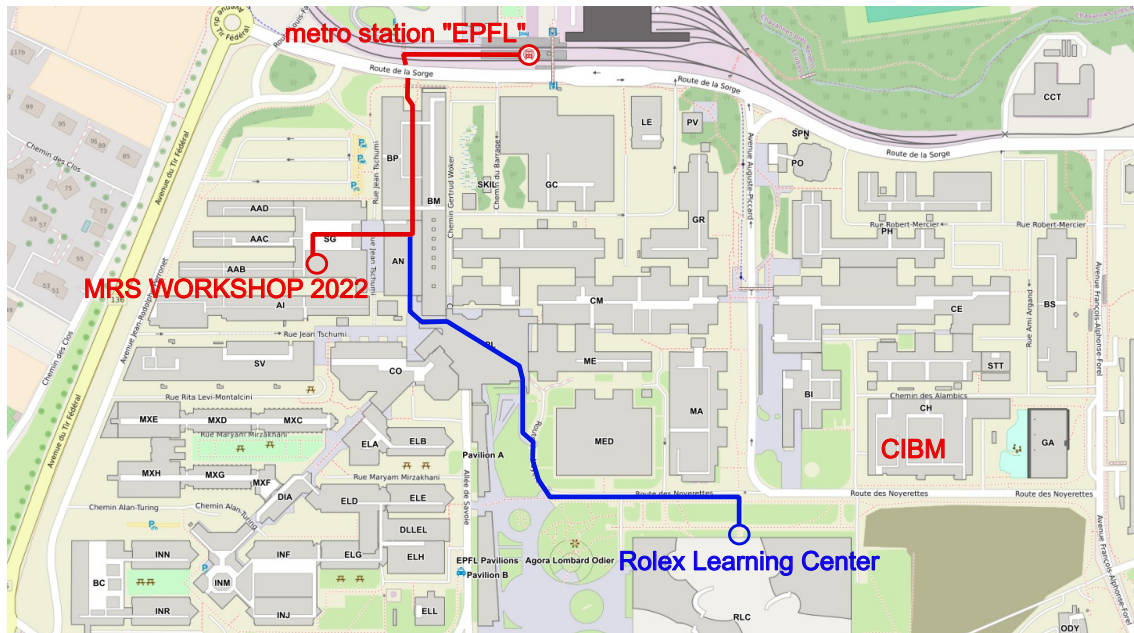
### 3.3 Online presence

**Talks**

For online participants an EPFL webinar was created to attend the talks related to Basics and advances in MRS as well as submitted abstracts. First, you need to open this link, where you sign in with you full name and your email address: "CLICK HERE". After that, you will get an email with the webinar link and passcode. You only have to sign up once for the three days. Please, note that the meeting will be auto-recorded on the EPFL cloud.

# 4 Social program

As a part of the workshop, we organized for all participants a pleasant event at the Olympic museum. The events in the Olympic museum will start at 6 p.m. with a welcome cocktail, which will be served until 7 p.m. After that, a museum visit will take place from 6 p.m. until 8 p.m. Our social gathering will be rounded with a dinner for all participants of the workshop. The dinner will start at 8 p.m. and finish at 11.30 p.m.

## 4.1 Transportation

There are two main options how to get to the dinner at the Olympic museum. First, to go by metro m1 from the station "EPFL" to the city center station "Flon", there, switch to the metro m2 and take a ride to the station "Ouchy-Olympique", and then, walk to the Olympic museum (650 m). Second, to take a nice walk (6.5 km) from the site of the MRS Workshop along Lac Léman to the Olympic museum.
Both route options are displayed below.

### 4.1.1 By public transport from Flon

This is the public transport connection for those who want to get to the dinner at the Olympic museum directly from the site of the MRS Workshop.
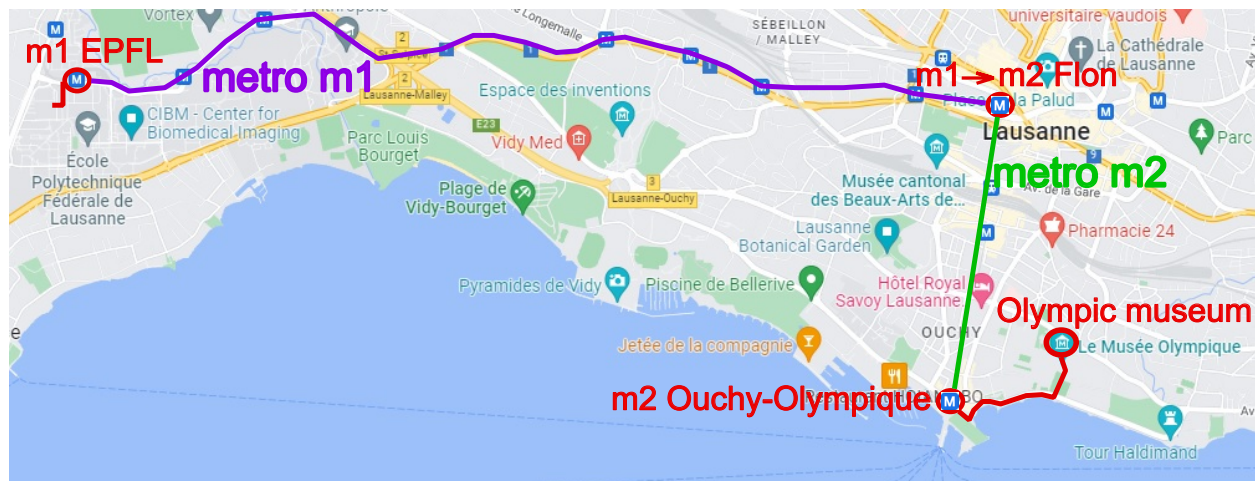
**MRS Workshop 2022**
Overcoming the Barriers to Clinical Use
DISCONNECT **2** RECONNECT
22-24 August 2022 @ EPFL, Lausanne, Switzerland

5

### 4.1.2   By foot from EPFL

This is a beautiful walk through a park, along beaches and ports on the shore of Lac Léman.



# 5   Scientific program

This workshop will feature three different types of scientific happenings. First, educational talks on different MRS topics. Second, talks related by submitted abstracts. Third, posters related to submitted abstracts.

## 5.1   Basics and advances

MRS experts will talk about basic and advanced concepts. Each of those talks will consist of a 20-minute presentation and a 5-minute discussion.

## 5.2   Abstracts

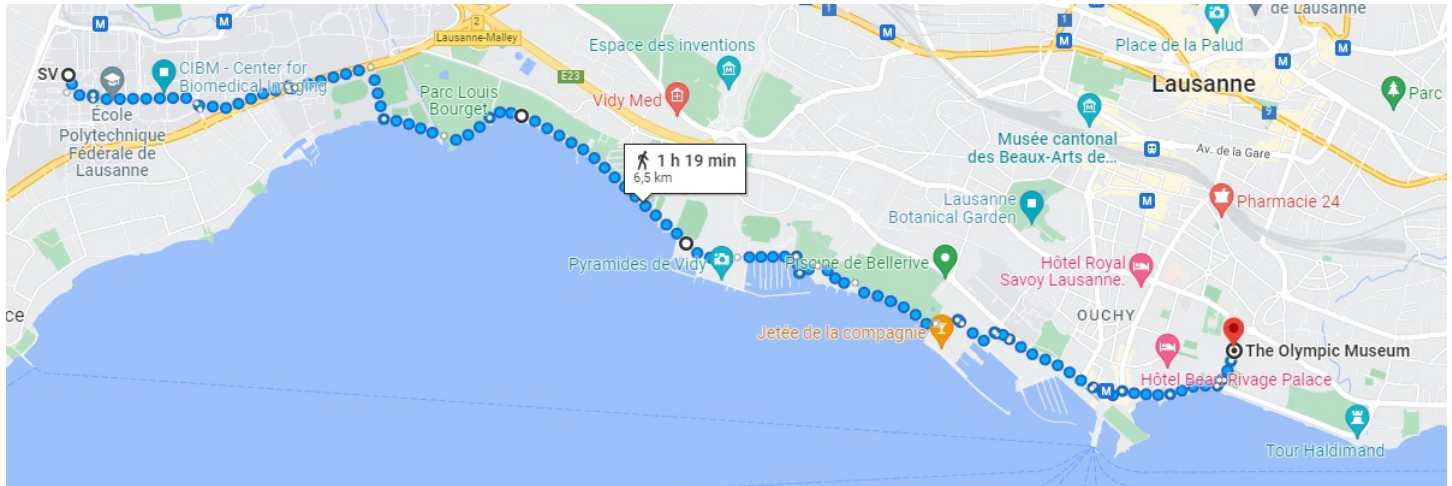Junior as well as senior scientists will present their abstracts either in the form of a 10min presentation with a 5min discussion, 18 abstracts, or in the form of a poster during one of the poster sessions. There will be 42 on-site posters and 8 online posters.

## 5.3   Meet the experts

During a part of our coffee and lunch breaks we are organizing, for the first time, "Meet the experts" sessions.

Each expert will participate in one session of 20min duration per day (the total duration of the coffee breaks is 30-40 min and the lunch break 1h 30min–1h 40min). The experts will be assigned to a table, where students can approach them freely (without prior introduction). There will be several experts at each table at the same time. The idea is that the experts reserve this 20min per day to talk to the students only. 44 experts will participate. We will also provide a box at each table with examples of some "ice-breaker" questions to start off the conversation.

As this is the first workshop since 2018, the idea is that the students have a chance to meet the experts and talk to them informally, without pressure and to expand the network in the field. We hope everyone will enjoy and benefit from it.

There will be dedicated coffee tables for these sessions only. The students will be split in 8 groups of approximately 7-8 trainees (PhD students and early PostDocs) and assigned to a table, where 2-3 experts will be. The students will rotate at every break (20min of two breaks per day are reserved for this), thus, the students will have a chance to meet as many experts as possible.

**MRS Workshop 2022**
Overcoming the Barriers to Clinical Use
DISCONNECT 2 RECONNECT
22-24 August 2022 @ EPFL, Lausanne, Switzerland

6

# 6 Full chronological program

In the full chronological program provided in this section, S stands for **"Session"**, B stands for **"Basics and advances"**, A stands for **"Abstract"**, and P stands for **"Panel discussion"**.

## 6.1 Day 1: Monday, 22nd August

**08:30-10:00**      **On-site registration (badges) and placing posters**

**10:00-10:20**      **Welcome and Introduction by Cristina Cudalbu, CIBM MRI EPFL**

**S1**    **10:20-12:20**      **MRS: back to basics**
**Moderators:**
François Lazeyras, CIBM MRI HUG-UNIGE Clinical MR Imaging Section
Gianna Nossa, Dydak Lab/ Health Science, Purdue University, USA

| Session | Time | Title | Presenter |
|---------|------|-------|-----------|
| S1B1 | 10:20-10:45 | Basics of MRS: SVS and MRSI | Georg Oeltzschner, Russell H. Morgan Department of Radiology and Radiological Science, The Johns Hopkins University School of Medicine, Baltimore, Maryland, USA and F. M. Kirby Research Center for Functional Brain Imaging, Kennedy Krieger Institute, Baltimore, Maryland, USA. |
| S1B2 | 10:45-11:10 | The neurochemical profile | Steve Williams, Imaging Science, University of Manchester |
| S1B3 | 11:10-11:35 | Spectral editing | Kimberley Chan, Advanced Imaging Research Center, University of Texas Southwestern Medical Center, Dallas, Texas, USA |
| S1B4 | 11:35-11:50 | MRS Hub - What's new? | Candace Fleischer, Emory University, Atlanta, U.S.A. |
| S1A1 | 11:50-12:05 | Adaptive Magnetic Resonance | Assaf Tal et al. |
| S1A2 | 12:05-12:20 | Does visual stimulation always lead to an increase in glutamate concentration? | Katarzyna Wasilewska et al. |

**12:20-14:00**      **Lunch on-site: Meet the experts! break the ice**
**Moderators:**
Dunja Simicic, CIBM MRI EPFL, Lausanne, Switzerland
Jessie Mosso, CIBM MRI EPFL, Lausanne, Switzerland
Brayan Alves, CIBM MRI EPFL, Lausanne, Switzerland
Rudy Rizzo, University of Bern, Switzerland
Kay Chioma Igwe, Columbia University, USA
Dario Goranovic, Medical University of Vienna, Austria
Gianna Nossa, Dydak Lab/ Health Science, Purdue University, USA
Ryan Armbuster (online), Center of Advanced Metabolic Imaging in Precision Medicine, University of Pennsylvania, USA
Kelley M. Swanberg (online), Columbia University, USA

**MRS Workshop 2022**
Overcoming the Barriers to Clinical Use
DISCONNECT 2 RECONNECT
22-24 August 2022 @ EPFL, Lausanne, Switzerland

7

**S2**    14:00- 15:30    **Artifacts and Correction (B0, B1, motion, ...)**

**Moderators:**

Ivan Tkac, Center for Magnetic Resonance Research, University of Minnesota, Minneapolis, Minnesota, USA

Ipek Ozdemir, School of Medicine/Neuroradiology, Johns Hopkins University, Baltimore, USA

| Session | Time | Title | Presenter |
|---------|------|-------|-----------|
| S2B1 | 14:00-14:25 | Artifacts and Correction in MRS and MRSI | Michal Povazan, Danish Research Centre for Magnetic Resonance, Centre for Functional and Diagnostic Imaging and Research, Copenhagen University Hospital Amager and Hvidovre, Hvidovre, Denmark |
| S2B2 | 14:25-14:50 | Quality control and preprocessing | Nuno Barros, Icometrix, Leuven, Belgium |
| S2A1 | 14:50-15:03 | Fast prospective motion correction for spectroscopic acquisitions | Isaac Adanyeguh et al. |
| S2A2 | 15:03-15:16 | Deep Learning Pipeline for Quality Filtering of MRSI Spectra | Mladen Rakic et al. |
| S2A3 | 15:16-15:30 | Effect of circadian rhythm on brain NAD: a magnetic resonance spectroscopy study at 7 T | Zhiwei Huang et al. |

**15:30-16:10    Break: Meet the experts! break the ice**

**S3**    16:10-18:00    **Accelerated MRSI and reconstruction**

**Moderators:**

Antonia Susnjar, Rispoli Lab/ Biomedical Engineering, Purdue University, West Lafayette, USA

Bernhard Strasser, High Field MR Center, Department of Biomedical Imaging and Image-guided Therapy, Medical University Vienna, Vienna, Austria

| Session | Time | Title | Presenter |
|---------|------|-------|-----------|
| S3B1 | 16:10-16:35 | Accelerated MRSI: conventional approaches | Ovidiu Andronesi, Athinoula A. Martinos Center for Biomedical Imaging, Department of Radiology, Massachusetts General Hospital, Harvard Medical School, Boston, Massachusetts |
| S3B2 | 16:35-17:00 | Accelerated MRSI: Advanced techniques | Antoine Klauser, Medical Informatics, University of Geneva, Switzerland; Center for Biomedical Imaging (CIBM), Geneva, Switzerland |
| S3A1 | 17:00-17:15 | Outlier Rejection for Fetal and Neonatal Brain MRS | Jack Highton et al. |
| S3A2 | 17:15-17:30 | Towards simultaneous concentration and T2 mapping of brain metabolites by multi-echo spectroscopic imaging | R Rizzo et al. |
| S3A3 | 17:30-17:45 | MP-PCA and LR-TGV denoising in $^{1}$H-FID-MRSI data at 14.1T: application and validation | Brayan Alves et al. |
| S3A4 | 17:45-18:00 | Downfield proton MRSI in the human brain with extended spatial coverage | İpek Özdemir et al. |

## 6.2  Day 2: Tuesday, 23rd August

**S4**    **08:30-10:15**    **Spectral Fitting and Quantification**
**Moderators:**
Phil Lee, Department of Radiology, Hoglund Biomedical Imaging Center, University of Kansas Medical Center, Kansas City, Kansas, US
Rudy Rizzo, University of Bern, CH

| Session | Time | Title | Presenter |
|---|---|---|---|
| S4B1 | 08:30-08:55 | Metabolite basis set simulations | Karl Landheer, Regeneron Pharmaceuticals, Tarrytown, NY, USA |
| S4B2 | 08:55-09:20 | Parametric fitting | Anke Henning, Advanced Imaging Research Center, University of Texas Southwestern Medical Center, Dallas, TX, United States |
| S4B3 | 09:20-09:45 | Quantification: references, T1, T2 and macromolecules | Niklaus Zölch, Department of Psychiatry, Psychotherapy and Psychosomatics, Psychiatric Hospital, University of Zurich, Zurich, Switzerland and Institute of Forensic Medicine, Department of Forensic Medicine and Imaging, University of Zurich, Zurich, Switzerland |
| S4A1 | 09:45-10:00 | Investigating Glutamate T2 relaxation time | Polina Emeliyanova et al. |
| S4A2 | 10:00-10:15 | Uncertainty Propagation in Absolute Metabolite Quantification for In Vivo Magnetic Resonance Spectroscopy of the Human Brain | Ronald Instrella et al. |

**10:15-10:45**    **Break: Meet the experts! break the ice**

**S5**    **10:45–12:30**    **Preclinical and Clinical Session**
**Moderators:**
Ralf Mekle, Center for Stroke Research Berlin, Charité-Universitätsmedizin Berlin, Berlin, Germany
Alireza Abaei, Core facility Small Animal Imaging / Medical Faculty, Ulm University, Germany

| Session | Time | Title | Presenter |
|---|---|---|---|
| S5B1 | 10:45-11:10 | Preclinical MRS | Bernard Lanz, CIBM MRI EPFL, Lausanne, Switzerland |
| S5B2 | 11:10-11:35 | Translational work bench-bedside | Itamar Ronen, The Clinical Imaging Sciences Centre,Brighton and Sussex Medical School, University of Sussex, UK |
| S5B3 | 11:35-12:00 | Methods for non-brain clinical MRS | Martin Krssak, Division of Endocrinology and Metabolism, Department of Internal Medicine III, Medical University of Vienna, Vienna, Austria and High-Field MR Center, Department of Biomedical Imaging and Image-Guided Therapy, Medical University of Vienna, Vienna, Austria |
| S5A1 | 12:00-12:15 | $\alpha$-ATP suppression in $^{31}$P MR spectroscopy by homonuclear BIRD editing: An approach to quantify NADH and NAD$^+$ at 3T in vivo in skeletal muscle | J. Mevenkamp et al. |
| S5A2 | 12:15-12:30 | Association of insulin resistance with the accumulation of saturated IMCL, compared with other fat stores | Mueed Azhar et al. |

**MRS Workshop 2022**
Overcoming the Barriers to Clinical Use
DISCONNECT **2** RECONNECT
22-24 August 2022 @ EPFL, Lausanne, Switzerland

9

**12:30-14:00**    **Lunch on-site: Meet the experts! break the ice**

**S6    14:00-15:40    Accuracy and rigor**

**Moderators:**
Julien Valette, Université Paris-Saclay, CEA, CNRS, MIRCen, Laboratoire des Maladies
Neurodégénératives (UMR 9199), Fontenay-aux-Roses, France
Jessie Mosso, CIBM MRI EPFL, Switzerland

| Session | Time | Title | Presenter |
|---|---|---|---|
| S6B1 | 14:00-14:25 | Validation, reproducibility/repeatability in MRS | Gulin Oz, Center for Magnetic Resonance Research, Department of Radiology, University of Minnesota, Minneapolis, Minnesota, USA |
| S6B2 | 14:25-14:50 | Vendor harmonization in MRS | Dinesh Deelchand, Center for Magnetic Resonance Research, Department of Radiology, University of Minnesota, Minneapolis, Minnesota, USA |
| S6B3 | 14:50-15:15 | Denoising for MRS and MRSI | William Clarke, Wellcome Center for Integrative Neuroimaging, FMRIB, Nuffield Department of Clinical Neurosciences, University of Oxford, Oxford, UK and MRC Brain Network Dynamics Unit, University of Oxford, Oxford, UK |
| S6B4 | 15:15-15:40 | Machine learning for MRS/MRSI | Hyeonjin Kim, Department of Medical Sciences, Seoul National University, Seoul, South Korea; Department of Radiology, Seoul National University Hospital, Seoul, South Korea |

**15:40-17:00**    **Break: Meet the experts! break the ice + POSTER SESSION**

**16:00-16:30**    **ONLINE: Meet the experts! break the ice**

**18:00-23:30**    **OLYMPIC MUSEUM**

| Session | Time | Title | Presenter |
|---|---|---|---|
| | **18:00-19:00** | **Welcome Cocktail** | |
| | **18:30-20:00** | **Museum visit** | |
| | **20:00-23:30** | **Dinner** | |

**MRS Workshop 2022**
Overcoming the Barriers to Clinical Use
DISCONNECT 2 RECONNECT
22-24 August 2022 @ EPFL, Lausanne, Switzerland

10

## 6.3   Day 3: Wednesday, 24th August

**S7      08:30-10:15      Clinical applications of MRS**

**Moderators:**
Peter Barker, Department of Radiology and Radiological Science, Johns Hopkins University, Baltimore, Maryland, USA
Kay Chioma Igwe, Columbia University, USA

| Session | Time | Title | Presenter |
|---|---|---|---|
| S7B1 | 08:30-08:55 | Brain MRS in psychiatry | Lawrence S Kegeles, New York State Psychiatric Institute (NYSPI), New York, NY |
| S7B2 | 08:55-09:20 | Brain MRS in cancer | Otto Rapalino, Athinoula A. Martinos Center for Biomedical Imaging, Department of Radiology, Massachusetts General Hospital, Boston, Massachusetts, USA and Harvard Medical School, Boston, Massachusetts, USA |
| S7B3 | 09:20-09:45 | MRS in pediatrics | Petra Pouwels, Department of Radiology and Nuclear Medicine, Amsterdam UMC, Amsterdam, The Netherlands |
| S7B4 | 09:45-10:15 | MRS application in liver and muscle | Vera Schrauwen-Hinderling, Department of Imaging / Nutrition and Movement Sciences NUTRIM School of Nutrition and Translational Research in Metabolism Faculty of Health, Medicine and Life Sciences, Maastricht University |

**10:15-10:45      Break: Meet the experts! break the ice**

**S8      10:45–12:30      Panel Discussions**

**Moderators:**
In-Young Choi, Department of Neurology, University of Kansas Medical Center, Kansas City, Kansas, US
Roland Kreis, Magnetic Resonance Methodology group of the University Institute for Diagnostic and Interventional Neuroradiology and the Department of Biomedical Research, University Bern, Bern, Switzerland

| Session | Time | Title | Presenter |
|---|---|---|---|
| S8P1 | 10:45–11:25 | Consensus papers: from consensus papers to impact - Panel discussion | Christoph Juchem, Department of Biomedical Engineering, Columbia University Fu Foundation School of Engineering and Applied Science, New York, New York, USA and Department of Radiology, Columbia University College of Physicians and Surgeons, New York, New York, USA with Jodi Weinstein, Stony Brook School of Medicine, Stony Brook, NY, USA |
| S8P2 | 11:25-12:05 | Accelerated MRSI: quality control and validation of fast methods - Panel discussion | Wolfgang Bogner, High Field MR Center, Department of Biomedical Imaging and Image-guided Therapy, Medical University Vienna, Vienna, Austria with Cristina Cudalbu, CIBM MRI EPFL, Lausanne, Switzerland and Jannie Wijnen, high Field MR Research, Centre for Image Sciences, University Medical Centre Utrecht, Utrecht, The Netherlands |
| S8A1 | 12:05-12:20 | Accurate prediction of IDH-mutation status of gliomas using SLOW- editing MRSI at 7 Tesla MR | Guodong Weng et al. |
| S8A2 | 12:20-12:35 | Probing diffusion of water and metabolites to assess white matter microstructure in Duchenne muscular dystrophy | R. Govaarts et al. |

**12:35-14:00     Lunch on-site: Meet the experts! break the ice + POSTER SESSION**

**S9   14:00-16:00    Emerging techniques X-nuclei, high field**
Moderators:
PG Henry, Center for Magnetic Resonance Research, Department of Radiology, University of Minnesota, Minneapolis, Minnesota, USA
Dario Goranovic, Medical University of Vienna, Austria

| Session | Time | Title | Presenter |
|---|---|---|---|
| S9B1 | 14:00-14:25 | Deuterium MRSI | Jeanine Prompers, Department of Radiology, University Medical Center Utrecht, Utrecht, The Netherlands |
| S9B2 | 14:25-14:50 | Hyperpolarized $^{13}$C: where are we in the clinic? | Christoffer Laustsen, The MR Research Center, Department of Clinical Medicine, Aarhus University, 8200 Aarhus, Denmark |
| S9A1 | 14:50-15:05 | Non-invasive 3D mapping of downstream brain glucose metabolism using $^1$H MRSI with deuterium labeling at 3T | Fabian Niess et al. |
| S9A2 | 15:05-15:20 | Comparing cerebral metabolism of hyperpolarized $^{13}$C-glucose and thermally polarized deuterated glucose under different anesthetic conditions | Mor Mishkovsky et al. |
| S9A3 | 15:20-15:35 | Retrospective under-sampled 3D Deuterium Metabolic Imaging (DMI) of the Human Liver with Low-rank and Subspace Modeling at 7T | Kyung Min Nam et al. |
| S9A4 | 15:35-15:50 | DMI using different doses of [6,6'-$^2$H$_2$]-glucose for real-time in vivo liver glucose mapping at 7 T | Simone Poli et al. |
| S9A5 | 15:50-16:05 | Anesthetic-related neuroenergetic changes measured with $^1$H- and $^{31}$P-MRS in mouse at 7 Tesla | Antoine Cherix et al. |

**16:00-17:00    Closing remarks and Au revoir ! by Wolfgang Bogner, Medical University Vienna, Austria – chair of the MRS Study Group at ISMRM**

MRS Workshop 2022
Overcoming the Barriers to Clinical Use
DISCONNECT 2 RECONNECT
22-24 August 2022 @ EPFL, Lausanne, Switzerland

12

# 7 Numbered list of posters

## 7.1 On-site posters

| Poster no. | Title | Presenter |
|---|---|---|
| 1 | A Multivariate Curve Resolution (MCR) analysis of multicenter MRSI data for prostate cancer localization | A Stamatelatou |
| 2 | The effect of signal-to-noise ratio and linewidth on neurochemical quantification by LCModel analysis | Phil Lee |
| 3 | Ultra-short TE semi-LASER sequence for small animal 1H MRS at 9.4 T | Ivan Tkac |
| 4 | Exposure study: Evaluating the neurotransmitter-metal relationship in welders | Gianna Nossa |
| 5 | Assessment of Oxidative Stress and Neuronal Activity Affected in PTSD Subjects | Antonia Susnjar |
| 6 | Super-fast assay of creatine kinase using 31P-MT-MR fingerprinting at 7T in the human brain | Mark Widmaier |
| 7 | A simulation study: toward accurate metabolite quantification of short-echo-time 1H MR spectra in LCModel by optimizing the basis set based on the spectral lineshape | Ying Xiao |
| 8 | Probing the medial temporal lobe with MRS | Nyman, Axel Karl Gottfrid |
| 9 | Validation, quality control and reproducibility of 1H FID-MRSI on a preclinical 14.1T | Dunja Simicic |
| 10 | Quantitative assessment of metabolite concentrations in 31P and 1H MRSI: Comparing age and gender related differences | Pilatus U |
| 11 | 31P and 1H MRS for in vivo metabolic profiling of diffuse large B-cell lymphoma | Katharina J. Wenger |
| 12 | Compressed Sensing for 2D-MRSI with Concentric Ring Trajectories at 7 T | Bernhard Strasser |
| 13 | Exploring ECCENTRIC sampling variants for accelerated high-resolution MRSI | Antoine Klauser |
| 14 | Initial experience using MRS in neonates on ultra-high field: a case series | Inge van Ooijen |
| 15 | Individual vs combined modeling of macromolecules in rat brain MRS | Wendy Oakden |
| 16 | 7T 1H-Magnetic resonance spectroscopy of thalamus and hypothalamus in chronic cluster headache | Anne Farestveit, Tore Wergeland Meisingset |
| 17 | Influence of signal-to-noise ratio on quantification of GABA concentration measured noninvasively in the human posterior cingulate cortex with 7 T ultra-short-TE MR spectroscopy | Guglielmo Genovese |
| 18 | Neurochemical profile of major depressive disorder in adolescents: 7 T MRS study | Guglielmo Genovese |
| 19 | Hyperpolarization of 129Xe gas via dissolution DNP: beneficial tips and tricks | Emma Wiström |
| 20 | A dictionary-based approach for the determination of pH values using 31P MRS | Vanessa L. Franke |
| 21 | Reduced glutamate levels correlate with decreased functional connectivity between the central visual field projection in V1 and V4 after central vision loss from Stargardt Macular Dystrophy | A.A. Sheldon |
| 22 | The association between stress-induced changes in dACC GABA levels and heart rate variability: a 7T 1H-MRS study | A. Kaiser |
| 23 | Repeatability of APTw imaging at 3T and 7T MRI | Iris Obdeijn |
| 24 | A simulation framework to assess the quantification reliability of 2HG in 1H MRS | Justyna Platek |
| 25 | Exploiting dual diffusion MRS and MRI acquisitions in the rat cerebellum at 14.1 T: a measurement of intra-extracellular water exchange | Jessie Mosso |

MRS Workshop 2022
Overcoming the Barriers to Clinical Use
DISCONNECT 2 RECONNECT
22-24 August 2022 @ EPFL, Lausanne, Switzerland

13

Continued...

| Poster no. | Title | Presenter |
| --- | --- | --- |
| 26 | Comparison between two quantification programs on the 1H-MRS data of the Alfa+ cohort | Margarida Julià-Sapé |
| 27 | Respiratory-triggered quantitative MR spectroscopy of the human cervical spinal cord at 7 T | Tangi Roussel |
| 28 | Whole brain 31P MRSI at 7 T with FSL-MRS | Tangi Roussel |
| 29 | Triple Repetition Time Saturation Transfer (TRiST) 31P MR Spectroscopy for Measuring ATP Synthesis in Human Liver at 3T | B. Korzekwa |
| 30 | Training a Convolutional Neural Network for Enhanced Spectral Quantification of whole-brain MRSI Data | Goranovic, D. |
| 31 | Novel urease inhibitors for the treatment of hepatic encephalopathy | Diana Evstafeva |
| 32 | 31P-MRS Analysis With Neural Networks: 31P-SPAWNN | Julien Songeon |
| 33 | Reproducibility of localized 31P-magnetic resonance spectroscopy using different surface coils for assessing human hepatic energy metabolism | M. Jonuscheit |
| 34 | Altered Brain Energy Metabolism Related to Astrocytes in Alzheimer's disease | Yuhei Takado |
| 35 | Effects of prefrontal TDCS on brain metabolites in the DLPFC of healthy subjects - a double-blind placebo-controlled MRS study | Gizem Vural |
| 36 | Integrating hybrid CSI/EPSI acquisitions with L2 regularization for fast lipid removal of MRSI | Yiling Liu |
| 37 | Magnetic resonance spectroscopic imaging visualized spatial mapping of decreased glutamate levels associated with tau depositions in Alzheimer's disease patients | Kiwamu Matsuoka |
| 38 | Spatial Lipid Signal Separation for Spectroscopic Imaging of Intramyocellular and Extramyocellular Lipids | P. Adany |
| 39 | B1+ Corrected Metabolite Concentration Estimates from 7T FID-CRT-MRSI | P. Lazen |
| 40 | Comparing 7T FID-CRT-MRSI with Amino Acid PET | P. Lazen |
| 41 | Linear combination modeling of complex relative to real 1H MR spectra improves quantification precision | Leonardo Campos |
| 42 | MRS-Sim: Open-Source Framework for Simulating In Vivo Clinical MR Spectroscopy Data | John LaMaster |

MRS Workshop 2022
Overcoming the Barriers to Clinical Use
DISCONNECT 2 RECONNECT
22-24 August 2022 @ EPFL, Lausanne, Switzerland

14

## 7.2 Online posters

There will be eight online poster sessions from participants who could not come in person. Each online poster will be presented in a separate chat room in the **Discord** app. You can easily download the app either on App Store or on Google Play.

Then, you need to create an account by selecting a nickname, giving your date of birth, and selecting a password. Your phone number is not required. In the table below are the links and QR codes to join the individual online poster sessions.

| Poster no. | Title | Presenter | Link | QR |
|---|---|---|---|---|
| 43 | Seasonal influences on brain GABA+ and Glx concentrations | Benjamin Spurny-Dworak | https://discord.gg/xkq4YQJ89D | |
| 44 | Measuring brain lactate and other metabolites at 3T using an enhanced MRS with macromolecule suppression | Xi Chen | https://discord.gg/Fh5mqCyvXb | |
| 45 | Establishing Reproducibility of Global Lactate Measurements in Healthy Subjects at 3T | Ryan Armbruster | https://discord.gg/XDBKcx8Cpt | |
| 46 | Prefrontal cortex metabolites measured by 7-Tesla proton magnetic resonance spectroscopy distinguish posttraumatic stress disorder and major depression from control with high sensitivity and specificity | Kelley M. Swanberg | https://discord.gg/tPheEAd839 | |
| 47 | Urea cycle deficiencies | A Gropman | https://discord.gg/FfuFJEHxZk | |
| 48 | Effect of temporal resolution on fMRS-measured GABA and Glx levels | Duanghathai Pasanta | https://discord.gg/UHqK6SvYRm | |
| 49 | Exponential Component Analysis and its Application to 1H-MRS Data | Ravi Kalyanam | https://discord.gg/Sj8wcGMqZ3 | |
| 50 | Correction of B0 drift in rapid high-resolution MR Spectroscopic Imaging | Sneha Vaishali Senthil | https://discord.gg/6HrFjhzZKp | |

**MRS Workshop 2022**
Overcoming the Barriers to Clinical Use
DISCONNECT 2 RECONNECT
22-24 August 2022 @ EPFL, Lausanne, Switzerland

15

# 8 Full abstracts

S1A1

## Adaptive Magnetic Resonance

Assaf Tal[1]
[1]Department of Chemical and Biological Physics, Weizmann Institute of Science, Rehovot, Israel

**Introduction**. Over the past several decades, the speed and precision of in-vivo magnetic resonance imaging (MRI) and spectroscopy (MRS) have increased by leaps and bounds, by utilizing sophisticated excitation and acquisition techniques, from parallel imaging[1] and compressed sensing[2] to magnetic resonance fingerprinting[3]. However, these approaches have all been static in nature, fixing measurement parameters in advance, in anticipation of a wide range of expected tissue parameter values, and are therefore sub-optimal for any given subject. We depart from the conventional framework of magnetic resonance and propose a new, adaptive approach to MR, which uses the measured signal from the subject in the scanner to update and fine-tune the sequence parameters in real time. We use this to estimate the transverse ($T_2$) relaxation time of n-acetyl-aspartate (NAA) in-vivo, a powerful biomarker in neurodegenerative diseases[4], and show our adaptive approaches accelerates the acquisition 2.5-fold.

**Theory**. The outline of our adaptive approach is shown in Fig. 1. It maintains a prior distribution $p(T_2)$ which quantifies the probability of each value of the tissue parameter $T_2$. This is used to estimate $T_2$ and select the next echo time (TE), which minimizes the Cramer Rao bound[5] on $T_2$. The measured signal $s_N$ is then used to calculate the likelihood $p(T_2|s_N)$ of the actual tissue parameter having a value $T_2$. The prior belief is updated using Bayes' rule, and the cycle repeats until reaching a set total acquisition time.

**Methods**. Seven healthy volunteers provided informed consent and were scanned on a 3T Siemens Prisma scanner using a Siemens 32-channel head coil, and a multi-echo (MTE) sequence, with a single 1.5×1.5×1.5 $cm^3$ voxel placed in parietal white matter. Two variations of the sequence were run: In the Static variation, the echo times were fixed in advance to minimize the Cramer Rao Lower Bound assuming a uniform prior distribution of $T_2$ values between 50 and 450 ms. The Adaptive variation followed the framework outlined in Fig. 1, starting from a uniform prior $p(T_2)$ for $p(T_2) \in [50,450]$ ms. Both variations set TR=6000 ms, NEX=20, TA=2:00 minutes. Each sequence was repeated 12 times per subject to increase statistical power. Data was analyzed using a linear mixed model which estimated the intra-subject standard deviation and 95% confidence interval for $T_2$ for each of the two variations (Static and Adaptive). The adaptive sequence was implemented using the ICE real-time image reconstruction framework of Siemens.



**Figure 1**. **Left**: Outline of adaptive approach (the flowchart represents a single excitation).

**Results**. Fig. 2 shows the estimated $T_2$ values of NAA for each of the 12 volunteers for both variations (Static vs. Adaptive). The mean $T_2$ did not differ significantly between the two methods. For each volunteer, the ratio R of the standard deviation of the static to the adaptive approach was quantified. The mean standard deviation, averaged over all subjects, was 1.7 smaller for the adaptive approach compared to the static one. Equivalently, the adaptive approach attained the same precision using only 40% of the excitations (NEX=8), yielding a 2.5-fold acceleration.

**Discussion**. Adaptive sequences, here demonstrated for $T_2$ relaxometry of NAA, offer a completely new venue for accelerating MR acquisitions several-fold. The proposed framework can be adopted to target any metabolite or tissue property ($T_1$, $T_2$, diffusion, etc), and the gains obtained are completely independent of any other sources of acceleration (including compressed sensing, MR fingerprinting and parallel imaging).



**Figure 2**. In-vivo results of $T_2$ estimations: Static vs. Adaptive approaches (7 volunteers × 12 measurements).

**Bibliography**. [1] Sodickson D. K. & Manning W. J., Magn Reson Med 38:591 (1997). [2] Lustig M., Donoho D. & Pauly J. M., Magn Reson Med 58:1182 (2007). [3] Ma, D et al, Nature 495:187 (2013). [4] Kirov II & Tal A, Magn Reson Med 83:22 (2020). [5] Cavassila S et al, NMR Biomed 14:278 (2001).

![MRS Workshop 2022 logo — IT'S TIME]
**MRS Workshop 2022**
Overcoming the Barriers to Clinical Use
DISCONNECT **2** RECONNECT
22-24 August 2022 @ EPFL, Lausanne, Switzerland

16

S1A2

**Does visual stimulation always lead to an increase in glutamate concentration?**

Katarzyna Wasilewska, Agnieszka Glica, Katarzyna Jednoróg, Bartosz Kossowski
Nencki Institute of Experimental Biology

**Introduction**
Functional magnetic resonance spectroscopy (fMRS) measures neurometabolic concentration changes during task performance. Action potential in the active brain area causes the release of glutamate to the synaptic cleft. Hypothetically, such glutamate is more visible in fMRS than glutamate stored in synaptic vesicles (Kauppinen et al., 1994). Despite the fact that block designs with visual stimuli are the most common fMRS experiments, a recent review (Mullins 2018) points out that event-related design is more specific to neurotransmission than block design. He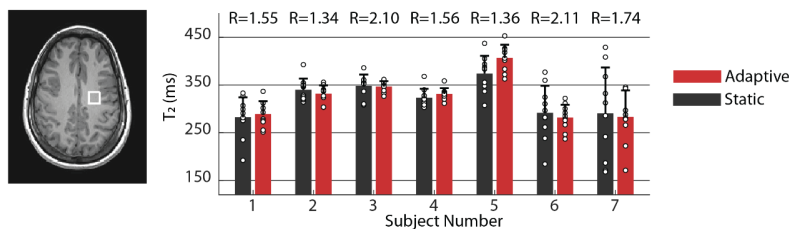re we aimed at studying glutamate concentration changes during a word reading event-related paradigm in brain areas of the reading network.

**Methods**
25 right-handed subjects (age range: 16-24 years) with different levels of reading skills were tested. Scans were performed on Siemens 3T Trio system using a 32 channel radiofrequency coil. fMRS data were acquired from 3 regions of interest (ROI) (Figure 1a): STS and VWFA from a classical reading network localized individually using fMRI localizer and the medial prefrontal cortex as the control region (CON). Event-related design with visual stimuli (words and false font strings) with variable delays between stimuli and MRS acquisition was performed. Single voxel spectroscopy was acquired using a Semi-Laser sequence (Deelchand *et al.*, 2021) (VOI=15x15x15 mm, TR/TE = 4000/28 ms, number of averages = 320). The FID-A MatLab toolkit (Simpson *et al.*, 2017) was used to preprocess fMRS data divided into three groups in terms of the time interval between stimuli onset and MRS data acquisition (**short**: 500 and 1000ms (104 averages); **long**: 3000 and 4500 ms (104 averages); **rest**: after more than 5s (99 averages)). Results were analyzed using LCModel (Provencher, 1993). Within-subject ANOVA with ROI (CON, STS, VWFA) and part of the spectrum (short, long, rest) was analyzed for an absolute glutamate concentration.

**Results**
We did not include VWFA estimates within the model due to a large number of missing data. We observed a significant main effect of "part" (F=3.48, p=0.04) regardless of the ROI (STS & CON) such as glutamate concentration in "short" is higher than for the "rest" condition (t=2.63 , p=0.035) (Figure 1c). Surprisingly, while "short" and "rest" conditions are different (BF10=8.220), we have found substantial evidence that the estimates for "long" and "rest" are the same (BF10=0.255). No significant differences were identified between the conditions within specific ROIs in post-hoc tests.

**Discussion**
Our results confirm the theory that glutamate released to the synaptic cleft is visible in MRS measured shortly after stimulus onset (500-1000 ms) but not in the "long" response (3000, 4500 ms). Our event-related design allows data to be split into different groups for e.g. based on time-lock between stimuli onset and data acquisition. This may allow for examination of the glutamate response function (Mullins, 2018) in more details. Our goal is to examine 120 subjects using data combined from 3T as well as a 7T scanner (work-in-progress).
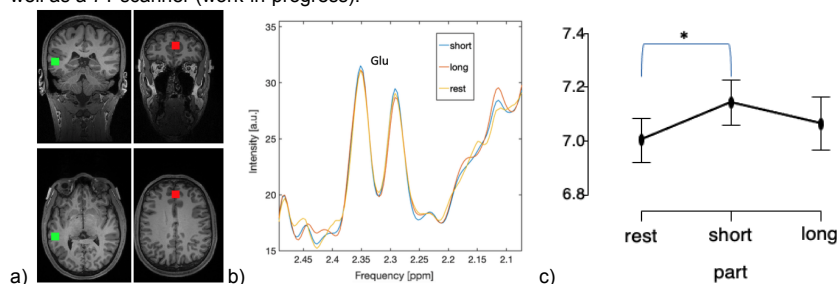


Figure 1. ROIs (green: STS, red: CON) (a) single-subject spectrum (b) anova results (c)

Deelchand, D.K. *et al.* (2021) 'Across-vendor standardization of semi-LASER for single-voxel MRS at 3T', *NMR in biomedicine*, 34(5), p. e4218.
Kauppinen, R.A. *et al.* (1994) 'Compartmentation of cerebral glutamate in situ as detected by 1H/13C n.m.r', *Biochemical Journal*, 298 ( Pt 1), pp. 121–127.
Mullins, P.G. (2018) 'Towards a theory of functional magnetic resonance spectroscopy (fMRS): A meta-analysis and discussion of using MRS to measure changes in neurotransmitters in real time', *Scandinavian journal of psychology*, 59(1), pp. 91–103.
Provencher, S.W. (1993) 'Estimation of metabolite concentrations from localized in vivo proton NMR spectra', *Magnetic resonance in medicine: official journal of the Society of Magnetic Resonance in Medicine / Society of Magnetic Resonance in Medicine*, 30(6), pp. 672–679.
Simpson, R. *et al.* (2017) 'Advanced processing and simulation of MRS data using the FID appliance (FID-A)-An open source, MATLAB-based toolkit', *Magnetic resonance in medicine: official journal of the Society of Magnetic Resonance in Medicine / Society of Magnetic Resonance in Medicine*, 77(1), pp. 23–33.

S2A1

## Fast prospective motion correction for spectroscopic acquisitions

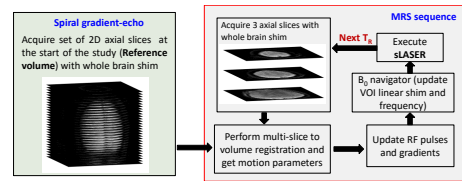Isaac Adanyeguh, Pierre-Gilles Henry, Dinesh K Deelchand

Center for Magnetic Resonance Research, University of Minnesota, Minneapolis, MN, United States

**Introduction**: Subject motion during MRS acquisition is a major issue leading to degraded spectral quality and incorrect localization. Several prospective motion correction techniques currently exist in the brain and use either external tracking devices[1,2] or are image-based navigators[3,4]. External devices are expensive due to the cost of the additional hardware and software requirements. Image-based navigators, on the other hand, can be implemented into custom spectroscopic sequences and do not require additional hardware. However, past studies that used image-based navigators had a relatively long time between measurement of motion and the acquisition of the MRS data ($\geq 1$ s)[3,4]. Any motion occurring during that time could not be corrected. Therefore, the aim of this study was to implement a fast image-based motion tracking method while minimizing the time between the start of the motion navigator and the start of the MRS acquisition. This new fast navigator is based on 2D spiral imaging with multi-slice-to-volume registration[5] for rapid computation of motion parameters.

**Methods**: The semi-LASER sequence[6] was modified to incorporate a 3-slice spiral motion navigator, a FASTMAP-like shim navigator (linear shims) and a frequency navigator[7]. The motion correction protocol consisted of first acquiring a reference volume, i.e. a set of spiral gradient-echo axial slices (30 slices, $T_R/T_E$=75/15 ms, matrix=64x64, thk=3 mm, FOV varies between subjects) covering the whole brain and acquired after shimming first and $2^{nd}$ order shims on the whole brain (referred to as brain $B_0$ shim). This was necessary because acquiring spiral images with all shims optimized on the MRS volume-of-interest (VOI) strongly degrades image quality. After positioning the VOI, 3 navigator slices (spNav) were acquired outside the VOI during each repetition and were registered to the reference volume to calculate motion (Figure 1). For each repetition, the brain $B_0$ shim was loaded before acquiring the spNav images, then the linear shims (lin-3) were adjusted in the MRS VOI using the shim navigator prior to sLASER. Second order shims were not updated at each repetition due to their long stabilization time. All experiments were performed on a 3T Prisma scanner using a 20-channel head coil. Five subjects participated in this study after obtaining written informed consent which was approved by the IRB. sLASER data (32 transients) with metabolite cycling and 3 modules of OVS pulses were acquired from the prefrontal cortex (PFC) under 3 conditions: without subject motion (Baseline), with subject motion and motion correction disabled (NoCo), and with subject motion and MoCo/shim/frequency enabled (shMoCo). Water signal was also measured in the PFC, pons and posterior cingulate cortex (PCC) to compare water linewidth with a) all shims adjusted in the VOI (using FASTESTMAP) and b) $2^{nd}$ order shims adjusted in the whole brain and linear shims adjusted in the VOI in these three regions.



**Figure 1**: Overview of the multi-slice to volume registration for prospective motion correction in MRS.
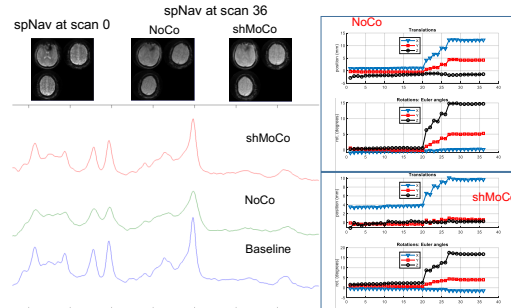


**Figure 2:** sLASER spectra ($T_R/T_E$=5000/30ms) from the last 16 transients for baseline, NoCo and shMoCo conditions. Translation and rotations plots during NoCo and shMoCo are also illustrated.

**Results & Discussion**: Figure 2 shows sLASER spectra acquired in one subject from the PFC between different conditions. Good agreement was observed between baseline shMoCo data even though the subject rotated their head by ~17° with an X translation of ~10 mm. Duration of each navigator: Moco (165 ms acquisition, 140 ms registration and feedback), shim (95 ms) and frequency (100 ms).



**Figure 3:** Water linewidth acquired using sLASER from PFC, PCC and pons using 3 different $B_0$ shims: 1) whole brain $B_0$ shim, 2) whole brain $B_0$ shim + lin-3 in VOI and 3) all shims in VOI.

Water linewidth was broader (>12 Hz) for hard to shim regions such as PFC and pons when shimming the whole brain vs. shimming in the MRS voxel. However, when the linear shims were adjusted in the voxel after shimming the whole brain, linewidth was significantly improved and within the recommend range[8], and was only slightly higher than when shimming all shims in the VOI.

**Conclusion**: This study shows that a fast (~300 ms) and accurate prospective motion correction for SVS MRS is feasible at 3T. This technique is not limited to SVS but can also be used for MRSI acquisitions.

**References:** [1] Zaitsev et al. NMR Biomed 2010; [2] Haeberlin et al. MRM 2015; [3] Keating et al. MRM 2010; [4] Hess et al. MRM 2011; [5] Hoinkiss & Porter MRM 2017; [6] Oz & Tkac MRM 2011; [7] Deelchand et al MRM 2019; [8] Juchem et al. NMR Biomed 2020.

MRS Workshop 2022
Overcoming the Barriers to Clinical Use
DISCONNECT 2 RECONNECT
22-24 August 2022 @ EPFL, Lausanne, Switzerland

18

S2A2

# Deep Learning Pipeline for Quality Filtering of MRSI Spectra

Mladen Rakić[1,2], Federico Turco[3], Guodong Weng[3],
Diana M. Sima[1], Johannes Slotboom[3]

[1]icometrix, Leuven, Belgium; [2]KU Leuven, Department of Electrical Engineering (ESAT), Processing Speech and Images (PSI) and Medical Imaging Research Center, Leuven, Belgium; [3]Institute for Diagnostic and Interventional Neuroradiology, Support Center for Advanced Neuroimaging (SCAN), University of Bern, Bern, Switzerland

With the rise of novel 3D MRSI acquisition protocols in clinical practice which are capable of capturing a large number of spectra from a subject, there is a need for a good preprocessing pipeline which would filter out the bad quality spectra prior to the quantification step. This work introduces such a pipeline, based on an ensemble of deep learning classifiers.

The dataset consists of 22878 spectra (70% training/30% validation) from a healthy subject, manually labelled two times by an expert. We define 4 classes of spectral quality as follows: (i) noise, (ii) spectra greatly influenced by lipids and macromolecules, (iii) spectra mildly influenced by lipids and (iv) good quality spectra. The spectra were collected with an EPSI-variant which implemented a novel type of spectral editing named SLOW-editing[1] at a UHF 7T MR-scanner (Terra, Siemens Healthineers, Erlangen, Germany) using the CE-labeled clinical mode. Whole brain spectral editing can be obtained within 10 minutes acquisition time (TE = 68 ms, TR = 1500 ms). Due to the implicit water and lipid suppression of SLOW-editing, no additional HLSVD based water removal is necessary.

The model consists of three pairs of networks, each comprising an autoencoder and a classification network. In the classification step, the encoding half of the autoencoder is kept as a dimensionality reduction tool, while the fully connected layers are added at its output. Each of the three pairs of networks is trained on different parts of spectra: (i) absorption, (ii) dispersion and (iii) concatenated absorption and dispersion, for a more robust decision making. The final class is assigned via a majority voting scheme.

The F1 scores obtained on the validation dataset for the 4 previously defined classes are 0.98, 0.94, 0.83 and 0.96, respectively. The arguably lower value of 0.83 was reached for the least represented class and future improvements will aim at diversifying the dataset in order to improve this value. The model was applied on an unseen and unlabelled data coming from another subject and the sample results are shown in Figure 1 for purposes of qualitative analysis.



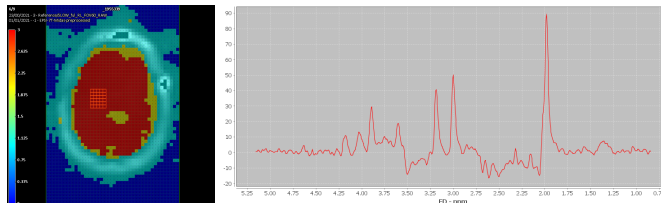Figure 1: Quality filtering model was applied on an unseen dataset, and the spatial representation matches what is expected (left). Average spectrum of the selected voxels is shown on the right.

[1] Weng G, Radojewski P, Sheriff S, Kiefer C, Schucht P, Wiest R, Maudsley AA, Slotboom J. SLOW: A novel spectral editing method for whole-brain MRSI at ultra high magnetic field. Magnetic resonance in medicine. 2022 Jul;88(1):53-70.

S2A3

**Effect of circadian rhythm on brain NAD: a magnetic resonance spectroscopy study at 7 T**

Zhiwei Huang[1], Bernard Cuenoud[2, 3, 4], Daniel Wenz[1], Lijing Xin[1]
1. Center for Biomedical Imaging, Ecole Polytechnique Fédérale de Lausanne, Lausanne, Switzerland.
2. Clinical Development Unit, Nestlé Research Center, Lausanne, Switzerland
3. Nestlé Institute of Health Sciences SA, Lausanne, Switzerland
4. Nestlé Health Science, Epalinges, Switzerland

**Introduction.** The circadian rhythm (CIR) plays a vital role in regulating cellular, physiological and behavioral processes. It was found that mammalian CIR are coordinated with metabolic activity through controlled expression of Nicotinamid Phosphoribosyltransferase (NAMPT)[1]. Regulation of NAMPT could result in oscillating $NAD^+$, an important metabolite involved in bioenergetics and cellular signaling processes[2]. The rhythmic oscillation of NAD+ could serve as a feedback timer in turn. Preclinical experiments showed that CIR is linked with the NAD levels and the NAD redox ratio[3]. However, no clinical study has been reported in human on the effect of the CIR on brain NAD levels. To explore how CIR could influence the brain NAD level in human, we conducted a MRS study at 7T.

**Methods.** To detect a similar effect size as observed in the red blood cells and mice livers[4, 5], 25 male subjects aging between 18-40 years old were recruited. Before the experiment, the participants were required to record their sleeping diary for one week to ensure regular sleeping habits. The experiment was implemented in fasted morning condition (8 am) and later afternoon condition (3 pm) during a day. For each session, the saliva sample was collected and analyzed to determine the cortisol level. Then, MR experiments were performed on a 7T/68cm MR scanner (Siemens Medical Solutions, Erlangen, Germany) with a $^1H$ surface coil and a single-loop $^{31}P$ coil (7cm-diameter) for the occipital lobe. $^{31}P$-MRS was performed by a pulse-acquire sequence (TR=3s, 320 averages) to measure $^{31}P$ metabolites including NADH and $NAD^+$. $^1H$-MRS was acquired by a short-TE STEAM sequence (TE/TM/TR=4.5/25/5500ms, 64 averages, voxel size = 35x20x25mm$^3$) for neurochemical profiling including lactate. BART[6] (Inquisit Lab) was implemented as a measure of individual risk-taking propensity. Breakfast and lunch were provided at certain time, and the participants were not allowed to consume other food or beverage before the PM session. All MR spectra were analyzed by LCModel.

**Results.** The cortisol level was significantly higher in the morning, confirming the existence of CIR; the BART performance was significantly higher in the afternoon. The redox ratio variance was significantly larger in the AM. By stratifying the subjects into a High (H) group and a Low (L) group relative to the AM ratio median value, significant increase of NAD ratio in the afternoon was found in L group, driven by the decrease of NADH, and the opposite was found in H group. Besides, BART performance was found to be significantly positively correlated with the cortisol level, indicating a higher risk preference in the afternoon.

**Discussion.** This is the first study to explore the relationship between CIR and brain metabolites in human. The success of the project could contribute to a greater molecular understanding of the CIR in human and open therapeutic perspectives for diseases. That H and L group exhibited different changes of the redox ratio during the day indicated that there might be two different metabolic processes.
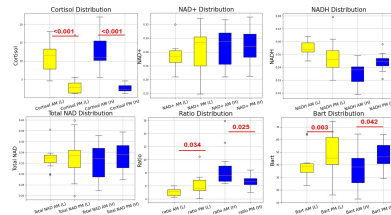


Figure 1. Cortisol level, metabolite level, and BART performance comparison in the AM and PM

### References

1. Cambronne XA, Kraus WL. Compartmentalization of $NAD^+$ Synthesis and Functions in Mammalian Cells. Trends Biochem Sci. 2020 Oct;45(10):858-873. doi: 10.1016/j.tibs.2020.05.010. Epub 2020 Jun 25. PMID: 32595066; PMCID: PMC7502477.
2. Yang, Yue, and Anthony A. Sauve. "NAD+ metabolism: Bioenergetics, signaling and manipulation for therapy." Biochimica et Biophysica Acta (BBA)-Proteins and Proteomics 1864.12 (2016): 1787-1800.
3. Xie N, Zhang L, et al. $NAD^+$ metabolism: pathophysiologic mechanisms and therapeutic potential. Signal Transduct Target Ther. 2020 Oct 7;5(1):227. doi: 10.1038/s41392-020-00311-7. PMID: 33028824; PMCID: PMC7539288.
4. Ramsey KM, Yoshino J, et al., Takahashi JS, Imai S, Bass J. Circadian clock feedback cycle through NAMPT-mediated $NAD^+$ biosynthesis. Science. 2009 May 1;324(5927):651-4. doi: 10.1126/science.1171641. Epub 2009 Mar 19. PMID: 19299583; PMCID: PMC2738420.
5. O'Neill JS, Reddy AB. Circadian clocks in human red blood cells. Nature. 2011 Jan 27;469(7331):498-503. doi: 10.1038/nature09702. PMID: 21270888; PMCID: PMC3040566.
6. Lejuez, Carl W., et al. "Evaluation of a behavioral measure of risk taking: the Balloon Analogue Risk Task (BART)." *Journal of Experimental Psychology: Applied* 8.2 (2002): 75.

**MRS Workshop 2022**
Overcoming the Barriers to Clinical Use
DISCONNECT **2** RECONNECT
22-24 August 2022 @ EPFL, Lausanne, Switzerland

20

S3A1

## *Outlier Rejection for Fetal and Neonatal Brain MRS*

Jack Highton[1], Maria Y. Lopez[1], Anthony N. Price[1], Vanessa Kyriakopoulou[1], Lisa Story[1], Mary A. Rutherford[1], Jo Hajnal[1], Enrico De Vita[1]
*1 Biomedical Engineering and Imaging Sciences, King's College London, London, United Kingdom*

### INTRODUCTION

MRS applications in the fetus are challenging due to the low SNR (fetal size, distance from the coil, the use of 1.5T scans) and signal disruption caused by unrestricted fetal motion. Outlier rejection of motion corrupted averages to improve spectral quality is particularly important. Spectral phase shifts are associated with motion, both during signal acquisition and between MRS repeats [1]. We propose a threshold-free method for optimal outlier rejection, "Ranked residual-water Phase Shift", using phase shifts in the residual water peak after suppression as a metric of potential motion in individual repeats.

### METHODS

The first MRS dataset used as a proof-of-concept (PRESS, TE/TR 42/1500ms, 20x20x20mm3, 1.5T Philips Achieva, 128 repeats saved in 32 'blocks' of 4) included 128 fetuses. From these, scans of 35 fetuses were selected based on key metabolite peaks being visually identifiable in the mean spectra, with median gestational age 29 weeks and range 12.6. In the second dataset (3T Philips Achieva, PRESS, TE/TR 80/2000ms, 25x25x25mm3, 80 repeats) the Thalamus of 15 preterm neonates were scanned before term (median birth Gestational Age 33.1 weeks range 12.4, median scan GA 35.1 weeks range 4.7) and 35 after term (median birth GA: 33.2 weeks range 13.1, median scan GA: 41.3 weeks range 8.3).
**Step 1**. The phase shift of the residual water peak (the peak in spectrum magnitude, 4.4-5 ppm) was estimated for each block of 4 repeats, as the cost metric and indicator of fetal motion. Due to the water peak's magnitude even after water suppression, this is robust to the low SNR. It is also insensitive to frequency drifts [2]. The water peak phase shift - relative to the first block - was used to rank each block; i.e. greater shifts rank lower due to association with greater motion [1].

| | Outlier Rejection Method | Number of repeat blocks rejected | Mean Fit SD of NAA+Cho+Cr over concentration | FWHM (Hz) |
|---|---|---|---|---|
| **Fetal** | None | 0 | 13.7 ± 13% | 2.71 ± 0.76 |
| | Ranked Phase Shift | 3.43 ± 0.5 | **7.86 ± 6.6%** | 2.66 ± 0.81 |
| | NSD 3.0 (default) | 3.43 ± 0.2 | 13.6 ± 15% | 2.70 ± 0.73 |
| **Neonatal** | None | 0 | 10.5 ± 6.0% | 5.45 ± 2.1 |
| | Ranked Phase Shift | 6.56 ± 5.9 | **7.86 ± 4.1%** | **4.77 ± 1.0** |
| | NSD 0.5 | 7.78 ± 5.4 | 8.10 ± 6.1% | 5.44 ± 1.3 |

**Figure 1** - Mean (±SD) repeat blocks rejected alongside fit quality metrics for each outlier rejection method. The proposed method is compared to FID-A with best performing NSD threshold (from 0.1,0.5,1,3) shown. Green: significant improvement relative to no outlier rejection (paired t-test).
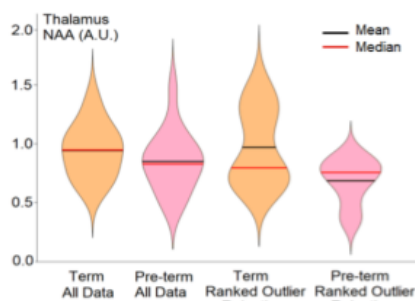
**Step 2**. Frequency & phase correction was applied to data in each block [3] using FID-A [4].
**Step 3**. Following ranking, an increasing number of blocks of repeats were cumulatively summed in the order of the rank calculated in the first step, i.e. (1st ranked block, 1st and 2nd ranked… all but the last block, all blocks).
**Step 4**. Metabolite concentrations, in each set containing more blocks, were quantified with TARQUIN [5].
**Step 5**. The quality metric for each of these fits was the standard deviation of the estimated concentration of the key metabolites - total N-Acetyl-Aspartate (NAA), total Choline (Cho), and total Creatine (Cr) - calculated using Cramér-Rao lower bounds [6]; the averages of these CRLBs was used as single summary metric weighting the contribution of these 3 groups of metabolites according to their concentration.

### RESULTS

Ranked residual-water Phase Shift outlier rejection algorithm improved the uncertainty in quantification of key metabolites relative to no outlier rejection, as indicated by the decreased average metabolite SD (p=0.003, Figure 1). FID-A's "op_rmbadaverages" outlier rejection could not achieve uncertainty reduction with any NSD threshold tried, even with a similar number of rejected repeats as our method. Thalamus NAA in neonates scanned preterm was lower than those scanned after term (Figure 2) as expected [7]. However, this only became significant (p=0.03) with Ranked Phase Shift Outlier Rejection. Metabolite linewidths slightly improved in both datasets (see Figure 2 FWHM & Figure 3 example fit).

**Figure 2** - The increased neonatal Thalamus NAA in the group scanned after-term was only significant (p=0.03) with our outlier rejection applied.
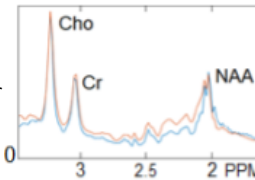
**Figure 3 -** The TARQUIN fit (arbitrary units) from a sample fetal scan (GA 26 wks), with (blue) & without (orange) Ranked Phase Shift outlier rejection.

### DISCUSSION

Our proposed outlier rejection algorithm significantly improved the quantification of key metabolites in a fetal and a neonatal cohort, by minimising rejected transients while maintaining the quality of the averaged spectrum. Fitting quality (measured as SD) improved, with no significant effects on linewidth and SNR compared to no outlier-rejection or conventional pre-processing. Noise dominates over motion artefact effects in the metabolic area (<4.6ppm), but we demonstrate that motion related phase shifts in the residual water peak are readily identifiable and can be used to perform optimised MRS outlier rejection. This is also consistent with the occasional observation of phase shift in online-displayed residual water peaks during neonatal MRS acquisitions, concurrent with observed motion of the neonate.

[1] MG Saleh, Edden RA, Chang L et al. MRM.April 2020.84(5).   [2] Hui SCN, Mikkelsen M, Zöllner HJ et al . Neuroimage. Nov 2021. 241.
[3] Near J, Edden R, Evans CJ et al. MRM.Jan 2015.73(1):44.    [4] Simpson R, Devenyi GA, Jezzard P et al. MRM.Jan 2017.77(1):23-33.
[5] Martin M et al. MRM.Jan 2011.65(1):1-12.  [6] Roland Kreis. MRM.March2015.75(1). [7] Chau V et al.Neurology.Dec 2013:81(24):2082.

MRS Workshop 2022
Overcoming the Barriers to Clinical Use
DISCONNECT 2 RECONNECT
22-24 August 2022 @ EPFL, Lausanne, Switzerland

21

S3A2

**Towards simultaneous concentration and $T_2$ mapping of brain metabolites by multi-echo spectroscopic imaging**

Rizzo R[1,2], Stamatelatou A[3], Heerschap A.[3], Scheenen T.[3], Kreis R[1,2]

**1.** MR Methodology, Institute of Diagnostic and Interventional Neuroradiology, University of Bern, Bern, Switzerland **2.** Translational Imaging Center, sitem-insel, Bern, Switzerland **3.** Department of Medical Imaging, Radboud University Medical Center, Nijmegen, Netherlands

**Introduction:** This study deploys multi-echo data from single readouts[1-4] to produce fast metabolite-specific $T_2$ and concentration maps. This approach can be of use in functional or multi-parametric MRS examinations[5,6], in which concentrations provide insight into functionality and pathophysiology, and relaxation rates act as further potential biomarkers of abnormalities, containing information on cellular microenvironment[7].

**Methods:** A metabolite cycled 2D-MRSI-sLaser scheme with weighted Cartesian k-space encoding and filtering, is optimized to acquire three consecutive echoes in one scan (multi-echo single-shot, MESS[2]) lasting 7 minutes: 16x16 grid, FOV: 200x160x15 mm, VOI: 80x60x15 mm, TR/(TEs) 1600/(35,156,278)ms, one healthy volunteer. The results are compared to a traditional multi-echo multi-shot approach (MEMS). A simultaneous 2D-fit is run in FitAID[8] with basis sets of 16 metabolites simulated in Vespa, assuming Voigt line shapes. A Macro Molecular Background (MMBG) pattern is simulated[9] and $T_2$s fit freely for 6 major metabolites and the MMBG. Concentrations are calculated in milli-*molal* units (mm) referencing to parenchymal water. Cramer Rao Lower Bounds (CRLBs) probe the achievable precision[10].

**Results & Discussion:** Fig.1 illustrates the acquisition setup, and MESS and MEMS signals from voxel number 20. Short TE MESS spectra show limited resolution. TE2 and TE3 show linear phase offsets due to partial echo acquisitions. Estimated concentrations and $T_2$ values (Fig.2) are in line with the literature[9]. The figures include fit uncertainties (CRLBs). MEMS and MESS yielded similar estimates whereas precision for concentration and $T_2$ estimates is better for MESS. Fig.3 displays concentration and $T_2$ maps.

**Conclusions:** The novel approach yields metabolite- and subject-specific $T_2$ maps and promises increased precision or inversely shorter experimental time compared to traditional approaches while achieving comparable accuracy of estimates, extending results from single-voxel experiments[4].

Fig. 2: Estimated concentrations, T2s and their CRLBs for 3 major metabolites plotted against voxel number after zero-filling in k-space domain (12x12 pixels) and cropping of voxels at the edge of the VOI to exclude partial volume effect.
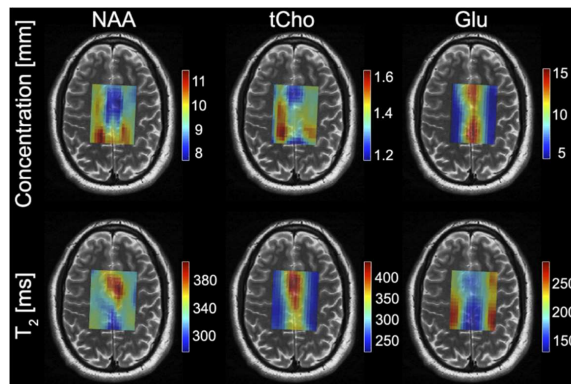


Fig.3: Concentration and $T_2$ maps for 3 major metabolites after zero-filling in spatial domain (18x18 pixels) and cropping of voxels at the edge of the VOI to minimize partial volume effects.



Fig. 1: (left) FOV and voxel numbering. (right) MESS and MEMS data.

**References: 1.** Ronen, I. et al. NMR Biomed. 26, (2013); **2.** Duyn, J. et al. MRM 30, (1993); **3.** Dydak, U. et al. MRM 50, (2003); **4.** Rizzo R. et al. ISMRM 2022, #0311; **5.** Ronen, I. ISMRM 2022, #WE-20; **6.** Tal, A. ISMRM 2022, #WE-27; **7.** Weinberg, B. ISMRM 2022, #WE-08; **8.** Chong, D. et al. MRMPBM. 24, (2011); **9.** Hoefemann, M. et al. NMR Biomed. 33, (2020).; **10.** Bolliger, C. et al. Neuroimage 83, (2013).

**MRS Workshop 2022**
Overcoming the Barriers to Clinical Use
DISCONNECT 2 RECONNECT
22-24 August 2022 @ EPFL, Lausanne, Switzerland

22

S3A3

## MP-PCA and LR-TGV denoising in ^{1}H-FID-MRSI data at 14.1T: application and validation

B. Alves[1,2#], D. Simicic[1,2,3#], J. Mosso[1,2,3], I.O. Jelescu[4], C Cudalbu[1,2*], A. Klauser[1,5*]

[1] CIBM Center for Biomedical Imaging, Switzerland; [2] Animal Imaging and Technology, EPFL, Lausanne, Switzerland; [3] LIFMET, EPFL, Lausanne, Switzerland; [4] Lausanne University Hospital CHUV, Service de radiodiagnostic et radiologie interventionnelle, Switzerland; [5] Department of Radiology and Medical Informatics, University of Geneva, Switzerland.; #, * -equal contribution

**Introduction:**

The constant appetite for higher spatial resolution in ^{1}H-MRSI leads to an increased search for post-processing methods that aim at reducing the noise variance, with several denoising methods proposed[1-5]. Reconstruction methods based on different low-rank assumptions have been implemented mainly on clinical applications[1-3]. In parallel, the Marchenko-Pastur principal component analysis (MP-PCA) based denoising has been implemented on MRI, DW-MRS and ^{1}H-MRSI data[5-9]. The MP-PCA technique exploits the fact that noise eigenvalues follow the universal Marchenko-Pastur distribution, a result of the random matrix theory. We recently implemented two noise-reduction techniques on prec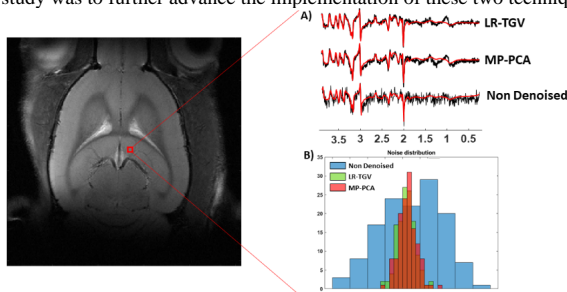linical 14.1T fast ^{1}H-FID-MRSI[10] datasets: the MP-PCA based denoising and the low-rank TGV reconstruction. The aim of the present study was to further advance the implementation of these two techniques, test their feasibility and routine usage at 14.1T.

**Methods**

^{1}H-MRSI datasets were acquired in the rat brain on a 14.1T MRI system (Bruker/Magnex Scientific) using a recently implemented single slice fast ^{1}H-FID-MRSI sequence (TE=1.3ms, TR=813ms, 2mm slice thickness centred on the hippocampus, FOV=24x24mm[2], matrix size=31x31, 1 average). The data was phase corrected based on the water signal, cleaned from lipid contamination using the metabolite-lipid orthogonality approach[4,11] and residual water was suppressed with HLSVD. The low-rank TGV reconstruction was applied[4] to the full dataset (31x31 matrix). For the MP-PCA, a sub-matrix X defined by the power map was selected. The complex-valued FIDs were split into real and imaginary parts, where the first dimension contained the time-domain sampling (1024 points) and the second dimension the number of spectra from the selected sub-matrix. The resulting



**Figure 1.** Denoised (via MP-PCA and LR-TGV) and non denoised : A) FID spectra for a voxel in the volume of interest, fitted by LCModel. B) Noise distribution, computed from a metabolite free region of the spectra

spectra: non-denoised, LR-TGV denoised and MP-PCA denoised were quantified with LCModel combined with a simulated basis set. The metabolite maps were created and overlaid to the corresponding MRI image using an in house written Matlab code. An automatic quality control process with a criterion on the SNR, FWHM, CRLB's was applied on the metabolic maps. Both the SNR and the FWHM were obtained from the LCModel outputs and averaged over the selected data. The effect of both denoising techniques on the metabolite map coverage was evaluated by computing: 1) the percentage of voxels accepted by the automatic quality control; and 2) the average relative concentration of Ins in a corresponding hippocampus region and a mix of striatum and cortex to assess well known brain regional difference of Ins after denoising[12].
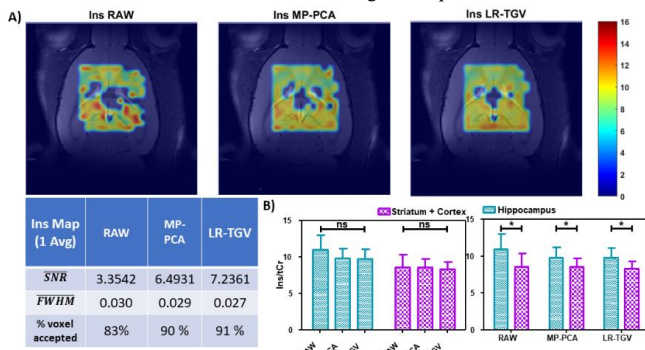
**Results and Discussion**

An averaged two-fold increase in apparent SNR as quantified by LCModel was observed when using both noise-reduction approaches, without any visual impact on linewidths or other features of the spectra (Fig 1A, Table and Fig 2A-quantitavive results). It has to be considered that the baseline estimate has an important contribution in the SNR calculations in addition to the residuals when using LCModel. The gaussian distribution of the noise in the MRSI slice was conserved, with a reduction of its standard deviation (Fig 1B). Both noise-reduction techniques improved the number of accepted voxels by at least 7%, leading to an



| Ins Map (1 Avg) | RAW | MP-PCA | LR-TGV |
|---|---|---|---|
| *SNR* | 3.3542 | 6.4931 | 7.2361 |
| *FWHM* | 0.030 | 0.029 | 0.027 |
| % voxel accepted | 83% | 90 % | 91 % |

**Figure 2.** A) Metabolite map coverage of the Ins for denoised (via MP-PCA and LR-TGV) and non-denoised (RAW) MRSI dataset. The blue table displays the average SNR, the average FWHM and the percentage of voxel accepted. B) Relative concentration of Ins quantified in the hippocampus, cortex and striatum for denoised and non-denoised datasets.

increased coverage of the metabolic maps while still preserving brain regional differences, particularly for spectra located at the edges of the brain (Fig 2A). No significant changes on the resulting concentrations of Ins per individual region were observed when applying either of the denoising techniques (Fig 2B, left), while its regional distribution was not affected[12] (Fig 2B, right). Moreover, both denoising approaches reduced the standard deviation of the estimated Ins concentration (Fig 2B).

We implemented, validated and showed the potential of two noise-reduction techniques on preclinical 14.1T ^{1}H-FID-MRSI datasets. The results show that these two techniques can increase the coverage while preserving relative concentration distribution, which offers enormous potential towards novel and fast MRSI developments. Further studies will be performed to further quantitatively assess the performance of both denoising techniques and their impact on low concentrated metabolites using Monte Carlo simulations and in vivo acquired 14.1T ^{1}H-FID-MRSI data.

**References:** 1.Abdoli, Magn Reson Mater Physics, Biol Med, 2016, 2.Nguyen, IEEE Trans Biomed Eng 2013, 3.Clarke, Magn Reson Med, 2021, 4.Klauser, Magn Reson Med, 2019, 5.Simicic, ISMRM, 2021 6.Veraart, Neuroimage, 2016, 7.Ades-Aron, Radiology, 2021, 8.Diao, Front Neurosci, 2021, 9.Jelescu, ISMRM, 2020, 10.Alves, ISMRM, 2022, 11.Bilgic, Magn Reson Med, 2013, 12.Tkac, Magn Reson Med, 2004

**MRS Workshop 2022**
Overcoming the Barriers to Clinical Use
DISCONNECT 2 RECONNECT
IT'S TIME
22-24 August 2022 @ EPFL, Lausanne, Switzerland

23

S3A4

## Downfield proton MRSI in the human brain with extended spatial coverage

İpek Özdemir Ph.D.[1], Sandeep Ganji Ph.D.[2], Joseph Gillen B.S.[1,3],
Michal Považan Ph.D.[4], and Peter B. Barker, D.Phil. [1,3]

[1]Department of Radiology, JHU SOM, Baltimore, MD, [2]Philips Healthcare, Best, The Netherlands, [3]Kennedy Krieger Institute, Baltimore, MD, [4]Danish Research Center for MR, Copenhagen, Denmark

**Background**

In proton MRS of the human brain, signals occur both upfield and downfield from the water resonance. Most studies to date have focused on the large upfield resonances, but there have also been some studies of the downfield peaks, usually using single voxel spatial localization. Recently, a single slice, 2D MRSI study of the downfield resonances in normal human brain was published at a nominal spatial resolution of 1.5 cm$^3$ (1).
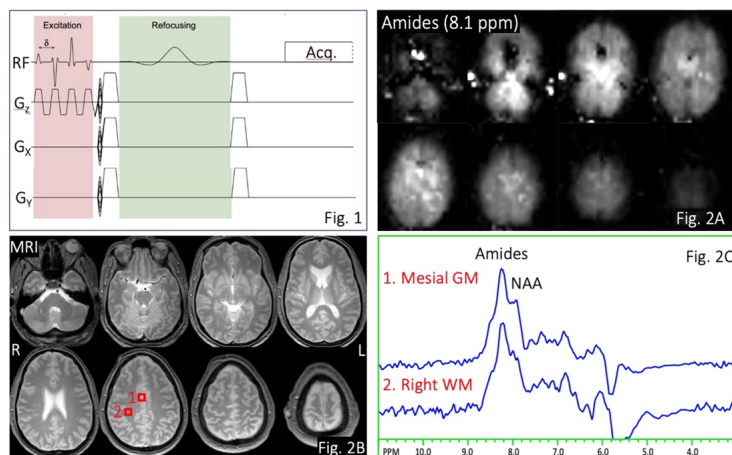
**Objective**

The objective of the current study was to develop a 3D downfield MRSI protocol with near full brain coverage and high spatial resolution at 3T.

**Methods**

Testing was performed in a normal human volunteer (M, 57 yr.) using a Philips 3T Elition scanner equipped with a 32-channel receive head coil. A 3D, circularly phase-encoded version of the previously developed 2D MRSI sequence (1) with $1\bar{3}3\bar{1}$ spectral-spatial excitation and frequency selective refocusing was implemented (Fig. 1). Scan parameters were TR/TE 287/22 ms, flip angle 78˚, FOV 200x180x120 mm, matrix size 29x26x8, nominal voxel size 7x7x15 mm ≈ 0.7 cm$^3$, 100mm slab excitation, 1 NEX, scan time 22m 40s. The $1\bar{3}3\bar{1}$ pulse delay (δ) was set to give maximum excitation at 7.4 ppm, and frequency-selective refocusing was achieved using a sinc-Gauss 180˚ pulse applied at 7.8 ppm (11ms, 400 Hz BW). An inferior saturation pulse was also applied. Data were post-processed using the LCModel, and images of the 8.1ppm amide proton resonance created by linear combination fitting.

**Results**

Fig. 2A shows images of the 8.1 ppm amide resonance from all 8 slices, as well as corresponding localizer MR images (Fig. 2B). Also shown are representative spectra (Fig. 2C) and corresponding voxel locations from 2 regions of interest illustrated in Fig. 2B.



Fig. 1



Amides (8.1 ppm)

Fig. 2A



MRI
R L
Fig. 2B



Amides
Fig. 2C
1. Mesial GM
NAA
2. Right WM

**Conclusions**

Downfield MRSI with 3D coverage is achievable at 3T in a clinically feasible scan time. Compared to upfield MRSI, some of the technical advantages include the ability to use short TR (due to the 'relaxation enhancement' effect), no need for additional water or lipid suppression, and also slightly less sensitivity to field inhomogeneity, since the downfield resonances have broader intrinsic linewidths compared to upfield. Scan time reductions should be possible in the future using fast MRSI techniques, such as EPSI readouts or parallel imaging. Downfield MRSI may give specific metabolic information on slowly exchanging molecules that is complementary to that observed using CEST MRI, which is more sensitive for intermediate exchange rates.

**References**

1. Povazan M, Schar M, Gillen J, Barker PB. Magnetic resonance spectroscopic imaging of downfield proton resonances in the human brain at 3 T. Magn Reson Med 2022;87(4):1661-1672.

MRS Workshop 2022
Overcoming the Barriers to Clinical Use
DISCONNECT 2 RECONNECT
22-24 August 2022 @ EPFL, Lausanne, Switzerland

24

S4A1

## Investigating Glutamate T2 relaxation time

*Polina Emeliyanova[1,2], Amy Stephen[1], Laura M. Parkes[1,2], Stephen R. Williams[3] and Caroline Lea-Carnall[1,2]*
*[1]Division of Neuroscience and Experimental Psychology, Faculty of Biology, Medicine and Health, The University of Manchester, Manchester, UK;*
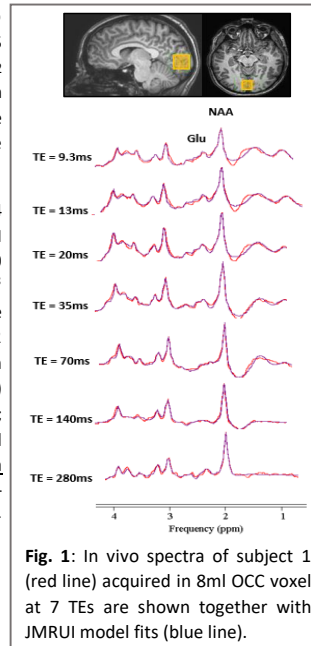*[2]Geoffrey Jefferson Brain Research Centre, Manchester Academic Health Science Centre, Manchester, UK; [3]Division of Informatics, Imaging and Data Science, University of Manchester, Manchester, UK*

**Introduction:** In-vitro studies have indicated that glutamate (Glu) bound to macromolecular structures within the vesicles may be invisible to ^{1}H-MRS due to very short T2 relaxation times[1–3]. Most studies reporting Glu T2 values only sample echo times (TE) within the range of $30 – 450$ ms[4,5] which is not adequate to observe a pool with ultra-short T2 ($< 20$ ms). Here, we acquire Glu at a range of TE values between 9.3 ms and 280 ms to examine whether there is a short-echo pool of Glu in vivo.
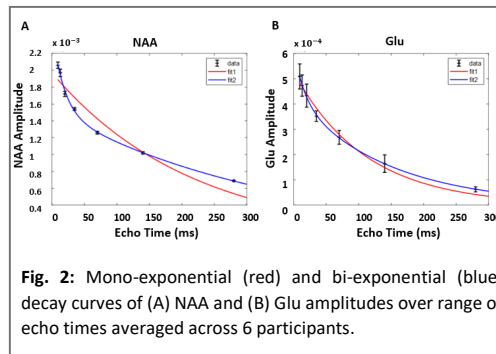
**Methods -** <u>MRS acquisition</u>:^{1}H-MRS data of 6 healthy volunteers (2 male; 4 female) were acquired on 3T Achieva Philips MR system, using SV STEAM (TR = 2 s, TM = 16 ms, NSA = 4) with 7 TEs (TE = 9.3, 13, 20, 35, 70, 140, 280 ms). The order of TEs was randomised for each participant. A $2 \times 2 \times 2$ cm$^3$ voxel was positioned in the occipital cortex (OCC), centred along the midline (Fig. 1). <u>Experimental design</u> consisted of 7 blocks (1 block = 512 seconds) with 4 trials of interleaved rest (black screen with white fixation dot) and visual stimulation (flashing checkerboard 8 Hz flicker, 4 cycles) each lasting 64 seconds. The fixation dot was present at all times; participants were required to press a button when it randomly changed colour to red (~10 times per block). Visual stimulation data not shown. <u>Data processing</u>: Metabolite signals were fitted and quantified using time-domain JMRUI QuasarY algorithm, and NMR-Scope-B to generate TE-appropriate basis functions for the analysis.

**Results** The signal was adjusted for T1 effects[4] and then we fit the T2 relaxation curve for Glu and NAA with mono- exponential and bi-exponential fits across 7 data points using the MATLAB function "fitnlm". The best fit was assessed using Akaike information criterion (AIC). We



**Fig. 1**: In vivo spectra of subject 1 (red line) acquired in 8ml OCC voxel at 7 TEs are shown together with JMRUI model fits (blue line).

found evidence of bi-exponential decay for both metabolites (Fig. 2). Fit parameters indicate the existence of 2 pools that contribute to the total signal as follows: Glu short- T2 pool (T2 = 17 ms) contributes 33% of the signal, long T2-pool (T2 = 187 ms) contributes 67% of the signal. NAA short- T2 pool (T2 = 17 ms) contributes 39% of the signal, long T2-pool (T2 = 350 ms) contributes 61% of the signal.

**Discussion and conclusions** These results provide preliminary evidence of bi-exponential decay of Glu and NAA in visual cortex at 3T indicating an echo-time dependence of the MRS-Glu signal. Our findings for the long- T2 Glu pool (187 ms) are in agreement with empirical literature using mono-exponential fit and a minimum TE $\geq 30$ ms (e.g. 181 ms)[6]. The results for NAA are less clear. Acetyl and Aspartyl moieties of NAA were fitted together as well as Glu protons of methine and methylene groups. Future analysis will incorporate fitting of each resonance component independently to examine resonance specific T2 relaxation times for both metabolites.



**Fig. 2:** Mono-exponential (red) and bi-exponential (blue) decay curves of (A) NAA and (B) Glu amplitudes over range of echo times averaged across 6 participants.

**References 1**. Lea-Carnall CA, et al. (2021). Bioarxiv doi: 10.1101/2021.03.11.434540. **2.** Kauppinen R & Williams S (1991) J Neurochem 57(4):1136-1144. **3.** Kauppinen R, et al. (1994) Biochem J 298((Pt1)):121-127. **4.** Träber F, et al. (2004) J Magn Reson Imaging 19(5):537-545. doi:10.1002/JMRI.20053. **5.** Wyss PO, et al. (2018) Magn Reson Med. 80(2):452-461. doi:10.1002/MRM.27067. **6.** Ganji SK et al. (2012) NMR Biomed. 25(4):523-529. doi:10.1002/NBM.1767

**MRS Workshop 2022**
Overcoming the Barriers to Clinical Use
DISCONNECT 2 RECONNECT
22-24 August 2022 @ EPFL, Lausanne, Switzerland

25

S4A2

## Uncertainty Propagation in Absolute Metabolite Quantification for *In Vivo* Magnetic Resonance Spectroscopy of the Human Brain

Ronald Instrella[1] and Christoph Juchem[1,2]
*[1]Department of Biomedical Engineering, Columbia University, New York, NY, USA. [2]Department of Radiology, Columbia University College of Physicians and Surgeons, New York, NY, USA.*

**Purpose**. Absolute spectral quantification in proton magnetic resonance spectroscopy (^{1}H-MRS) is the standard method for deriving concentration estimates of metabolite signals in absolute units, such as molar concentration. Derived concentrations are often reported with minimum variance estimators, specifically the Cramér-Rao Lower Bound (CRLB),[1] which serves as a proxy for the standard deviation. However, characterizing the precision of absolute quantification relies on more than simply the CRLB of the metabolite's signal amplitude from MR signal models. The uncertainty of metabolite-specific ($T_{1m}$, $T_{2m}$), water reference-specific ($T_{1w}$, $T_{2w}$) and sequence-specific ($TR$, $TE$) parameters are generally ignored, potentially leading to an overestimation of the reported concentration's precision. In this study, we present an analysis using the *law of propagation of uncertainty* to examine this additive effect, and calculate a more comprehensive estimate of the overall precision from concentrations derived using an internal water reference.

**Methods**. The absolute concentration of metabolite $m$ is estimated using a tissue-specific internal water reference (eq. 1),[2] where $A_m$ is the relative scaling factor of a metabolite basis function, $S_w$ is the internal water signal amplitude, $c_{w,i}$ and $f_i$ are the absolute water concentration and fractional estimates of grey matter, white matter and CSF, respectively. $T_{1w,i}$, $T_{2w,i}$ are the tissue-specific relaxation rates of the water reference, $T_{1m}$, $T_{2m}$ are the metabolite relaxation rates, $D(TR, T1_m)$ and $D(TR, T1_{w,i})$ are correction factors for partial longitudinal relaxation, and $TE$, $TR$ are the echo time and repetition time, respectively.

$$(1) \quad C_m = \frac{A_m e^{\frac{TE}{T2_m}} D_m(TR, T1_m)}{S_w(1 - f_{csf})} * \sum_{i=1}^{3} \frac{f_i D_{w,i}(TR, T1_{w,i}) c_{w,i}}{e^{\frac{TE}{T2_{wi}}}}$$

$$(2) \quad \delta C_m(\mathbf{x}) = \sqrt{\sum_{i=1}^{n}\left(\frac{\partial C_m}{\partial x_i}\delta x_i\right)^2 + 2\sum_{i=1}^{n-1}\sum_{j=i+1}^{n}\frac{\partial C_m}{\partial x_i}\frac{\partial C_m}{\partial x_j}\sigma_{x_i,x_j}}, i \neq j$$
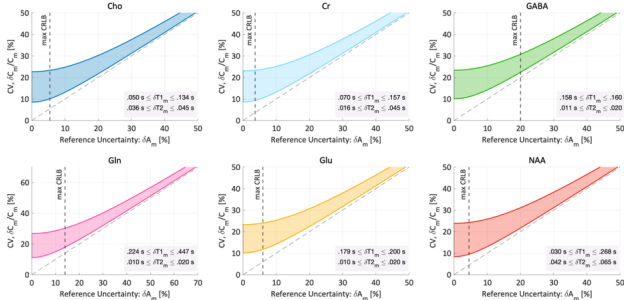


**Figure 1**. Propagated uncertainty boundary curves by metabolite

The overall uncertainty of a functionally-derived measurement outcome $C_m(\mathbf{x})$ for $n$ dependent parameters in $\mathbf{x}$ is calculated using a generalized equation of the propagation of uncertainty (eq. 2),[3] where $\delta x_i$ is the standard deviation of quantification parameter $x_i$ and $\sigma_{x_i,x_j}$ is the covariance between $x_i$, $x_j$. This is applied for the parameter uncertainties in eq. 1 and typical CRLBs for *in vivo* MRS of the brain from literature. The uncertainty is also estimated using Monte Carlo methods, where normally distributed random variable $X \sim N(\mu_{x_i}, \sigma_{x_i})$ is used to produce simulated concentrations, with $\mu_{x_i}$ and $\sigma_{x_i}$ set to the parameter constant and uncertainty extrema, respectively. The propagated uncertainty is reported for 6 example metabolites: Cho, Cr, GABA, Gln, Glu and NAA.

**Results**. Boundary curves for the metabolite-specific propagated uncertainty are expressed using the coefficient of variation (CV) of $C_m$, and are compared to the CRLB alone (Fig 1). The CRLB ($\delta A_m$) is plotted as a linear term, with a shaded region denoting the space of possible uncertainties bounded by the two higher order terms. The CV at the highest reported reference uncertainty is as high as 30% for Gln, and increases as much as 14% between uncertainty extrema for Cr and NAA. Simulated metabolite concentrations using reported parameter uncertainty extrema are consistent with analytically derived CVs (Fig 2). Metabolite signals that are more easily quantifiable, such as NAA and Cho, show narrower distributions, while those that are less distinguishable at low SNR (e.g. Gln, GABA) show wider distributions.



**Figure 2**. Monte Carlo validation of the propagated uncertainty by metabolite

**Discussion**. The range of possible precision estimates demonstrates the need to carefully consider whether potential error sources in quantification are negligible. Potential factors, including the effect of various parameter covariances, the use of other internal or external signal references, other signal model variable CRLBs, systematic errors from limited sequence performance, erroneous timing events, and miscellaneous hardware failures are not yet considered.

**Conclusion**. The precision of metabolite quantification is shown to be systematically overestimated if measurement uncertainty of various absolute quantification-dependent correction factors are ignored. Since these uncertainties are added in quadrature, the total hypothetical uncertainty increases monotonically with each error source by varying degrees across metabolites. The results of this study should motivate investigators to consider more comprehensive reporting of potential sources of error in *in vivo* MRS experiments.

**References.** [1] Cavassila S, et al. NMR Biomed. 2001;14(4). doi:10.1002/nbm.701. [2] Landheer K, et al. NMR Biomed. 2020;33(9). doi:10.1002/nbm.4324. [3] Taylor BN, et al. Guidelines for Evaluating and Expressing the Uncertainty of NIST Measurement Results. Vol 1297. National Institute of Standards and Technology (NIST); 1994.

# MRS Workshop 2022
## Overcoming the Barriers to Clinical Use
### DISCONNECT 2 RECONNECT
22-24 August 2022 @ EPFL, Lausanne, Switzerland

26

S5A1

## α-ATP suppression in $^{31}$P MR spectroscopy by homonuclear BIRD editing:
## An approach to quantify NADH and NAD$^+$ at 3T in vivo in skeletal muscle

**Authors:** *J. Mevenkamp[1,2], Y.M.H. Bruls[1,2], L. Grevendonk[2], J.E. Wildberger[1], M.K.C Hesselink[2], P. Schrauwen[2], J. Hoeks[2], M. Buitinga[1,2], R.A. de Graaf[3], L. Lindeboom[1,2], V.B. Schrauwen-Hinderling[1,2]*

**Affiliations:**  *[1] Maastricht University Medical Center+, Department of Radiology & Nuclear Medicine*
*[2] Maastricht University, Department of Nutrition & Movement Sciences, Maastricht*
*[3] Yale School of Medicine, Department of Radiology & Biomedical Imaging*

**Introduction & Background:** NAD$^+$ and NADH play important roles in metabolism and metabolic health [Stein & Imai et al 2012]. However, non-invasive quantification of NAD$^+$/H in $^{31}$P-MRS at clinical field strength is challenging as there is strong overlap of α-ATP and NAD$^+$/H resonances. Hence, we developed a MRS sequence to suppress α-ATP resonances based on homonuclear Bilinear Rotation Decoupling (BIRD) [Garbow et al. 1982], uncovering NAD$^+$/H resonances.

**Methods:** We confirmed the α-ATP suppression capability of our novel homonuclear BIRD (HB) editing sequence, depicted in figure 1, in phantoms. Furthermore, we tested whether acute physiological changes in NAD$^+$/H concentrations can be detected by HB editing. Therefore, we acquired HB edited spectra from calf muscles of eight healthy, young and lean volunteers during normal perfusion and ischemia, which is known to increase NADH at the cost of NAD$^+$ [Sahlin et al. 1983]. Values are reported in arbitrary units (.A.U.). Moreover, we measured NAD$^+$/H concentrations in two groups of an older adult population (Age 65 - 80), differing strongly in physical activity and fitness. Spectra in these two groups were acquired during rest, whereby NAD$^+$ concentrations in the highly active group were expected to be elevated [de Guia et al. 2019]. Values are reported as ratios relative to γ-ATP.

**Results:** Phantom tests showed an effective α-ATP suppression of 85% with signal loss of 22.9% for NAD$^+$/H between FID and HB editing, see figure 2. HB edited spectra during rest and ischemia showed that NADH rose significantly by 19.5% (0.41±0.03 vs. 0.5±0.02 A.U., p = 0.047), whereas NAD$^+$ concentrations dropped significantly by 22.9% (1.14±0.04 vs. 0.88±0.07 A.U., p = 0.001), leading to an average decrease of 35.2% in NAD$^+$/NADH ratios (2.81±0.18 vs. 1.82±0.19, p = 0.004). Cross-sectional comparisons of older adults varying in physical fitness showed a significant difference in NAD$^+$ (5.38±0.35 vs. 3.94±0.31, p = 0.005) and total NAD metabolite pool (6.47±0.24 vs. 5.45±0.26, p = 0.012) with higher concentrations in the active individuals. NAD$^+$/NADH ratios were also significantly higher in trained older adults (6.64±1.46 vs. 3.03±0.51, p = 0.023). However, no significant differences in NADH concentrations were detected (1.09±0.25 vs. 1.5±0.24, p = 0.265).

**Conclusion & Discussion:** We successfully suppressed the α-ATP resonance and measured acute changes in NADH and NAD$^+$ concentrations at 3T using a novel $^{31}$P-MRS HB editing in vivo in skeletal muscle. Moreover, differences between groups of older adults with different physical activity levels were also detectable with the help of HB editing. However, as α-ATP suppression successfully uncovers NAD-metabolites, a clear separation of NADH and NAD$^+$ resonances remains challenging due to incomplete resolution of these resonances at 3T. The two metabolite resonances could only be separated analytically by using a robust fitting model.
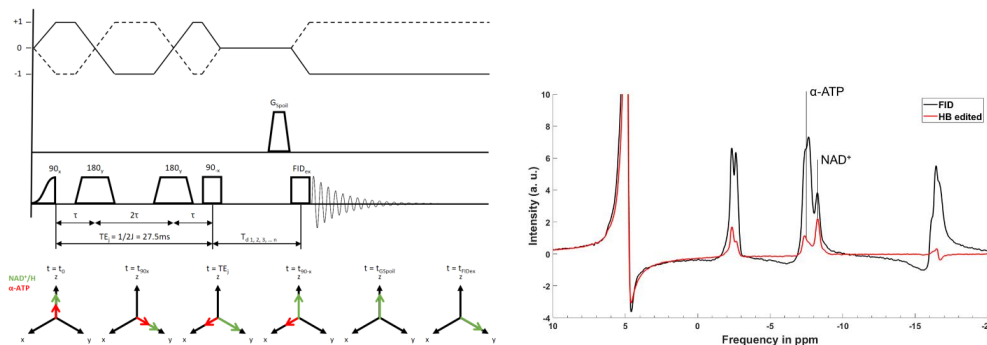


*Figure 1: Scheme of homonuclear BIRD (HB) editing. After an adiabatic double echo with $TE_J = 1/2J$, J-coupled α-ATP spins end up aligned with x. The following 90º hard pulse flips spins about the x-axis back towards the z-axis. Spins remaining in the x-y plane are then dephased by $G_{Spoil}$. A varying delay reduces potential effects of zero quantum coherences (ZQC)*



*Figure 2: Comparison of spectra resulting from FID and HB edited acquisition in a phantom composed of ATP and NAD$^+$. α-ATP suppression of 85% with an approximate signal loss of 22.9%, determined on NAD$^+$ was achieved*

# MRS Workshop 2022
## Overcoming the Barriers to Clinical Use
### DISCONNECT 2 RECONNECT
22-24 August 2022 @ EPFL, Lausanne, Switzerland

27

S5A2

**Association of insulin resistance with the accumulation of saturated IMCL, compared with other fat stores**

Mueed Azhar[1*], Laura Watson[2*], Ema De-Lucia Rolfe[3], Katie Carr[2], Jieniean Worsley[2], Leanne Hodson[4], Chris Boesch[5], Krishna K Chatterjee[2,3], Graham J. Kemp[6], David Savage[3], Alison Sleigh[1,2,3]

[1] Department of Clinical Neurosciences, [2] NIHR Cambridge Clinical Research Facility, [3] WT-MRC Institute of Metabolic Science, University of Cambridge, Cambridge Biomedical Campus, UK , [4] OCDEM, University of Oxford, Oxford, [5] AMSM, University Bern, Switzerland [6] Department of Musculoskeletal & Ageing Science, University of Liverpool, Liverpool, UK.

**Introduction**
A recently validated [1] marker of the saturation of intramyocellular lipid (IMCL) is more closely associated with whole-body measures of insulin resistance than IMCL concentration independent of composition [2,3]. Here we investigate whether this marker's association with insulin resistance is stronger than previously-reported associations with other ectopic and adipose tissue stores, and whether it remains a significant predictor when these are taken into account.

**Methods**
38 healthy females (F) and 27 age- and BMI- matched males (M) had MR scanning on a Siemens 3T Verio/Skyrafit, DXA for fat mass, and fasting blood samples for HOMA-IR. $^1$H MRS  was used to assess soleus (SOL) and tibialis anterior (TA) IMCL and intrahepatic lipid (IHL), and MRI for calf intramuscular fat (IMF) and subcutaneous adipose tissue ($SCAT_{calf}$), and abdominal visceral and subcutaneous adipose tissue (VAT, $SCAT_{adb}$). Acquisition/analysis methods are as in [1-3] other than a single slice for MRI. IMCL saturation index adjusted for quantity, a marker of the accumulation of saturated IMCL [2,3], was calculated as ($CH_2:CH_{3adj}$) = $CH_2 – (mCH_3 +c)$, where m and c are the regression slope and intercept of $CH_2$ vs $CH_3$ for the female individuals [2]. Statistics were performed in IBM SPSS v 28. Non-normal measures were log-transformed prior to Pearson correlation or regression analysis. Benjamini-Hochberg adjusted P values were used to correct for multiple comparisons within the Table.

**Results**
The mean±SEM age, BMI, and whole-body insulin resistance (HOMA-IR) were 36.4±2.1 y, 24.3±0.6 kg/m$^2$, 1.14±0.13 respectively in females, and 34.2±2.3 y, 24.9±0.6 kg/m$^2$, 1.10±0.17 respectively in males.

*Pearson correlation coefficients with HOMA-IR*

| | F (n=38) | M (n=27) | F+M (n=65) |
|---|---|---|---|
| *IMCL Concentration* | | | |
| SOL $CH_3$ | 0.080 | 0.054 | 0.057 |
| TA $CH_3$ | 0.275 | 0.387 ‡ | 0.315 * |
| *IMCL Composition* | | | |
| SOL $CH_2:CH_{3adj}$ | 0.342 ‡ | 0.429 * | 0.358 * |
| TA $CH_2:CH_{3adj}$ | 0.260 | 0.447 * | 0.306 * |
| *Others* | | | |
| IHL | 0.429 * | 0.539 * | 0.457 * |
| IMF | 0.216 | 0.118 | 0.155 |
| $SCAT_{calf}$ | 0.355 ‡ | 0.431 * | 0.362 * |
| VAT | 0.517 * | 0.292 | 0.367 * |
| $SCAT_{abd}$ | 0.210 | 0.329 | 0.293 * |
| DXA total fat mass | 0.403 * | 0.463 * | 0.394 * |

*Adjusted P values:  ‡ p<0.10, * p<0.05*



*HOMA-IR vs (A) SOL $CH_2CH_{3adj}$ and (B) IHL*
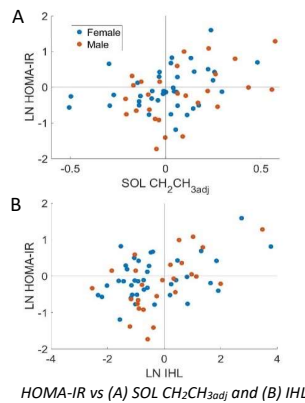
Starting with the measure that has the strongest association and performing stepwise linear regression, the only significant predictors of HOMA-IR were VAT in females (R=0.517, p<0.001), IHL in males (R=0.539, p=0.004), and IHL and fat mass in females and males combined (R=0.513, IHL p=0.010, fat mass p=0.039).

**Discussion/Conclusion**
As well as the accumulation of saturated IMCL, several other markers were, as previously reported [4], significantly associated with whole-body insulin resistance, namely visceral adipose tissue, intrahepatic lipid, calf subcutaneous adipose tissue, total fat mass and abdominal subcutaneous adipose tissue (M and F combined). Disentangling these relationships by stepwise regression did not reveal the accumulation of saturated IMCL to be a significant predictor of whole-body insulin resistance, which implies this measure carries no more information in practice than the predictors we found, such as intrahepatic lipid. However, the performance of any marker depends on factors such as measurement precision and accuracy, biological variation and dynamic range in addition to the underlying biology; and as the dynamic range and precision of the predictors is much greater than that of the saturated IMCL marker, this negative finding does not rule out a role for saturated IMCL accumulation in the pathogenesis of insulin resistance.

**References**
[1] Thankamony *et al*., 2018, Sci. Rep, **8**, 2750.
[2] Savage *et al*., 2019, J. Lipid Res., **60(7)**, 1323.
[3] Watson *et al*., 2020, Proc. ISMRM virtual conference, 2554.
[4] Kirchhoff *et al*., 2007, J. Diab Sci Technol, **1(5)**, 573

* Joint first authors

**MRS Workshop 2022**
Overcoming the Barriers to Clinical Use
DISCONNECT 2 RECONNECT
22-24 August 2022 @ EPFL, Lausanne, Switzerland

28

S8A1

# Accurate prediction of IDH-mutation status of gliomas using SLOW-editing MRSI at 7 Tesla MR

Guodong Weng[1,2], Johannes Slotboom[1,2], Piotr Radojewski[1,2]

[1]Institute for Diagnostic and Interventional Neuroradiology, Support Center for Advanced Neuroimaging (SCAN), University of Bern, Bern, Switzerland. [2]Translational Imaging Center, sitem-insel, Bern, Switzerland.

## Introduction

2-Hydroxy-glutarate (2HG) is a metabolite that accumulates in IDH-mutated gliomas and can be detected non-invasively using MR-spectroscopy. However, due to the low concentration of 2HG, established magnetic resonance spectroscopic imaging (MRSI) techniques at low-field have limitations with respect to signal-to-noise and to spatial resolution that can be obtained within clinically acceptable measurement-times. Recently a tailored editing-method for 2HG detection at 7T named SLOW-EPSI was developed. The underlying prospective study aimed to compare SLOW-EPSI to established techniques at 7T and 3T for IDH-mutation status determination.

## Methods

The applied sequences were MEGA-SVS and MEGA-CSI at both field strengths and SLOW-EPSI at 7T only. Measurements were performed on a MAGNETOM-Terra 7T MR-scanner in clinical-mode using a Nova 1Tx32Rx head-coil and on a 3T MAGNETOM-Prisma scanner with a standard 32-channel head-coil.

## Results

Fourteen patients with suspected glioma were enrolled. Histopathological confirmation was available in 12 patients. IDH-mutation was confirmed in 9 out of 12 cases and 3 cases were characterized as IDH-wildtype. SLOW-EPSI at 7T showed highest accuracy for IDH-status prediction (91.7% accuracy, 11 of 12 predictions correct with 1 false negative case). At 7T, MEGA-CSI had an accuracy of 58.3% and MEGA-SVS an accuracy of 75%. At 3T, MEGA-CSI showed an accuracy of 63.6% and MEGA-SVS of 33.3%. In addition, the co-edited cystathionine was detected in 2 out of 3 patients with oligodendrogliomas.

## Conclusion

Depending on the pulse sequence, spectral editing can be a powerful tool for noninvasive determination of the IDH-status. SLOW-editing EPSI sequence is the preferable pulse sequence when used at 7T for IDH-status characterization.
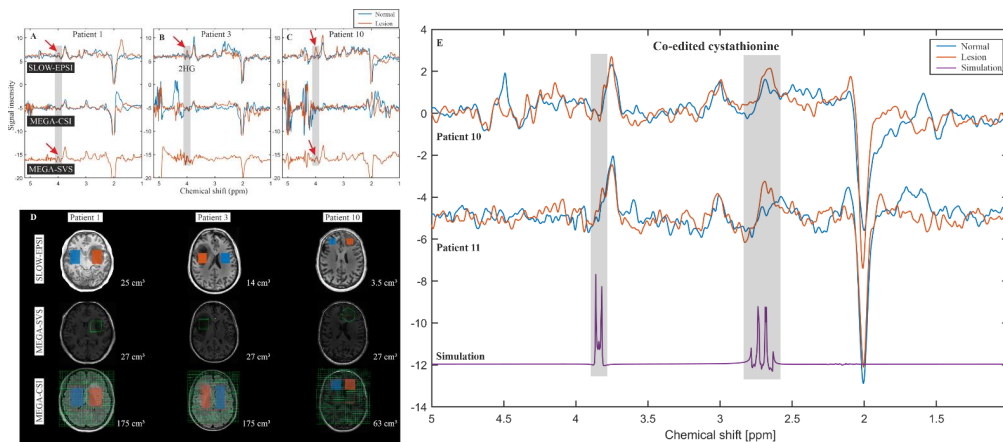


**Figure: A-C)** The in vivo spectral editing difference (editing-partial minus editing-full for SLOW-editing, editing-on minus editing-off for MEGA-editing) within lesion/tumor (orange line) and mirror-symmetric normal tissue (blue line). The red arrows indicate the 2HG-signals. **D)** The MRI and corresponding MRSI/MRS VOI of three patients. The displaced volumes are indicated as orange (lesion) and blue (normal tissue) rectangular for SLOW-EPSI and MEGA-CSI. The size of the displaced volume is as indicated. **E)** The cystathionine peaks are shown (orange) at 2.7 and 3.85 ppm in patient #10 and 11, respectively.

**MRS Workshop 2022**
Overcoming the Barriers to Clinical Use
DISCONNECT 2 RECONNECT
22-24 August 2022 @ EPFL, Lausanne, Switzerland

29

S8A2

**Probing diffusion of water and metabolites to assess white matter microstructure in Duchenne muscular dystrophy**

R. Govaarts[1], N. Doorenweerd[1,2,3], E.M. Broek[1], M.E. Tamsma[1], I. Ronen[1], C. Najac[1], K.G. Hollingsworth[2], E.H. Niks[1], V. Straub[2,3], H.E. Kan[1]
[1]Leiden University Medical Center, Netherlands, [2]Newcastle University, United Kingdom, [3]Newcastle Hospitals NHS Foundation Trust, United Kingdom

Duchenne muscular dystrophy (DMD) is a progressive X-linked neuromuscular disorder caused by the absence of functional dystrophin protein. In additional to muscle, dystrophin is expressed in the brain in both neurons and glial cells. Approximately 30% of DMD patients experience behavioural and cognitive deficits[1,2]. Previously, altered white matter microstructure has been shown with diffusion tensor imaging (DTI)[3-5]. In this study, we investigate if this altered white matter microstructure is due to intra- or extracellular microstructural changes, using $^1$H diffusion-weighted spectroscopy (DWS) and DTI.

Scans were obtained at 3 Tesla (Philips Achieva) using an 8-channel head coil. 3DT$_1$-weighted scans were obtained for anatomical reference (TE/TR 4.6/9.8 ms; spatial resolution 1.17x0.92x1.17 mm). DTI scans were obtained to determine the diffusion of water (TE/TR 59/9440ms; spatial resolution 1.96x2x2 mm; 32 directions, $b$=0 and $b$=1000 s/mm$^2$). DWS data were acquired with and without water suppression using a cardiac triggered PRESS sequence to determine diffusion and concentration of metabolites (TE=125 ms, TR=2 cardiac cycles; 24 signal averages; $b$=0 and $b$=3765 mm/s$^2$; three diffusion directions; non-water suppressed two signal averages, 24s). A volume of interest (VOI; 30x20x15 mm) was positioned in the left parietal white matter (Fig. A). DWS spectra (Fig. B) were analyzed using an in-house Matlab routine, including corrections for individual frequency and phase drifts and eddy currents, and subsequently fitted using LCModel[6]. Apparent diffusion coefficients (ADC) were calculated for total N-acetyl aspartate (tNAA), choline compounds (tCho), and total creatine (tCr). Volume fractions of cerebrospinal fluid, white matter and grey matter within the VOI were determined using an overlay of the VOI with tissue maps derived from FSL[7,8]. The ratios of tNAA/tCr and tCho/tCr were calculated from the fitted non-diffusion weighted spectrum. DTI scans were co-registered with T$_1$ and DWS using ExploreDTI[9] to obtain mean diffusivity (MD), radial diffusivity (RD), and axial diffusivity (AD) of water within the VOI.

DWS and DTI data from 18 DMD patients (mean age 15.5 ± sd 4.6 years) and 10 age-matched healthy controls (HCs; mean age 16.3 ± sd 3.3 years) were included. No differences in metabolite diffusion (tNAA (Fig. C), tCho and tCr) and metabolite levels (tNAA/tCr and tCho/tCr ratios) were found between DMD patients and HCs. Water diffusion (MD (Fig. D), RD and AD) within the VOI was significantly higher in DMD patients compared to HCs.

The mean ADC of all three metabolites (tNAA, tCr, and tCho) and their ratios were comparable between DMD patients and HCs. In the same VOI, DMD patients did show increased water diffusivity. This suggests that altered white matter microstructure is likely due to extracellular, rather than intracellular, changes.

*[1] Banihani et al. (2015). DOI: 10.1177/0883073815570154. [2] Doorenweerd et al. (2020). DOI: 10.1016/j.nmd.2020.05.001. [3] Doorenweerd et al. (2014). DOI: 10.1002/ana.24222. [4] Preethish-Kumar et al. (2020). DOI: 10.3174/ajnr.A6604. [5] Fu et al. (2016). DOI: 10.21037/atm.2016.03.19. [6] Provencher (1993). DOI: 10.1002/mrm.1910300604. [7] Zhang et al. (2001). DOI: 10.1109/42.906424. [8] Smith (2002). DOI: 10.1002/hbm.10062 [9] Leemans et al. (2009). www.exploredti.com.*
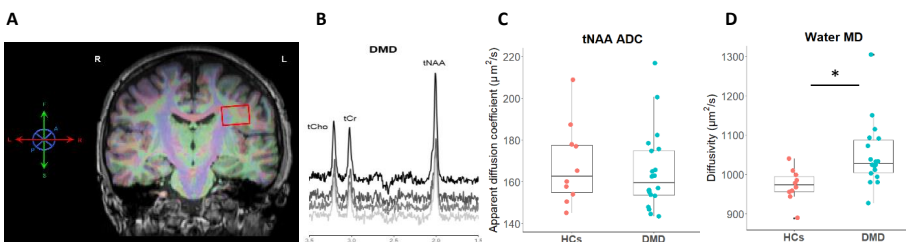
**Figure A)** Merged T1, DTI colour-coded FA map, and VOI (red box). **B)** Representative spectrum of a DMD patient with the non-diffusion weighted signal in black and three directions in grey, showing the peak heights for tCho, tCr and tNAA. Boxplots overlaid with scatter of **C)** ADC of tNAA within the VOI for HCs and DMD (F(1,29) = .221, $p$ = .642) and **D)** water MD within the VOI for HCs and DMD (t = -2.727, $p$ = .011).

MRS Workshop 2022
Overcoming the Barriers to Clinical Use
DISCONNECT 2 RECONNECT
22-24 August 2022 @ EPFL, Lausanne, Switzerland

30

S9A1

**Non-invasive 3D mapping of downstream brain glucose metabolism using 1H MRSI with deuterium labeling at 3T**

Fabian Niess[1], Lukas Hingerl[1], Bernhard Strasser[1], Petr Bednarik[1], Dario Goranovic[1], Eva Niess[1], Gilbert Hangel[1,2], Martin Krssak[3], Benjamin Spurny-Dworak[4], Thomas Scherer[3], Rupert Lanzenberger[4], Siegfried Trattnig[1], Wolfgang Bogner[1]

[1] High Field MR Center, Department of Bioimaging and Image-Guided Therapy, Medical University of Vienna [2]Department of Neurosurgery, Medical University of Vienna [3]Division of Endocrinology and Metabolism, Department of Internal Medicine III, Medical University of Vienna [4]Department of Psychiatry and Psychotherapy, Medical University of Vienna

**Purpose** Impairment of glucose metabolism in the human brain has been linked to several pathologies e.g. cancer, Alzheimer's disease and diabetes. FDG-PET is the current gold standard in clinical routine for assessing whole-body glucose uptake, but it requires invasive administration of expensive and unstable radioactive tracers and lacks information on glucose downstream metabolites. Therefore, non-invasive, reliable and cheap mapping of brain glucose metabolism is of critical interest not only for clinical research but also clinical routine application. Recently, a novel approach to map glucose metabolism in the human brain has been presented on non-clinical MR scanners by detecting orally or intravenously administered deuterium ($^2$H) labeled glucose and downstream metabolites directly via $^2$H MRS[1] or indirectly via $^1$H MRS/MRSI[2,3]. This method could evolve to a non-invasive and cheap alternative to PET, which is in contrast to FDG-PET even capable of separating normal oxidative and pathologic glycolytic metabolism. Our methodology enables 3D mapping of human brain glucose metabolism for the first time on a clinical 3T MR scanner using $^1$H MRSI.
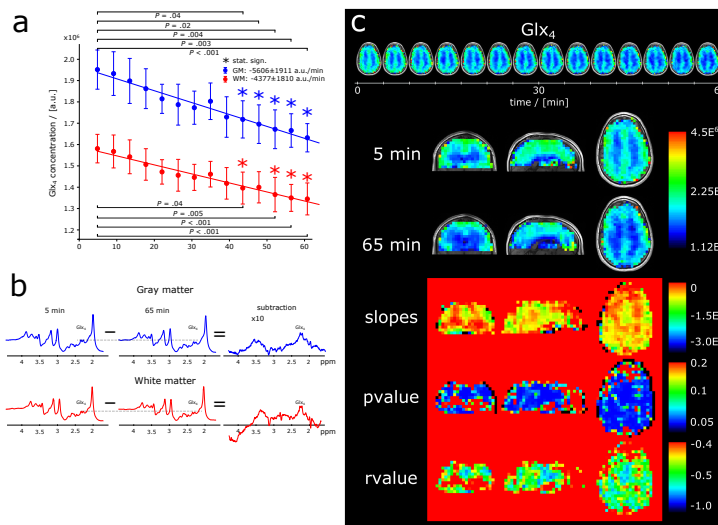
**Methods** Eight healthy participants (3f/5m) were scanned after overnight fasting and oral [6,6']-$^2$H glucose administration (0.8g per kg body weight) using a dynamic real-time motion, shim and frequency drift corrected 3D FID $^1$H-MRSI sequence with non-cartesian concentric ring trajectory readout[4]. Over the course of ~60 min 14 whole-brain metabolic maps of Glx (Glutamate+Glutamine), total Creatine (tCr), total N-acetylaspartate (tNAA) were acquired every ~5 min with ~0.24 ml isotropic resolution. Glx signal decay (proportional to the speed of Glu+Gln synthesis) was linearly fitted voxel-wise and over regional means (whole gray and white matter).

**Results** A statistically significant signal decrease of the $^2$H labeled resonance Glx$_4$ (p<0.001) over time was observed in both gray (17±4%) and white matter (16±5%). Slopes of the linear fits revealed a 28% faster decrease in GM compared to WM, representing faster metabolic activity, which is in good agreement with literature (Fig a). The decrease of the Glx$_4$ resonance is visually discernable in averaged spectra of GM and WM, in the subtraction spectra (first minus last time point see Fig b) and in the Glx$_4$ map time courses shown from one representative subject (Fig c). Voxel-wise linear fitting resulted in moderate to strong negative correlations of Glx$_4$ and time with p-values <0.05 over the majority of the brain. The resulting slopes revealed a visible contrast in metabolic activity between GM and WM. Other non-labeled metabolites (tCr and tNAA) showed no significant changes with a coefficient of variation < 3%.

**Conclusion** Our novel approach makes deuterium metabolic imaging, which is a safe, cheap, and versatile (also other substances than glucose can be labeled e.g., choline) alternative to PET, widely available on routine clinical MR scanners without specialized hardware, while adding information on downstream metabolism that exceeds the possibilities of PET.

**References**
[1] De Feyter et al. Science Adv. 2018 [2]Rich et al. Nature Biomed. Eng. 2020 [3]Cember et al. Neuroimage 2022 [4]Moser et al. MRM 2020

**MRS Workshop 2022**
Overcoming the Barriers to Clinical Use
DISCONNECT 2 RECONNECT
22-24 August 2022 @ EPFL, Lausanne, Switzerland

31

S9A2

## Comparing cerebral metabolism of hyperpolarized $^{13}$C-glucose and thermally polarized deuterated glucose under different anesthetic conditions

Emmanuelle I. Flatt[1], Bernard Lanz[1,2,3], Rolf Gruetter[1], and Mor Mishkovsky[1]

[1]Laboratory of Functional and Metabolic Imaging, École Polytechnique Fédérale de Lausanne (EPFL), Lausanne, Switzerland. [2]CIBM Center for Biomedical Imaging, Switzerland. [3]Animal Imaging and Technology (AIT), École Polytechnique Fédérale de Lausanne (EPFL), Lausanne, Switzerland
mor.mishkovsky@epfl.ch

Dissolution dynamic nuclear polarization (dDNP) of metabolites dramatically enhances MR sensitivity, allowing for monitoring of real-time intermediary metabolism[1,2]. This dramatic increase in sensitivity paves the way for a new class of metabolic neuroimaging [3,4]. Glucose is the primary fuel molecule for the brain. However, due to the short lifetime of its hyperpolarized carbons, it is the most challenging precursor for *in vivo* metabolic studies with dDNP. We have developed a unique protocol for detecting real-time lactate production through glycolysis shortly after injection of hyperpolarized ($^2$H$_7$,$^{13}$C$_6$)-D-glucose in naïve mouse brain[5]. We applied, for the first time, hyperpolarized glucose MRS to study brain tumor metabolism and found a reduction in aerobic glycolysis in a glioblastoma model representing the tumors' infiltrative zone, in opposition to what is expected by the "Warburg effect"[6].

Recently a renewed interest in deuterium MRS has emerged[7]. The potential of deuterium molecular imaging post intake of $^2$H-labelled glucose was shown to provide new perspectives for molecular imaging[8]. Hence, we investigated the difference between hyperpolarized glucose $^{13}$C MRS and thermally-polarized glucose $^2$H MRS to interrogate cerebral glycolysis. Brain metabolism of hyperpolarized $^{13}$C-glucose and thermally-polarized $^2$H-glucose was monitored in two groups of mice under different anesthetic conditions in a 9.4 T MRI system. We found that the very different duration and temporal resolution of the two techniques enable highlighting different aspects in glucose metabolism. We show that variations in cerebral glucose metabolism, under different anesthesia, are reflected differently in hyperpolarized and thermally polarized X-nuclei MRS of glucose[9].
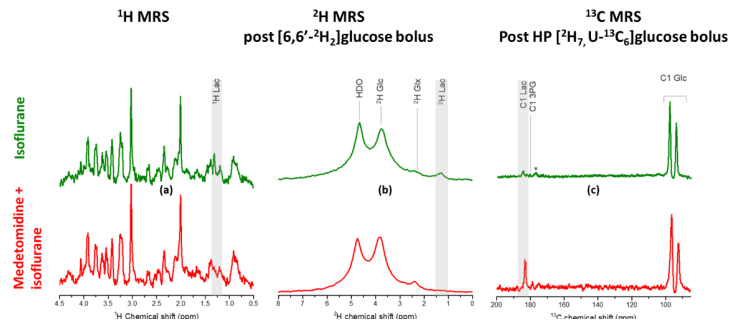


**Figure 1:** Typical summed spectra measured with $^1$H MRS (a,d), $^2$H MRS (b,e) and hyperpolarized $^{13}$C MRS (c,f) under isoflurane solely ('ISO', in green) and under medetomidine combined with isoflurane anesthesia ('MED–ISO', in red).

**References:**
1. Ardenkjær-Larsen, J. H. *et al. Proc. Natl. Acad. Sci.* **100**, 10158–10163 (2003).
2. Golman, K., Ardenkjaer-Larsen, J. H., Petersson, J. S., Månsson, S. & Leunbach, I. *Proc. Natl. Acad. Sci. U. S. A.* **100**, 10435–10439 (2003).
3. Mishkovsky, M. & Comment, A. *Anal. Biochem.* **529**, 270–277 (2017).
4. Le Page, L. M., Guglielmetti, C., Taglang, C. & Chaumeil, M. M. *Trends Neurosci.* **43**, 343–354 (2020).
5. Mishkovsky, M. *et al. Sci. Rep.* **7**, 11719 (2017).
6. Mishkovsky, M. *et al. Sci. Rep.* **11**, 5771 (2021).
7. Lu, M., Zhu, X.-H., Zhang, Y., Mateescu, G. & Chen, W. *J. Cereb. Blood Flow Metab.* **37**, 3518–3530 (2017).
8. Feyter, H. M. D. *et al. Sci. Adv.* **4**, eaat7314 (2018).
9. Flatt, E. *et al. Metabolites* **11**, 413 (2021).

# MRS Workshop 2022
## Overcoming the Barriers to Clinical Use
### DISCONNECT 2 RECONNECT
22-24 August 2022 @ EPFL, Lausanne, Switzerland

32

S9A3

## Retrospective under-sampled 3D Deuterium Metabolic Imaging (DMI) of the Human Liver with Low-rank and Subspace Modeling at 7T

Kyung Min Nam[1], Ayhan Gursan[1], Nam G. Lee[2], Jannie Wijnen[1], Dennis Klomp[1], Jeanine Prompers[1], Alex Bhogal[1], and Arjan Hendriks[1]

*[1]Radiology, University of Medical Center Utrecht, Utrecht, Netherlands, [2]Biomedical Engineering, University of Southern California, Los Angeles, CA, USA*
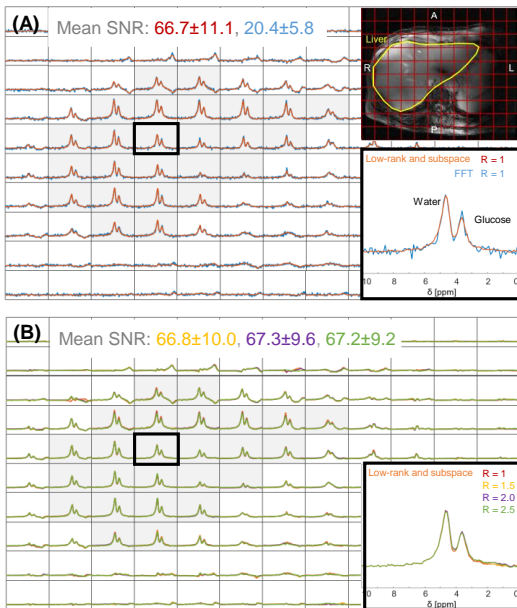
**Introduction** Deuterium Metabolic Imaging (DMI)[1] is an emerging non-invasive MR modality that can spatially map metabolism in vivo through the intake of deuterium-labelled substrates. The sensitivity and signal-to-noise ratio of DMI has been shown to scale supra-linearly with the magnetic field strength[2]. Nevertheless, it remains challenging to obtain 3D high resolution data of the human liver within a reasonably short scan time. To address this, we have implemented low-rank and subspace modeling (LRSM) reconstruction, an unconstrained SPICE reconstruction framework, and have evaluated the fidelity of accelerated MRSI acquisitions at various acceleration rates using retrospectively undersampled 3D data.

**Methods**  **Experiment:** A volunteer was scanned using a 7T MR system (Achieva, Philips, Netherlands) and transmit-receive body array. A 3D DMI dataset of the human liver was obtained 2.5h after the oral glucose intake. **Scan parameters:** DMI with Hamming weighted-acquisition (Fig. 1A): resolution=25×25×25mm³, FOV=250×300×300mm³, TR/TE=333/1.95 ms, spectral bandwidth=5kHz, weighted average=4, and acquisition time=10min 35s.

**Reconstruction:** Our approach employs a low-rank and subspace modeling[3] where a temporal subspace is estimated from the fully sampled k-space center region (6x6x6 voxels). The unknown spatial basis U is estimated by solving the following least-squares problem:

$$\hat{\mathbf{U}} = \underset{\mathbf{U}}{\operatorname{argmin}} \|\mathbf{d} - \Omega(\mathbf{F}\mathbf{U}\hat{\mathbf{V}})\|_{\ell_2}^2$$

where a linear operator (Ω) selects k-space data according to a Poisson disk sampling pattern[4] (Fig. 1B) where a central region (6x6x6 voxels) is fully sampled. All data were processed using in-house scripts in MATLAB (The MathWorks, Inc, Natick, MA). **Analysis**: Glucose and water maps were calculated by fitting each spectrum with the AMARES algorithm[5] implemented in the OXSA toolbox[6].



**(A)** Mean SNR: 66.7±11.1, 20.4±5.8

Low-rank and subspace  R = 1
FFT  R = 1

Water  Glucose

δ [ppm]

**(B)** Mean SNR: 66.8±10.0, 67.3±9.6, 67.2±9.2
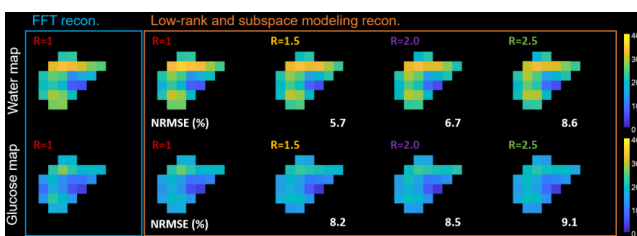
Low-rank and subspace  R = 1
R = 1.5
R = 2.0
R = 2.5

δ [ppm]

*Fig. 2. The MRI image and DMI spectra. (A) FFT and LRSM reconstruction with fully sampled data (R=1). (B) LRSM reconstruction with undersampled data (R=1 to 2.5)*



**(A)**  Nkz  Averages 1 2 3 4  Nkx  Nky

**(B)**  Nkz  Nkx  Nky
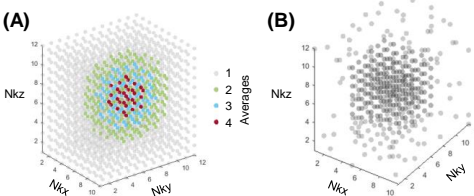
*Fig. 1. (A) Hamming sampling pattern (reduction factor, R=1.0) (B) Poisson disk sampling pattern (R=2.5)*

**Results and Discussion**   2D DMI spectra were reconstructed by FFT and LRSM. The LRSM reconstruction showed a noise level reduction in the spectra compared to FFT (Fig. 2A) and mean SNR from R=1 to R=2.5 in the middle slice (Fig. 2B). Deuterated glucose and water metabolite maps (Fig. 3) were generated from fully sampled data (FFT and LRSM, R=1) and from undersampled data (LRSM, R=1.5, 2.0, and 2.5). Overall normalized root-mean-square error (%) was calculated and gradually increased as the reduction factor increases.

**Conclusion**  We implemented an unconstrained SPICE reconstruction and investigated MRSI spectra quality by retrospectively undersampling 3D DMI data. Our retrospective analysis suggests that the scan time of a 3D Hamming weighted DMI acquisition could be further reduced by a factor of 2.5.



FFT recon.  Low-rank and subspace modeling recon.
Water map  R=1  R=1  R=1.5  R=2.0  R=2.5
NRMSE (%)  5.7  6.7  8.6
Glucose map  R=1  R=1  R=1.5  R=2.0  R=2.5
NRMSE (%)  8.2  8.5  9.1

*Fig. 3. Deuterated glucose and water maps of the DMI data using FFT and LRSM reconstructions. R: reduction factor. NRMSE (%): overall normalized root-mean-square error $= \|\theta - \hat{\theta}\|_2 / \|\theta\|_2$ .*

**References**  [1] De Feyter et al. 2018 Science Advances [2] de Graaf et al. 2020, NMR in Biomed. [3] Lam et al. 2014 MRM [4] Lustig et al. 2010 MRM [5] Vanhamme et al. 1997 JMR [6] Purvis et al. 2017 PLOS One

# MRS Workshop 2022
## Overcoming the Barriers to Clinical Use
### DISCONNECT 2 RECONNECT
22-24 August 2022 @ EPFL, Lausanne, Switzerland

33

S9A4

## DMI using different doses of [6,6′-²H₂]-glucose for real-time in vivo liver glucose mapping at 7 T

Simone Poli[1,2], Ahmed Fahiem Emara[3], Edona Ballabani[3], Naomi Lange[4,5], Andreas Melmer[3], David Herzig[3], Luc Tappy[3], Lia Bally[3], and Roland Kreis[1,2]

[1]Magnetic Resonance Methodology, Institute of Diagnostic and Interventional Neuroradiology, University of Bern, Bern, Switzerland, [2]Translational Imaging Center, sitem-insel, Bern, Switzerland, [3]Department of Diabetes, Endocrinology, Nutritional Medicine and Metabolism UDEM, Inselspital, University Hospital Bern, Bern, Switzerland, [4]Department of Visceral Surgery and Medicine, Inselspital, Bern University Hospital, University of Bern. [5]Graduate School for Health Sciences, University of Bern.

**Introduction**: Quantitative non-invasive exploration of hepatic glucose metabolism is of high importance due to its central role in glucose homeostasis and relevance for various metabolic diseases[1]. Deuterium metabolic imaging (DMI) has emerged as novel tool to dynamically assess the metabolic fate of administered deuterated glucose (and other substrates) in animals[2] and humans[3]. For the mapping of orally administered [6,6′-²H₂]-glucose (D-Glc) in brain and liver, initial work suggested doses of 60 g or 0.75 g/kg body weight[4]. Due to the high costs of D-Glc and the positive correlation of the load with both ingestion-difficulty and time for complete absorption (and hence scanning time), it is tempting to explore the feasibility of lower doses. The objective of this work was to explore the feasibility of lower than currently suggested doses of D-Glc for dynamic hepatic glucose mapping. In this work, we try to estimate the minimal dose of D-Glc for evaluation of Glc dynamics in the liver. Our project extends previous works[4] that focus on non-invasive techniques to assess glucose and glycogen turnover, respectively, with DMI and ¹³C-MRS[5].
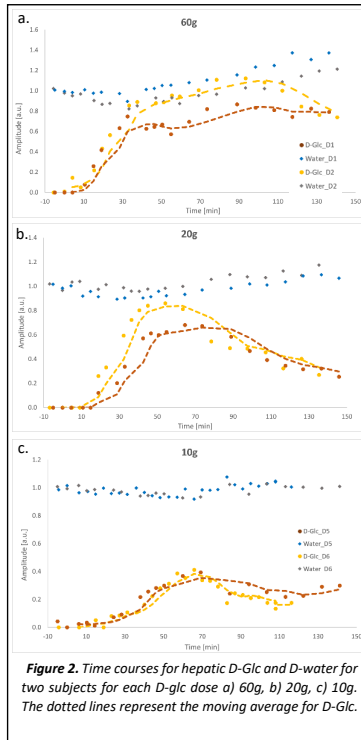
**Methods**: Exams are performed at 7T (Terra, Siemens) with a triple-tuned surface coil (¹H: quadrature-driven dual loop, ²H and ¹³C: linearly driven single loops, outer dimensions: 30x10x30 cm) from Rapid, Biomedical GmbH. Chromium-doped acetone (8 mL, 1% deuterated) inserted in a vial near the coil center served as external reference.

- DMI: conventional 3D-MRSI (0.50 ms rectangular excitation pulse, 0.35 ms phase-encoding gradient, TR500 ms, 4 averages with acquisition-weighting, 12x12x8 phase encodings, nominal resolution of18.3x18.3x27.5 mm³, 1000 Hz spectral width, 4:08 min acquisition time). Placement of the MRSI grid uses reference markers on the coil.
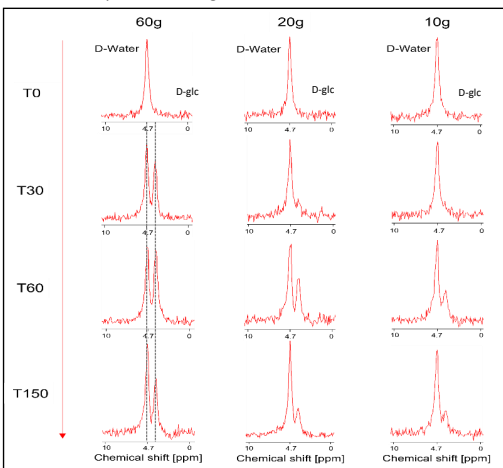
Data processing and fitting was performed in jMRUI using AMARES[6].

Study population according to D-Glc intake: Six healthy subjects received an oral glucose load of 60g, 20g or 10g (n=2 for each dose). Subjects underwent 48h of standardized diet and withdrawal from strenuous exercise (40% carbs, 40% fat, 15% proteins, no caffeine, no alcohol) prior to ingestion of 60/20/10g of D-Glc in 200 ml of water in a supine position. Scanning was performed until 150min after D-Glc ingestion. Blood sampling is performed for plasma concentration of (enriched) glucose, insulin, glucagon and C-peptide.

**Results and Discussion:** Fig. 1 shows the spectral quality at different time points (T0, T30, T60, T150) of three subjects receiving different D-Glc dose (60, 20 or 10 g, respectively). Each spectrum is the average of 6 central voxels in the liver, manually selected for optimal signal. The 60 g dose resulted in a hepatic D-Glc signal (3.7 ppm) comparable to the amplitude of the water signal (4.7 ppm) around T60 and it is still visible at the end of the acquisition. For 20 g and 10 g, the D-Glc signal amplitude was reduced and almost decayed to baseline at the end of the acquisition period, suggesting capturing of the completely absorbed dose. SNR of water of a single voxel spectrum from near the center coil is ~34 and linewidths ~21 Hz. Fig.2 shows the time course of the signal with a time resolution of 5-10 minutes for D-Glc and D-water for two subjects for each dose. With 10 g, the signal was well visible, adequate for fitting and reached almost baseline at the end of the acquisition. With the 60 g, an increase in the water signal was observed, indicating metabolisation into end products of the TCA cycle. For 20 g the increase is lower, while for 10 g it is almost undetectable.



*Figure 2. Time courses for hepatic D-Glc and D-water for two subjects for each D-glc dose a) 60g, b) 20g, c) 10g. The dotted lines represent the moving average for D-Glc.*

**Conclusions:** These first results suggest the feasibility of D-Glc as low as 10g for liver DMI. The benefit is two-fold: 1) the whole dynamic of increase and decay to baseline of the D-Glc signal can be observed (beneficial for metabolic modelling); 2) the cost for the examination is drastically reduced (from ~1000$ to ~200$). However, the concomitant conversion of glucose to glycogen by natural abundance ¹³C MRS, which is necessary to fully understand the metabolic fate of D-Glc, is limited at such low doses (data not shown).

**References:** [1] Petersen MC, et al. Nat Rev Endocrinol. 2017 Oct;13(10):572-587. [2] Lu M, et al. J Cereb Blood Flow Metab. 2017;37(11):3518-3530. [3] De Feyter HM, et al. Sci Adv. 2018 Aug 22;4(8):eaat7314. [4] Poli S, et al. ISMRM. 2022. [5] Buehler, T., et al. NMR Biomed. 2016.29: 796– 805. [6] Vanhamme L, et al. J Magn Reson. 1997 Nov;129(1):35-43. Supported by the Swiss National Science Foundation (PCEGP3_186978) and Diabetes Center Bern.

*Figure 1. ²H-MRSI spectra from DMI datasets of one subject per D-Glc dose at selected time points (T0 corresponds to the time of Glc intake).*

**MRS Workshop 2022**
Overcoming the Barriers to Clinical Use
DISCONNECT 2 RECONNECT
22-24 August 2022 @ EPFL, Lausanne, Switzerland

34

S9A5

**Abstract: Anesthetic-related neuroenergetic changes measured with ^{1}H- and ^{31}P-MRS in mouse at 7 Tesla**

Antoine Cherix[1], Mohamed Tachrount[1], Jason Lerch[,1,2]

[1.] Wellcome Centre for Integrative Neuroimaging, WIN-FMRIB, Nuffield Department of Clinical Neurosciences, University of Oxford, Oxford, UK. [2.] Mouse Imaging Centre (MICe), Hospital for Sick Children, 25 Orde Street, Toronto, ON, Canada

**Introduction:** Medetomidine has recently become a popular anesthetic regime as opposed to isoflurane to study brain function in rodents[1,2]. While it is well known that isoflurane changes levels of brain lactate[3] by potentially altering mitochondrial function[4] or changing metabolite diffusion[5], it is unclear whether isoflurane changes overall brain energy metabolism homeostasis compared to medetomidine[6]. To test this, we measured the differences in energy homeostasis induced by switching medetomidine and isoflurane within the same experimental session using either edited proton ([1]H-) or phosphorous ([31]P-) Magnetic Resonance Spectroscopy (MRS). **Methods:** Adult male C57BL/6 mice were scanned on a 7 Tesla (70/20) MRI scanner (Bruker), equipped with ^{1}H cryoprobe and ^{31}P RT-surface coil. Mice were exposed to A) 1-2% isoflurane or B) 0.4mg/kg/h medetomidine + 0.2% isoflurane, which were switched in the middle of the scan. The initial anesthetic regime was randomized in two groups of mice (Fig.1A) to compensate for exposure time. Respiration, rectal temperature, blood $O_2$ saturation and heart rate were monitored with SAI. Scans consisted of either edited single-voxel ^{1}H-MRS (n=12 per group, $time_{acq}$=32min) in the dorsal hippocampi (TR=3s, Lactate offset:4.1ppm,TE=100ms; GABA offset:1.9ppm,TE=68ms) or ^{31}P-MRS (n=7 per group, $time_{acq}$=34min) in the whole brain (3D-ISIS, TR=4s). Spectra were processed with jMRUI and quantified with AMARES. All statistics were done in GraphPad Prism 9. **Results:** As expected, we observed a significant increase in breathing rate (19%,p=0.007) and decrease in heart rate (-19%p=0.004) under medetomidine as compared to isoflurane (Fig.1D), while no difference was observed in temperature and blood oxygen saturation (n.s.). Hippocampal lactate levels were higher under isoflurane (32%,p=0.037) with an associated drop in pH ($\Delta$pH=-0.04,p=0.036) (Fig.1E), while no difference was observed in energy metabolites ATP/PCr or Pi/PCr (n.s.), nor in neurotransmitter GABA and Glx levels (n.s.). Finally, lactate level correlated only with heart rate (Fig.1F; $r^2$=0.42, 95%CI=0.11-0.65; Linear Regression: p=0.009). **Discussion**: Our results support the idea that isoflurane induces a glycolytic switch from oxidative metabolism, but do not suggest this is associated with a significant change in energy homeostasis. Interestingly, levels of lactate correlated positively with the heartbeat only, which could reflect neurovascular contributions to isoflurane's effects on glycolysis.

**References: 1** Grandjean, J. *et al. NeuroImage* 102, 838–847 (2014) **2** Hyppönen, V. *et al. NMR Biomed.* 35, (2022) **3** Horn, T. *et al. Neurochem. Int.* 57, 940–947 (2010) **4** Schwarzkopf, T. M. *et al. Exp. Biol. Med.* 238, 84–89 (2013) **5** Valette, J. *et al. J. Cereb. Blood Flow Metab.* 27, 588–596 (2007) **6** Flatt, E. *et al. Metabolites* 11, 413 (2021)
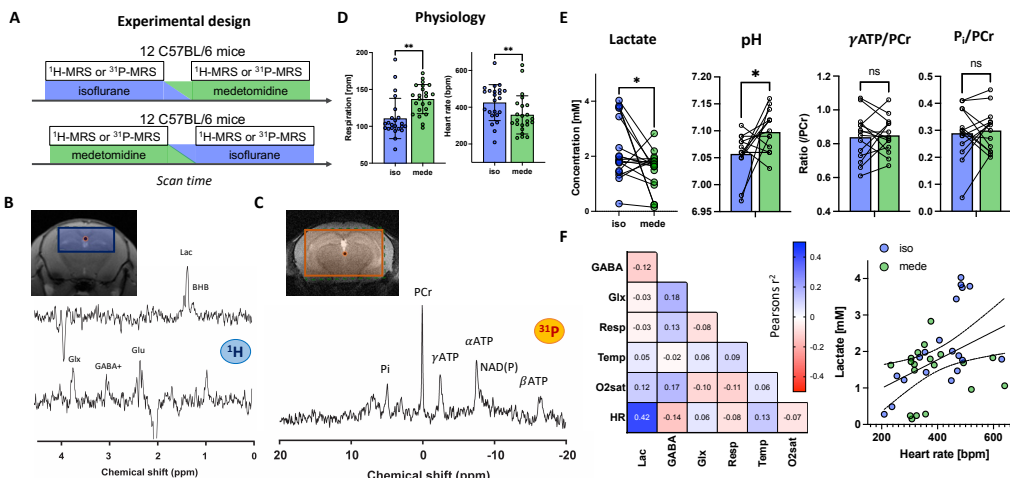
**Figure 1** : **A** Experimental design (medetomidine vs. isoflurane). **B.** Typical Edited ^{1}H-MRS spectrum acquired in mouse dorsal hippocampi. **C.** Typical ^{31}P-MRS spectrum acquired in mouse brain. **D.** Anesthesia-induced physiological differences **E.** Anesthesia-induced neuroenergetic differences **F.** physiological and metabolic correlations. **\***p<0.05, \*\*p<0.01, paired Student's t-test.

# MRS Workshop 2022
## Overcoming the Barriers to Clinical Use
### DISCONNECT 2 RECONNECT
22-24 August 2022 @ EPFL, Lausanne, Switzerland

35

IT'S TIME

Poster no. 1 (on-site poster)

**A Multivariate Curve Resolution (MCR) analysis of multicenter MRSI data for prostate cancer localization**

A Stamatelatou[1], CG Bertinetto[2], JJ Jansen[2], GJ Postma[2], A. Heerschap[1], TWJ Scheenen[1]
[1]Radboud UMC, Nijmegen, The Netherlands, [2]Radboud University, Nijmegen, The Netherlands

**Introduction:** Automated and reliable spectral evaluation is essential for the clinical use of 3D ^{1}H-MRSI of the prostate[1]. The multivariate Curve Resolution-Alternating (MCR) method aims at reconstructing the relative intensity of spectral profiles of individual chemical components within a sample[2], providing an easily interpretable model. Aim of this work is to apply the data-driven MCR method to prostate MRSI data for rapid automated localization and classification of cancer and healthy tissue, reducing the requirement for in-house expertise and improving objectiveness by avoiding subjective human intervention.

**Method:** Multicenter prostate cancer MRSI data from 85 patients were acquired on a 3T MR system (MAGNETOM Trio or Skyra, Siemens Healthcare, Erlangen, Germany) from 7 centers[3], with a body array coil for signal reception. The acquisition protocol was PRESS, TE 145ms and TR 750 ms. 62 patients were used as a training set and 23 as a test set.

Magnitude spectra (n=61122) of the training set were used to perform MCR, which models the data $X$ as a linear mixture of components: $X=C\,S$, where $C$ and $S$ are matrices of the pure components' relative abundances and spectral profiles respectively. These profiles $S$ are obtained by imposing mathematical constraints based on physicochemical principles. The number of components in the model was estimated with Singular Value Decomposition (SVD) and initialized by entropy minimization[4].

The model's components were interpreted following the patterns of in-vivo prostate spectroscopy spectra[1]. The component with the higher intensity in the Choline ppm region (3.2ppm) was further investigated as the most suspicious for the presence of tumor. After training, the relative intensities of each component for each voxel were normalized across all voxels from the patients in the test set, and were mapped slice-by-slice for a qualitative validation of the model, using histopathology reports as gold standard. As a second independent quantification method, individual voxels previously assigned as definitely tumorous or benign were used. The relative intensity of the component of these assigned voxels was employed to separate benign from tumorous voxels in the test set.

**Results and Discussion:** The optimal number of components was 5 for the training set (Fig.1). The spectroscopic profile of S1 and S2 correlates to benign prostate spectra, high levels of Cit (2.6ppm) and low Cho (3.2ppm) and Cre (3.03ppm). The spectroscopic profile of S5, with elevated intensity in the Cho ppm range, is deemed representative for tumor spectra. Examples of relative intensity maps of the components combinations are presented for a slice in a patient with a non-aggressive tumor (Fig.2) and for a patient with an aggressive tumor (Fig.3). Qualitatively in all 23 patients in the testing group, the regions of increased levels of S1+S2 and S5 seemed to correlate with histopathologically benign and tumor tissue, respectively.

The relative intensity of the cancerous component (S5) discriminated benign from tumorous voxels without overlap in the test set (Fig.4). In benign assigned voxels, S1+S2=0.7±0.2 AU and S5=0.2±0.1 AU. In tumor assigned voxels, S1+S2= 0.4±0.1 AU and S5= 0.5±0.1 AU. We need to investigate whether the intensity of the S5 component correlates to the aggressiveness of the tumor.

**Conclusion:** MCR can be used for the extraction of common spectroscopic components without a need of prior knowledge. The assigned components can be used to classify prostate regions as suspicious and non-suspicious for cancer, with potential to also assess tumor aggressiveness. Altogether, our approach can be considered as a step towards the development of an automated tool for classification of prostate MRSI spectra.

**References:**

[1]    A. Stamatelatou et al, *Magn. Reson. Mater. Physics, Biol. Med.*, 2022.
[2]    A. De Juan et al *Anal. Methods*, 2014.
[3]    PCa-MAP; ClinicalTrials.gov Identifier NCT01138527.
[4]    C. G. Bertinetto et al, *J. Chemom.*, 2018.

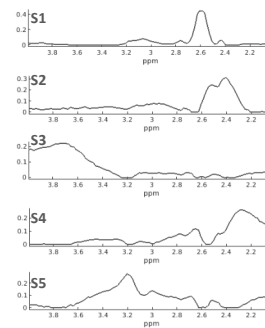**Figure 1.** spectral profiles of the components S1 benign, S2 benign with lipids, S3 water residual, S4 lipids, S5 tumor



Gleason score 2+3
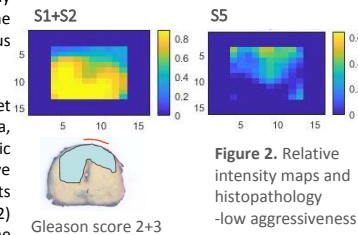
**Figure 2.** Relative intensity maps and histopathology -low aggressiveness


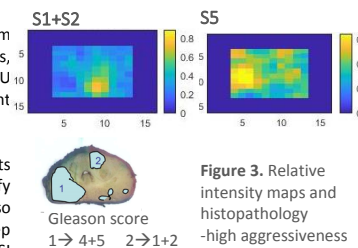
Gleason score
1→ 4+5    2→1+2

**Figure 3.** Relative intensity maps and histopathology -high aggressiveness
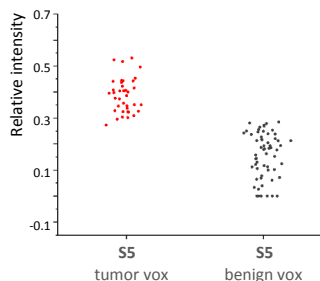


**Figure 4.** Relative intensity of S5 in tumor and benign assigned voxels

**MRS Workshop 2022**
Overcoming the Barriers to Clinical Use
DISCONNECT **2** RECONNECT
22-24 August 2022 @ EPFL, Lausanne, Switzerland

36

Poster no. 2 (on-site poster)

## The effect of signal-to-noise ratio and linewidth on neurochemical quantification by LCModel analysis

Phil Lee,[1,2] Wen-Tung Wang,[1] and In-Young Choi[1-3]

[1]Hoglund Biomedical Imaging Center, [2]Department of Radiology, [3]Department of Neurology,
University of Kansas Medical Center, Kansas City, Kansas, USA

INTRODUCTION Precision of quantitative analysis of *in vivo* [1]H MR spectra, performed in the frequency domain or in the time domain, depends on quality of the spectra, in particular on the spectral signal-to-noise ratio (SNR) and linewidth. [1] LCModel [2] is one of commonly used software packages that analyze spectra in the frequency domain by fitting them as a linear combination of basis spectra. In this work, we examined the dependence of neurochemical quantification of ^{1}H MR spectra on SNR and water linewidths.

METHODS Proton MR spectra were acquired as a series of blocks of FIDs from the cerebral neocortex of 5 Sprague-Dawley rats using a short echo-time stimulated echo acquisition mode (STEAM) sequence (TE/TM/TR = 2/20/5000 ms) and from the hippocampus of 4 Sprague-Dawley rats using the SPECIAL [3] sequence (TE/TR = 2.7/4000 ms). *In vivo* MRS experiments were performed at a 9.4 T Varian system (Agilent Technologies, Santa Clara, CA) using an 18-mm diameter quadrature surface RF coil consisting of two geometrically decoupled loops. The nominal sizes of the volume of interest (VOI) were 48 μl for the neocortex, and 22.5 μl for the hippocampus. Magnetic field homogeneity in the VOI was adjusted using FASTMAP [4], resulting in water linewidths of 13, 16, 19, and 22 Hz for the STEAM sequence and 10, 13, 16, and 19 Hz for the SPECIAL sequence, respectively. LCModel quantification was performed on the spectra obtained by averaging 16 - 800 FIDs, resulting spectral SNR (reported by LCModel) ranging from 11 to 78. Fig. 1 shows the effect of averaging on spectral SNR.

RESULTS A total of 19 neurochemicals were quantified using LCModel. Quantification of strongly and weakly represented neurochemical signals showed distinct dependences on SNR and linewidth. Quantification of strongly represented neurochemicals (e.g., NAA, Tau, Glu) was relatively insensitive to SNR and lindwidth and the quantification was relatively reliable at SNR as low as 11 with water linewidth of 22 Hz (data not shown). Quantification of other neurochemicals showed various dependence patterns.

Fig. 2 shows the quantification dependence of alanine (Ala), ascorbate (Asc), aspartate (Asp), phosphocreatine (PCr), and phosphorylethanolamine (PE) on SNR with linewidths of (A) 16 and (B) 22 Hz using the STEAM sequence. With the same numbers of average, the SNRs of spectra with lindwidth of 16 Hz were higher than those with linewidth of 22
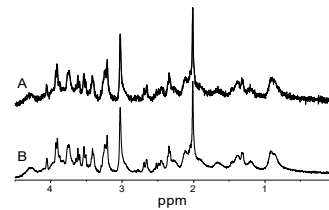


**Fig. 1**. Averaged spectra of 16 (A) and 640 (B) FIDs obtained from neocortex of rat brain.

Hz, as expected. With lindwidth of 13 Hz, reliable quantification of PCr and Ala can be obtained from spectra with SNR as low as 15, yet reliable quantification of Asc, Asp, and PE can only be obtained when SNR > 30 (Fig. 2A). As SNR increases, the neurochemical levels and their standard-deviation (SD) are relatively stable and consistent. This observation applies to Fig. 2B in which linewidth was 22 Hz. When SNRs are lower than 30, however, wider linewidth (or poor shimming) results in less precise quantifications with larger SDs.

Figure 3 shows the quantification of the aforementioned neurochemicals from the spectra acquired using the SPECIAL sequence as a function of SNR and linewidth. Similar to the STEAM sequence, quantification with SNR > 30 yielded reliable neurochemical concentrations for linewidths from 10 Hz to 16 Hz. When SNR is lower than 30, quantifications were less reliable with larger SDs.



**Fig. 2**. Dependence of neurochemical quantification using the STEAM sequence on spectral SNR with water linewidths of 16 (A) and 22 (B) Hz.
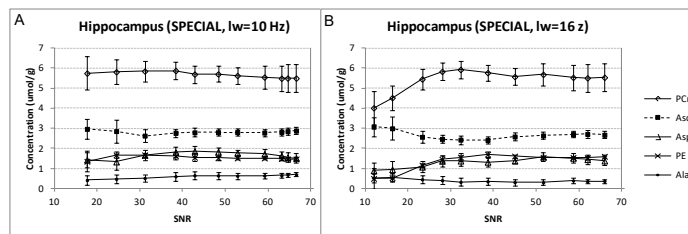


**Fig. 3**. Dependence of neurochemical quantification using the SPECIAL sequence on spectral SNR with water linewidths of 16 (A) and 22 (B) Hz.

DISCUSSION The results of this study suggest that SNR and linewidth of MR spectra play important roles in the precision of neurochemical quantification using LCModel. Quantification of strongly represented neurochemicals that have high and distinctive peaks did not show strong dependence on SNR and linewidth. Reliable quantification of those neurochemicals can be obtained from spectra with SNR as low as ~10. For other neurochemicals, however, quantification becomes more reliable as the spectral SNR improves over 30 and linewidth improves.

REFERENCES 1. Lanz et al., *NMR Biomed*, e4325 (2020) 2. Provencher, *Magn Reson Med* 30:672-9 (1993) 3. Mlynarik et al., *Magn Reson Med* 56:965-70 (2006) 4. Gruetter et al., *Magn Reson Med* 29:804-11 (1993)
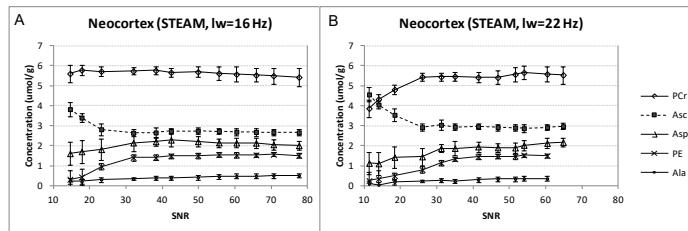
**MRS Workshop 2022**
Overcoming the Barriers to Clinical Use
DISCONNECT 2 RECONNECT
22-24 August 2022 @ EPFL, Lausanne, Switzerland

37

Poster no. 3 (on-site poster)

# Ultra-short TE semi-LASER sequence for small animal $^1$H MRS at 9.4 T

**Ivan Tkáč**

*Center for Magnetic Resonance Research, University of Minnesota, Minneapolis, MN, USA*

**INTRODUCTION** Spectral quality is the key factor for reliable *in vivo* neurochemical profiling by $^1$H MRS. Ultra-short TE(min) is desirable for reducing $T_2$ relaxation effects and minimizing the J-modulation in metabolites with coupled spin systems. TE(min) < 3 ms is feasible for rodent brain $^1$H MRS when STEAM[1] and SPECIAL[2] sequences are used. However, STEAM provides only 50% of available signal intensity and SPECIAL is not a single-scan technique and requires subtraction of unwanted magnetization (1D ISIS). In the LASER sequence optimized for rodents[3,4], TE(min) can be reduced only to about 15 ms due to three pairs of AFP pulses. Up to now, the semi-LASER sequence has been utilized for rodent $^1$H MRS studies only sparsely[5]. The purpose of this study was to implement and optimize ultra-short TE semi-LASER sequence for rodents at 9.4 T.

**METHODS** The semi-LASER sequence was implemented on a Varian/Agilent 9.4T MR scanner. The $B_0$ shimming was accomplished using FASTMAP[6]. Spontaneously breathing rats were anesthetized with 1.2 – 1.5% isoflurane.

**RESULTS** The semi-LASER was implemented with the slice-selection order Z-X-Y-Y-X originally proposed for 4T human MR scanner[7]. The echo-time TE(min) was possible to reduce down to 7.0 ms without sacrificing the spectral quality (unwanted coherences). The semi-LASER localization was combined with VAPOR water suppression interleaved with OVS[1]. Achieved spectral quality is shown in Figure 1.

**DISCUSSION**

Figure 1 demonstrates that ultra-short TE semi-LASER localization is feasible at 9.4T. The semi-LASER sequence provides full signal intensity from the selected VOI. The echo time as short as 7 ms minimizes $T_2$ relaxation effects, which provides a potential for improved accuracy of metabolite quantification. The advantage of this sequence over the original LASER technique is not only reduced TE(min), but also semi-LASER excites less magnetization from outside of the VOI that reduces the probability of spurious echoes.

*References: 1.* Tkac et al., Magn Reson Med 1999; *2.* Mlynarik et al., Magn Reson Med 2006; *3.* de Graaf et al., Magn Reson Med 2006; *4.* Oz et al., J Neurosci 2010; *5.* Deelchand et al., Magn Reson Med 2021; *6.* Gruetter et al., Magn Reson Med 2000; *7.* Oz et al., Magn Reson Med 2011.
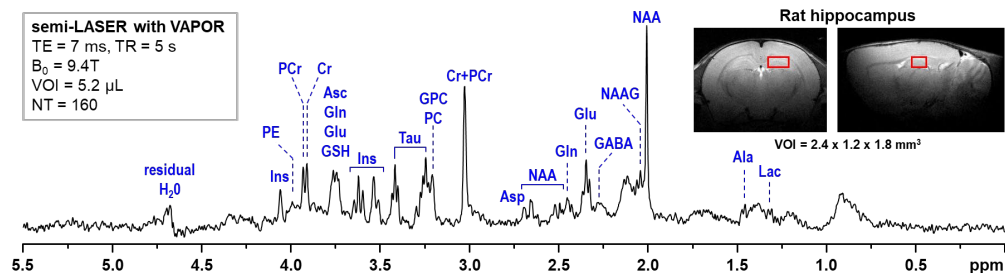
**Figure 1.** Representative $^1$H MR spectrum acquired from the hippocampus of rat on postnatal day 30.

Poster no. 4 (on-site poster)

### Exposure study: Evaluating the neurotransmitter-metal relationship in welders

[1]Gianna Nossa, [1]Chang Geun Lee, [1]Humberto Monsivais, Sa Liu[1], Jae Hong Park[1],[1,2]Ulrike Dydak

[1] School of Health Sciences, Purdue University, West Lafayette, IN, USA

[2] Department of Radiology and Imaging Sciences, Indiana University School of Medicine, Indianapolis, IN, USA

**Background:** High exposure to manganese (Mn) through inhalation of welding fumes has been shown to have a toxic effect to the human brain leading to a parkinsonism syndrome (manganism). Our group has demonstrated elevated thalamic γ-aminobutyric acid (GABA) levels, measured by edited magnetic resonance spectroscopy (MRS), in response to high exposure to Mn in welding fumes,[1] which was found to be reversible if exposure is decreased.[2] Furthermore, we have shown that toenail metal levels are a good biomarker for exposure to Mn over the past year.[4] This study investigates whether toenail Mn and iron (Fe) levels are predictive of brain GABA and Glutamate (Glu) levels in two brain regions of Mn-exposed welders: the thalamus, a region responsible for relaying sensory and motor signals, and the cerebellum, the region that maintains balance, posture, and coordination. Since toenail metal levels reflect an exposure window of 7-12 months prior to clipping,[3] while brain Mn levels reflect exposure in more recent time windows (~0-3 months), metabolite levels are expected to best correlate with metal levels from toenails collected ~6-12 months after the MRS measurement.

**Methods:** Toenails are collected every 3 months, with the initial clippings and MRS acquired at the first visit (baseline). Levels of GABA, the primary inhibitory neurotransmitter, and Glu, the primary excitatory neurotransmitter, are acquired using MEGA-PRESS (TE/TR:68/2000ms, 256 averages, $30\times30\times25mm^3$ VOI), in the thalamus and cerebellum of welders. Spectra were processed in Osprey and analyzed using LCModel (Version 6.3-1M). Toenail metal levels were analyzed via inductively coupled plasma- optical emission spectrometry (ICP-OES).

**Results:** A preliminary analysis from 16 stainless-steel welders recruited from a truck trailer manufacturer yields no significant correlations between toenail Mn and brain GABA levels. However, thalamic GABA levels tend towards positive correlations with toenail Mn at later time points, whereas cerebellar GABA levels and thalamic Glu levels tend towards negative correlations at later time points. In contrast, a significant correlation was found between cerebellar GABA and toenail Fe at baseline (R=0.75, p=0.005), and a trend was seen between thalamic GABA and toenail Fe at 12 months (R=0.72, p=0.07).

**Conclusion:** While data collection is still in progress, we see trends pointing towards GABA-Fe correlations, which indicates that increased toenail Fe concentrations may represent an increase in GABA values. Furthermore, this suggests that other metals, including Fe, that play a role in Mn homeostasis, should not be neglected in the study of Mn neurotoxicity. (Supported by the R01 ES032478 and the International Manganese Institute)
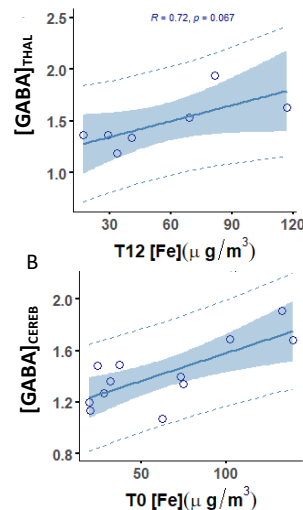


*Figure1:* A) Correlation between *thalamic* GABA and Toenail Fe (clipped at the final timepoint, 12 months after acquisition of the brain GABA levels) approaching significance; B) Significant correlation between *cerebellar* GABA and Fe at the first timepoint.

References:

1. Ma RE, et al. *Neurotoxicology*. 2018 Jan; 64:30-42.
2. Edmondson DA, et al. *Toxicol Sci*. 2019;172(1):181-190. doi:10.1093/TOXSCI/KFZ174
3. Yeh CL, et al. Toxicol Sci suppl. 2015;144(1):2739.
4. Ward EJ, et al. *Ann Work Expo Heal*. 2018;62(1):101-111. doi:10.1093/ANNWEH/WXX091

# MRS Workshop 2022
## Overcoming the Barriers to Clinical Use
### DISCONNECT 2 RECONNECT
22-24 August 2022 @ EPFL, Lausanne, Switzerland

39

Poster no. 5 (on-site poster)

## Assessment of Oxidative Stress and Neuronal Activity Affected in PTSD Subjects

Antonia Susnjar[1], Gianna Nossa[2], Joseph Rispoli[1,3], Ulrike Dydak[2], Meden Issac Lam[4]

1.Weldon School of Biomedical Engineering, Purdue University; 2. School of Health Sciences, Purdue University; 3.Elmore Family School of Electrical and Computer Engineering, Purdue University; 4. Department of Chemistry and Physics, Purdue University Northwest.

### Introduction and Methods

The applications of MRS to investigate the metabolic window on a wide range of biochemical processes are extremely diverse. MRS was the first tool that demonstrated biological changes in mental health patients, namely imbalances in brain metabolism, changing the stigma of mental health. However, research evidence for altered in vivo metabolite levels across post-traumatic stress disorder (PTSD) are lacking. This study evaluates edited and unedited single voxel spectroscopy (SVS) of ten clinically diagnosed PTSD participants and their age and gender-matched healthy controls. Four brain regions (anterior cingulate cortex (ACC), dorsolateral prefrontal cortex (DLPFC), insula, hippocampus) related to the underlying PTSD symptoms have been investigated for assessment of alterations in cognitive-affective processing, such as lack of extinction of the fear response, flashbacks, heightened physiological responses to trauma cues, and general hyperarousal symptoms and hypervigilance[1]. Fifth brain region, the amygdala, was only investigated using unedited MRS (sLASER,TE/TR:30/2000ms, 64avgs,VOI: $15x15x15mm^3$) due to difficulty in acquiring usable and reliable edited MRS. Unedited SVS was obtained using Point RESolved Spectroscopy(PRESS,TE/TR:30/2000ms,64avgs,VOI:$40x25x27mm^3$), processed in Osprey and analyzed using LC Model. Edited MRS was obtained using HERMES (TE/TR:80/2000ms,256avgs, VOI:$40x25x27mm^3$) and analyzed using Gannet. To overcome acquisition downfalls, we have conducted critical optimization for each voxel of interest (VOI) by finding the optimal voxel rotation and slice order selection to enhance data quality and reproducibility (**Figure 1**).
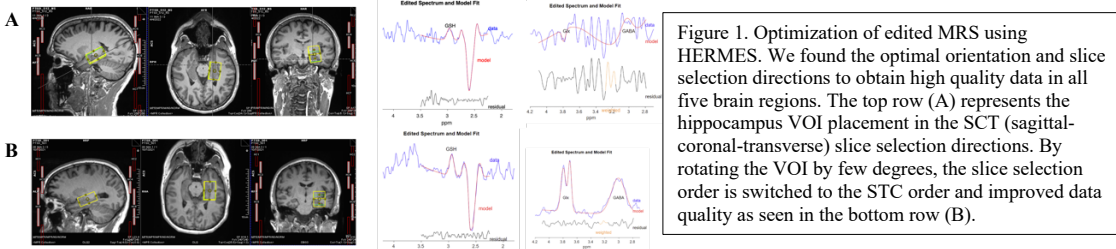


Figure 1. Optimization of edited MRS using HERMES. We found the optimal orientation and slice selection directions to obtain high quality data in all five brain regions. The top row (A) represents the hippocampus VOI placement in the SCT (sagittal-coronal-transverse) slice selection directions. By rotating the VOI by few degrees, the slice selection order is switched to the STC order and improved data quality as seen in the bottom row (B).
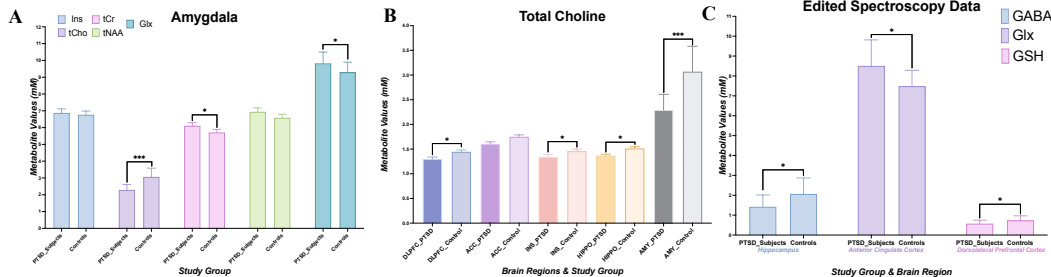
### Results and Discussion



Figure 2. A) The amygdala is a core component in neurobiological models of stress-related pathologies. We found statistically significant changes in PTSD participants compared to healthy controls indicating neurotrauma with elevated glutamate-glutamine (Glx, p = 0.039), and creatine (tCr, p = 0.023) values. Additionally, a decrease in choline (tCho, p = 0.0014) seems to indicate neurotrauma related metabolic changes in the brain region in charge of "flight or fight" state. B) Statistically significant decrease is observed in tCho, a cell membrane turnover marker, in four out of five brain regions (p = 0.0215, 0.044, 0.0249, 0.0014). C) Edited MRS depicted the important role of three brain regions in PTSD. Lower concentration of GABA (p =0.004) in the hippocampus is a biological marker of vulnerability for development of mood disorders, anxiety, depression, and insomnia which are common symptoms of PTSD[3]. While the findings for Glx levels are somewhat inconsistent, a meta-analysis suggests that Glx concentration are increased in frontal brain regions in neurological disorders, confirmed by our findings in the ACC (p= 0.03). Glutathione (GSH, p =0.05), an antioxidant in charge of disposal of peroxides, is decreased in DLPFC of PTSD subjects because of incomplete REDOX and active protection against toxicity[2].

**References:**

1.Karl, Anke, et al. "The Use of Proton Magnetic Resonance Spectroscopy in PTSD research—Meta-Analyses of Findings and Methodological Review." *Neuroscience and biobehavioral reviews* 34.1 (2010): 7–22

2.Schür, Remmelt R et al. "Brain GABA Levels Across Psychiatric Disorders: A Systematic Literature Review and Meta-Analysis of (1) H-MRS Studies." *Human brain mapping* 37.9 (2016): 3337–3352

3.Schmitz, Taylor W et al. "Hippocampal GABA Enables Inhibitory Control over Unwanted Thoughts." *Nature communications* 8.1 (2017): 1311–12.

Poster no. 6 (on-site poster)

**Super-fast assay of creatine kinase using ^{31}P-MT-MR fingerprinting at 7T in the human brain**

Mark Widmaier[a,b,c], Song-I Lim[a,b,c], Daniel Wenz[a,c], Lijing Xin[a,c]

[a]CIBM Center for Biomedical Imaging, Lausanne, Switzerland; [b] Laboratory for Functional and Metabolic Imaging, École polytechnique fédérale de Lausanne, Lausanne, Switzerland; [c] Animal Imaging and Technology, EPFL, Lausanne, Switzerland

Introduction: Energy buffering and transport via phosphocreatine (PCr)/creatine kinase (CK) shuttle play important roles in cellular energy metabolism to maintain neuronal activity and normal brain function. Non-invasive measurement of CK reaction rates has been possible using ^{31}P magnetic resonance spectroscopy (MRS) combined with magnetization transfer (MT). However, MT methods typically require long acquisition time, which limits their clinical applications. In this study, we introduce a SAR efficient ^{31}P-MT-MRF approach to accelerate in vivo assay of CK at 7T in the human brain and evaluate its test-retest reproducibility.

Methods: The ^{31}P-MT-MRF approach is based on a b-SSFP-type sequence, with varying phase alternating flip angles [1,2]. A 20 mm slice in the occipital lobe was excited using a 1D slice selective RF pulse. Excitation profile, dictionary creation and fitting process are elaborated in Widmaier et al. [3]. The approach is compared with the state-of-the-art EBIT MT approach [4]. 38 averages and 1 dummy scan were acquired for MRF and 16+1 scans for the EBIT, resulting in a similar scan time of 18.5 min. In vivo data were acquired from 6 healthy subject (3 female; 3 males; age 18-30 years), who provided written informed consent. To evaluate the reproducibility of our method subjects were scanned 2 times with the
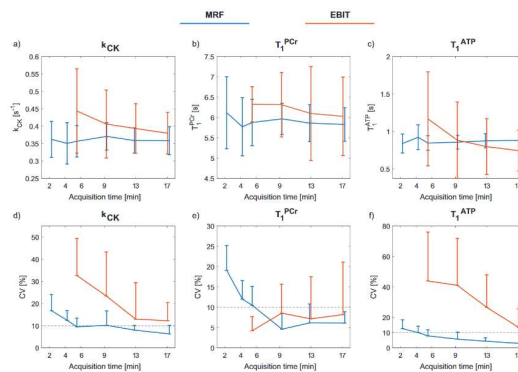


Figure 1: (a,b,c) Estimated parameters for MT-31P-MRF and the EBIT method over the acquisition time. (d,e,f) CV [%] of MT-31P-MRF and the EBIT method over the acquisition time. All Values are shown in mean and STD.

same MRF and EBIT protocol (15 min break). All MR experiments were performed on a 7T/68cm MR scanner (Siemens Medical Solutions, Erlangen, Germany) with a ^{1}H quadrature surface coil and a single-loop ^{31}P coil for the occipital lobe.

Results: Table 1 shows the estimated mean values of $T_1^{PCr}$, $T_1^{\gamma ATP}$, $M_0^{PCr}$ and $k_{CK}$ obtained by both ^{31}P-MT-MRF and EBIT with different acquisition times. The MT-^{31}P-MRF provides $T_1^{PCr}$, $T_1^{ATP}$, and $k_{CK}$ estimates in good agreement with those obtained by the EBIT method and literature values [4-8]. Furthermore, the test-retest reproducibility results showed that the MT-^{31}P-MRF achieves less than 10% of the coefficient of variations with 4 min 15 s scan time (Figure 1), which is more than four times faster than the EBIT method.

| | MT-^{31}P-MRF | | | | | | EBIT |
|---|---|---|---|---|---|---|---|
| Averages | 37 | 27 | 19 | 11 | 8 | 4 | 16 |
| $t_{acq}$ [min] | 17:24 | 12:50 | 9:17 | 5:30 | 4:15 | 2:18 | 17:04 |
| $SNR_{PCr}$ [dB] | 12.0 | 11.3 | 9.9 | 8.0 | 6.5 | 4.3 | - |
| $SNR_{ATP}$ [dB] | 9.8 | 9.1 | 7.8 | 5.8 | 4.6 | 2.6 | - |
| $k_{CK}$ [s$^{-1}$] | 0.36±0.04 | 0.36±0.04 | 0.37±0.04 | 0.36±0.06 | 0.35±0.07 | 0.34±0.08 | 0.38±0.06 |
| $T_1^{PCr}$ [s] | 5.83±0.37 | 5.86±0.42 | 5.96±0.41 | 5.93±0.79 | 5.97±0.64 | 5.74±1.51 | 6.03±0.97 |
| $T_1^{ATP}$ [s] | 0.88±0.10 | 0.87±0.09 | 0.86±0.10 | 0.87±0.14 | 0.89±0.14 | 0.90±0.18 | 0.74±0.27 |
| $C_r$ [mM] | 4.03±0.36 | 4.04±0.40 | 4.02±0.43 | 4.04±0.42 | 4.08±0.48 | 4.06±0.66 | |

Table 1: Estimated parameters (mean ± STD), SNR and acquisition time for different number of averages.

Conclusions: We conclude that MT-^{31}P-MRF is a fast and reproducible approach for in vivo creatine kinase metabolic rate assay in the human brain, which enables the potential for investigating energy metabolism in a clinical setting.

References: [1] Ma, D. et al., Nature 495 (2013); [2] Wang et al. NMR Biomed. (2017) 30:1–14 [3] Widmaier, M., et al., Research Square (2022); [4] Ren, J. et al., Magnetic resonance in medicine 78.5 (2017); [5] Valkovic, L. et al., Eur. J. Radiol. 82 (2013); [6] Xin, L. et al. Front. nutrition 62 (2018); [7] Lei H. et al., Magnetic resonance in medicine (2003) 49; [8] Du F. et al., Magnetic resonance in medicine (2007) 57

# MRS Workshop 2022
## Overcoming the Barriers to Clinical Use
### DISCONNECT 2 RECONNECT
22-24 August 2022 @ EPFL, Lausanne, Switzerland

41

Poster no. 7 (on-site poster)

## A simulation study: toward accurate metabolite quantification of short-echo-time 1H MR spectra in LCModel by optimizing the basis set based on the spectral lineshape

**Ying Xiao[1,2,3], Bernard Lanz[1,2], Ivan Tkáč[4], Lijing Xin[1,2]**

1. CIBM Center for Biomedical Imaging, Switzerland  2. Animal Imaging and Technology (AIT), EPFL, Lausanne, Switzerland
3. Laboratory for Functional and Metabolic Imaging (LIFMET), EPFL, Lausanne, Switzerland
4. Center for Magnetic Resonance Research, University of Minnesota, Minneapolis, Minnesota, USA

### Synopsis

In this study, we investigated the short-TE 1H MR spectra quantification accuracy using basis sets with different lineshapes in LCModel through the simulations. Simulation results showed that the estimated metabolite concentrations depend on the linewidths and lineshapes of the basis sets as well as the spectral lineshape. With a basis set that has a similar lineshape to that of the spectrum to be fitted, the quantification accuracy, the scan-rescan reproducibility, and the inter-subject variability can be improved.

### Introduction

Accurate quantification of in vivo short-TE 1H MR spectra provides essential information in cerebral metabolism. LCModel (Stephen Provencher Inc. Oakville, ON, Canada) is one of the frequently used software packages for metabolites quantification through decomposition of the 1H MR spectra into individual metabolite spectra based on the input basis set in the frequency domain.[1] The experimentally acquired spectra are not always of good quality, which affects the quantification accuracy. For example, due to the imperfect shimming, the spectral lineshape may be distorted and vary with measurements. This may introduce the bias, which is different among the measurements[2,3,4]. Therefore, we aim to investigate the influence of spectral lineshape on the accuracy of metabolite quantification and how to improve the quantification accuracy by optimizing the basis sets. The short-TE 1H MR spectra with Lorentzian, Gaussian, Voigt, and experimentally acquired irregular lineshapes were simulated, and fitted with the basis sets that were broadened by the multiple lineshapes.

### Method

All the simulations were performed in MATLAB R2021b (The MathWorks Inc., Natick, MA, USA). The metabolite basis spectra were simulated by the density matrix formalism with chemical shifts and J-coupling constants taken from the literature[6]. The concentrations of metabolites used in simulations were the mean concentrations measured from in vivo human occipital lobe. The experimentally measured macromolecular spectrum[7] was also included in basis sets and in the simulated spectra. Random noise and random spline baseline were added to the simulated 1H MR spectra.
The linebroadening of model functions was achieved in time domain by the four decay functions: (a) Lorentzian; (b) Gaussian; (c) Voigt; (d) real-lineshape (the methyl group of total creatine from the in vivo spectra regarded as the spectral lineshape reference).



**Figure 1**: Estimation errors of concentrations of Glx, tCr, tNAA, tCho measured by basis sets of different linewidths and lineshapes from simulated 1H MR spectra broadened to 12Hz by the Lorentzian, Voigt (FWHM$_g$/FWHM$_v$=0.5), Gaussian functions, and convoluted by one real lineshape function taken from one of in vivo 1H MR spectra at 7T.
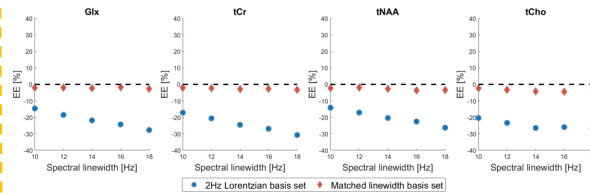


**Figure 2**: EEs versus the spectral linewidths. The spectral lineshape is a typical Voigt (FWHM$_g$/FWHM$_v$=0.5). The matched linewidth basis sets were the basis sets in which all the basis spectra were broadened to the same linewidth of the spectra to be fitted.

| Spectra | basis sets | | Gln | Glu | Ins | Lac | GABA | tCr | tNAA | tCho |
|---|---|---|---|---|---|---|---|---|---|---|
| Irregular | 2Hz lorentzian | EE (%) | -5,8 | -1,4 | -5,1 | -37,3 | 1,3 | -8,2 | 2,5 | -3,2 |
| | | SD of EE (%) | 3,6 | 2,9 | 3,9 | 18,0 | 9,1 | 3,2 | 3,3 | 2,9 |
| | matched | EE (%) | 3,4 | 6,6 | 6,7 | -0,1 | 12,1 | 4,7 | 5,0 | 4,9 |
| | | SD of EE (%) | 0,8 | 0,5 | 0,5 | 6,6 | 3,1 | 0,6 | 0,5 | 2,5 |
| Voigt | 2Hz lorentzian | EE (%) | -3,9 | 1,3 | -3,5 | -38,6 | 16,2 | -6,9 | 5,3 | -2,9 |
| | | SD of EE (%) | 0,8 | 0,6 | 0,6 | 8,8 | 2,8 | 0,6 | 0,5 | 1,6 |
| | matched | EE (%) | 4,4 | 6,6 | 6,3 | -2,0 | 11,5 | 4,5 | 4,8 | 3,3 |
| | | SD of EE (%) | 0,9 | 0,4 | 0,7 | 6,4 | 3,0 | 0,6 | 0,4 | 2,1 |

**Table 1**: EEs of the metabolite concentrations and standard deviations of EEs. All the spectral lineshape were experimentally acquired that derived from the tCr peak at 3.03ppm. Each of the lineshape libraries contained 20 lineshapes. The 2Hz Lorentzian basis set and the matched basis sets (which have the same spectral profile as the simulated spectra) were used to fit in LCModel.

### Result and discussion

The estimated metabolite concentrations are spectral-lineshape, basis-set-lineshape, and basis-set-linewidth dependent as shown in Figure 1. Figure 2 demonstrates large deviations when quantifying the simulated spectra with the typical Voigt lineshape with linewidths exceeding 10 Hz. Using a basis set in which all the basis spectral linewidths are close to the spectral linewidth results approximately in the ground truth. The estimation errors vary with the metabolites, which is more evident in spectra with irregular lineshapes. Table 1 demonstrates that the standard deviations for metabolites with lower concentrations like GABA (9%) and Lactate (18%) are higher for those spectra with irregular lineshapes than for a typical Voigt profile. In the case of the basis set that had the same spectral lineshape as the spectrum to be fitted, the standard deviation of GABA dropped to 3% at the expense of collective overestimation.

### Conclusion

In LCModel, estimation errors of metabolite concentration are highly dependent on the spectral lineshape and the basis sets used to fit the spectra. Considering the real spectral lineshape when preparing the basis sets for each spectrum to be fitted is recommended. In theory, this can reduce the bias of the estimated metabolite concentration caused by the spectral lineshape for short-TE 1H MR spectra when using LCModel.

### Reference

[1] Provencher, S.W., 2001. [2] Near, J., 2013. [3] Dehghani, M., 2020. [4] Lim SI, 2022 [5] Tkáč, I. and Gruetter, R., 2005. [6] Govindaraju, V., Young, K. and Maudsley, A.A., 2000. [7] Tkáč, I., 2009
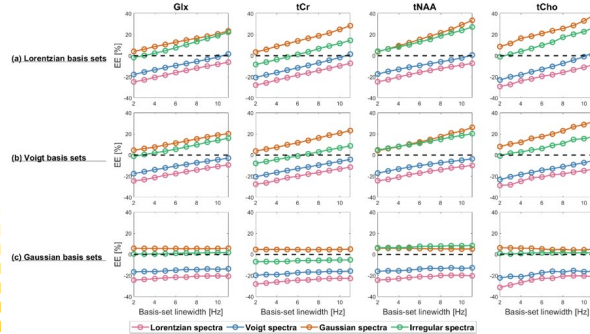
**MRS Workshop 2022**
Overcoming the Barriers to Clinical Use
DISCONNECT 2 RECONNECT
22-24 August 2022 @ EPFL, Lausanne, Switzerland

42

Poster no. 8 (on-site poster)

# Probing the medial temporal lobe with MRS

**Nyman, Axel Karl Gottfrid**[1,2]; Doan, Thanh Pierre[2,3]; Tse, Desmond[4]; Navarro Schröder, Tobias [5]; Bråthen, Geir[1,2]

[1] K. G. Jebsen Center for Alzheimer's research (JCA), Norwegian University of Science and Technology (NTNU), Trondheim, Norway
[2] St Olav's University Hospital, Trondheim, Norway
[3] Department of Neuromedicine and Movement Science, NTNU, Trondheim, Norway
[4] Norwegian 7T MR Center, NTNU, Trondheim, Norway
[5] Kavli Institute for Systems Neuroscience, NTNU, Trondheim, Norway

**Background**

The brain medial temporal lobe (MTL) is severely affected in many disorders such as Alzheimer's disease (AD), which is the most common cause of dementia. AD affects the MTL initially, as manifested by episodic memory and spatial cognition deficits as earliest symptoms [1]. Ground-breaking research in rodents and humans have established detailed neurophysiological correlates of a higher cognitive function in the MTL (i.e. spatial sense) [2, 3]. Although this promises understanding of disease mechanisms affecting the MTL [4], corresponding metabolic processes remain unexplored. Interestingly, high field *in vivo* MR spectroscopy (MRS) has demonstrated that patients developing AD have decreased N-acetylaspartate (NAA) and increased myo-inostiol (ml) in their posterior cingulate cortex before symptom onset, which could provide a window for earlier diagnosis and therapeutic interventions [5]. Furthermore, Transient global amnesia (TGA) is a neurological syndrome whose acute phase present a comparable clinical phenotype to AD [6]. In spite of strikingly similar clinical phenotypes, metabolic changes in AD and TGA pathologies haven't been compared and remain enigmatic.
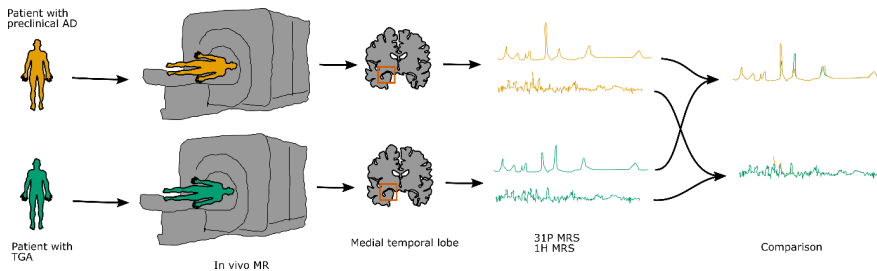


**Methods**

We wish to develop methods for studying the metabolism and neurophysiology of the MTL to decipher function in healthy and pathological states. Using 7T MR, we have found that simultaneous ${}^1$H MRS and fMRI of the MTL in the acute, subacute and recovery phase of TGA is feasible. We aim to use this dataset together with ${}^{31}$P MRS and comparable methods in preclinical AD in order to investigate potential stereotypical metabolic changes during acute and chronic MTL dysfunction.

**References**

1.  Dubois B, Hampel H, Feldman HH, Scheltens P, Aisen P, Andrieu S, et al. *Alzheimer's Dement.* 2016;**12**:292–323.
2.  Moser EI, Moser M-B, McNaughton BL. *Nat Neurosci.* 2017;**20**:1448–64.
3.  Jacobs J, Weidemann CT, Miller JF, Solway A, Burke JF, Wei XX, et al. *Nat Neurosci.* 2013;**16**:1188–90.
4.  Kunz L, Schröder TN, Lee H, Montag C, Lachmann B, Sariyska R, et al. *Science (80- ).* 2015;**350**:430–3.
5.  Waragai M, Moriya M, Nojo T. *J Alzheimer's Dis.* 2017;**60**:1411–27.
6.  Bartsch T, Deuschl G.. *Lancet Neurol.* 2010;**9**:205–14.

MRS Workshop 2022
Overcoming the Barriers to Clinical Use
DISCONNECT 2 RECONNECT
22-24 August 2022 @ EPFL, Lausanne, Switzerland

43

Poster no. 9 (on-site poster)

## Validation, quality control and reproducibility of ^{1}H FID-MRSI on a preclinical 14.1T

D Simicic[1,2,3], B Alves[1,2], J Mosso[1,2,3], Lê T Phong[3,4], J Starcukova[5], A Klauser[1,6], B Strasser[7], W Bogner[7], C Cudalbu[1,2]

[1]CIBM Center for Biomedical Imaging, Switzerland; [2] Animal Imaging and Technology, EPFL, Lausanne, Switzerland;[3] LIFMET, EPFL, Lausanne, Switzerland;[4]HEdS, HES-SO, Geneva, Switzerland; [5] Institute of Scientific Instruments, Czech Academy of Sciences, Brno, Czech Republic;[6]Department of Radiology and Medical Informatics, University of Geneva, Switzerland.;[7]Department of Radiology, MR Center of Excellence, Medical University Vienna, Vienna, Austria

**Introduction:** Availability of UHF, advanced pulse sequences and new encoding methods improved the quality and speed of MRSI[1,2]. At UHF in the clinical setting, ^{1}H FID-MRSI acquisitions are increasingly used[2], but not yet widely applied in the preclinical setting mostly due to the small rodent brain[3]. The low SNR arises from a very small nominal voxel size in rodents (e.g. $0.75x0.75x2mm^3$)[4] while in the human brain it remains fairly big even at high spatial resolution (e.g. $1.7x1.7x10mm^3$)[5]. There are additional challenges in terms of shimming of large volumes with many tissue interfaces, long measurement times[4,6,7], water suppression artifacts and lipid contamination[3]. We recently showed the feasibility of implementing ^{1}H FID-MRSI at 14.1T in the rat brain[8]. In this study we propose to go one step further by implementing an automatic quality control and validating the obtained brain regional difference while additionally testing the reproducibility of the results.



**Methods:** The data were acquired in the rat brain (n=4) at 14.1T (Bruker/Magnex) using a homemade transmit /receive quadrature surface coil. For the high-resolution 2D fast ^{1}H-MRSI, a slice selective pulse acquire sequence was used (TE=1.3ms, TR=813ms, Cartesian k-space sampling, Figure.1A)[8]. The FOV was set to $24x24mm^2$, matrix size to 31x31 with a nominal voxel size of $0.77x0.77x2mm^3$. Shims were adjusted using MAPSHIM. Two datasets with one and two averages were acquired (per animal). Lipid removal was performed using the metabolite-lipid spectral orthogonality approach[9]. All spectra were
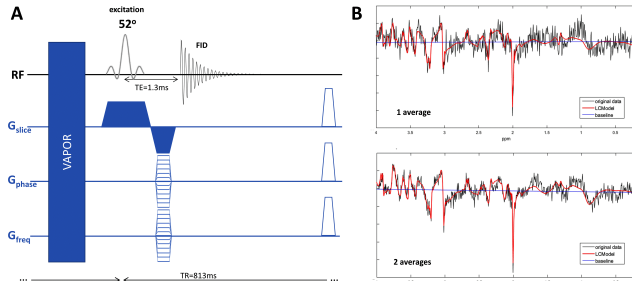
Figure 1. (A) A schematic drawing of the ^{1}H FID-MRSI sequence used for data acquisition (TE=1.3ms, TR=813ms leading to a total acquisition time of 13min for 1 average). (B) The quality of LCModel quantification is shown for one and two averages.

quantified using LCModel (Figure.1B) with a simulated basis set (NMRScope-B/jMRUI[10]) and in vivo MM[8,11]. An automatic quality assessment of the data was implemented using general (power map selection, SNR - 0.75* average SNR and LW - 1.25* average LW) and a metabolite specific (CRLB<40%) criteria. Average of quantifications from nominal voxels in two regions (Figure.2A) within the



MRSI slice were used for validation and reproducibility assessment. Ins and Gln were chosen to be presented due to their known regional distribution in the rodent brain[12].

**Results:** The LCModel quantifications provided reliable fits of the data (Figure.1B) leading to accurate metabolic maps. MAPSHIM proved to be efficient leading to an increased brain coverage (not limited to a standard rectangular volume). This resulted in good quality metabolic maps for a number of metabolites (NAA, Glu, tCho, GABA, Ins, Gln etc.). The obtained metabolic maps were
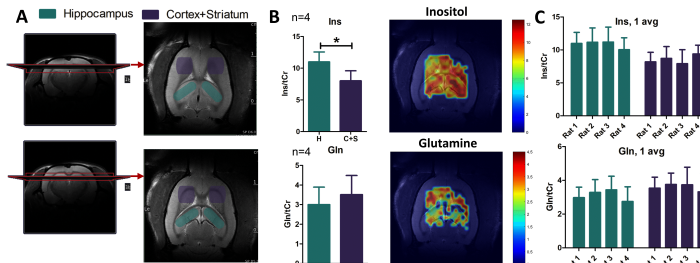
Figure 2. (A) The slice position shown in both axial and coronal directions with marked brain regions within the slice. (B) Regional differences in resulting concentrations of Ins and Gln (average from n=4 animals and up to 28 nominal voxels per animal using the quantifications of 2avg MRSI data, on the left) derived from the metabolic maps (1 animal example, on the right). (C) Reproducibility of metabolite quantifications (Ins and Gln) between 4 different animals/MRSI acquisitions with 1 average.

accurate enough to confirm the previously known[12] brain regional distribution of metabolites (Ins and Gln, Figure.2B). Although the slice thickness was 2mm, we quantified up to 28 region specific nominal voxels, potentially accessing more anatomical/regional in plane information. Despite the small nominal voxel size ($0.77x0.77x2mm^3$) we reproducibly obtain an average SNR~3 for 1avg acquisitions (SNR values from LCModel). Figure.2C confirms the reproducibility of our MRSI acquisition displaying the Ins and Gln concentration ratios obtained from 4 different animals/acquisitions, proving the accurate estimation of these metabolites even with 1avg (13 min).

**Discussion and conclusion:** We presented the first implementation and validation of fast ^{1}H FID-MRSI in the rat brain at 14.1T with an increased brain coverage, reliable, accurate quantification results and metabolic maps which allowed us to highlight the brain regional distribution of metabolites. We showed that our results are reproducible, setting the grounds for a wider application of ^{1}H FID-MRSI in the preclinical setting with a potential for further improvement and acceleration.

[1]De Graaf (2007);[2]Maudsley et al., NMR Biomed (2021); [3]Lanz et al., NMR Biomed (2021); [4]Mlynarik et al., Magn. Reson. Med (2008); [5]Hangel et al., Neuroimage (2018); [6]Cudalbu et al., Metab. Brain Dis. (2013); [7]Delgado-Goni et al., NMR Biomed (2016); [8]Simicic et al., ISMRM 2022. [9]Klauser et al., Magn. Reson. Med. (2019); [10]Starcuk et al, Anal. Biochem (2017); [11]Simicic et al., Magn. Reson. Med. (2021); [12]Tkac et al., Magn. Reson. Med. (2003).

# MRS Workshop 2022
## Overcoming the Barriers to Clinical Use
### DISCONNECT 2 RECONNECT
22-24 August 2022 @ EPFL, Lausanne, Switzerland

44

Poster no. 10 (on-site poster)

## Quantitative assessment of metabolite concentrations in ^{31}P and ^{1}H MRSI: Comparing age and gender related differences

Pilatus[1,4] U, Ludin[2] N, Silaidos[5] C, Wachter[5] L, Matura[3] S, Pantel[2] J, Eckert[5] GP, Hattingen[1] E

[1]Institut für Neuroradiologie, [2]Institut für Allgemeinmedizin, [3]Klinik für Psychiatrie, Psychosomatik und Psychotherapie and [4]Brain-Imaging-Center, Goethe-Universität Frankfurt; [5]Institut für Ernährungswissenschaft, Justus-Liebig-Universität Gießen

**Background & Purpose:** Information of the main signals from ^{1}H MRS refers to metabolite groups: tNAA (N-Acetyaspartate and N-Acetylaspartate-Glutamate), tCho (Glycerophosphocholine and Phosphocholine), tCr (Creatine and Phosphocreatine). In addition, ^{31}P-MRS can be used to quantify the ratio of the choline components and, via absolute concentrations, even the creatine components. We used combined ^{31}P and ^{1}H MRSI to specify age related changes observed for the ^{1}H-MRSI metabolites.

**Methods:** ^{1}H-MRSI and ^{31}P-MRSI data were obtained from 130 healthy volunteers (33 young female, 35 old female, 32 young male and 30 old male; mean age young 26.5; mean age old 71). Data were analyzed from parietal WM and GM. [1]H data were quantified according to [1] while for ^{31}P data an external reference (phosphate solution in phantom) was used applying correction for coil loading regarding the transmit power (to adjust flip angle) and receive sensitivity. Absolute metabolite concentrations were calculated in mmol/l refering to tissue water, which was obtained from segmented anatomical MRI data and published data on water content for GM and WM.

**Results:** Focusing on tCho and tCr we found: The concentration of tCho is significantly lower in young females. while tCr is lower in younger subjects with the lowest concentration in young females. Based on the quantitative analysis we found a choline fraction ($[rCho] = [tCho] – ([GPC] +[PCho])$) which is only visible in ^{1}H MRSI. This fraction is low in young females. Elderly subjects show increased tCr which is accompanied by increased [PCr], while young females exhibit the lowest [Cr] ($[Cr ]= [tCr] – [PCr]$).

**Discussion:** Increased rCho concentration may indicate increased lipid mobility [2], hinting at a higher integrity of the membrane phospholipids in the brain of young females which may be attributed to higher estrogen levels. Increased PCr and tCr concentrations in elderly subjects provide higher buffering capacity for high energy metabolites which may compensate for reduced mitochondrial activity with age.

**Conclusion:** Combined quantitative ^{1}H and ^{31}P MRSI provides new insights into metabolic changes in the brain related to age and gender.

References:

1 Silaidos, C., Pilatus, U., et al.  Sex-associated differences in mitochondrial function in human peripheral blood mononuclear cells (PBMCs) and brain. Biology of sex differences 2018; 9:34
2 Hattingen et al., Combined 1H and 31P spectroscopy provides new insights into the pathobiochemistry of brain damage in multiple sclerosis; NMR Biomed. 2011; 24: 536–546.

**MRS Workshop 2022**
Overcoming the Barriers to Clinical Use
DISCONNECT 2 RECONNECT
22-24 August 2022 @ EPFL, Lausanne, Switzerland

45

Poster no. 11 (on-site poster)

### ^{31}P and ^{1}H MRS for *in vivo* metabolic profiling of diffuse large B-cell lymphoma

Katharina J. Wenger[1-4], Ulrich Pilatus[1-4], Seyma Alcicek[1-4], Florian Buettner[3,4],
Elke Hattingen[1-4], Thomas Oellerich[2-5]

[1] *Institute of Neuroradiology,* [2] *University Cancer Center Frankfurt (UCT),* [3] *Frankfurt Cancer Institute (FCI),* [4] *German Cancer Research Center (DKFZ) Heidelberg, Germany and German Cancer Consortium (DKTK), Partner Site Frankfurt/Mainz,* [5] *Department of Hematology/Oncology, Goethe University, Frankfurt, Germany*

Because of their extreme genetic, phenotypic, and clinical heterogeneity, aggressive lymphomas serve as a model for the dissection of cancers into molecularly distinct subtypes that require different therapeutic strategies. Altered metabolic fingerprints offer novel opportunities on the path to personalizing cancer therapy. Past attempts aiming at metabolic subtyping in patient tumor tissue were met with caution, as *ex vivo* metabolomic studies of tissue can suffer from bias due to the collection procedure and artificial *ex vivo* microenvironment. (Smith et al. 2020). We therefore propose MRS to non-invasively collect metabolic fingerprints of tumor manifestations in patients.

Prior MRS research on lymphoma patients is sparse, both with regard to prognosis and therapy response, and restricted to 1.5T. Several fairly small studies have demonstrated that a wide variety of human cancers (lymphoma among others) show a decrease in the phosphomonoesters (PME) peak of the ^{31}P MR spectrum in the early stages of successful therapy. [31]P MR spectra of tumors before treatment might contain information to predict subsequent tumor response to treatment. (Negendank et al. 1992, Griffiths et al. 2002).

The initiated ^{31}P and ^{1}H MRS study aims to examine patients with superficial lymphnode manifestations of diffuse large B-cell lymphoma (DLBCL) on a 3T MRI Scanner (Siemens MAGNETOM Prisma), using two dual tuned Flex Surface Coils for ^{1}H/[31]P (sizes S and M from RAPID Biomedical GmbH). The protocol includes:

1. [1]H decoupled ^{31}P MR spectroscopic imaging (MRSI) with chemical shift imaging (2D-CSI-FID). 25 mm slice, FOV 320 mm$^2$, 16x16 matrix, extrapolated to 32x32 yielding 10x10x25 mm$^3$ voxel size. NA 4, TR 2 s, 60° flip angle (15 min. total acquisition time)
2. a Single-voxel (SVS) semi-LASER sequence (TE 144 ms, TR 3 s) for detection of lactate, alanine and total choline (5 min. total acquisition time)

As a first step, critical parameters i.e., coil sensitivity, location accuracy and Bo homogeneity were established the on the gluteus minimus muscle in healthy volunteers (mimicking the location of inguinal lymphoma manifestations with regard to its position in relation to subcutaneous fat tissue and hip joint). Figure 1 demonstrates feasibility of the protocol to monitor energy and lipid metabolism in DLBLC.

The ultimate goal is to identify metabolic signatures, some of which have been described in preclinical cohorts e.g., OxPhos-DLBCL compared to „non-OxPhos"-DLBCL with differences in lactate and alanine concentrations (as a surrogate for pyruvate) due to pyruvate dehydrogenase (PDH) enzyme activity. Patient recruitment has just started.
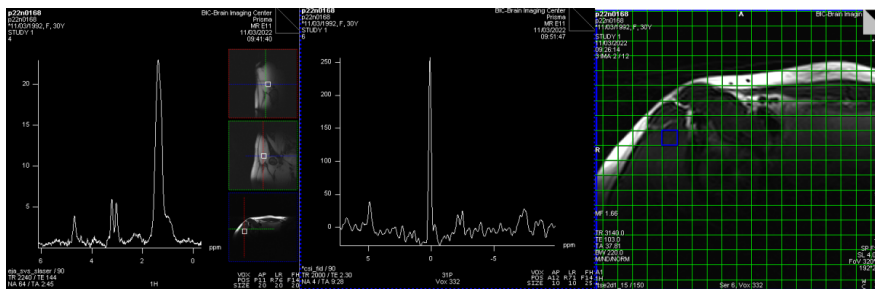


Figure 1: SVS-^{1}H data (left) and 2D-FID-CSI-^{31}P data (middle) from muscle tissue gluteus minimus muscle in healthy volunteers (mimicking the location of inguinal lymphoma manifestations with regard to its position in relation to subcutaneous fat tissue and hip joint). Note the sufficient S/N for detection of phosphomonoesters with ^{31}P MRSI and excellent spectral resolution to discriminate tCho and tCr. The most prominent signals for muscle are lipids at 1.2 ppm in ^{1}H MRS and PCr at 0 ppm for ^{31}P MRSI.

Poster no. 12 (on-site poster)

**Compressed Sensing for 2D-MRSI with Concentric Ring Trajectories at 7 T**

Bernhard Strasser[1], Antoine Klauser[2], Lukas Hingerl[1], Stanislav Motyka[1], Siegfried Trattnig[1], Wolfgang Bogner[1], Ovidiu C. Andronesi[3]

[1]Department of Radiology, Medical University of Vienna, Vienna, Vienna, Austria; [2]Department of Radiology and Medical Informatics, University of Geneva, Geneva, Switzerland; [3]A. A. Martinos Center for Biomedical Imaging, Massachusetts General Hospital, Charlestown, MA, USA

**Introduction:** The clinical usefulness of 1H MR spectroscopic imaging has been shown in many studies, but is held back by its long measurement times. Several acceleration methods have been proposed, e.g. spatio-spectral encoding like concentric ring trajectories (CRT)[1]. However, even CRT sequences can be too slow for 3D MRSI with measurement times≥15 min[2]. Therefore, in this study we test to combine 2D-CRT with compressed sensing (CS), which can be applied to 3D MRSI in the future.



Fig. 1: Undersampling pattern for two acceleration factors.

**Methods**: 2D CRT was measured in a volunteer at 7 T with the following parameters: TR 600 ms; TE 1.3 ms; 840 FID points; spatial resolution 3.4×3.4 mm²; FoV 220×220×12 mm³; 2778 Hz spectral bandwidth; up to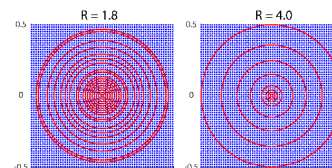 3 variable temporal interleaves; 7 averages; measurement time 4:45 min:s. We used HSVD to partially remove nuisance signal in k-space. Acceleration was simulated by retrospective circle trajectories undersampling (see figure 1). The undersampled data were iteratively reconstructed, using a model including the coil sensitivity profiles, the non-cartesian encoding and Total-Generalized-Variation spatial regularization. All reconstructed data were fitted with LCModel.

**Results**: Figure 2 shows the Glx, tCho and tNAA maps for the gold standard and five different acceleration factors. Figure 3 shows a spectrum from the position marked with a red rectangle in Figure 2 for accelerations 1 (red), 1.8 (blue) and 4.0 (black). Metabolic maps and spectra show high similarity to the ground truth for moderate acceleration (R≤2), but visible differences at higher acceleration.
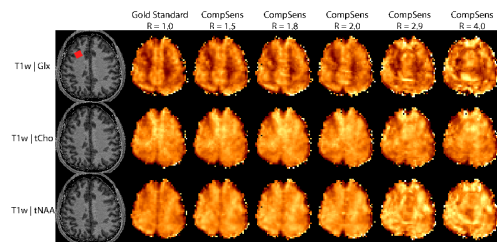


Fig. 2: T1w, Glx, tCho and tNAA maps for the gold standard and five accelerations.
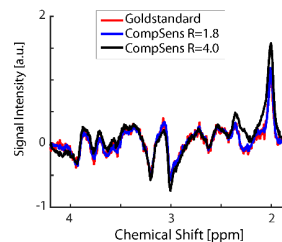


Fig. 3: Spectra for gold standard (red), R=1.8 (blue) and R=4.0 (black).

**Discussion**: We have shown the feasibility of 2D-CRT sequence acceleration with CS for the first time. Higher accelerations (R≥2.9) led to deviations f the ground truth. This is expected, since the measurement time without acceleration was only 5 minutes, and only 32 circles were available for random undersampling. The translation to 3D CRT is thus expected to achieve higher accelerations of at least 3, which represents a significant acceleration e.g. from 15 min to 5 min. Partial nuisance removal was necessary, as otherwise only the water and lipid signal could be reconstructed accurately, but not the metabolites.

**References**:
1. Furuyama et al., DOI: 10.1002/mrm.23184
2. Hingerl et al., DOI: 10.1097/RLI.0000000000000626

MRS Workshop 2022
Overcoming the Barriers to Clinical Use
DISCONNECT 2 RECONNECT
22-24 August 2022 @ EPFL, Lausanne, Switzerland

47

Poster no. 13 (on-site poster)

## Exploring ECCENTRIC sampling variants for accelerated high-resolution MRSI

*Antoine Klauser[a,b,d], Bernhard Strasser[b,c], Wolfgang Bogner[c], François Lazeyras[a,d], Ovidiu C. Andronesi[b]*
*[a]Department of Radiology and Medical Informatics,University of Geneva, Switzerland; [b] Athinoula A. Martinos Center for Biomedical Imaging,Massachusetts General Hospital, Harvard Medical School, Boston,USA [c]High-Field MR Center, Department of Biomedical Imaging and Image-guided Therapy, Medical University of Vienna,Austria [d]CIBM Center for Biomedical Imaging, Switzerland*

**Introduction:** The acquisition of high-resolution MRSI is generally prohibitively long and strategies for accelerating this process are often limited by magnetic field gradient system capacities. ECCENTRIC [1] is a new MRSI sampling strategy that was designed to address both problems by combining actual random k-space under-sampling for compressed-sensing (CS) and trajectories with low demand of gradient slew-rate. By design, ECCENTRIC acquisition are characterized by: the circle radius (CR), CS acceleration factor (CS), matrix size (MS) (See Fig.1 for illustration). These parameters have different impact on the measured signal-to-noise ratio (SNR) and acquisition time (TA) :

| Effect on | SNR | TA |
|---|---|---|
| Circle Radius ↗ | ↘ | ↘ |
| CS Acceleration ↗ | → (image smoothness ↗) | ↘ |
| Matrix Size ↗ | ↘ | ↗ |

While successful in-vivo ECCENTRIC was performed [2] with standard parameters: $CR=k_{max}/4,CS=2$, $MS=64x64x31$, we aim here to explore the variants of ECCENTRIC with different values for these parameters.
**Methods:** 2D FID-MRSI ECCENTRIC was implemented on a 7T MRI Terra (Siemens) with 1.15ms TE, 27° FA and 450ms TR, 2300Hz spectral bandwidth . Acquisitions were performed on a structural metabolite phantom over a 224mm Field-of-View, 10mm slice and with the following matrix size: 48,64,80,96,112. Data were accelerated retrospectively with circle undersampling (CS): 2,4,6,8,10,12 and reconstructed with the CS-SENSE-LR model [1]. ECCENTRIC data were simulated with various SNR values, matrix size: 48,64,80,96,112 and CS: 1,2,3,4,5,6. Finally, 3D FID-MRSI ECCENTRIC data were acquired at a 3T MRI Prisma (Siemens), TE=0.8ms, 27° excitation flip-angle and 450ms TR, 1250Hz spectral bandwidth on a volunteer. 3 protocols with the same TA=14min and MS=42x42x21 were acquired with: $(CR=k_{max}/4,CS=1)$, $(CR=k_{max}/8,CS=2)$ and $(CR=k_{max}/16,CS=4)$. For comparison, these ECCENTRIC acquisitions are 7-fold faster than equivalent Cartesian FID-MRSI with full elliptical sampling (98min).
**Results:** Analysis of the phantom data reveal that CS acceleration performs well with increasing MS despite the loss in SNR (Fig.2). It is assumed that even though the SNR decreases with the voxel volume, the gain in spatial resolution permits a better MRSI reconstruction (with TGV regularization). Simulation data demonstrated the known results that CS acceleration is more efficient with higher SNR for constant MS. Finally the in-vivo data at fixed 14min acquisition demonstrated a very similar metabolite map quality for $(CR=k_{max}/4,CS=1)$ and $(CR=k_{max}/8,CS=2)$ but with a gain in spectral SNR (+41%) thanks to the smaller CR (Fig.2). Acquisition with $(CR=k_{max}/16,CS=4)$ exhibits over-smoothing due to high CS acceleration but with the highest SNR (Fig.2).
**Discussion:** ECCENTRIC is a new sampling strategy for fast and high resolution MRSI that permits acceleration via either CR and CS parameter. These parameters permit to optimize ECCENTRIC sampling based on the type of acquisition (high or low SNR) or the desired spatial resolution and TA.
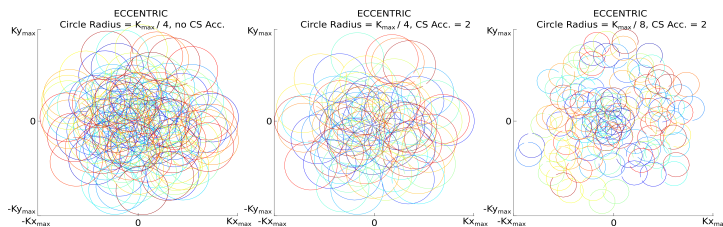


*Figure 1: Examples of ECCENTRIC k-space trajectories with different CR or CS acceleration factors. MS = 48.*
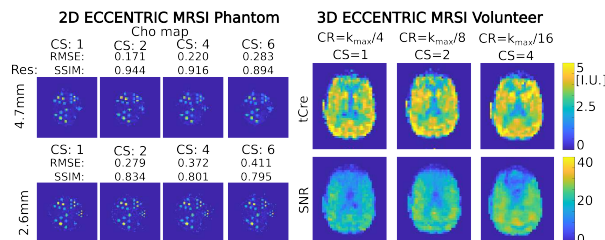


*Figure 2: (Left) ECCENTRIC acceleration performance measured on a phantom with MS =46,80. (Right) Results of the volunteer data acquired with varying CR and CS but same TA=14min.*

[1] A Klauser, et al. ECcentric Circle ENcoding TRajectorIes for Compressed-sensing (ECCENTRIC): A fully random non-Cartesian sparse k-space sampled MRSI at 7 Tesla. ISMRM Annu Meet. 2021 #0835.
[2]A Klauser, et al. Whole-brain high-resolution MRSI at 7T with non-Cartesian FID-ECCENTRIC in glioma patients
. ISMRM Annu Meet. 2022 #4799.

**MRS Workshop 2022**
Overcoming the Barriers to Clinical Use
DISCONNECT **2** RECONNECT
22-24 August 2022 @ EPFL, Lausanne, Switzerland

48

Poster no. 14 (on-site poster)

### Initial experience using spectroscopy in neonates on ultra-high field: a case series.

I.M. van Ooijen[a,b], K.V. Annink[a], J. Dudink[a], F. Groenendaal[a], M. Lequin[b], F. Visser[b], D.W.J. Klomp[b], M.J.N.L. Benders[a], N.E. van der Aa[a], E.C. Wiegers[b] & J.P. Wijnen[b]

*From the Department of [a]Neonatology/[b]Radiology, University Medical Center Utrecht, Utrecht, The Netherlands.*

**Introduction**: Cerebral MRI in infants is usually performed on 3 Tesla MRI. Using 7 Tesla MRI we can potentially increase the spatial resolution and improve the use of advanced imaging, such as MR spectroscopy[1]. MR spectroscopy in neonates at ultra-high field has never been performed before. In this study we show four spectra in neonates with various types of brain damage.

**Methods**: This data is part of the 7 Tesla MRI in neonates study[2-3]. From this dataset we selected four cases with: ischemic lesions (patient A; female; born pre-/dysmature; MRI at 40 weeks GA); an intraventricular hemorrhage (IVH) and thalamus bleeding (patient B; male; born term; MRI at 3 months of age); an extensive ischemic stroke (patient C; female; born term; MRI at 3 months of age) and a patient with SCOT deficiency (i.e. a metabolic disease resulting in episodes of ketoacidosis) (patient D; female; born term; MRI at 42 weeks GA). We acquired single voxel spectroscopy data (sLASER; TE 36 ms; TR 5000 ms; 48 NSA (Patient A) or 64 NSA (Patient B, C, D) with an ROI in the left basal ganglia/thalamic region, with a voxel size of 1.5cm isotropic (Figure 1E). The MR spectra were analyzed with LCModel[4] using 22 simulated metabolites and the simulated macromolecules by LCModel. Creatine (Cr+Pcr) was used as an internal reference for quantification.

**Results:** Patient A, B and C show good quality spectra and shims (Figure 1 A-C; Table 1), e.g. NAA and NAAG can be separated by visual inspection. In these patients all major metabolites were fitted with a CRLB < 20% (Table 1). Linewidths in Patient D are higher, but still acceptable (Figure 1D; Table 1). There were no differences in metabolite levels between patient A, B and C. In patient D the NAA seems lower.

**Discussion and conclusion:** We could acquire good quality MRS data in neonates at ultra-high field MRI. Metabolic profiles of these neonates are fairly similar. We did observe lower NAA levels in the neonate with SCOT deficiency which has been described in other diseases resulting in ketoacidosis before[5-6]. However, this research should be replicated on big scale, to evaluate differences between various neonatal brain pathologies.
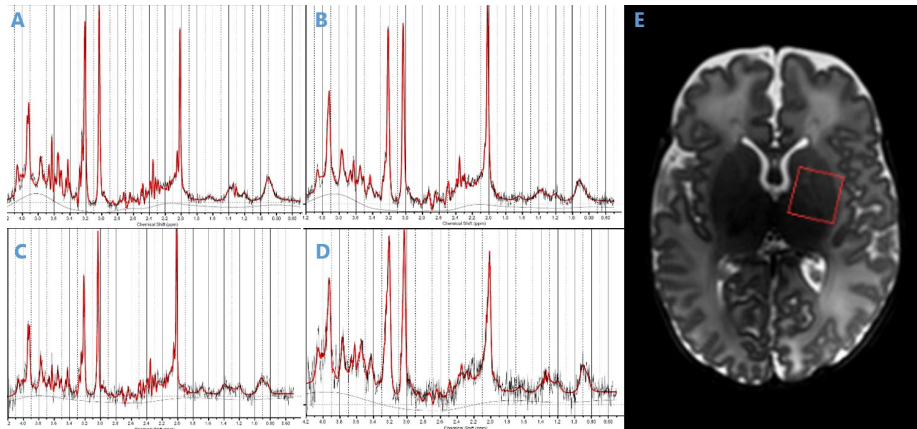


**Figure 1:** MR spectroscopy of the four patients (A-D). MRS voxel placement on 7T in patient A (E).

**Table 1:** Overview of the metabolite levels (/Cr+PCr) (%CRLB), the FWHM and the S/N.

|  | Patient A | Patient B | Patient C | Patient D |
|---|---|---|---|---|
| **Gln** | 0.233 (16%) | 0.202 (24%) | 0.398 (16%) | 0.229 (41%) |
| **Glu** | 0.765 (5%) | 0.961 (4%) | 0.909 (7%) | 0.809 (10%) |
| **GSH** | 0.127 (8%) | 0.151 (7%) | 0.168 (10%) | 0.199 (12%) |
| **Ins** | 0.598 (4%) | 0.459 (5%) | 0.404 (9%) | 0.684 (7%) |
| **Gly** | 0.100 (14%) | 6.1E-02 (24%) | 6.8E-02 (35%) | 6.8E-02 (54%) |
| **Tau** | 0.592 (4%) | 0.403 (6%) | 0.466 (8%) | 0.595 (7%) |
| **NAA+NAAG** | 0.739 (2%) | 1.060 (2%) | 0.937 (3%) | 0.793 (4%) |
| **Glu + Gln** | 0.997 (5%) | 1.163 (5%) | 1.306 (7%) | 1.037 (11%) |
| **Cho + GPC + PC** | 0.721 (2%) | 0.748 (2%) | 0.575 (4%) | 1.155 (30%) |
| **FWHM** | 4.8 Hz | 7.8 Hz | 4.8 Hz | 9.9 Hz |
| **S/N** | 29 | 26 | 17 | 10 |

References:
(1) Dagia & Ditchfield, 2008. Eur J Radiol. 68(2):309-319.
(2) Annink, et al., 2020. Am J Neuroradiol. 41(8):1532-1537
(3) Ooijen et al., 2022. ISMRM.
(4) Provencher. 1993. Magn Reson Med 30, 672.
(5) Wootton-Gorges, et al., 2007. American journal of neuroradiology, 28(5), 895-899.
(6) Cameron, et al., 2014. Diabetes care, 37(6), 1554-1562.

# MRS Workshop 2022
## Overcoming the Barriers to Clinical Use
### DISCONNECT 2 RECONNECT
22-24 August 2022 @ EPFL, Lausanne, Switzerland

49

Poster no. 15 (on-site poster)

## Individual vs combined modeling of macromolecules in rat brain MRS

Wendy Oakden[1], Jamie Near[1,2], Greg Stanisz[1,2,3]

[1]Physical Sciences Platform, Sunnybrook Research Institute, Toronto, Canada, [2]Medical Biophysics, University of Toronto, Toronto, Canada, [3]Neurosurgery and Pediatric Neurosurgery, Medical University of Lublin, Lublin, Poland

**Intro:** Deciding how to acquire and process macromolecular data is difficult as there are many different ways to go about doing it, and any choices may affect the final metabolite concentrations – not always in a predictable way. The consensus recommendation regarding macromolecules is that for short TE they must be included in the basis set, and that they should be quantified based on field strength and acquisition sequence[1]. However, it is not clear whether the macromolecule signals should be combined into a single basis function, or fitted separately. The aim of this work is to compare individual vs. combined modelling of macromolecules in rat brain MRS at 7T.

**Methods:** Macromolecule (MM) data were acquired on a 7T Bruker BioSpec 70/30 (Bruker BioSpin, Ettlingen, Germany) using an 8 cm inner diameter volume transmit coil, and a 20 mm loop receiver coil. Animals were maintained under anesthesia using 1.5-2% isoflurane. A double inversion recovery PRESS sequence[1], with adiabatic hyperbolic secant inversion pulses (12ms, 2000 Hz BW, Bruker calculated with sharpness 3), outer volume suppression, and VAPOR water suppression was used to null the metabolite resonances. Data were acquired in the left cortex+hippocampus in Long Evans rat brain with TR 3s, TE 16ms, inversion times of 1250 and 1550 ms, 1200 averages, 30uL voxels. Each dataset took 1 hour to acquire, and a total of 10 datasets in 5 different rats were combined to achieve adequate SNR. Eddy current correction was performed automatically on the scanner. Each MM spectrum was loaded into MatLab(Natick MA, USA) and FID-A[2] was used to apply a zeroth order phase correction based on the peak between 3.7 and 4.2ppm, remove the water peaks, and average the spectra were averaged. LCModel was used to fit the averaged MM data. The basis set consisted of Creatine (Cr) and Taurine (Tau), along with a set of 17 simulated Voigt lines defined using chsimu using values obtained from the literature, and no ratio priors. Peaks at 0.9, 1.28, and 1.43 ppm were used for referencing, as water had been removed. Positions of the simulated Voigt lines were adjusted iteratively as described by Birch et al. [3]. Fits were loaded in to MatLab and MM peaks were summed to obtain a combined MM signal, omitting the peaks near 0.9 ppm as these varied significantly in size between datasets.

In order to test the MM fitting, data from a different study were used. PRESS data were acquired in the left cortex of 32 male Long Evans rats. Parameters were TR 2.5s, TE 16ms, 1024 averages, 4.5 x 1.4 x 2.0 mm$^3$ voxels, with outer volume suppression and VAPOR water suppression.

Data were analyzed using LCModel, with a basis set consisting of metabolites plus either the combined MM signal, or the optimized set of 17 Voigt lines determined using the MM data.



Rat Brain Macromolecules

**Results:** The fitted MM signal is shown on the right. Comparison of combined and individual MM analyses showed that, with the exceptions of Ace and NAAG, all of the metabolite concentration estimates were correlated. NAA, Gly, Ala, and GABA were all roughly equivalent. The remainder were all either overestimated or underestimated when analyzed using combined vs individual MM signals. Cr, Gln, Glu, GPC, PE, tNAA, and Tau were all overestimated using the individual MMs vs the combined, while Asp, Asc, Glc, GSH, Lac, PCr, PCh, tCr, tCh, and Ins were all underestimated, with examples shown on the right. NAAG was estimated to have a concentration of 0 for all datasets when using the combined MM signal, but values ranged from 0 to 1.5 mM when using the individual MMs.
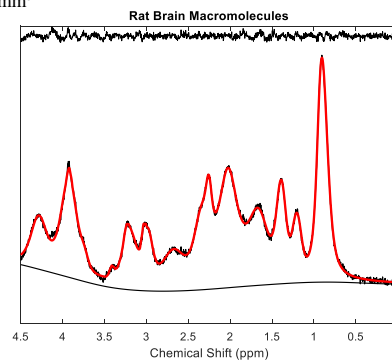
**Discussion:** While the differences in concentrations were small for most metabolites, they were systematic. As it is impossible to measure the ground truth, it is extremely difficult to know which of these methods is more accurate. Additionally, there are many other subtle changes that could be made. Rather than using a single combined MM signal, it might be better to use smaller combinations of MMs which are known to be related. In situations where the MMs are expected to change it will likely be necessary to use individual MMs. However, the standard deviations of metabolite concentrations were increased for most metabolites when using the individual MMs, so it might be best to start by using the individual MMs to check for variability, but, if possible, to fit using the combined MMs.



Total NAA



Total Creatine
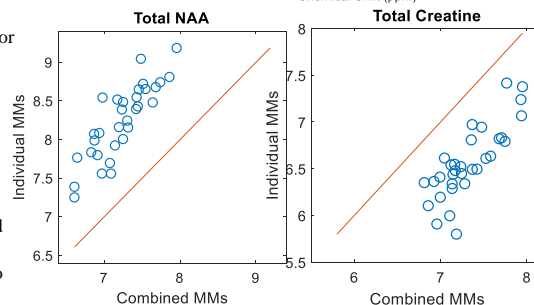
**References:** 1. Cudalbu, C. *et al.* Contribution of macromolecules to brain 1 H MR spectra: Experts' consensus recommendations. *NMR Biomed.* **34**, e4393 (2021). 2. Simpson, R., Devenyi, G. A., Jezzard, P., Hennessy, T. J. & Near, J. Advanced Processing and Simulation of MRS Data Using the FID Appliance (FID-A)— An Open Source, MATLAB-Based Toolkit. *Magn. Reson. Med.* **77**, 23–33 (2017). 3. Birch, R., Peet, A. C., Dehghani, H. & Wilson, M. Influence of Macromolecule Baseline on 1H MR Spectroscopic Imaging Reproducibility. *Magn. Reson. Med.* **77**, 34–43 (2017).

MRS Workshop 2022
Overcoming the Barriers to Clinical Use
DISCONNECT 2 RECONNECT
22-24 August 2022 @ EPFL, Lausanne, Switzerland

50

Poster no. 16 (on-site poster)

**7T [1]H-Magnetic resonance spectroscopy of thalamus and hypothalamus in chronic cluster headache**

Anne Farestveit[1], Tore Wergeland Meisingset[2,3]

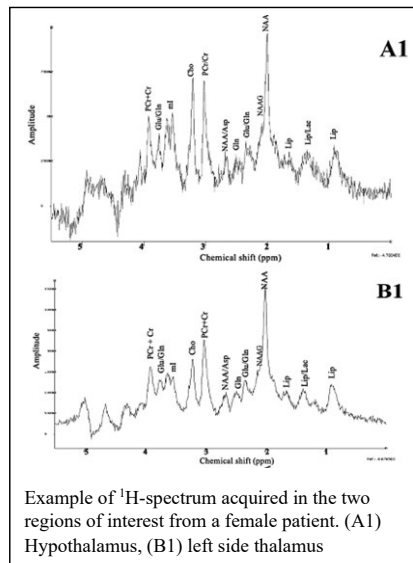[1] Faculty of Medicine and Health sciences, NTNU
[2] Norwegian headache research center (NorHEAD), Institute of neuromedicine and movement science, NTNU
[3] Department of neurology and neurophysiology, St. Olav's university hospital

**Background:** Cluster headache (CH) is a primary headache disorder, classified amongst the trigeminal autonomic cephalalgias. Patients with chronic CH (cCH) undergo frequent, unilateralt, painful attacks with short remission periods. Modulation of thresholds in the trigeminovascular system, the trigeminal autonomic reflex and the hypothalamus seems to be the crucial for pathological mechanisms in CH. In addition, CH patients display anatomical and widespread functional connectivity (FC) abnormalities across multiple networks and multiple cortical and subcortical areas in the brain. The neurotransmitters GABA and glutamate are important for modulating nociceptive information in the hypothalamus, thus making these metabolites central for the understanding pain in CH. The objectives of this study were to investigate feasibility recruiting patients with chronic cluster headache to 7T MR scanning; Investigate spectral ^{1}H 7T MRS quality with a new scan protocol; And compare interictal metabolite concentration between patients and healthy controls in thalamus and hypothalamus.

**Method:** 17 participants, 10 with cCH and 7 controls, were included in the analyses. Hypothalamic and thalamic ^{1}H MRS absolute metabolite concentrations and metabolite ratios from 14 metabolites were collected.

**Results:** When comparing metabolite concentration in thalamus ipsilateral to cluster headache attacks (ipsi-thalamus) in patients with cCH to the average metabolite concentration of healthy volunteers and the thalamus contralateral to pain in cCH patient (contra-thalamus), a significant decrease in NAA in the thalamus ipsilateral to the headache was detected (mean difference -0.44, 95% CI -0.87 – 0.08, p-value=0.022). When restricting comparison to cCH population, NAA difference between ipsi-thalamus and contra-thalamus showed a similar tendency, though not statistically significant (mean contra-thalamus 9,14±0,75, mean ipsi-thalamus 8,65±0,63, mean difference 0,49, 95% CI -0,05 - 1,03, p-value=0.07). This preliminary study could not reproduce the reduction in NAA in hypothalamus of cCH patients, as demonstrated by Wang et al. in eCH.



Example of [1]H-spectrum acquired in the two regions of interest from a female patient. (A1) Hypothalamus, (B1) left side thalamus

**Conclusion:** ^{1}H MRS of thalamus and hypothalamus is feasible and yields high quality spectra. A reduction in NAA in thalamus ipsilateral to cluster headache was demonstrated. No metabolic alterations in the hypothalamus were detected. Study results gives merit to a hypothesis that NAA might be a marker of neuronal dysfunction in the thalamus of patients with cluster headache.

Wang SJ, Lirng JF, Fuh JL, Chen JJ. Reduction in hypothalamic 1H-MRS metabolite ratios in patients with cluster headache. Journal of Neurology, Neurosurgery & Psychiatry. 2006;77(5):622.

MRS Workshop 2022
Overcoming the Barriers to Clinical Use
DISCONNECT 2 RECONNECT
22-24 August 2022 @ EPFL, Lausanne, Switzerland

51

Poster no. 17 (on-site poster)

**Influence of signal-to-noise ratio on quantification of GABA concentration measured noninvasively in the human posterior cingulate cortex with 7 T ultra-short-TE MR spectroscopy**

Guglielmo Genovese[1], Dinesh K. Deelchand[1], Melissa Terpstra[2] and Małgorzata Marjańska[1]
[1]Center for Magnetic Resonance Research, University of Minnesota, Minneapolis, MN, USA.
[2]NextGen Imaging Facility, University of Missouri, Columbia, MO, USA.

**Purpose:** Even though the increased spectral dispersion achieved at ultra-high field permits reliable quantification of γ-aminobutyric acid (GABA) concentrations at ultra-short echo time without editing[1,2], the influence of signal-to-noise ratio (SNR) remains uninvestigated and unclear. This abstract investigated the influence of SNR on a quantification of GABA.

**Methods:** *In-vivo* spectra were acquired at 7 T system (Siemens, Syngo VB17, Erlangen, Germany) using a 16-channel receive-transmit coil and an ultra-short-STEAM sequence (TR = 5 s, TE = 8 ms, TM = 32 ms and 128 shots)[2] from the posterior cingulate cortex of five volunteers (mean ± standard deviation (SD): 21 ± 1 years; two men). Synthetically altered spectra were generated by adding *in-silico* GABA signal to the acquired spectra[3]. The *in-silico* GABA signal was normalized to match the amplitude and linewidth of the LCModel[4]-fitted GABA and intensities were varied over the range: 0%, ± 5%, ± 10%, ± 20%, ± 30%, ± 50%, ± 100%. Four datasets of synthetically altered spectra (Figure 1) were obtained by computing the final spectra with 128, 64, 32, and 16 shots. Measured percent changes in GABA concentrations were linearly regressed as a function of the imposed change in GABA signal for all cases studied. The coefficients of variation ($C_V$ = SD/mean) were reported for all cases studied at each level of the imposed change in GABA signal.

**Results and discussion:** The slopes of the regression lines were 0.98, 0.94, 0.90, and 0.87 respectively for 128, 64, 32, and 16 shots (Figure 2A). Mean GABA concentrations at baseline from the three low-SNR datasets were higher than those from the 128-shot dataset. Absolute Cramer-Rao lower bounds remained constant from -50% to 100% imposed change for all datasets (0.13, 0.15, 0.19, and 0.24 mM, respectively for 128, 64, 32, and 16 shots). The lower SNR data produced an overall overestimation of GABA concentrations and increased $C_V$s (Figure 2B). The reliability of GABA quantification strongly depends on GABA concentration at lower SNR (< 128 shots) since $C_V$s did not remain constant across the imposed changes (Figure 2B). Probably, with 128 shots the linearity of GABA SD is preserved, because LCModel estimates with high accuracy the overlapped neurochemicals with GABA.

**Conclusion:** Decreasing SNR dramatically compromises reliability of GABA evaluations.

**References:** [1] Tkáč I *et al.*, Magn. Reson. Med. (2001); [2] Marjańska M *et al.*, Neuroscience (2017); [3] Deelchand DK *et al.*, NMR Biomed. (2016); [4] Provencher SW, Magn. Reson. Med. (1993).
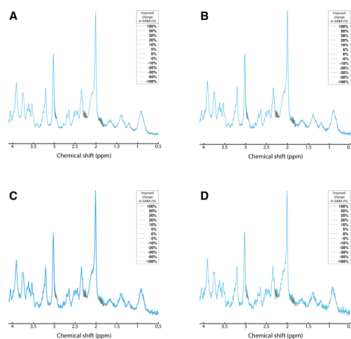
**Figure 1. Synthetically altered spectra.** Examples of synthetically altered spectra generated using (A) 128, (B) 64, (C) 32, and (D) 16 shots from one subject. Contributions of GABA resonances are shown with different colors. Spectra are shown without apodization and with the same vertical scale, normalized to the signal intensity at 0.90 ppm.
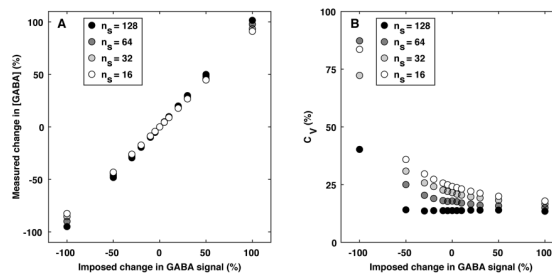
**Figure 2. Influence of SNR on GABA quantification.** (A) Mean values of measured percent changes and (B) $C_V$s of GABA concentration. The synthetically altered spectra with 128, 64, 32, and 16 shots (number of shots, $n_s$), are plotted *versus* imposed change in GABA signal

Poster no. 18 (on-site poster)

**Neurochemical profile of major depressive disorder in adolescents: 7 T MRS study**

Guglielmo Genovese[1], Paul E. Croarkin[2], and Małgorzata Marjańska[1]
[1]Center for Magnetic Resonance Research, University of Minnesota, Minneapolis, MN, USA.
[2]Department of Psychiatry and Psychology, Mayo Clinic, Rochester, MN, USA.

**Purpose:** Major depressive disorder (MMD) in adolescence is a substantial public health problem and it increased with the onset of the COVID-19 pandemic[1]. Existing treatment approaches are often ineffective and do not target relevant neurobiological markers[2]. However, it has been hypothesized that the neurobiological mechanism underlies MMD involves a dysfunction of the neurotransmitters glutamate (Glu) and γ-aminobutyric acid (GABA)[3]. So far, $^1$H-MRS studies in patients with MDD have reported inconsistent results[4-6], probably because findings are biased by different regions of interest, magnetic field strengths, and MRS sequences. To our knowledge, this is the first study, which compares the neurochemical profile from the occipital lobe of adolescents with MDD and healthy volunteers (HV) acquired at 7 T.
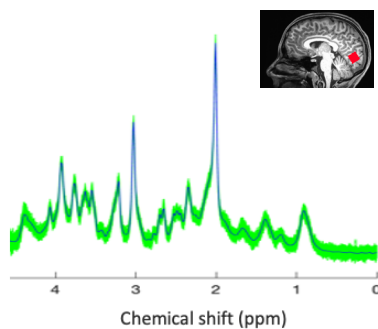
**Methods:** *In-vivo* spectra were acquired on 7 T system (Siemens, Syngo VB17, Erlangen, Germany) using a quadrature surface coil and an ultra-short-STEAM sequence (TR = 5 s, TE = 8 ms, TM = 32 ms and 128 shots) in twenty-two MDD (mean ± standard deviation (SD): 16 ± 2 years; ten men) and in nineteen HV (16 ± 2 years; eight men). $B_0$ shimming was performed in the VOI[7](8 ml). Spectra were individually saved (spectral width: 6 kHz; 2048 complex points) and post-processed with phase and frequency correction. Non-suppressed water spectra were acquired for eddy-current correction and as internal reference in LCModel[8]. Quantification of GABA, Glu, Gln, NAA, NAAG, and Cr+PCr (tCr) were corrected for gray matter (GM), white matter (WM), and cerebral spinal fluid (CSF) content. Unpaired t-tests were performed to assess which metabolites exhibited significant difference between MDD and HV.

**Results and discussion:** High signal-to-noise ratios (340 ± 60) and narrow linewidths (12 ± 1 Hz) were obtained in both groups (Figure 1). No thresholds based on Cramer-Rào lower bounds (CRLBs) of metabolites were used[9]. Mean values, SDs and CRLBs for metabolites of interest are reported in Table 1. No significant differences were observed between groups for metabolite concentrations. These findings are in agreement with a previous study[6], which investigated metabolic differences in pregenual anterior cingulate cortex of adult MDD *versus* HV at 7 T with a similar group size than this current abstract. However, data reported are preliminary (acquisitions are still in progress) and current conclusion could be influenced by the small group size. GABA difference, which is a major interest in this work, smaller than 10 % is expected to be detectable with a group size larger than 40 individuals per group.

**Conclusion:** Although these results are not completely surprising, a larger cohort may reveal significant difference in GABA.

**References:** [1] L Lebrun-Harris *et al.*, JAMA Pediatr. (2022), [2] D Warden *et al.*, Curr. Psychiatric Rep. (2007), [3] W Shamseddeen *et al.*, J. Am. Acad. Child. Adolesc. Psychiatry (2011), [4] P Bhattacharyya *et al.*, Front. Psychiatry (2021), [5] J Levitt *et al.*, J. Psychiatry Neurosci. (2019), [6] J Evans *et al.*, AMCN (2018), [7] R Grutter *et al.*, Magn. Res. Med. (2006), [8] SW Provencher, Magn. Res. Med. (1993), [9] R Kreis, Magn. Res. Med. (2016).



| | MDD | | HV | |
|---|---|---|---|---|
| | Conc. (mM) | CRLB (mM) | Conc. (mM) | CRLB (mM) |
| GABA | 1.0 ± 0.1 | 0.1 | 1.0 ± 0.3 | 0.1 |
| Glu | 9.2 ± 0.4 | 0.2 | 9.2 ± 0.5 | 0.2 |
| Gln | 2.6 ± 0.2 | 0.1 | 2.6 ± 0.3 | 0.1 |
| NAA | 11.4 ± 0.4 | 0.1 | 11.5 ± 0.4 | 0.1 |
| NAAG | 1.4 ± 0.2 | 0.1 | 1.6 ± 0.2 | 0.1 |
| tCr | 8.1 ± 0.3 | 0.1 | 8.2 ± 0.2 | 0.1 |
| GM (%) | 69 ± 2 | | 66 ± 3 | |
| WM (%) | 24 ± 2 | | 26 ± 5 | |
| CSF (%) | 7 ± 1 | | 7 ± 2 | |

**Figure 1. *In-vivo* spectrum in MDD.** 128 shots (green) and the mean spectrum from one representative participant with MDD after post-processing, which shows great spectral quality. Shots and mean spectrum are shown without apodization. Inset: location of the 2x2x2-cm$^3$ VOI shown on the MPRAGE image acquired at 3 T.

**Table 1. Neurochemical concentration in MDD and HV.** Mean values ± standard deviations, and CRLBs are reported for GABA, Glu, glutamine (Gln), *N*-acetylaspartate (NAA), *N*-acetylaspartylglutamete (NAAG), and creatine + phosphocreatine (tCr = Cr + PCr). Content of GM, WM, and CSF of the VOIs are also reported

# MRS Workshop 2022
## Overcoming the Barriers to Clinical Use
### DISCONNECT 2 RECONNECT
22-24 August 2022 @ EPFL, Lausanne, Switzerland

53

Poster no. 19 (on-site poster)

**Hyperpolarization of 129Xe gas via dissolution DNP: beneficial tips and tricks**

*Emma WISTRÖM (1), Andrea Capozzi (1), Thanh Phong Lê (1,2), Rolf Gruetter (1), Jean-Noël Hyacinthe (2).*
*(1) Laboratory of Functional and Metabolic Imaging, EPFL (Swiss Federal Institute of Technology in Lausanne), Lausanne, Switzerland*
*(2) Geneva School of Health Sciences, HES-SO University of Applied Sciences and Arts Western Switzerland, Geneva, Switzerland*

Dissolution DNP (dDNP) is an alternative for hyperpolarizing $^{129}Xe$ to the well acknowledged method spin exchange optical pumping (SEOP)[1]. As opposed to SEOP, DNP takes place in the solid state at very low temperatures, which can potentially produce a large volume of hyperpolarized gas after dissolution. In this study, by implementing a new way of preparing the sample, we ease the overall process and establish a superior incorporation of the gas atoms into the solvent. Additionally, due to a surprisingly short radical electron $T_1$, we show that a higher polarization was achieved by applying microwave frequency modulation. Sample preparation of $^{129}Xe$ for DNP had superior incorporation of the gas atoms into the solvent with the help of ultrasonication. A higher polarization was achieved by applying microwave frequency modulation. Acquired DNP profiles Fig.1. Microwave FM efficiently enhanced the polarization on both samples, causing higher polarization levels and decreasing the buildup time (Fig.2A). Ultrasonic mixing did not have an effect on the initial polarization rate compared to manual mixing, but resulted in a substantially higher polarization level (Fig.2b). Furthermore, ultrasonic mixing resulted in a 29% longer apparent $T_2$ in on the NMR FID signal (Fig.3). The radicals electronic properties of TEMPO were drastically influenced by the sample matrix. In isobutanol, the $T_{1e}$ was only 29.7ms compared to about 150ms in a classical water:glycerol matrix, and further halved by the addition of Xe to the sample (Fig.4). Xenon hyperpolarized via DNP could be successfully extracted and measured in the gas-state (Fig.5).

[1] G. Norquay, G. J. Collier, M. Rao, et al. 129Xe-Rb Spin-Exchange Optical Pumping with High Photon Efficiency. *Phys. Rev. Lett*. 2018; **121**

Figure 1


Figure 2


Figure 3


Figure 4


Figure 5

# MRS Workshop 2022
## Overcoming the Barriers to Clinical Use
### DISCONNECT 2 RECONNECT
22-24 August 2022 @ EPFL, Lausanne, Switzerland

54
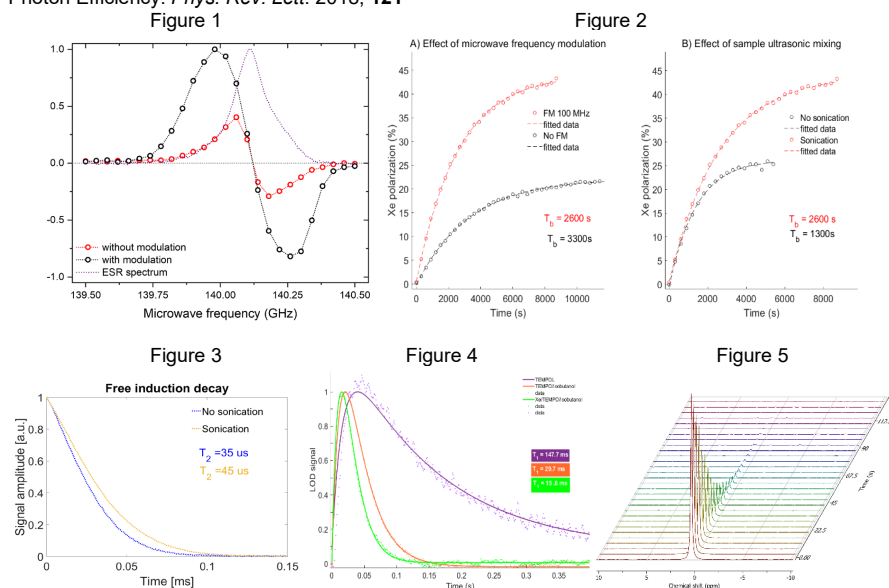
Poster no. 20 (on-site poster)

## A dictionary-based approach for the determination of pH values using $^{31}$P MRS

Vanessa L. Franke[1,2], Johannes Breitling[1], Renate Bangert[1], Mark E. Ladd[1,2,3], Peter Bachert[1,2], and Andreas Korzowski[1]

[1]Division of Medical Physics in Radiology, German Cancer Research Center (DKFZ), Heidelberg, Germany
[2]Faculty of Physics and Astronomy, University of Heidelberg, Heidelberg, Germany
[3]Faculty of Medicine, University of Heidelberg, Heidelberg, Germany

### Introduction

The pH value of living tissue is a valuable biomarker for numerous pathologies, e.g. cancer, and can be non-invasively determined by $^{31}$P MRS. As gold standard, the pH-dependent chemical shift of inorganic phosphate ($P_i$) is used for pH calculation via a modified Henderson-Hasselbalch equation, assuming physiological conditions[1]. However, challenges of this method are (I) altered ion homeostasis in pathologies and (II) the low signal of $P_i$ in vivo.

In this work, we present results of preliminary work on a dictionary-based approach for the estimation of pH applicable for various chemical conditions using not only one, but multiple chemical shifts of $^{31}$P compounds. We demonstrate the feasibility of this approach on a limited subspace using the chemical shifts of adenosine-5'-triphosphate (ATP) and their dependencies on pH and [$Mg^{2+}$].

### Methods

A total of 154 model solutions with a base concentration of 5mM $P_i$, ATP and phosphocreatine (PCr) were prepared with different pH values and different concentrations of Mg, Na and K. $^{31}$P spectra of all model solutions were acquired at a 9.4T small-animal scanner (Bruker BioSpec) with an unlocalized FID sequence while temperature was maintained at 37°C. Evaluation of data was performed in MATLAB R2020a (The Mathworks). The chemical shifts of PCr, $P_i$ and ATP were quantified using a home-built implementation of the AMARES algorithm[2,3].

For demonstrating the concept, we focused on a subset of 24 model solutions with [$Na^+$] = 29mM, [$K^+$] = 160mM, and the limited pH range [6.8–7.4], for which the dependency of the chemical shifts $\delta_i$ of ATP on the pH value and the ratio R=[$Mg^{2+}$]/[$ATP^{4-}$] can be described by empirically developed approximations of the Hill equation:

$$\delta_i(pH, R) = k - \frac{m \cdot (pH - 7.1) + b}{1 + e^{d \cdot R}} , \quad i = \alpha, \beta, \gamma. \tag{1}$$

Equation (1) was fitted to the quantified chemical shifts of γ, α and β-ATP, resulting in three defined functions $\delta_\gamma$(pH, R), $\delta_\alpha$(pH, R) and $\delta_\beta$(pH, R). These relations define the dictionary, allowing for an assignment of input values $\delta_{\gamma,input}$, $\delta_{\alpha,input}$, $\delta_{\beta,input}$ to possible pairs of pH and R values.

To incorporate uncertainties in the input chemical shifts $\sigma_{\delta_i}$, (assumed to be 0.01 ppm), pH was calculated as a normal probability density function ($N(\mu, \sigma^2)$) using Gaussian error propagation. The estimated pH value is then obtained as the weighted mean pH with the weighted standard deviation as error estimate.

### Results

The acquired spectra from the model solutions were of good quality, enabling a robust quantification of the chemical shifts of all contained metabolites and showing clear spectral changes with changing pH (Fig. 1) and R.

The obtained relations $\delta_i$(pH,R) were used to calculate probability density functions $P_i$(pH,R) for specific input values $\delta_{i,input}$. For the shown example (Fig. 2), the estimated values $pH_{est}$ = 7.25 ± 0.05 (with $R_{est}$ = 0.77 ± 0.01) are in good agreement with the prepared conditions $pH_{prep}$ = 7.2 and $R_{prep}$ = 0.75.

When applying this method to all datasets of the shown subspace, the estimated pH values are in good agreement with the prepared values for datasets with small R (Fig. 3). For the datasets with higher R, the estimated pH values deviate more strongly from the prepared values.

### Discussion and Conclusion

We present initial results of the preliminary work on a dictionary-based approach for pH estimation using $^{31}$P MRS under various chemical conditions and demonstrated its feasibility for a limited subspace using the chemical shifts of ATP and their dependencies on pH and Mg. Further refinement and extension of the dictionary by other influences, is, however, required for potential application to in vivo data.



Figure 1: Representative $^{31}$P spectra of the model solutions of the chosen subset. Spectral variation with changing pH is shown for fixed R. spectra were acquired with TR=0.3s, FA=20°, BW=10kHz, 2018 spectral points, averages = 1024, $T_{meas}$ = 5 min.



Figure 2: Estimation of pH based on the proposed dictionary approach for one specific example. Calculated probability density functions $P_i$(pH,R) are shown for the measured chemical shifts $\delta_{input}$, as well as the joined probability density function P(pH, R).



Figure 3: Performance of pH estimation via the proposed dictionary-based approach for the entire chosen subset. Estimated pH values (red dots) are compared with prepared values (black dots).

1. de Graaf RA. In Vivo NMR Spectroscopy: Principles and Techniques: 2nd Edition.; 2007. doi: 10.1002/9780470512968.
2. Vanhamme L, et al. AMARES. J. Magn. Reson. 1997;43:1–2.
3. Korzowski A, et al. Magn. Reson. Med. 2020;84:1707–1723 doi: 10.1002/mrm.28255.

**MRS Workshop 2022**
Overcoming the Barriers to Clinical Use
DISCONNECT 2 RECONNECT
22-24 August 2022 @ EPFL, Lausanne, Switzerland

55

Poster no. 21 (on-site poster)

**Reduced glutamate levels correlate with decreased functional connectivity between the central visual field projection in V1 and V4 after central vision loss from Stargardt Macular Dystrophy**

A.A. Sheldon[1], J. K. Jolly[1,2,3,4], I.B. Ip[1], H.E. Willis[1], W.T. Clarke[1], S. Jbabdi[1], S.M. Downes[2,3], H. Bridge[1]

[1] Oxford Centre for Functional Magnetic Resonance Imaging of the Brain (FMRIB), Wellcome Centre for Integrative Neuroimaging (WIN), Nuffield Department of Clinical Neuroscience, University of Oxford, Oxford, United Kingdom, OX3 9DU. [2] Nuffield Laboratory of Ophthalmology, Nuffield Department of Clinical Neuroscience, University of Oxford, Oxford UK. [3] Oxford Eye Hospital, Oxford University Hospitals NHS Foundation Trust, Oxford, UK. [4] Vision and Eye Research Institute, Anglia Ruskin University, Cambridge, UK.

Stargardt Macular Dystrophy (STGD1) causes retinal degeneration predominantly affecting the cone photoreceptors, resulting in loss of central vision and colour vision. Understanding how this loss affects cortical visual processing will be important for evaluating outcomes following therapy to restore retinal function. The retinotopic organisation of the visual cortex allows us to compare regions of the visual cortex that are affected or unaffected by STGD1. Here we used resting state functional connectivity to determine the relationship between ventral visual region V4 (involved in colour processing) and the posterior region of the primary visual cortex (V1), representing the central visual field and the anterior region reflecting the periphery. These measures of functional connectivity were then correlated with the concentration of neurometabolites glutamate, NAA and myo-inositol (*myo*-Ins) measured using magnetic resonance spectroscopic imaging (MRSI).

Sixteen STGD1 participants (age 36.8 ± 16SD) and 16 controls (age 39.7 ± 14.7SD) undertook a 3T MRI session that included DW-CRT MRSI acquired over the calcarine sulcus (3 runs, resolution=5x5x10mm, FOV=240x240x15mm, TR:1350ms, TE:32ms) and resting state fMRI (TR:1355ms, TE:32.4ms, 2mm$^3$, 72 slices, orientated axially, 644 volumes). MRSI data were analysed with FSL-MRS, and NAA, *myo*-Ins and glutamate relative to total creatine (:tCr) were quantified for each individual voxel (Clarke et al., 2021). Neurometabolite concentrations for all voxels within V1 were then averaged to give a mean concentration for each neurometabolite. FMRI data were pre-processed using principal component analysis (Beckmann and Smith, 2004) with FSL. The mean timeseries for anterior and posterior V1 were regressed as seed-regions in FEAT to generate cortical connectivity maps. The mean BOLD activation within V4 was correlated with seed-region timeseries from the connectivity maps using *featquery* in FSL. Neurometabolite concentrations were then correlated with the functional connectivity between V4 and anterior and posterior V1 separately.

Functional connectivity was significantly reduced for STGD1 compared to controls between posterior V1 and V4 ($F_{(1, 16)}$=63.00, p>0.01) but not between anterior V1($F_{(1,15)}$=63.00, p=0.06) and V4. Glutamate concentration was significantly lower for STGD1 compared to controls between posterior V1 and V4 ($F_{(1,9)}$=48.00, p>0.01) but not for anterior V1 and V4 (($F_{(1,13)}$=48.00, p=0.98). Glutamate concentration were correlated significantly with functional connectivity between posterior V1 and V4 ($R^2$=0.09, p=0.02), but not with connectivity between anterior V1 and V4 ($R^2$=0.02,p=0.35; Fig 1A). Neither NAA, nor *myo*-Ins concentrations correlated with the measures of functional connectivity between V4 and either posterior (NAA (Fig 1B): $R^2$=0.01, p=0.56; *myo*-Ins (Fig 1C): $R^2$=0.01, p=0.44) or anterior (NAA: $R^2$=0.03, p=0.22; *myo*-Ins: $R^2$=0.01, p=0.74) V1.
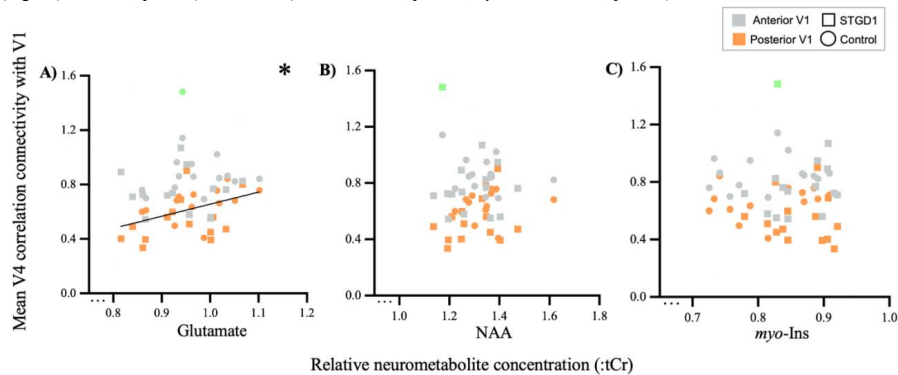


*Figure 1: Mean glutamate (A) (:tCr), NAA (:tCr) (B) and myo-Ins (:tCr) (C) levels within V1 correlated with functional connectivity between anterior (grey) and posterior (orange) V1 and V4. Individual data points for controls (circles) and STGD1 (squares) are plotted with lines of best fit and asterisks to represent significance. Graphs include outliers (green) removed from the statistical analysis.*

Lower glutamate levels are related to decreased functional connectivity between posterior V1 and V4. This may reflect the central vision loss and reduced colour perception present in STGD1. NAA and *myo*-Ins, markers of neuronal degeneration, did not show this relationship with functional connectivity which suggests that changes are linked to neuronal excitation rather than degeneration.

Beckmann, C. F., and S. A. Smith, 2004, Probabilistic independent component analysis for functional magnetic resonance imaging: Ieee Transactions on Medical Imaging, v. 23, p. 137-152.

Clarke, W. T., C. J. Stagg, and S. Jbabdi, 2021, FSL-MRS: An end-to-end spectroscopy analysis package: Magnetic Resonance in Medicine, v. 85, p. 2950-2964.

MRS Workshop 2022
Overcoming the Barriers to Clinical Use
DISCONNECT 2 RECONNECT
22-24 August 2022 @ EPFL, Lausanne, Switzerland

56

Poster no. 22 (on-site poster)

**The association between stress-induced changes in dACC GABA levels and heart rate variability: a 7T 1H-MRS study.**

A. Kaiser[1], L. Reneman[1], P.J. Lucassen[2,12], A.M. Kaag[3], W. van der Zwaag[4], T. Jurhar[1,5], C. Kirschbaum[6], O.A. van den Heuvel[7,8], E.J. Hermans[9], H.L. Tan[10,11], A. Schrantee[1,12]

1 Amsterdam UMC, University of Amsterdam, Department of Radiology and Nuclear Medicine, Amsterdam Neuroscience, the Netherlands; 2 Brain Plasticity group, Swammerdam Institute for Life Sciences, University of Amsterdam, Amsterdam Neuroscience, the Netherlands; 3 Vrije Universiteit Amsterdam, Department of Clinical, Neuro and Developmental Psychology, Amsterdam Neuroscience, the Netherlands; 4 Spinoza Centre for NeuroImaging, Royal Dutch Academy of Sciences, Amsterdam, the Netherlands; 5 University of Veterinary Medicine, Vienna, Austria; 6 Technical University of Dresden, Department of Psychology, Dresden, Germany; 7 Amsterdam UMC, Vrije Universiteit Amsterdam, Department of Psychiatry, Amsterdam Neuroscience, the Netherlands; 8 Amsterdam UMC, Vrije Universiteit Amsterdam, Department of Anatomy and Neuroscience, Amsterdam Neuroscience, the Netherlands; 9 Radboud university medical center, Donders Institute for Brain, Cognition and Behaviour, Nijmegen, the Netherlands; 10 Amsterdam UMC, University of Amsterdam, Department of Clinical and Experimental Cardiology, Amsterdam, the Netherlands; 11 Netherlands Heart Institute, Utrecht, The Netherlands; 12 Center for Urban Mental Health, University of Amsterdam, The Netherlands

**Background:** Stress affects our body and brain in many ways. It can strongly impact mental, but also cardiovascular health. Sudden cardiac death (SCD), for instance, has been associated with stress exposure and may be triggered by a disrupted autonomic nervous system (ANS) control of the heart. How exactly the ANS controls cardiac physiology remains however unclear. In particular, the gamma-aminobutyric acid (GABA) system can modulate anxiety and stress responses in both the brain and heart [1]. A previous study found that GABA-levels significantly decreased after induced anxiety compared to a control condition [2], although another study could not replicate this [3]. Furthermore, withdrawal from GABA agonists (e.g., baclofen) can induce Takotsubo cardiomyopathy, potentially resulting from a sudden decrease in GABA-ergic signalling [4].

**Study design:** We investigated the effects of an established stress paradigm on GABA-levels in the dorsal anterior cingulate cortex (dACC). We used 7T dynamic MRS, while at the same time assessing heart rate variability (HRV) and saliva cortisol. Fifty-six healthy adult male volunteers (mean age = 24.1 years) were stratified into a stress and control condition. Groups were matched on age, IQ, drug use and score on the Perceived Stress Scale. We obtained interleaved dynamic MRS data and functional magnetic resonance imaging (fMRI) data. MRS parameters were: sLASER localization, VAPOR water suppression, TR/TE=3600/36ms, dACC voxel size=18x18x25mm, HOS-DLT shim. MRS and fMRI scans and HRV parameters were obtained before and after the stress/control intervention. The stress group underwent the MRI-compatible, socially-evaluated cold pressor task (SECPT) and a mental arithmetic task, the control group underwent an appropriate non-stressful control procedure using warm water and a corresponding easier arithmetic task [5].

**Analysis:** Linear mixed models in R were used to assess between-group differences. LC-Model was used for fitting using a basis-set with 23 metabolites and a measured MM baseline. HRV was operationalized as the root mean square of successive differences (RMSSD).

**Results:** The preliminary results show a significant increase in cortisol levels in the stress condition (p=0.02). Our data hint towards the opposite of our hypothesis, namely higher GABA levels in the dACC (p=0.03) and an increase in HRV after stress induction (p=0.03; peaking at ~22 min; Figure 1). No changes in glutamate levels were found (p=0.56).

**Discussion:** Prevention of sudden cardiac death has so far been hampered by a lack of knowledge of the underlying neural mechanisms. Further analysis should provide us with an explanation of why we observed an increase rather than a decrease in GABA levels. When replicated in chronic stress situations (e.g., patients suffering from anxiety disorders), these results may help develop novel targets for preventive strategies and treatments.
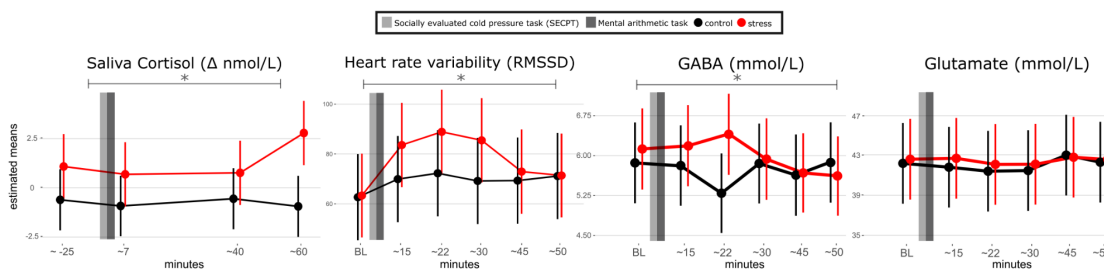


**Figure 1.| Outcome measures.** Estimated marginal means and confidence intervals at the measured time points in minutes after the start of the intervention are shown for the stress condition in red and the control condition in black. Significant interaction effects between time and condition are indicated with a gray bar and an asterix on top (*; p<0.05).

**References:** [1] Delli Pizzi, S., et al., 2017, Brain Structure and Function, 22(7), 3217-3229. [2] Hasler, G. et al., 2010, American Journal of Psychiatry, 167(10), 1226-1231. [3] Houtepen, L. C., et al., 2017., NeuroImage: Clinical, 14, 195-200. [4] Levy, J., et al., 2016, Annals of Physical and Rehabilitation Medicine, 59, 340-342. [5] Vogel, S., et al., 2015., Biol. Psychiatry, 78, 830–839.

# MRS Workshop 2022
## Overcoming the Barriers to Clinical Use
### DISCONNECT 2 RECONNECT
22-24 August 2022 @ EPFL, Lausanne, Switzerland

57

Poster no. 23 (on-site poster)

**Repeatability of APTw imaging at 3T and 7T MRI**

Iris Obdeijn[1], Maarten Lequin[1,2], Sabine Plasschaert[2], Wybe van der Kemp[1], Hans Hoogduin[1], Dennis Klomp[1], Jannie Wijnen[1] and Evita Wiegers[1]

[1]Department of Radiology and Nuclear Medicine, University of Medical Centre Utrecht, Utrecht, the Netherlands
[2]Department of paediatric neuro-oncology, Princess Maxima Centre, Utrecht, the Netherlands

**Introduction**

Amide proton transfer weighted (APTw) imaging is a potential imaging biomarker to assess treatment effects in brain tumours [1][2]. The improved signal-to-noise-ratio and spectral resolution and prolonged $T_1$ relaxation time at 7T would enable the acquisition of APTw imaging with a higher resolution compared to 3T; which is relevant for the monitoring treatment effects in inherently heterogeneous brain tumours [3][4][5]. However, 3T MRI is more widely used in clinical practice. Embedding of APTw imaging in clinical decision making requires insight in the repeatability of APTw imaging. Therefore, we evaluated the repeatability of APTw imaging at both 3T and 7T.

**Methods**

APTw images were obtained at 3T MRI (Ingenia Elition X, Philips Healthcare) and 7T MRI (Achieva, Philips Healthcare) with a dedicated head coil. The APTw images were acquired with a 3D turbo spin echo (3T) or 3D gradient echo sequence (7T), both with 35 frequency offsets. Imaging parameters at 3T: saturation time= 2s; $B_1$= 2.0 µT; recon voxel size= 0.9x0.9x6.0 mm$^3$ ; TE=8.3 ms. Imaging parameters at 7T: saturation time=1.4s; $B_1$= 2.1 µT; recon voxel size=1.8x1.8x2.0 mm$^3$; TE=1.8 ms.

APTw images were acquired on both MR systems first in a cylindrical phantom filled with 0.9% saline solution and five submerged falcon tubes (nicotinamide (NAM; 20, 50 and 100 mM), glutamate (Glu; 10 mM) and glycine (Gly; 20 mM)) and then in supratentorial and infratentorial brain region of five healthy subjects (2m/3f; age: 25.8±1.7 years). Z-spectra of both field strengths were fitted pixel-wise with a five (in vivo) or six-pool (phantom) Lorentzian model after $B_0$-correction. No $B_1$-correction was performed.

**Results**

Figure 1 illustrates repeatable APTw maps between the two time points in the phantom and in the brain at both 3T and 7T MRI. Higher APTw values and more heterogenous APTw maps are acquired in the brain at 7T. Within-coefficient-of-variation (wCV) for the phantom and the brain tissue types was comparable at 3T and 7T (Table 1).

**Conclusion**

Repeatable and specific APTw maps were obtained at both 3T and 7T, which facilitate the potential of comparing longitudinal APTw images and detecting metabolic changes in brain tumours. APTw values in vivo were not similar comparing 3T and 7T, probably due to the differences in acquisition protocols.

**References**

[1] Sagiyama et al. PNAS. 2014. DOI: https://doi.org/10.1073/pnas.1323855111. [2] Meissner et al. JMRI. 2019. DOI: https://doi.org/10.1002/jmri.26702. [3] van Zijl et al. MRM. 2011.  DOI: https://doi.org/10.1002/mrm.22761. [4] Barisano et al. BJR. 2019. DOI: https://doi.org/10.1259/BJR.20180492. [5] Morrison et al. MRIC NA 2021. DOI: https://doi.org/10.1016/J.MRIC.2020.09.007.
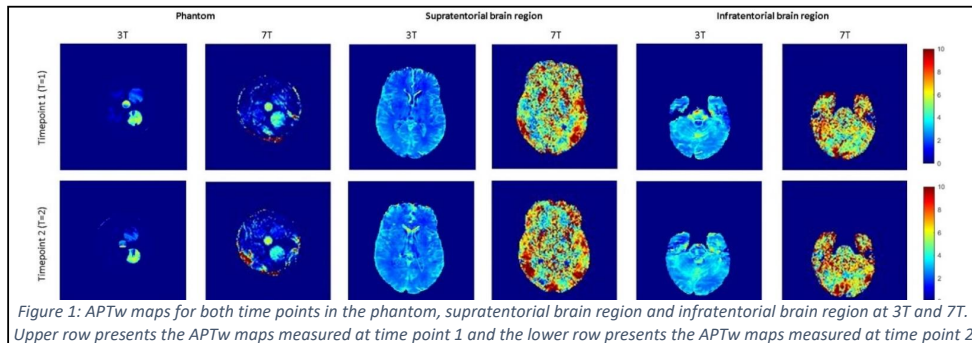
*Figure 1: APTw maps for both time points in the phantom, supratentorial brain region and infratentorial brain region at 3T and 7T. Upper row presents the APTw maps measured at time point 1 and the lower row presents the APTw maps measured at time point 2*

Table 1: Mean ± standard deviation and repeatability metrics of APTw maps of the in the phantom, supratentorial brain region and infratentorial brain region at 3T and 7T

| | | ROI/ Segment | 3T | | | | 7T | | | |
|---|---|---|---|---|---|---|---|---|---|---|
| | | | Mean ± STD | | RMSD | wCV (%) | Mean ± STD | | RMSD | wCV (%) |
| | | | T=1 | T=2 | | | T=1 | T=2 | | |
| **Phantom** | | NAM 20 mM | 1.73±0.62 | 1.73±0.69 | 0.33 | 9.16 | 1.36±0.93 | 1.11±0.67 | 0.52 | 14.28 |
| | | NAM 50 mM | 4.77±0.86 | 4.09±1.54 | | | 4.36±1.32 | 3.76±0.78 | | |
| | | NAM 100 mM | 6.12±1.11 | 5.95±1.40 | | | 6.35±1.38 | 6.02±0.46 | | |
| | | GLU 10 mM | 0.35±0.28 | 0.19±0.21 | | | 1.01±1.27 | 0.84±1.21 | | |
| | | GLY 20 mM | 0.42±0.30 | 0.24±0.22 | | | 0.11±0.32 | 1.01±0.79 | | |
| **In vivo brain** | Supratentorial | GM | 2.79±0.17 | 2.89±0.16 | 0.27 | 6.64 | 6.47±0.28 | 6.78±0.50 | 0.69 | 7.35 |
| | | WM | 2.33±0.20 | 2.41±0.13 | 0.24 | 7.23 | 5.39±0.39 | 5.40±0.49 | 0.70 | 9.14 |
| | | WM small | 1.91±0.28 | 2.00±0.24 | 0.25 | 9.02 | 4.82±0.78 | 5.19±0.86 | 1.12 | 15.83 |
| | Infratentorial | GM | 3.35±0.28 | 3.33±0.20 | 0.41 | 8.76 | 6.71±0.59 | 7.11±0.48 | 0.55 | 5.61 |
| | | WM | 2.79±0.25 | 2.85±0.25 | 0.42 | 10.43 | 5.98±0.91 | 5.46±0.83 | 1.03 | 12.74 |
| | | WM small | 2.87±0.32 | 3.05±0.45 | 0.58 | 13.79 | 6.10±1.21 | 5.23±0.97 | 1.60 | 19.98 |
| | | Pons | 3.24±0.59 | 3.06±0.44 | 0.59 | 13.18 | 5.70±0.68 | 5.54±0.75 | 0.61 | 7.68 |
| | | Pons small | 3.00±0.83 | 2.95±0.41 | 0.98 | 23.32 | 6.05±0.60 | 5.95±0.37 | 0.38 | 4.42 |

MRS Workshop 2022
Overcoming the Barriers to Clinical Use
DISCONNECT 2 RECONNECT
22-24 August 2022 @ EPFL, Lausanne, Switzerland

58

Poster no. 24 (on-site poster)

# A simulation framework to assess the quantification reliability of 2HG in ¹H MRS

Justyna Platek[1,2], Vanessa L. Franke[1,2], Mark E. Ladd[1,2,3], Peter Bachert[1,2], and Andreas Korzowski[1]

[1]Division of Medical Physics in Radiology, German Cancer Research Center (DKFZ), Heidelberg, Germany
[2]Faculty of Physics and Astronomy, University of Heidelberg, Heidelberg, Germany
[3]Faculty of Medicine, University of Heidelberg, Heidelberg, Germany

## Introduction

The non-invasive detection of the onco-metabolite 2-hydroxyglutarate (2HG)[1,2,3] via ¹H magnetic resonance spectroscopy (MRS) is of particular interest in brain tumors[4], but quantification of 2HG may be challenging due to the spectral overlap with Glutamate (Glu) and Glutamine (Gln), particularly in the case of limited signal-to-noise-ratio (SNR) and low 2HG concentration. The purpose of this study was to establish a simulation framework for the assessment of the quantification reliability for 2HG under realistic conditions i.e. low SNR levels, in order to identify a range of optimal acquisition parameters, i.e. echo time (TE), for the application in small animal models at $B_0$=9.4T

## Methods

A simulation framework was implemented in Matlab R2021a (The MathWorks) using the open-source spin dynamics simulation library Spinach5[5], in order to (I) generate noiseless ¹H spectra at $B_0$=9.4T for a PRESS sequence with 29 different TEs ([10–150]ms), and (II) to create corresponding ¹H basis sets. The simulations omitted relaxation effects. The spectra were line-broadened by 15 Hz, included 21 ¹H metabolites present *in vivo* ((cf. Fig.1) and their concentration ratios were adjusted to mimic observed conditions in glioma mouse models (2HG/Cr=1, Gln/Cr=1, Glu/Cr=1, Cr=Creatine).

To investigate the influence of SNR on the quantification reliability, four different noise levels (SNR = [1,5,10,100] referenced to Cr) each with 20 different noise realizations were applied. All spectra were analyzed with LCModel[6] using the custom-created ¹H basis sets. The relative deviation of the quantified concentration from noisy spectra to the true concentration (e.g. 1 for 2HG) was calculated. Mean values and standard deviations of the relative deviations and the Cramér-Rao lower bounds (CRLB) were calculated across all noise realizations.

## Results

Figure 1 shows representative spectra for TE=120ms without (A) and with noise (B-D), along with the corresponding fits. While the fits of the spectra with SNR≥5 (Fig.1 B,C) yield reasonable concentration estimates, the fitting quality of the spectrum with SNR=1 (Fig. 1D) could be considered as insufficient due to the larger CRLBs. Across all investigated SNR levels, it could be observed that depending on the echo time, the individual metabolite concentrations are estimated with varying accuracy. For the overlapping metabolites 2HG, Gln and Glu, the smallest deviation from the true concentration with lowest variance occurred at a TE around 120ms. At very high SNR, long TEs outperformed short TEs in terms of reliability (Fig. 2).

## Discussion and Conclusion

In this example, a PRESS sequence with equally spaced TE intervals ($TE_1$=$TE_2$) was simulated, showing the most reliable detection at long TEs (110–135ms), which is in agreement with other studies using different approaches[1,2,3]. These other approaches can be incorporated into the framework e.g. PRESS with unequal TE intervals or J-difference editing. Moreover, the simulations can be easily extended for more TEs and noise realizations, as well as for different shimming conditions and $T_2$ decays in order to better mimic *in vivo* conditions.

In the future, this optimized framework will enable us to identify optimal sequence schemes and parameters for the application in small animal models at $B_0$=9.4T.



**Fig.1** Simulated ¹H spectra for a PRESS sequence with TE = 120 ms at $B_0$ = 9.4T with the corresponding LCModel fits.
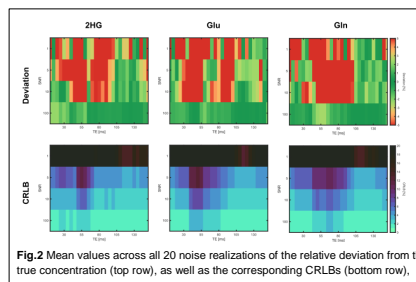


**Fig.2** Mean values across all 20 noise realizations of the relative deviation from the true concentration (top row), as well as the corresponding CRLBs (bottom row),

## References

[1] Choi C et al. Nat Med. (2012) 18:624–9. doi: 10.1038/nm.2682
[2] Andronesi OC et al. Sci Transl Med. (2012) 4:116ra4. doi: 10.1126/scitranslmed.3002693
[3] Tiwari V et al. Magn Reson Med. 2020; 84(3): 1152- 1160. https://doi.org/10.1002/mrm.28183
[4] Dang L et al. Annals of Oncology 27 (2016): 599–608. doi:10.1093/annonc/mdw013
[5] Hogben HJ et al. 208 (2011) 179-194. doi: 10.1016/j.jmr.2010.11.008
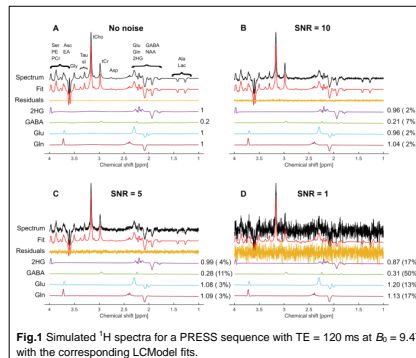[6] Provencher SW. Magn Reson Med. 1993;30:672–679: doi: 10.1002/mrm.1910300604

Poster no. 25 (on-site poster)

# Exploiting dual diffusion MRS and MRI acquisitions in the rat cerebellum at 14.1 T: a measurement of intra-extracellular water exchange

Jessie Mosso[1,2,3*], Michael Chan[1,2*], Mickaël Rey[1,2], Ileana O. Jelescu[4], and Cristina Cudalbu[1,2]

[1]CIBM Center for Biomedical Imaging, Lausanne, Switzerland, [2]Animal Imaging and Technology (AIT), EPFL, Lausanne, Switzerland, [3]LIFMET, EPFL, Lausanne, Switzerland, [4]Service de radiodiagnostic et radiologie interventionnelle, Lausanne University Hospital CHUV, Lausanne, Switzerland, *Joint first authors

## Abstract

**Background**: Recent studies have highlighted the need to account for inter-compartment water exchange when estimating diffusion models of gray matter (GM) at diffusion times longer than 20 ms [1] [2]. This often requires multi-diffusion time protocols, which can substantially increase the total acquisition time. In the context of hepatic encephalopathy (HE), where poor ammonia detoxification results in an excessive synthesis of glutamine in the astrocytes and in an osmotic pressure which may alter water exchange, we have recently presented paralleled results of diffusion MRS (dMRS) and diffusion MRI (dMRI) in the cerebellum of an HE rat model, using non-exchanging models only [3].

**Aims**: In the present study, we propose a dual modelling of these preclinical dMRS and dMRI data at 14.1 T [3]. We obtain a reliable estimate of cerebellar GM intra-extracellular water exchange time ($t_{ex}$) without additional dMRI data at multiple diffusion times ($T_d$). This methodology was tested on a small sample-size of SHAM (n=3) and HE rats (n=2).

**Methods**: dMRS and dMRI acquisition parameters have been detailed in [3]: dMRS was performed using the STE-LASER sequence [4] with $T_d = 63$ ms, and dMRI using a multi-slice 2D SE EPI sequence with $T_d = 12$ ms. The pipeline for $t_{ex}$ estimation is described in Figure 1. We assumed that the exchange could be neglected: 1) in white matter (WM) due to the myelin sheath; 2) in GM at $T_d = 12$ ms; and 3) between the soma and the extracellular space in GM at $T_d = 63$ ms [5].

**Results and Discussion**: The fitted values were: mean $t_{ex}$ SHAM: $40.1 \pm 24.4$ ms, mean $t_{ex}$ HE: $50.3 \pm 7.8$ ms, in good agreement with literature [1]. No statistically significant difference was found between the 2 groups, but an increased sample-size may help further investigate this matter. Overall, our approach enables an estimation of: geometric features of GM and WM from biophysical models at short diffusion time, diffusion coefficients of compartment-specific metabolites, and, using the dMRS water signal jointly with dMRI, an estimation of membrane permeability in GM, without the need for prohibitively long acquisition times.
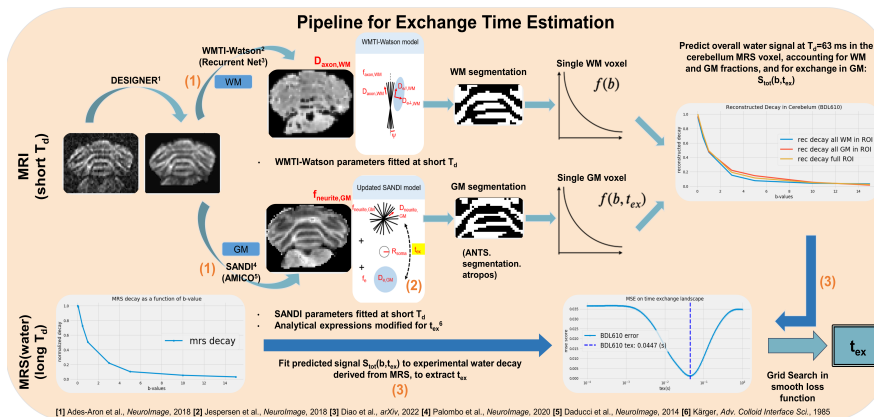
Figure 1: Pipeline for the exchange time estimation from dMRS and dMRI water acquisitions: (1)-SANDI [5] and WMTI-Watson [6] parameters were fitted at short diffusion time ($T_d = 12$ ms); (2)-the SANDI model formulation in GM was then modified to account for exchange between the sticks and the extracellular space [7]; (3)-the predicted water decay in the MRS voxel $S_{tot}$(b,tex) was reconstructed by summing weighted contributions of GM (SANDI with exchange) and WM (WMTI-Watson) voxels, and fitted to the experimental dMRS water decay at long diffusion time ($T_d = 63$ ms) to estimate $t_{ex}$. Other model parameters (relative fractions, compartment diffusivities, orientation dispersion...) were assumed unchanged between $T_d = 12$ ms and $T_d = 63$ ms

**References:** [1] Jelescu et al., *NeuroImage*, 2022 [2] Olesen et al., *NeuroImage*, 2022 [3] Mosso et al., *Proc. Intl. Soc. Mag. Reson. Med. 30 (ISMRM)*, 2022 [4] Ligneul et al., *MRM*, 2017 [5] Palombo et al., *NeuroImage*, 2020 [6] Fieremans et al., *NeuroImage*, 2011 [7] Käger, *Adv. Colloid Interface Sci.*, 1985

**MRS Workshop 2022**
Overcoming the Barriers to Clinical Use
DISCONNECT 2 RECONNECT
22-24 August 2022 @ EPFL, Lausanne, Switzerland

60

Poster no. 26 (on-site poster)

## Comparison between two quantification programs on the $^1$H-MRS data of the Alfa+ cohort

**Margarida Julià-Sapé[1,2,3], Marina Garcia-Prat[2], Paula Montesinos[4], Javier Sánchez[4], Juan Domingo Gispert[1,2], Carles Falcón[1,2] , on behalf of the ALFA Study**

[1]Centro de Investigación Biomédica en Red (CIBER-BBN), Spain
[2]BarcelonaBeta Brain Research Center. Fundació Pasqual Maragall, Spain
[3]Universitat Autònoma de Barcelona (UAB), Spain
[4]Philips Healthcare, Madrid, Spain

***INTRODUCTION:*** The ALFA project (Alzheimer's and Families) is a research study started by the Barcelonaβeta Brain Research Center (BBRC) for the prospective follow-up of a cohort of 2743 cognitively normal subjects, from the 45-75 age range [1], [2]. The cohort is enriched in offspring of Alzheimer's disease (AD) patients. The ALFA project focuses into the study of the preclinical phase of (AD) to find early biomarkers and pathophysiological events of the disease. Patients undergo a full cognitive evaluation, questionnaires of lifestyle, Apolipoprotein E typing and full-genome wide association study (GWAS), and an MRI study. In this context, ALFA+ is a nested study of 440 volunteers who also undergo extended cognitive testing, CSF, blood and urine sampling, extended MRI, PET/CT of amyloid, Tau and/or FDG, and a follow up every three years. Among the MR techniques included in the advanced MRI study, they undergo SV MRS, being mI the metabolite of greatest interest to detect potential neuroinflammation in AD-related areas, with the idea that neuroinflammation would precede neuronal damage. The aim of this study was to compare different quantification programs for the SV MRS data of the ALFA+ volunteers.
***METHODS:*** SV MRS data were acquired at the BBRC with a 3T Philips *Ingenia-CX*, using a PRESS sequence, TE=100 ms (TE$_1$= 37 ms), and CHESS water suppression. SV MRS data were available for 370 of the 440 ALFA+ volunteers in three different brain localizations: angular, hippocampus and precuneus. Data were acquired from 2017 to 2019 (visit 1).  We processed the SV MRS using two different software tools: LCmodel [3] and Tarquin [4]. For LCmodel, a basis set tailored for TE=100ms, provided by Prof S. Provencher, was used. For Tarquin, we used the default "1H+glth" basis set. Other parameters were W_att = 0.7 for LCmodel and 0.65 for Tarquin. All spectra were processed in batch and a data dictionary was created in order to compare the spectral quality and quantification results from both programs.
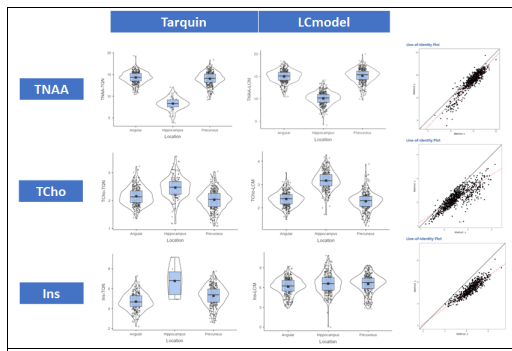


Figure 1: Boxplots for three different metabolites with the two programs, in the three localizations, as well as line-of identity plot to assess bias.

***RESULTS AND DISCUSION:*** As expected, spectra from hippocampus had the worst quality due to the poor magnetic field homogeneity in the medial temporal area. In the angular region, a frequent artifact was the signal from subcutaneous fat. Using a CRLB threshold of 20, Tarquin generated more CRLB values above accepted limits than LCmodel, therefore ending up with less metabolites with reliable quantified values for further analysis. As an example, for total creatine (TCr), LCmodel gave 98.91% of the spectra of hippocampus with CRLB<20, whereas with Tarquin this happened only for 39.34% of the same spectra. We could reliably quantify a majority of cases with both programs only for the main metabolites: TCho, TCre, TNAA, Ins and Glx, but in hippocampus Tarquin gave CRLB> 20 for most of the cases for these metabolites. There was also some bias in the quantified values between the two programs, but quantification results were similar between them (Figure 1), even considering the minor differences in some parameters.
***CONCLUSION AND FUTURE DIRECTIONS:*** There are marked differences in the number of quantifiable peaks using LCmodel or Tarquin although in aggregate, results are similar between the two programs.

**References:**

[1]     J. L. Molinuevo *et al.*, "The ALFA project: A research platform to identify early pathophysiological features of Alzheimer's disease," *Alzheimers Dement (N Y)*, vol. 2, no. 2, pp. 82–92, Mar. 2016, doi: 10.1016/j.trci.2016.02.003.

[2]     J. Huguet *et al.*, "Management and Quality Control of Large Neuroimaging Datasets: Developments From the Barcelonaβeta Brain Research Center ," *Frontiers in Neuroscience* , vol. 15. 2021. [Online]. Available: https://www.frontiersin.org/article/10.3389/fnins.2021.633438

[3]     S. W. Provencher, "Estimation of metabolite concentrations from localized in vivo proton NMR spectra," *Magnetic Resonance in Medicine*, vol. 30, no. 6, pp. 672–679, 1993, doi: 10.1002/mrm.1910300604.

# MRS Workshop 2022
## Overcoming the Barriers to Clinical Use
### DISCONNECT 2 RECONNECT
22-24 August 2022 @ EPFL, Lausanne, Switzerland

61

Poster no. 27 (on-site poster)

## Respiratory-triggered quantitative MR spectroscopy of the human cervical spinal cord at 7 T

**Tangi Roussel, Yann Le Fur, Maxime Guye, Patrick Viout, Jean-Philippe Ranjeva, Virginie Callot**

1. Aix-Marseille Univ, CNRS, CRMBM, Marseille, France
2. APHM, Hôpital Universitaire Timone, CEMEREM, Marseille, France

**Introduction**

Ultra-high field (7T and higher) ^{1}H MRS is of great interest to help characterizing human spinal cord (SC) pathologies. However, very few studies have been reported so far in this small size structure at these fields due to challenging experimental difficulties caused by static and dynamic radiofrequency field heterogeneities, as well as physiological motion. In this work, in line with recent developments to strengthen ^{1}H SC MRS feasibility [1,2], and benefiting from the improved SNR provided by ultra-high field system, we demonstrate the necessity of respiratory-gated acquisition and present original post-processing and quantitative approaches dedicated to robust ^{1}H human cervical SC MRS at 7 T.

**Methods**

Experiments were performed on a 7 T system (MAGNETOM, Siemens Healthcare) on 14 healthy subjects using an 8-channel RF transmit/receive neck coil array (Rapid Biomedical). Respiratory-triggered single-voxel MRS was performed using a semi-LASER sequence with a TE of ca. 40 ms. 128 averages were collected from an average 0.97 mL voxel placed in the SC at a C3 vertebral level (Fig. 2C) with a minimum TR of 3.5-4.5 s. $B_0$ field homogenization was performed using a respiratory-gated FASTESTMAP sequence. The respiration signal was recorded using a bellow elastic belt.

Additional acquisitions were performed to evaluate the influence of respiration on the recorded MRS signal. Similar to the procedure described in [3], these experiments consisted in acquiring repeatably the water STEAM spectrum (TE/TM = 3.5/8.1 ms) without any triggering, while asking the subject to breathe normally.

The raw MRS data were processed and quantified using a home-made Python software (PASTIS) [4] which included a specific routine to automatically improve spectral quality by discarding corrupted individual acquired MR spectra.
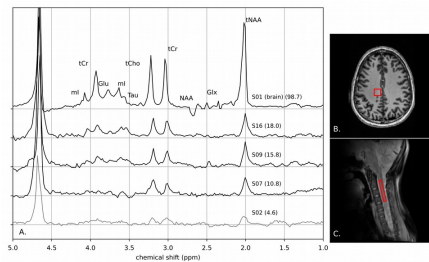


*Fig. 1: One brain and 4 spinal cord semi-LASER MRS datasets acquired at 7 T (A). For each spectrum, the SNR estimated on the NAA peak is indicated. VOI volumes were 15x15x15 $mm^3$ (3.38 mL) in the brain (B) and 6x6x20 $mm^3$ (0.72 mL) in the spinal cord (C).*

**Results & Discussion**

Fig. 1 shows a set of 4 SC and 1 brain MR semi-LASER spectra acquired on different healthy volunteers. Fig. 2 shows an example of data post-processing based on individual spectra analysis and rejection. This approach led to an average data discard rate of 5.9 %. During non-triggered MRS acquisitions, strong correlations were found between the water resonance linewidth and chemical shift variations and the respiration signal.

At the group level, the average water linewidth and NAA signal-to-noise ratio reached 0.04 ppm and 11.01, respectively. The group-average metabolic ratios NAA/tCr, tCho/tCr and mI/tCr were in good agreement with previous studies and showed inter-session reproducibility variations below 30%.

To conclude, we demonstrated the interest of respiratory-triggered acquisition to collect robust ^{1}H MRS data from the cervical SC at 7 T. A dedicated raw data processing algorithm was developed to enhance MR spectral quality by discarding corrupted scans. This processing and quantification tool has been made open source and available at (https://crmbm.univ-amu.fr/softwares/pastis). This high-quality MRS data approach would be of particular relevance to assess SC metabolism in multiple sclerosis, amyotrophic lateral sclerosis and injury metabolism.



*Fig. 2: Data discard stage of a SC MRS acquisition. Individual spectra were extracted from raw data (E); the residual water peak was analyzed in terms of amplitude (A), linewidth (B), chemical shift (C) and phase variations (D). In this case, the data rejection algorithm allowed a final SNR increase of 4.80%.*

**References**

[1] Henning A, Koning W, Fuchs A et al. NMR Biomed 2016;29:1231-1239 [2] Hock A, Henning A. NMR Biomed 2016;29:490-498 [3] Vannesjo SJ, Miller KL, Clare S et al. Neuroimage 2018;167:191-202 [4] Roussel T, Le Fur Y, Guye M et al. MRM 2022;87:2600-2612
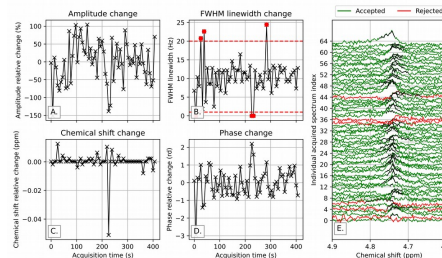
# MRS Workshop 2022
## Overcoming the Barriers to Clinical Use
### DISCONNECT 2 RECONNECT
22-24 August 2022 @ EPFL, Lausanne, Switzerland

62

Poster no. 28 (on-site poster)

# Whole brain ^{31}P MRSI at 7 T with FSL-MRS

**Tangi Roussel[1,2], Patrick Viout[1,2], Thomas Troalen[3], Jean-Philippe Ranjeva[1,2], Maxime Guye[1,2]**

1. Aix-Marseille Univ, CNRS, CRMBM, Marseille, France
2. APHM, Hôpital Universitaire Timone, CEMEREM, Marseille, France
3. Siemens Healthcare SAS, Saint-Denis, France

## Introduction

Phosphorus NMR allows the detection of all metabolites that play key roles in tissue energy metabolism. Biologically relevant parameters such as intracellular pH may also be indirectly deduced [1]. While non-localized ^{31}P MRS has been employed to explore energy metabolism of skeletal muscles, only few studies have reported ^{31}P MRS imaging of whole brain at ultra-high fields [2-4]. In this work, a complete ^{31}P imaging protocol compatible with a scan time compatible with clinical use has been designed at 7 T including a data processing and quantification pipeline based on FSL-MRS [5]. First results on healthy subjects are discussed.
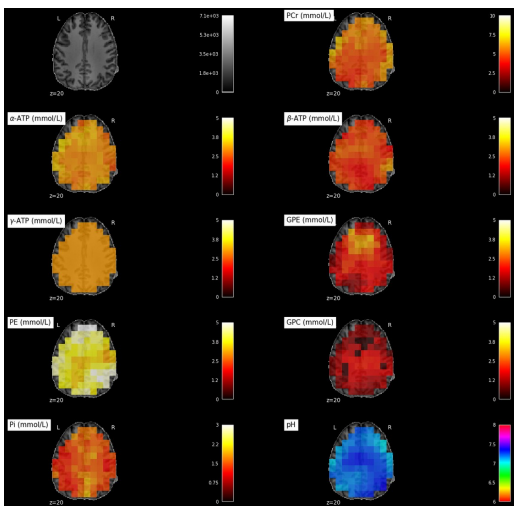
## Methods

Experiments were performed on a 7 T system (Magnetom TERRA, Siemens Healthcare) on 5 healthy subjects using a dual ^{1}H/^{31}P RF transmit/receive head coil (Rapid Biomedical). 3D MRSI acquisitions were performed using a prototype FID-CSI sequence (TE/TR = 0.2/300 ms) with a nominal isotropic spatial resolution varying between 2 and 8 cm$^3$. The number of averages were set to reach a 20-min scan time (half-cosinus weighted k-space sampling). Anatomical $T_1$-weighted images were acquired using a 32-channel receive head coil (Nova Medical).

Data processing and quantification were performed using a modified version of the FSL-MRS package [5] and the NIFTI-MRS format [6] to handle ^{31}P MRSI data quantification. Metabolites ATP-α, ATP-γ, ATP-β, PC, PCr, Pi, PE, GPC and GPE were quantified and absolute estimations were attempted by assuming a 3-mmol/L concentration for ATP-γ [4]. pH maps were also computed [7].

## Results & Discussion

Fig. 1 shows the 3D ^{31}P metabolic concentration and pH maps obtained for one healthy volunteer with a nominal an effective spatial resolution of respectively 6.16 (1.83$^3$ cm) and 55.12 (3.81$^3$ cm). Metabolites ATP-α, ATP-γ, ATP-β, PCr, Pi and PE were quantified with brain-averaged Cramér-Rao Bounds (CRB) below 20%. Metabolite concentrations are in good agreement with literature [4] except for PCr (Fig. 1). The latter likely



*Fig. 1: Phosphorus metabolic concentration and pH maps obtained on a healthy subject at 7 T in 20min with a nominal resolution of 6.16 cm3. K-space was zero-filled to 16x16x16.*

originated from the extra-cranial temporalis muscles and will be suppressed soon by the use of BISTRO saturation bands [8].

Considering the current set-up and scan time constraints and an arbitrary CRB threshold of 20%, the optimal nominal spatial resolution was of ca. 6 cm3. Future efforts will focus on [31]P $B_1$ field correction and a new protocol design to enhance spatial resolution allowing white and gray brain matter phosphorus content profiling [9]. To conclude, we presented a ^{31}P MRS whole-brain imaging protocol at 7 T and a FSL-MRS-based data processing pipeline. Promising first results were obtained showing homogeneous metabolic maps with concentrations in agreement with literature.

## Acknowledgements

*Fig. 2: [31]P MR magnitude spectrum (black) extracted from the MRSI dataset shown in Fig. 1. Frequency-domain complex quantification was performed using FSL-MRS (red).*

## References

[1] de Graaf RA. Wiley-Interscience; 2019. 569 p. [2] Korzowski A, Bachert P. Magn Reson Med 2018;79:1251-1259 [3] Rowland BC, Driver ID, Tachrount M et al. Magn Reson Med 2020;83:765-775 [4] Ruhm L, Dorst J, Avdievitch N et al. Magn Reson Med 2021 [5] Clarke WT, Stagg CJ, Jbabdi S. Magn Reson Med 2021;85:2950-2964 [6] Clarke WT, Mikkelsen M, Oeltzschner G et al. BioRxiv 2021 [7] Ren J, Sherry AD, Malloy CR. NMR Biomed 2015;28:1455-1462 [8] Luo Y, de Graaf RA, DelaBarre L et al. Magn Reson Med 2001;45:1095-1102 [9] Hetherington HP, Spencer DD, Vaughan JT et al. Magn Reson Med 2001;45:46-52

**MRS Workshop 2022**
Overcoming the Barriers to Clinical Use
DISCONNECT 2 RECONNECT
22-24 August 2022 @ EPFL, Lausanne, Switzerland

63

Poster no. 29 (on-site poster)

**Triple Repetition Time Saturation Transfer (TRiST) ^{31}P MR Spectroscopy for Measuring ATP Synthesis in Human Liver at 3T**

_B. Korzekwa[1,2], M. Jonuscheit[1,2], M. Schär[3], Y. Kupriyanova[1,2], M. Roden[1,2,4] and V.B. Schrauwen-Hinderling[1,2,5]_

[1]_Institute for Clinical Diabetology, German Diabetes Center, Leibniz Institute for Diabetes Research at Heinrich Heine University, Düsseldorf, Germany._ [2]_German Center for Diabetes Research (DZD e.V.), München-Neuherberg, Germany._ [3]_Division of Magnetic Resonance Research, Department of Radiology, Johns Hopkins University School of Medicine, Baltimore, United States of America._ [4]_Department of Endocrinology and Diabetology, Medical Faculty and University Hospital, Heinrich Heine University Düsseldorf, Germany._ [5]_Department of Radiology and Nuclear Medicine, Maastricht University Medical Center, Maastricht, The Netherlands._

**Introduction**

Saturation transfer (ST) magnetic resonance spectroscopy (MRS) techniques enable the measurement of in vivo chemical reaction kinetics [1]. Phosphorus (^{31}P) ST MRS can be applied for studying the adenosine triphosphate (ATP) synthesis flux in human liver and discovered a decreased ATP synthetic flux in metabolic disease [2,3]. However, this technique generally offers low signal-to-noise-ratio (SNR) at 3 T, and thus long measurement times. Furthermore, the method needs to allow accurate localized measurements and a robust frequency-selective saturation of hepatic ATP. The aim of this study was to set up a robust and fast ^{31}P ST MRS method to investigate ATP synthase flux in human liver. For this, we adapted the TRiST method, previously applied in human calf muscle and heart [4], for application in the liver. Finally, day-to-day and intra-session variabilities of this method were assessed.

**Methods**

For the ATP synthase flux, a two-site model of chemical exchange between inorganic phosphate ($P_i$) and γATP is assumed. During the ST experiment, the γATP resonance is completely saturated by frequency-selective irradiation using delay alternating with nutation for tailored excitation (DANTE) pulse trains of short hard pulses. In response, the equilibrium longitudinal magnetization of $P_i$ is reduced from $M_{0,Pi}$ to $M'_{z,Pi}$ and with this the spin-lattice relaxation time of $P_i$ is reduced from $T_{1,Pi}$ to an apparent $T'_{1,Pi}$ caused by chemical exchange of $P_i$ with the saturated γATP pool. In the TRiST experiment, one measures the partially saturated magnetization $M'_{z,Pi}$ at short ($TR_{short}$) and long ($TR_{long}$) repetition periods in the presence of saturating irradiation applied to the exchanging γATP moiety at -2.5 parts per million (ppm), relative to $P_i$. Then $M_{0,Pi}$ ($TR_{mirrored}$) is measured fully relaxed in the presence of control irradiation applied at +2.5 ppm. $T'_{1,Pi}$ is obtained from $TR_{short}$ and $TR_{long}$ according to the 2TR method [5].

Finally, the rate constant $k_f$ is determined by: $k_f = \frac{1}{T'_{1,Pi}}\left(1 - \frac{M'_{0,Pi}}{M_{0,Pi}}\right)$

Three healthy volunteers (2 male/1 female; age 24 to 29 years; body mass index 23.4 to 26.9 kg/m^{2}) participated in the study. Two volunteers underwent measurements on three different days within a week to assess the day-to-day variation, after an overnight fast. To determine the intra-session variation, one volunteer was examined two times, with repositioning between measurements. All examinations were performed on a clinical 3 T MR system (3 T Philips Achieva dStream, Best, Netherlands). A quadrature surface coil (transmit-receive coil; RAPID Biomedical, Rimpar, Germany) with total ^{31}P loop size of 220 mm x 160 mm was used. Liver MR spectra were obtained using a 2D localized Image-Selected In vivo Spectroscopy (ISIS) sequence with a hyperbolic secant (HS) adiabatic pulse for excitation, voxel size 120 mm x 30 mm, repetition time (TR) 0.7 s, 2.7 s and 4.2 s with number of signal averages (NSA) 732, 384 and 244 for $TR_{short}$, $TR_{long}$ and $TR_{mirrored}$, respectively. Shimming was performed using localized second-order shimming based on acquired static magnetic field [6]. All spectra were acquired with 512 sample points (N) and 3 kHz spectral bandwidth (BW) and processed with the jMRUI software, using AMARES.

**Results**

Figure 1 shows a representative $TR_{long}$ spectrum demonstrating full saturation of the γATP resonance at -2.5 ppm. Table 1 summarizes the data of the day-to-day and intra-day variability study. The mean coefficient of variation (CV) of $T'_{1,Pi}$ is 4.9 % and $k_f$ is 13.2 % for the day-to-day variability study.

**Discussion and Conclusion**

This study demonstrates the feasibility of the TRiST method for assessing hepatic ATP synthase flux via a pseudo-first-order reaction rate in human liver. The obtained values for $T'_{1,Pi}$ and $k_f$ are in agreement with literature [2,3]. Additionally, the 2TR method in TRiST only requires the acquisition of two spectra and therefore provides faster assessment of $T'_{1,Pi}$ compared to previously published approaches using a multiple point inversion recovery [2,3]. The combination of TRiST and 2D ISIS provides a higher degree of localization and therefore better exclusion of muscle signal. The assessed CVs for $k_f$ of less than 15% for day-to-day and intra-day variability indicate the robustness of the method and suggest its application in interventional studies.

**References**

[1] Forsen et al. _J. Chem. Phys._ 1963; [2] Schmid et al. _NMR Biomed._ 2008; [3] Buehler et al. _NMR Biomed._ 2015; [4] Schär et al. _MRM_ 2010; [5] El-Sharkawy et al. _MRM_ 2009; [6] Schär et al. _MRM 2004_

**Figures:**

Table 1: Day-to-day and intra-day results and variability (CVs):

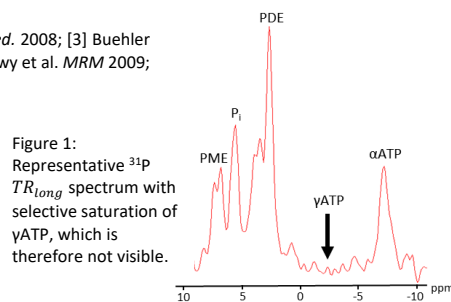| Volunteer | | Mean ± SD | | CV [%] | |
|---|---|---|---|---|---|
| | | $T'_{1,Pi}$ [ms] | $k_f$ [$s^{-1}$] | $T'_{1,Pi}$ | $k_f$ |
| Day-to-day | 1 | 550 ± 20 | 0.253 ± 0.043 | 3.6 | 16.8 |
| | 2 | 683 ± 42 | 0.258 ± 0.024 | 6.1 | 9.4 |
| Intra-day | 3 | 660 ± 28 | 0.253 ± 0.032 | 4.3 | 12.7 |



Figure 1: Representative [31]P $TR_{long}$ spectrum with selective saturation of γATP, which is therefore not visible.

# MRS Workshop 2022
## Overcoming the Barriers to Clinical Use
### DISCONNECT 2 RECONNECT
22-24 August 2022 @ EPFL, Lausanne, Switzerland

64

Poster no. 30 (on-site poster)

Goranovic, D. (1), Strasser, B. (1), Motyka, S. (1), Weiser, P. (2), Langs, G. (2), Bogner, W. (1)
(1) High Field MR Center - Department of Biomedical Imaging and Image-Guided Therapy, Medical University of Vienna, Austria
(2) Computational Imaging Research Lab - Department of Biomedical Imaging and Image-guided Therapy, Medical University of Vienna, Austria

**Training a Convolutional Neural Network for Enhanced Spectral Quantification of whole-brain MRSI Data**

**Purpose:** Magnetic resonance spectroscopic imaging (MRSI) is a non-invasive imaging method, which uses spectroscopic information in addition to the relaxation times of the tissue being imaged. This approach combines anatomic and metabolic information into one imaging technique. A critical tasks in the field of MRSI lies in the time consuming quantification of individual metabolites through means of linear fitting models. State-of-the-art post-processing steps may take up to several hours before the final spectroscopic images can be analysed for medical purposes. In order to mitigate the aforementioned post-processing times, a deep learning (DL) approach is proposed for enhanced spectral quantification of MRSI data.

**Methods:** A supervised convolutional neural network (CNN) was trained (n = 28.000), validated (n = 3.500) and tested (n = 3.500) on simulated 7T magnetic resonance brain real spectra to perform robust spectral quantification on different levels of SNR (6.8-18.2). The networks architecture is designed to first predict and correct for unknown baselines, before estimating metabolite concentrations and spectral parameters from baseline-removed spectra, which are then put into a spectral model for reconstruction purposes. The basis set was generated with the software package jMRUI, utilizing NMR-SCOPE and QUEST for the quantummechanical simulation of combined creatine and phosphocreatine (tCr=Cr+PCr), glutamate (Glu), glutamine (Gln), N-acetylaspartate (NAA), N-acetylaspartylglutamate (NAAG), combined phosphorylcholine and glycerophosphorylcholine (tCh=PC+GPC), myo-Inositol (mI), taurine (Tau) and γ-aminobutyric acid (GABA). The predicted spectral fitting parameters include zero-order phase (±90 deg), frequency shift (±12 Hz), lorentzian and gaussian $T_2^*$ decay constants (0.04-0.25 ms, 0.1-1.0 ms). Spectra with a linewidth below 5 Hz and above 12 Hz for tCr were excluded during the simulation and were thus not present during the training process. Pearson correlation coefficients r and paired student t-test were calculated to evaluate the networks performance on simulated data compared to linear combination model (LCModel) analysis.

**Results:** The networks performance on metabolite quantification was compared to LCModel by calculating MAE (mmol/L), shown in Fig 1. Comparable performance was achieved for Glu (0.74±0.68; 0.68±0.63) and Tau (0.52±0.39; 0.40±0.33), while underperforming for NAAG (0.36±0.31; 0.18±0.16) and GABA (0.51±0.39; 0.29±0.26). The quantification of the network for tCr (0.44±0.42; 9.07±2.26), Gln (0.68±0.65; 5.55±2.53), NAA (0.58±0.52; 0.92±0.59), tCh (0.18±0.17; 1.60±0.48) and mI (0.58±0.49; 0.89±0.59) was more accurate compared to LCModel. Overall, the CNN has a MAE of ≤ 1 mmol/L across all metabolites. The correlation test between both approaches reports very high correlation (r ≥ 0.8) for tCr, Glu, NAA; high correlation (0.6 ≤ r ≤ 0.79) for NAAG, tCh, mI and moderate correlation (0.4 ≤ r ≤ 0.59) for Tau, GABA. For all r values, the two-tail p<0.001. Spectral fitting parameters show MAE of 0.78±0.93 Hz for frequency shifts, 0.13±0.16 rad for zero-order phase and 0.05±0.04 and 0.22±0.17 ms for lorentzian and gaussian $T_2^*$ decay constants respectively. Analysing the testing dataset took the CNN 15 s and LCModel 2548 s, which corresponds to a time difference by the factor of ~170. Sample fitting spectra are given in Fig 2.

**Conclusion:** The possibility of combining physical models with means of DL gives rise to improved means of quantification. To ensure optimal performance on in-vivo data in the future, ranges for the simulation and network parameters need to be extended though, by including first-order phase and further baseline variations (macromolecule signals and lipid artifacts). Nevertheless, this project improves the spectral quantification of whole-brain MRSI (wbMRSI), as the robust CNN approach significantly speeds up quantification times, which brings us closer to MRSI being part of routine clinical practices.
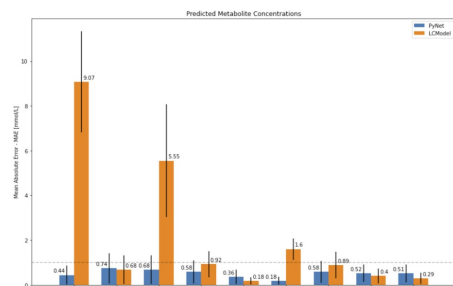


Fig 1: Mean absolute error (MAE) and standard deviations (STDEV) for the metabolite concentrations of the test dataset of major metabolites for the CNN approach (blue) the and LCModel (orange). The dashed Line indicates the 1 mmol/L error mark.
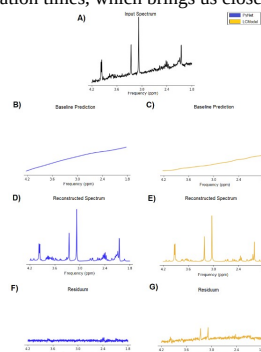
Fig 2: Comparing spectral fitting capabilities of the CNN (blue) and LCModel (orange), plotted over the frequency range in ppm. Sample Input spectrum is depicted in (A), corresponding baseline in (B-C) and the it in (D-E). The residual error is given in (F-G).

**MRS Workshop 2022**
Overcoming the Barriers to Clinical Use
DISCONNECT 2 RECONNECT
22-24 August 2022 @ EPFL, Lausanne, Switzerland

65

Poster no. 31 (on-site poster)

### Novel urease inhibitors for the treatment of hepatic encephalopathy

Diana Evstafeva[1], Filip Ilievski[1], Yinyin Bao[1], Sunghyun Kang[1], Dario Sessa[2], Stefanita-Octavian Mitrea[2], Katarzyna Pierzchala[2], Dunja Simicic[2], Cristina Ramona Cudalbu[2], Jean-Christophe Leroux[1]

[1]*Institute of Pharmaceutical Sciences, ETH Zurich, 8093 Zurich, Switzerland*
[2]*Center for Biomedical Imaging (CIBM), EPFL, 1015 Lausanne, Switzerland*

Hepatic encephalopathy (HE) is a frequent complication of liver disease manifesting as a broad range of neuropsychiatric abnormalities (*1*). The dysfunctional liver shows reduced ureagenesis leading to elevation of systemic ammonia levels. Excess ammonia induces accumulation of glutamine in astrocytes causing osmotic stress and alteration of cell metabolism (*2, 3*). Due to its neurotoxic effect, ammonia has been the main target for HE therapy. Current treatment options for HE focus on either reducing ammonia production and absorption or on promoting its elimination. They, however, exhibit various limitations such as persistent side effects, risk of resistance (in case of antibiotics), and/or moderate efficacy (*4, 5*).

Urea hydrolysis by urease-producing bacteria is one of the key pathways of ammonia production in the human body (*6*). Therefore, urease inhibitors such as hydroxamic acids (HAs) represent an alternative treatment for HE. In the present work, we synthesized a series of HA derivatives and screened them for their urease inhibitory activity in rat caecum content. We identified 2-octynohydroxamic acid (2-octynoHA) as a lead candidate. Its potency exceeded that of HAs tested in previous clinical trials. It was further shown to be neither cytotoxic nor mutagenic up to 1 mM. *In vivo* efficacy studies showed that 2-octynoHA (30 mg/kg) was able to reduce ammonia blood levels in bile-duct ligated (BDL) rats. Additionally, *in vivo* 1H MRS measurements performed at 9.4T in the cerebellum (SPECIAL sequence, TE=2.8ms, VOI=2.5x2.5x2.5mm$^3$) showed a significant decrease in brain glutamine levels after 5 days of treatment compared to non-treated BDL rats (Figure 1) confirming the therapeutic effects of 2-octynoHA. In summary, 2-octynoHA represents a promising oral candidate for the treatment of HE. Carigest SA is acknowledged for financial support.
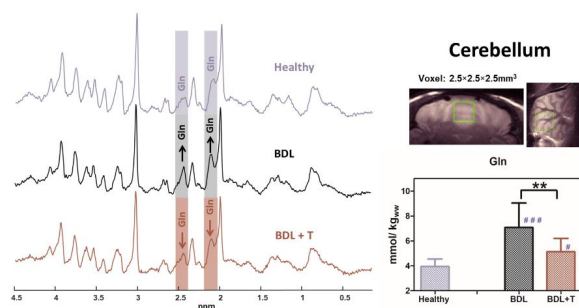


**Figure 1.** Left: Representative 1H MRS spectra acquired at 9.4T in the cerebellum in healthy, BDL and BDL rats treated with 2-octynoHA (BDL + T) (SPECIAL, TE=2.8ms, 160av); Right: corresponding VOI position and brain Gln concentrations estimated using LCModel (** $p < 0.01$; # $p < 0.05$, ### $p < 0.001$ compared to the healthy group).

References
1. H. Vilstrup *et al.*, *Hepatology*. 60, 715–735 (2014).
2. C. F. Rose *et al.*, *J Hepatol*. 73, 1526–1547 (2020).
3. O. Braissant *et al.*, *J Hepatol*. 71, 505–515 (2019).
4. L. L. Gluud, H. Vilstrup, M. Y. Morgan, *Cochrane Database Syst Rev*. 4, CD003044 (2016).
5. Z. D. Jiang, H. L. DuPont, *Chemotherapy*. 51, 67–72 (2005).
6. V. Walker, *Adv Clin Chem*. 67, 73–150 (2014).

**MRS Workshop 2022**
Overcoming the Barriers to Clinical Use
DISCONNECT **2** RECONNECT
22-24 August 2022 @ EPFL, Lausanne, Switzerland

66

Poster no. 32 (on-site poster)

## ^{31}P-MRS Analysis With Neural Networks: 31P-SPAWNN

Julien Songeon[1], Sébastien Courvoisier[1,2], Lijing Xin[2,3], Thomas Agius[4], Oscar
Dabrowski[1], Alban Longchamp[4], François Lazeyras[1,2], and Antoine Klauser[1,2]

[1]*Department of Radiology and Medical Informatics, University of Geneva, Geneva, Switzerland*
[2]*CIBM Center for Biomedical Imaging, Lausanne, Switzerland*
[3]*Animal Imaging and Technology, Ecole Polytechnique Fédérale de Lausanne (EPFL), Lausanne, Switzerland and*
[4]*Department of Vascular Surgery, Centre Hospitalier Universitaire Vaudois and University of Lausanne, Lausanne, Switzerland*

### I. ABSTRACT

Introduction and Purpose: ^{31}P-MRS is a non-invasive technique that allows to measure high-energy phosphate metabolites in-vivo that are associated with the metabolic activity of the cell [1, 2]. ^{31}P-MRS acquisition displays a lower relative sensitivity than [1]H [3], and its acquisition is usually performed using larger voxel sizes to achieve a sufficient SNR. Preliminary application of convolutional neural network (CNN) [4, 5] in proton MRSI revealed high robustness to noise. Application of CNN to ^{1}H-MRS has demonstrated this method to display equal or better level of performance, while having a faster computational time than current standard MRS metabolites quantification methods like LCModel [6]. We propose to introduce an artificial intelligence framework, 31P-SPAWNN, in order to fully analyze ^{31}P magnetic resonance spectra. In this work, we compared the performance of 31P-SPAWNN with traditional least-square fitting LCModel method.

Theory and Methods: Convolutional neural network architectures have been proposed for the analysis and quantification of ^{31}P-spectroscopy. The generation of training and test data have been developed with a fully parameterized model. In-vivo unlocalized free induction decay and three-dimensional ^{31}P-magnetic resonance spectroscopy imaging data were acquired from healthy volunteers before being quantified using either 31P-SPAWNN or LCModel.

Results: The presented experiment has demonstrated both the reliability and accuracy of 31P-SPAWNN for estimating metabolite concentrations and spectral parameters. Simulated test data showed improved quantification using 31P-SPAWNN compared to LCModel, evaluated with the coefficient of determination $R^2$. In-vivo data analysis revealed higher accuracy at low signal-to-noise ratio using 31P-SPAWNN, yet with equivalent precision. Processing time using 31P-SPAWNN can be further shortened up to two orders of magnitude.

### II. FIGURES
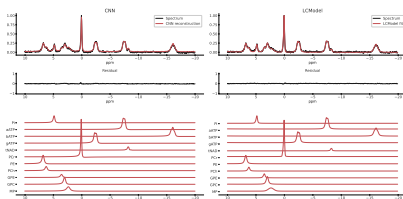


(a) Comparison of in-vivo ^{31}P-MRSI spectrum evaluated and reconstructed with SPAWNN (left) and fitted with LCModel (right). The figure displays SPAWNN reconstruction and the LCModel fit (top), the residuals (middle), and the contribution of each metabolite (bottom). No preprocessing applied before analysis.
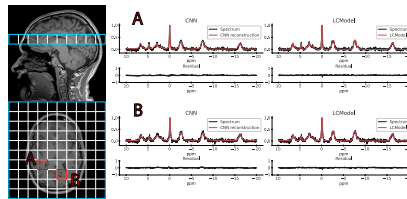
(b) Examples of SPAWNN evaluation of a 3D ^{31}P-MRSI acquired on a human brain. The spectra on the left represent the SPAWNN reconstruction with the measurement data, and the spectra on the right the LCModel fitting for voxels A and B.

### III. REFERENCES

[1] Buchli Reto, Meier Dieter, Martin Ernst, Boesiger Peter. Assessment of absolute metabolite concentrations in human tissue by 31P MRS in vivo. Part II: Muscle, liver, kidney *Magnetic Resonance in Medicine.* 1994;32:453-458.

[2] Rudin M.. , ed.*In-Vivo Magnetic Resonance Spectroscopy III: In-Vivo MR Spectroscopy: Potential and Limitations.* Springer Berlin Heidelberg 1992.

[3] Boulangé Claire L.. Nuclear Magnetic Resonance Spectroscopy-Applicable Elements| Phosphorus-31 in *Reference Module in Chemistry, Molecular Sciences and Chemical Engineering*Elsevier 2017.

[4] Hatami Nima, Sdika Michaël, Ratiney Hélène. Magnetic Resonance Spectroscopy Quantification Using Deep Learning in *Medical Image Computing and Computer Assisted Intervention – MICCAI 2018*:467–475Springer International Publishing 2018.

[5] Courvoisier S., Klauser A., Lazeyras F.. High-Resolution Magnetic Resonance Spectroscopic Imaging quantification by Convolutional Neural Network in *Proceedings of the 2019 Annual Meeting of the International Society for Magnetic Resonance in Medicine (ISMRM).*

[6] Lee Hyeong Hun, Kim Hyeonjin. Deep learning-based target metabolite isolation and big data-driven measurement uncertainty estimation in proton magnetic resonance spectroscopy of the brain *Magnetic Resonance in Medicine.* 2020;84:1689–1706.

# MRS Workshop 2022
## Overcoming the Barriers to Clinical Use
### DISCONNECT 2 RECONNECT
22-24 August 2022 @ EPFL, Lausanne, Switzerland

67

Poster no. 33 (on-site poster)

**Reproducibility of localized $^{31}$P-magnetic resonance spectroscopy using different surface coils for assessing human hepatic energy metabolism**

*M. Jonuscheit[1,2], B. Korzekwa[1,2], S. Wierichs[1,2], Y. Kupriyanova[1,2], M. Roden[1,2,3] and V.B. Schrauwen-Hinderling[1,2,4]*
[1]*Institute for Clinical Diabetology, German Diabetes Center, Leibniz Institute for Diabetes Research at Heinrich Heine University, Düsseldorf, Germany.* [2]*German Center for Diabetes Research (DZD e.V.), München-Neuherberg, Germany.* [3]*Department of Endocrinology and Diabetology, Medical Faculty and University Hospital, Heinrich Heine University Düsseldorf, Germany.* [4]*Department of Radiology and Nuclear Medicine, Maastricht University Medical Center, Maastricht, The Netherlands*.

### Introduction
Noninvasive quantification of phosphorus metabolites in the liver is established as a valuable tool to investigate energy metabolism and made it possible to detect alterations in hepatic adenosine triphosphate (ATP) and inorganic phosphate ($P_i$) contents in people with type 1 or type 2 diabetes mellitus (T1DM/T2DM) when compared to healthy humans [1-3]. Most persons with T2DM are overweight or obese, making the determination of hepatic phosphorous metabolites challenging due to a high distance of the region of interest (liver) from the coil and limited sensitivity of standard single loop coils. For this reason, a quadrature coil was custom-made and compared to a multi-purpose standard single loop coil regarding $^{31}$P-magnetic resonance spectroscopy (MRS) in the liver.

### Methods
Seven healthy volunteers (6 m/1 f, mean ± SD 38.0 ± 11.6 years; body mass index (BMI) 28.3 ± 3.6 kg/m$^2$) underwent measurements with both coils on three different days within a week (4-7 days interval) to assess the day-to-day variation. In order to provide for standardized physiological conditions, each volunteer was measured at the same time of the day after a 4.5 h fast. To assess intra-session variation (reproducibility) of the quadrature coil, a group of 3 volunteers were examined multiple times during a single session with repositioning of the volunteer between measurements. All examinations were performed on a clinical 3-T MR system (3T Philips Achieva dStream, Best, Netherlands). Two different surface coils were used: a flat 14 cm circular, single loop surface coil (transmit-receive coil; Philips Healthcare, Best, Netherlands) and a custom created curved quadrature surface coil (transmit-receive coil; RAPID Biomedical, Rimpar, Germany) with total $^{31}$P loop size of 220 mm x 160 mm. The $^1$H body coil was used for imaging, $^1$H decoupling and Nuclear Overhauser enhancement (NOE). Liver spectra were obtained using a 3D localized Image-Selected In vivo Spectroscopy (ISIS) sequence with a 5.42 ms and 3.83 ms hyperbolic secant (HS) adiabatic pulse for excitation (excitation bandwidth 1.15 kHz and 1.63 kHz) for Philips and Rapid, respectively, repetition time (TR) 6 s, number of signal averages (NSA) 128, total acquisition time 13 min, samples (N) 2048, spectral bandwidth (BW) 3 kHz, broadband decoupling (WALTZ-4) and continuous wave (CW) NOE. Typical line width of the automatic Philips shimming procedure was ~30 Hz. Spectra of the external reference methylphosphonic acid (MeP) were acquired in separate scans using a pulse-acquire sequence with the identical HS adiabatic pulse of the corresponding coil for excitation, TR 8 s, NSA 16, total acquisition time ~2 min, N 8192, BW 6 kHz, no proton decoupling or NOE was applied. Absolute concentrations were measured by using the phantom-replacement method [4]. Spectra from the phantom were acquired with the same acquisition parameters as in vivo. Corrections were applied for coil loading by measuring the external reference, $T_1$ relaxation times by using the reported values at 3T by Schmid et al [5], the excitation profile of the adiabatic pulse and $B_1$ inhomogeneities of the surface coil in all three spatial directions [4].
All liver spectra were processed using jMRUI software (15 Hz Gaussian apodization, zero order phasing) with the AMARES algorithm together with in-house established prior knowledge. Statistical analysis for changes in γ-ATP and Pi of day-to-day-/intra-session variability and test for difference of the two coils was performed with a paired t-test.

### Results
Table 1 summarizes the data of day-to-day- and intra-session coefficient of variation (CV) of hepatic γ-ATP and Pi of both coils. The absolute concentrations of γ-ATP and Pi was 2.29 ± 0.24 mM and 1.75 ± 0.25 mM for the Philips P140 coil and 2.19 ± 0.23 mM and 1.72 ± 0.20 mM for the Rapid quadrature coil, respectively. Paired t-test showed no statistical differences in phosphorus metabolites concentrations, determined with the two coils.

### Discussion and Conclusion
Single voxel (ISIS) $^{31}$P-MRS allowed robust detection of γ-ATP and Pi concentrations within a reasonable time frame. Good reproducibility was shown with both coils (CV < 10 %) and determining the metabolites on another day did not introduce additional variation. There was no benefit of the bigger coil loops of the quadrature coil for lean and overweight healthy volunteers, however, using the quadrature coil may be beneficial for measurements of people with BMI > 33 kg/m$^2$. The similarity of metabolite concentrations, measured with the two coils shows the robustness of the phantom-replacement method for absolute quantification.

### References
[1] Szendroedi et al. *Hepatology* 2009; [2] Gancheva et al. *Diabetes* 2016; [3] Kupriyanova et al. *J. Hepatol.* 2021; [4] Laufs et al. *MRM* 2014; [5] Schmid et al. *NMR Biomed.* 2008

### Figure
Table 1: Day-to-day and intra-session variability (CVs):

| | | Intra-session CV | | Day-to-day CV | |
|---|---|---|---|---|---|
| | | γ-ATP | Pi | γ-ATP | Pi |
| Philips P140 | with repositioning | 9 % [n=5]* | 7 % [n=5]* | 7.1 % [n=7] | 8.2 % [n=7] |
| Rapid quadrature | w/o repositioning | 3.5 % [n=3] | 5.7 % [n=3] | 7.5 % [n=7] | 7.1 % [n=7] |
| | with repositioning | 6.1 % [n=3] | 7.3 % [n=3] | | |

*Intra-session CV data of Philips P140 are from[4].

MRS Workshop 2022
Overcoming the Barriers to Clinical Use
DISCONNECT 2 RECONNECT
22-24 August 2022 @ EPFL, Lausanne, Switzerland

68

Poster no. 34 (on-site poster)

**Altered Brain Energy Metabolism Related to Astrocytes in Alzheimer's disease**

Yuhei Takado[1,2], Kosei Hirata[1,3], Kiwamu Matsuoka[1], Maiko Ono[1], Kenji Tagai[1], Hironobu Endo[1], Naomi Kokubo[1], Xiaoyun Zhou[1], Hitoshi Shinotoh[1], Keisuke Takahata[1], Takayuki Obata[1,3], Kazunori Kawamura[1], Ming-Rong Zhang[1], Hitoshi Shimada[1], Takashi Saito[4], Takaomi Saido[5], Naruhiko Sahara[1], Takahiko Tokuda[1], Takanori Yokota[3], Tetsuya Suhara[2], Makoto Higuchi[1]

1. Institute for Quantum Medical Science, National Institutes for Quantum Science and Technology, Chiba, Japan
2. Institute of Quantum Life Science, National Institutes for Quantum Science and Technology, Chiba, Japan
3. Department of Neurology and Neurological Science, Tokyo Medical and Dental University, Tokyo, Japan
4. Department of Neurocognitive Science, Institute of Brain Science, Nagoya City University Graduate School of Medical Sciences, Nagoya, Japan
5. Laboratory for Proteolytic Neuroscience, RIKEN Center for Brain Science, Saitama, Japan

【Background】 Recent large-scale proteomic analysis revealed early changes in the energy metabolism of Alzheimer's disease (AD) brains. In AD brains, amyloid and tau proteins are two hallmarks of the disease. However, how they influence altered energy metabolism remains unknown.

【Aim】 To clarify how amyloid and tau are involved in altered energy metabolism and astrocyte function changes in AD patients.

【Methods】 We performed magnetic resonance spectroscopy (MRS) at the cingulate gyrus regions in AD patients (n = 30), progressive supranuclear palsy (PSP) patients (n = 30) and healthy subjects (n = 30). We also performed MRS at hippocampus and cortex regions in mouse models with AD-like accumulation of amyloid (APP[NL-G-F/NL-G-F]-knock-in mice) and tau (rTg4510).

【Results】 The MRS results showed increased levels of lactate, glucose, and myoinositol, an astrocytic marker, in AD patients compared to healthy subjects. Moreover, lactate levels were positively correlated with myoinositol levels in the posterior cingulate gyrus region of AD patients. While the APP[NL-G-F/NL-G-F]-knock-in mice showed a more pronounced increase of lactate and myoinositol levels, the changes were not evident in the mouse model of tau accumulation in neurons (rTg4510), suggesting the more relevant association between astrocyte dysfunction and amyloid than tau in AD pathology. Moreover, lactate and myoinositol levels were positively correlated in the amyloid-accumulated mouse model. The additional clinical MRS results in PSP patients, a tauopathy characterized by tau accumulation in astrocytes, showed increased lactate and myoinositol levels in the anterior cingulate region, indicating that internal tau accumulation in astrocytes could be a trigger for functional changes of astrocytes in case of primary tauopathies. Moreover, elevated lactate and myoinositol levels in the cingulate cortex reflected the cognitive decline of AD and PSP, respectively.

【Conclusion】 This study in humans and mice suggested that astrocytes functional changes caused by extracellular amyloid or internal tau accumulation in astrocytes contribute to altered energy metabolism in dementia, which may serve as therapeutic targets for the diseases.

**MRS Workshop 2022**
Overcoming the Barriers to Clinical Use
DISCONNECT 2 RECONNECT
IT'S TIME
22-24 August 2022 @ EPFL, Lausanne, Switzerland

69

Poster no. 35 (on-site poster)

EFFECTS OF PREFRONTAL TDCS ON BRAIN METABOLITES IN THE DLPFC OF HEALTHY
SUBJECTS - A DOUBLE-BLIND PLACEBO-CONTROLLED MRS STUDY

Gizem Vural[1], Aldo Soldini[1,2], Eva Mezger[1], Esther Dechantsreiter[1], FrankPadberg[1], Daniel Keeser[1].

[1] Department of Psychiatry and Psychotherapy, University Hospital of Munich, München, Germany;
[2] Max Planck Institute for Psychiatry, Germany

Abstract

Background: The efficacy of prefrontal transcranial direct current stimulation (tDCS) in the treatment of various clinical conditions has been demonstrated in initial pilot studies, but the mechanisms of tDCS action are not fully understood. Studies investigating the balance between neuronal excitation and inhibition in the dorsolateral prefrontal cortex (DLPFC) using magnetic resonance spectroscopy (MRS) of glutamate and gamma aminobutyric acid (GABA) have shown heterogeneous results. The aim of this double-blind, placebo-controlled study was to investigate the effects of prefrontal tDCS on glutamate and GABA in the left DLPFC using combined tDCS/MRS in healthy participants. Thus, this study extends the previous tDCS/MRS approach to other target regions.

Methods: Fourty-one healthy participants were screened and recruited. Prefrontal tDCS (Anode: F3, Cathode: F4) was applied inside an MRI Siemens Prisma scanner using a neuroConn DC-Stimulator MR device. Active stimulation consisted of a 2mA electrical current delivered for a duration of 20 minutes, while the sham condition consisted only of a ramp-up/ramp-down sequence to induce tactile sensations. We recorded three MEGA-PRESS spectroscopy sequences before, during, and after stimulation with tDCS, as well as fMRI sequences at baseline and post-stimulation in the resting state condition. Spectroscopy was analyzed using the software packages Gannet and LCModel to calculate GABA and glutamate concentrations, respectively.

Results: Although an interim analysis with a smaller sample size revealed no significant differences between active and sham tDCS, the results for the full sample (N=41) will be presented and further discussed together with a correction of neurotransmitter concentration using only grey matter tissue for MRS calculations.

Keywords: Magnetic Resonance spectroscopy (MRS), transcranial direct current stimulation (tDCS), dorsolateral prefrontal cortex (DLPFC)

# MRS Workshop 2022
## Overcoming the Barriers to Clinical Use
### DISCONNECT 2 RECONNECT
22-24 August 2022 @ EPFL, Lausanne, Switzerland

70

Poster no. 36 (on-site poster)

## Integrating hybrid CSI/EPSI acquisitions with L2 regularization for fast lipid removal of MRSI

Yiling Liu[1], Jianfeng Bao[2], Hao Chen[1], Guiqin Liu[3], and Zhiyong Zhang[1]

[1]School of Biomedical Engineering, Shanghai Jiao Tong University, Shanghai, China. [2]The First Affiliated Hospital of Zhengzhou University, Zhengzhou University, Zhengzhou, China. [3]Renji Hospital Affiliated to Shanghai Jiaotong University School of Medicine, Shanghai Jiao Tong University, Shanghai, China.

**Synopsis:** Lipid suppression is one of the major challenges for magnetic resonance spectroscopic imaging (MRSI). The widely used placements of lipid saturation bands not only demand a skillful scanning operation but also restrict the full brain coverage. Therefore, post-processing for lipid removal becomes clinically attractive and valuable [1-2]. Chemical shift imaging (CSI) acquisition generally has limited k-space coverage but a high Signal-to-Noise Ratio (SNR). Echo-planar spectroscopic imaging (EPSI) significantly accelerates MRSI, which allows an extended k-space coverage with a low SNR within a short period. The hybrid of them can help reduce truncation artifacts [3]. A union-of-subspaces (abbreviated as UOS in this manuscript) model [4] was proposed to remove nuisance signals in hybrid data with limited and sparse (k-t)-space coverage. However, the UOS algorithm requires accurate prior knowledge of spectral supports and takes a long reconstruction time. In this work, a simple but effective method by integrating hybrid CSI/EPSI acquisitions with L2 regularization is proposed for fast lipid removal of MRSI. In-vivo brain studies demonstrate the effectiveness and low computational cost of the proposed method.

**Methods:** The hybrid CSI/EPSI acquisitions rely on the same excitation and refocusing evolution on the modified CSI and EPSI sequence. There is a tilting $k_x$-t trajectory of EPSI and a small interval of starting acquisition times of CSI and EPSI. All those trajectory differences are correctable by synchronizing the center CSI/EPSI acquisitions with time-shifting correction and re-gridding. As the flowchart is shown in Fig. 1, a hybrid dataset is generated by adding the consistent CSI/EPSI acquisitions and then followed by a lipid penalty with L2-regularization.
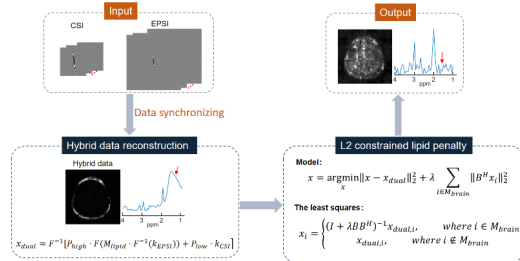


**Figure 1. The flowchart of the proposed method.**
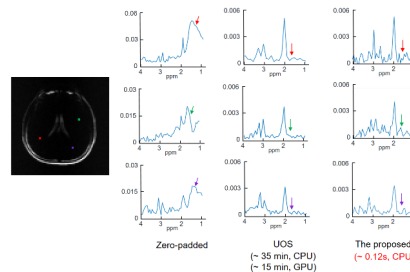


**Figure 2. The lipid removal result.**

**Results and Discussion:** One of the lipid removal results compared with the state-of-the-art UOS method is depicted in Fig. 2. It can be seen that our method achieved comparable lipid suppression results within 1 second while the UOS takes about 15 minutes. It indicates the effectiveness and efficiency of the proposed method, which is of great clinical value.

**Conclusions:** Integrating hybrid CSI/EPSI acquisitions with L2 regularization is proposed for fast lipid removal of MRSI. In-vivo brain studies demonstrate its effectiveness and low computational cost.

**References**

[1] Bilgic B, Chatnuntawech I, Fan A P, et al. Fast image reconstruction with L2-regularization. Journal of magnetic resonance imaging, 2014, 40(1): 181-191.

[2] Bhattacharya I, Jacob M. Compartmentalized low-rank recovery for high-resolution lipid unsuppressed MRSI. Magnetic resonance in medicine, 2017, 78(4): 1267-1280.

[3] Metzger G, Sarkar S, Zhang X, et al. A hybrid technique for spectroscopic imaging with reduced truncation artifact. Magnetic resonance imaging, 1999, 17(3): 435-443.

[4] Ma C, Lam F, Johnson C L, et al. Removal of nuisance signals from limited and sparse 1H MRSI data using a union-of-subspaces model. Magnetic resonance in medicine, 2016, 75(2): 488-497.

MRS Workshop 2022
Overcoming the Barriers to Clinical Use
DISCONNECT 2 RECONNECT
22-24 August 2022 @ EPFL, Lausanne, Switzerland

71

Poster no. 37 (on-site poster)

**Magnetic resonance spectroscopic imaging visualized spatial mapping of decreased glutamate levels associated with tau depositions in Alzheimer's disease patients**

Kiwamu Matsuoka, [1,2], Kosei Hirata [1], Naomi Kokubo [1], Kenji Tagai [1], Hironobu Endo [1], Keisuke Takahata [1], Hitoshi Shinotoh [1], Maiko Ono [1], Chie Seki [1], Kazunori Kawamura [3], Ming-Rong Zhang [3], Hitoshi Shimada [1,4], Yuhei Takado [1], Makoto Higuchi [1]

1. Department of Functional Brain Imaging, Institute for Quantum Medical Science, Quantum Life and Medical Science Directorate, National Institutes for Quantum Science and Technology,

2. Department of Psychiatry, Nara Medical University,

3. Department of Advanced Nuclear Medicine Sciences, Institute for Quantum Medical Science, Quantum Life and Medical Science Directorate, National Institutes for Quantum Science and Technology,

4. Department of Functional Neurology & Neurosurgery, Center for Integrated Human Brain Science, Brain Research Institute, Niigata University.

**ABSTRACT**

**Objective**: Despite accumulating evidence for impaired glutamatergic neurotransmission in the cingulate cortex in Alzheimer's disease (AD) brains, its significance in neurofunctional and neuropathological alterations remains elusive. We hypothesized the regional alterations of glutamate (Glu) at the level of the cingulate gyrus in relation to tau and A$\beta$ depositions in AD patients. To test this hypothesis, we performed magnetic resonance spectroscopic imaging (MRSI) at the level of the cingulate gyrus for evaluation of metabolic levels.

**Methods**: We enrolled 19 patients with AD, consisting of 8 cases with mild cognitive impairment due to AD and 11 cases with AD dementia, and 26 cognitively healthy controls (HCs). We performed tau and amyloid-$\beta$ (A$\beta$) PET with $^{18}$F-florzolotau (also known as $^{18}$F-PM-PBB3 or $^{18}$F-APN-1607) and $^{11}$C-PiB, respectively, and single-plane MRSI for evaluating Glu, total N-acetylaspartate (tNAA), myo-inositol, and total choline to total creatine (tCr) ratios. PET probe retentions were quantified as standardized uptake value ratio (SUVR) using the cerebellar cortex as a reference region.

**Results**: Z-score maps of the AD group compared to the HC group demonstrated marked tau and A$\beta$ depositions in extensive cortical gray matter regions, and reduced Glu and tNAA to tCr ratios in more confined areas. Glu/tCr ratios were correlated with tau but not A$\beta$ burdens in some regions, including the posterior cingulate cortex (PCC). In an analysis of combined voxels covering PCC, Glu and tNAA to tCr ratios were significantly decreased ($p < 0.05$ for both ratios). Glu/Cr ratios were correlated negatively with tau deposits in the AD group ($r = -0.46$, $p < 0.05$) and positively with mini-mental state examination scores ($r = 0.66$, $p < 0.05$) in AD dementia cases.

**Conclusions**: MRSI revealed the regional vulnerability of the glutamatergic system to tau depositions in AD brains. In the PCC, tau accumulations are likely to induce disrupted glutamatergic transmissions, aggravating cognitive functions.

MRS Workshop 2022
Overcoming the Barriers to Clinical Use
DISCONNECT 2 RECONNECT
IT'S TIME
22-24 August 2022 @ EPFL, Lausanne, Switzerland

72

Poster no. 38 (on-site poster)

**Spatial Lipid Signal Separation for Spectroscopic Imaging of Intramyocellular and Extramyocellular Lipids**

Peter Adany,[1] In-Young Choi,[1-3] and Phil Lee[1,3]

[1]Hoglund Biomedical Imaging Center, [2]Department of Neurology, [3]Radiology, University of Kansas Medical Center, Kansas City, Kansas, USA

INTRODUCTION Measurement of skeletal muscle lipids provides valuable information regarding muscle physiology and function in health and disease, associated with insulin resistance and physical activity status. Magnetic Resonance Spectroscopic Imaging (MRSI) of the leg muscles offers improved specificity and quantitative measurement of intramyocellular and extramyocellular lipids (IMCL, and EMCL) compared to the Dixon and other imaging-based techniques. However, removing the strong interfering lipid signals from subcutaneous fat presents a significant challenge to quantify metabolite and lipid signals in the muscles. In this work, we evaluate the feasibility of our recently developed Fast Lipid Processing (FLIP) spatial lipid removal algorithm [1] to separate subcutaneous lipid signals from signals from muscles (e.g., IMCL and EMCL) in high resolution 2D MRSI of the human thigh.

METHODS ^{1}H MRSI data were acquired at 3T (Skyra, Siemens) using a four-channel flex receiver coil, with a 2D echo planar spectroscopic imaging sequence (EPSI) [2] (TE/TR = 87/1551 ms; 280×280 mm$^2$ field of view; matrix size 50×50; Grappa with 76% fill factor; 1000 time points; spatial resolution 5.5×5.5×15 mm; acquisition time of 2 minutes). T1 weighted images were acquired with a gradient echo sequence (0.9×0.7×2.0 mm resolution). Anatomic segmentation was done manually using the USHIRT shape interpolation algorithm [3]. Lipid removal was performed by using the FLIP algorithm. The FLIP processing was modified to include additional compartments, and muscle compartments were reconstructed using Spectral Localization by Imaging (SLIM) [4,5] on the subcutaneous lipid-removed data. Spectral fitting was performed using LCModel [6] using the muscle analysis setting.

RESULTS Fig. 1 shows results of spatial lipid reconstruction and removal using FLIP. Raw spectra are shown (left), with strong lipid signal contributions from the subcutaneous tissue layer and the bone marrow. Since FLIP uses a spatial rather than spectral model, it could avoid removing the interior signals, e.g. lipids within the bone marrow (Fig. 1). The subtracted spectra show highly effective removal of the subcutaneous lipid signals.

Fig. 2 shows tissue compartments and corresponding compartmental spectra obtained using SLIM, after removal of subcutaneous lipid signals using FLIP. The spectrum from the first compartment shows EMCL and IMCL of similar height, indicating efficient removal of lipid signals from subcutaneous lipid. Manual anatomical segmentation of the slices was facilitated by drawing four key slices and interpolating to high resolution using USHIRT.



Fig. 1. Input data overlaid with T1-weighted anatomical images (left). FLIP reconstructed lipid spectra (middle). Residual spectra after subcutaneous lipids have been subtracted.

This work shows a promising capability to expand applications of high resolution MRSI to muscles, by effectively removing the subcutaneous lipid signals without further lipid mitigation methods. Effective spatial lipid removal helps to avoid the need for additional lipid signal mitigation approaches that attenuate all lipid signals. The methods will benefit from further developments, such as corrections for B$_0$ and B$_1$ inhomogeneities, as well as refined compartment models addressing the muscle fiber orientations.



Fig. 2 Compartmental spectra reconstructed using FLIP and SLIM. Compartments of the subcutaneous layer and major muscles are shown based on manual segmentation and USHIRT shape interpolation.

[1] Adany et al. Magn Reson Med 86(6):2930-2944 (2021). [2] Maudsley et al. Magn Reson Med 61(3):548-559 (2009). [3] Adany et al. Proc Intl Soc Mag Reson Med 23:3755 (2015). [4] Hu et al. Magn Reson Med (1988). [5] Adany et al. Neuroimage 134:355-364(2016). [6] Provencher, Magn Reson Med 30:672-9 (1993).

Poster no. 39 (on-site poster)

## B₁⁺ Corrected Metabolite Concentration Estimates from 7T FID-CRT-MRSI

Philipp Lazen[1,2], Wolfgang Bogner[1], Karl Rössler[2], Siegfried Trattnig[1,3], Gilbert Hangel[1,2]

[1]High-field MR Center, Department of Biomedical Imaging and Image-guided Therapy, Medical University of Vienna, Austria; [2]Department of Neurosurgery, Medical University of Vienna, Austria, [3]Institute for Clinical Molecular MRI, Karl Landsteiner Society, Austria.

### Introduction

7T magnetic resonance spectroscopic imaging (MRSI) suffers from inhomogeneities of the $B_1^+$ field. We calculated concentration estimates (CE)[1] in healthy volunteers and implemented a $B_1^+$ inhomogeneity correction process.

### Methods

Seven volunteers (4 male, 3 female, mean age 24.3±4 years) were measured using a protocol consisting of an MP2RAGE, a whole-brain CRT-FID-MRSI (64x64x39, 3.4 mm resolution), a water reference MRSI scan, and a $B_1^+$ map[1,2]. The spectroscopic data was fitted using LCModel. For the $B_1^+$ correction process, the measured $B_1^+$ map was interpolated to the MRSI's matrix size and corrected for its pulse profile and transmit voltage U. Next, for every voxel, the anticipated signal was calculated[3] based on the flip angle $α_L$ as given by the $B_1^+$ map and the respective TR and T1 for each of the metabolites of interest (as well as water) according to

$$S_{B1} = M_0 \, sin(α_L) \cdot (1 - e^{-TR/T1}) / (1 - cos(α_L) \, e^{-TR/T1}).$$

Additionally, an analogous signal map containing T1 correction only was created. The signal maps were calculated for gray and white matter and combined based on a segmentation and used for normalization of the metabolite and water amplitude maps. Internal water referencing was then performed using literature water concentrations, yielding CEs for every metabolite[1]. The resulting CE maps were numerically analyzed using averages and standard deviations.

### Results

In absolute terms, the CE with T1 correction over the whole brain over all volunteers was 1.82±0.82 mM for tCho, 6.63±2.69 mM for tCr, 8.92±4.89 mM for Glu, 5.52±2.03 mM for Ins and 9.97±4.15 for NAA. The $B_1^+$ corrected CEs were 1.89±0.86 mM for tCho, 6.70±2.74 mM for tCr, 9.09±5.04 mM for Glu, 5.83±2.15 mM for Ins and 10.25±4.31 mM for NAA. This difference is relatively small and changes in the maps are mainly visible in border regions, where the excitation by the $B_1^+$ field is relatively weak.



Concentration Estimate Maps — Vol 1 — tCho, tCr, Glu, Ins, NAA
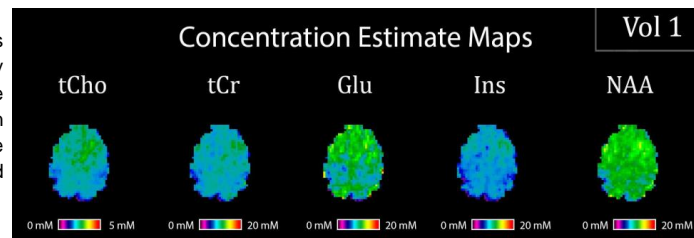
### Conclusion

$B_1^+$ correction has a very small effect on metabolite CEs for our method. The $B_1^+$ correction increased the CEs compared to our previous publication slightly[1], and results remained within literature value ranges.

### References

1. Hangel G et al. Inter-subject stability and regional concentration estimates of 3D-FID-MRSI in the human brain at 7 T, 2021. NMR in Biomed. https://doi.org/10.1002/nbm.4596
2. Hingerl L et al. Clinical High-Resolution 3D-MR Spectroscopic Imaging of the Human Brain at 7 T, 2020. Invest Radiol. https://doi.org/10.1097/RLI.0000000000000626
3. Bernstein MA et al. Handbook of MRI Pulse Sequences. Elsevier; 2004. https://doi.org/10.1016/B978-0-12-092861-3.X5000-6

Poster no. 40 (on-site poster)

## Comparing 7T FID-CRT-MRSI with Amino Acid PET

Philipp Lazen[1,2], Julia Furtner[1], Ivo Rausch[3], Wolfgang Bogner[1], Georg Widhalm[2], Karl Rössler[2], Tatjana Traub-Weidinger[1], Siegfried Trattnig[1], Gilbert Hangel[1,2]

[1]Department of Biomedical Imaging and Image-guided Therapy, [2]Department of Neurosurgery and [3]Center for Medical Physics and Biomedical Engineering, Medical University of Vienna, Austria

**Introduction**

Magnetic resonance spectroscopic imaging (MRSI) and positron emission tomography (PET) are both imaging modalities capable of going beyond the mere structural contrasts delivered by other modalities, instead delivering information about metabolic processes in physiological and pathological tissues. Due to their similar nature, we decided to compare the results from our 7T MRSI with clinical PET scans in glioma patients. This study represents the first quantitative comparison of 7T MRSI and PET.

**Methods**

We retroactively included 24 glioma patients who had participated in a 7T MRSI tumor study and had undergone a PET scan within two months of the MRI in this study[1]. The MRI protocol consisted of an MP2RAGE, a FLAIR and a whole-brain CRT-FID-MRSI (64x64x39, 3.4 mm resolution)[2]. Spectroscopic quantification used our processing pipeline in conjunction with LC Model. For PET, both FET and MET were used as tracers, and imaging used a reconstructed pixel size of 2 x 2 mm.

For analysis, regions of interest (ROIs) were defined based on the PET tracer uptake, where the ratio of the ROI to normal appearing white matter (tumor to brain ratio, TBR) was classified using three distinct threshold values (1.15, 1.6 and 2.0). For the MRSI, ROIs were based on the ratio of total choline to N-acetyl aspartate (NAA) using the same threshold values as the PET, which were additionally masked with a tumor segmentation by a radiologist. PET and MRI were coregistered using mutual information, and the main focus of the analysis was on Sørensen–Dice similarity coefficients (DSC), which were calculated together with the distances between the centers of intensity for both modalities' ROIs for every patient.

**Results**

We found that the metabolite ratios that showed the best correspondence to PET were glutamine to NAA (Gln/NAA) and glycine to NAA (Gly/NAA), not choline to NAA (Cho/NAA), which is commonly used clinically as a tumor marker in MRSI. The best correspondence between PET and MRSI was achieved when using stricter threshold values for both PET and MRSI. For a threshold value of 1.6 for the TBR and the metabolite ratios, DSCs for PET and MRSI can be seen in the table on the right.

| Metabolite Ratio to NAA | DSC between Metabolite and PET |
|---|---|
| Gln | 0.66 ± 0.40 |
| Gly | 0.57 ± 0.36 |
| Cho | 0.53 ± 0.36 |

**Conclusion**

Gln and Gly ratios correspond better to PET hotspots than Cho. This study is limited by the number of participants and its findings need to be confirmed in larger cohorts.



Comparison of PET and MRSI Ratio Maps
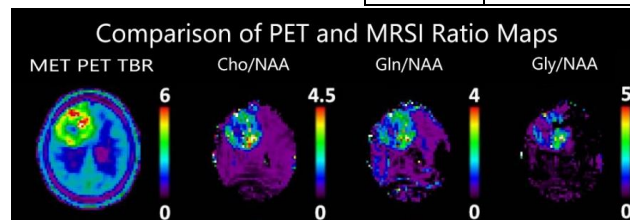
**References**

1. Hangel G et al. 7T HR FID-MRSI Compared to Amino Acid PET: Glutamine and Glycine as Promising Biomarkers in Brain Tumors, 2022. Cancers. https://doi.org/10.3390/cancers14092163
2. Mauler J et al. Spatial Relationship of Glioma Volume Derived from 18F-FET PET and Volumetric MR Spectroscopy Imaging: A Hybrid PET/MRI Study, 2018. Journal of Nuclear Medicine. https://doi.org/10.2967/jnumed.117.196709

Poster no. 41 (on-site poster)

**Linear combination modeling of complex relative to real ^{1}H MR spectra improves quantification precision**

Leonardo Campos[1], Kelley M. Swanberg[1], Martin Gajdošík[1], Karl Landheer[1], and Christoph Juchem[1,2]

1. Biomedical Engineering, Columbia University, New York, NY, USA 2. Radiology, Columbia University, New York, NY, USA

Spectral fitting over the real domain remains a common method for in vivo ^{1}H MRS quantification.[1,2] To determine the extent to which additional information provided by the full complex data might further inform this process, we systematically compared complex and real fitting schemes (Fig. A).

In Analysis 1, five hundred unique noisy Lorentzian singlets (3.00ppm; linewidth 7Hz; 2048 points) were generated for each of nine distinct SNR values using INSPECTOR[3] and additional batch scripting.[4,5] This was conducted for both correlated and uncorrelated noise conditions (Fig. B), analyzed to account for sources of noise of varying correlation that may be present in vivo. The spectra were then quantified using linear combination modeling over either the complex or real domains with no additional processing, scaling only solved by the fit, and relative quantification errors compared against results from noiseless fits. For Analysis 2, we simulated metabolite spectra (semi-LASER; 3T; $T_E$=20.1ms, linewidth 8Hz, 2048 points)[6] consisting of 19 metabolites with literature-informed physiological $T_2$ and concentration values from the occipital cortex. Five hundred noisy spectra were created for each of six SNR values for both noise conditions. With the same metabolite bases used in simulation and no additional processing applied, these spectra were quantified with amplitude scaling and offset, zero-order phase, frequency shift, and Lorentzian broadening solved by the fit. In Analysis 3, noiseless simulated metabolite spectra were combined with 20 measured (semi-LASER; 3T; $T_E$=20.1ms)[6] in vivo macromolecule signals to consider baseline effects at realistic noise floor (average SNR 300). In addition to the aforementioned parameters solved, Gaussians were added to the basis set for macromolecule modeling and a cubic spline baseline (knot interval 1ppm; no smoothing)[5] was included in the fit.

For the first two analyses, the use of complex fitting consistently improved precision independent of SNR, noise correlation, and to a lesser degree metabolite by a factor of approximately √2 (Fig. C-D). Including the baseline, complex fitting provided improvements in precision and accuracy on average, although with greater variability by metabolite (Fig. E).

This provides insight into the improvements provided by complex relative to real fitting of ^{1}H MR spectra, demonstrating potential suboptimal use of the available data in fits considering the real domain only without further processing. This can help to inform future studies regarding improvements in quantification, with further consideration for more conditions reflective of in vivo spectra for greater translatability.
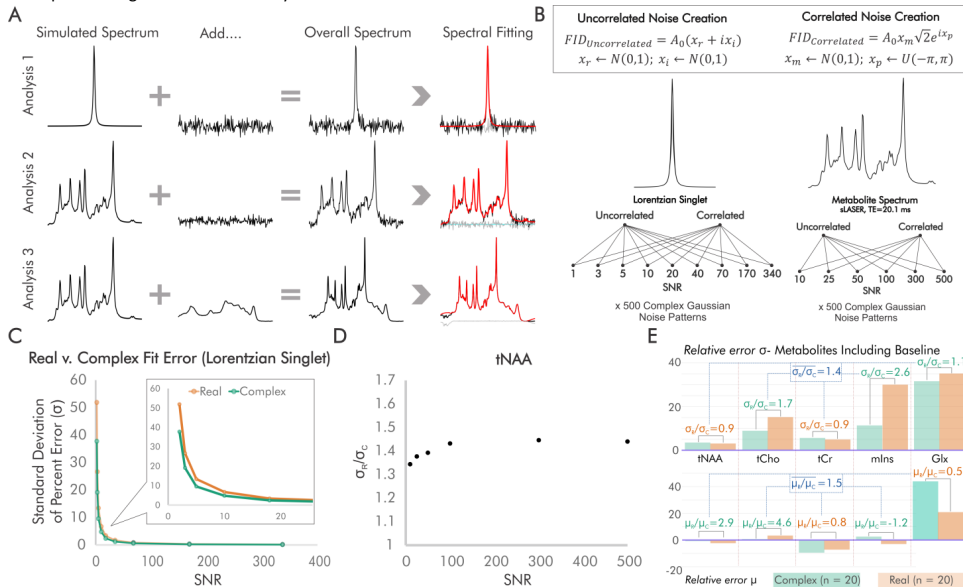


**Figure. Overall methodology and results**. A) Overview of three analyses comparing linear combination modeling of complex and real spectra. B) Definition of correlated and uncorrelated noise conditions, and SNR values for the first two analyses. Example results for C) Lorentzian (Analysis 1), D) metabolite (Analysis 2), and E) metabolite with baseline conditions (Analysis 3).

**1.** Provencher SW. *Magnetic Resonance in Medicine* 30:672-679 (1993). **2.** Swanberg KM et al. *Frontiers in Neurology* 10, 1173 (2019). **3.** Gajdošík M et al. *Scientific Reports* 11, 2094 (2021). **4.** Swanberg KM et al. *Proc Int Soc Magn Reson Med* 4327 (2019). **5**. Swanberg KM et al. *Proc Int Soc Magn Reson Med* 2856 (2020). **6.** Landheer K et al. *NMR in Biomedicine* 33:e4324 (2020).

Poster no. 42 (on-site poster)

## MRS-Sim: Open-Source Framework for Simulating In Vivo Clinical MR Spectroscopy Data

**J. T. LaMaster[1], D. Das[2], G. Oeltzschner[3], J. Crane[4], Y. Li[4], and B. H. Menze[5]**

[1]Technical University of Munich, Faculty of Computer Science; [2]Gabrieli Laboratory, Massachusetts Institute of Technology; [3]Russel H. Morgan Department of Radiology and Radiological Sciences, The Johns Hopkins University, School of Medicine; [4]University of California San Francisco, Center for Intelligent Imaging; [5]University of Zurich, Department of Quantitative Biomedicine

**Background:** Deep learning research for MRS is a budding field with many promising applications. The greatest challenge currently is to generate enough data to train robust deep learning (DL) models. Clinical datasets tend to be very small while DL projects can require 1E5 to 5E5 or more individual spectra. A promising solution is to train on inexpensive synthetic data and apply the DL model to clinical data. Such pre-trained models translate well only when the distribution of the training data is similar enough to that of the target domain, i.e. clinical data, meaning that realistic training data is a requirement. While there are many software applications for metabolite basis set simulation, no publicly available resource is currently available for simulation of realistic, clinical in-vivo data and labs must re-develop individual solutions. This work presents an open-source framework that applies a sophisticated MRS signal forward physics model to generate large datasets of synthetic in-vivo-like spectra.

**Method:** This framework proposes a rich MRS signal physics model, Eqn. 1, which leans heavily on the physical parameters that are incorporated into models used by popular spectral fitting algorithms like LCModel, TARQUIN, etc. First, the framework uses a combination of high-quality metabolite basis functions from MARSS[1], which accurately capture the effects of spatial localization, vendor-specific RF pulses, and sequence timings, and MM/lipid basis functions from Osprey[2]. Next, the physics model modulates these basis functions by scaling their amplitudes and then models Voigt lineshapes, accounting for B0 inhomogeneities, zero- and first-order phase offsets, a uniform frequency shift for metabolites and a second one for lipid and macromolecular signals, and then Gaussian noise. Finally, the framework includes a generator for the baseline and residual water components which are added to the scaled and shifted synthetic spectra. This generator uses a bounded, pseudo-random walk followed by smoothing function with one set of parameters for the broad, smooth nature of baselines and another set for the more irregular residual water line shapes. The Hilbert transform produces the imaginary component for these two terms and the noise. The simulated spectra are then re-sampled using a cubic Hermite modified Akima spline interpolation to the desired ppm range and number of points.

$$F(\omega) = \mathcal{F}\left( \left( \sum_n^N \underbrace{M_n * basisfcn_n}_{amplitude\ scaling} \underbrace{e^{-d_n t - g_n t^2}}_{lineshape} \underbrace{e^{-i\Delta f_n t}}_{fshift} + \mathcal{H}\left( \underbrace{\mathcal{N}(0, \mathrm{snr}_0, l)}_{noise} + baseline + resWater \right) \right) \underbrace{e^{i(\phi_0 + \phi_1)}}_{phase} \underbrace{\sum_{r=1}^R e^{-i\Delta\omega_r t}}_{B_0\ inhomog.} \right) \qquad \textbf{Eqn. 1}$$

**Examples:**
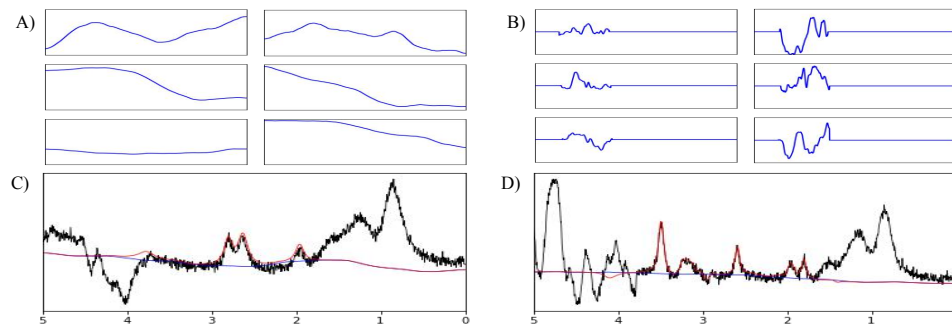


**Figure 1**: Generator samples. **A)** Baselines with various flexibilities (arbitrary ppm); **B)** Residual Water ([6,0] ppm); **C)** Long Echo (Cho, Cre, NAA, + 4 MM, 2 Lip); and **D)** Short Echo (Cho, Cre, NAA, Glu, Gln, Lac, Ins, + 4 MM, 2 Lip)

**Discussion:** This work presents an open-source framework to simulate realistic, clinical in-vivo MRS data with the primary goal of facilitating deep learning research for MRS applications. This framework uses accurate metabolite basis functions and a rich, highly modular physics model with a high number of degrees of freedom. Due to the modularity of the implementation, it is very easy to turn artifacts on and off and generate spectra with different metabolites, different nuclei, different sequences, and different clinical scenarios. The model is run in the terminal via a command line function and a .json config file. It is accompanied by a Jupyter notebook manual giving an overview of the model, how to use it, and how to customize the dataset. This framework will enable researchers to explore deep learning research for MRS/MRSI, even when access to in-vivo data is limited.

**References:**
[1] Landheer, K., Swanberg, K. M., & Juchem, C. (2019). Magnetic resonance Spectrum simulator (MARSS), a novel software package for fast and computationally efficient basis set simulation. In NMR in Biomedicine (Vol. 34, Issue 5). Wiley. https://doi.org/10.1002/nbm.4129
[2] Oeltzschner, G., Zöllner, H. J., Hui, S. C. N., Mikkelsen, M., Saleh, M. G., Tapper, S., & Edden, R. A. E. (2020). Osprey: Open-source processing, reconstruction &amp; estimation of magnetic resonance spectroscopy data. In Journal of Neuroscience Methods (Vol. 343, p. 108827). Elsevier BV. https://doi.org/10.1016/j.jneumeth.2020.108827

**MRS Workshop 2022**
Overcoming the Barriers to Clinical Use
DISCONNECT 2 RECONNECT
22-24 August 2022 @ EPFL, Lausanne, Switzerland

77

IT'S TIME

Poster no. 43 (online poster)

*MRS workshop 2022, Lausanne, Switzerland*
**Seasonal influences on brain GABA+ and Glx concentrations**

Spurny-Dworak B[1], Reed MB[1], Handschuh P[1], Vanicek T[1], Spies M[1], Bogner W[2], Lanzenberger R[1]

[1]*Department of Psychiatry and Psychotherapy, Medical University of Vienna, Austria* [2]*Department of Biomedical Imaging and Image-guided Therapy, High Field MR Centre, Medical University of Vienna, Austria*

**Introduction:** Seasonal influences on neurotransmitter systems have been shown in the dopaminergic and foremost the serotonergic system. GABA serves as important modulator to regulate the circadian rhythm in the suprachiasmatic nucleus (Albers, 2017). Thus, there is a potential seasonal effect on derived measures of GABA+ (GABA and macromolecules) and Glx (glutamate+glutamine) from GABA-edited magnetic resonance spectroscopy imaging (MRSI). If so, a need for seasonal correction of neurotransmitter ratios in statistical models would become necessary. We therefore investigated seasonal effects on brain GABA+ and Glx ratios to total creatine (tCr) in 5 brain regions of healthy participants using MRSI.

**Methods:** Baseline measurements of 159 healthy subjects taken from multiple studies (79, female, mean age ± SD= 25.4 ± 5.3 years) could be included in this analysis. MRSI measurements were conducted using a 3D GABA-edited MEGA-LASER sequence described in (Bogner, 2014) including real-time correction for rigid body motion and center frequency changes on a 3 Tesla MR Scanner (MAGNETOM Prisma, Siemens Medical, Erlangen, Germany), with a TE of 68 ms, volume of interest (VOI) = 80 (l-r) x 90 (a-p) x 80 (s-i) mm$^3$ and field of view (FOV) = 160 x 160 x 160 mm$^3$. All spectra within the VOI were processed using MATLAB, MINC and LCModel software. For region of interest (ROI)-based analysis, structural T1-weighted images, acquired prior to each MRSI scan, were segmented using FreeSurfer. Maps of GABA+, Glx and tCr were interpolated to the resolution of structural images, overlaid with masks and mean GABA+/tCr and Glx/tCr ratios calculated for each ROI: hippocampus, insula, putamen, pallidum and thalamus bilaterally, details can be found in (Spurny, 2019). GABA+/tCr and Glx/tCr ratios were compared between the 4 seasons (spring n=48, summer n=35, autumn=46, winter n=30). ANCOVAs for each ROI were run with and without accumulated daily sunshine and global radiation of the last 3,7,15,30 and 90 days of Vienna, respectively. Furthermore, sex was also included as covariate in each model. Information on global radiation (containing solar radiation and diffuse sky radiation, in J/cm²) in and daily sunshine duration (in h) was provided by the Central Institute for Meteorology and Geodynamics in Vienna, Austria (ZAMG, http://www.zamg.ac.at).

**Results:** No differences between seasons could be observed for any ROI or neurotransmitter ratio after correcting for multiple comparisons ($p_{corr.} > 0.05$).

**Discussion:** In this study, we examined seasonal differences in neurotransmitter ratios in a large study cohort consisting of 159 healthy individuals showing stable patterns over the course of the year. Hence, correction for season does not seem necessary when analyzing GABA and glutamate levels in healthy individuals.

Albers HE, Walton JC, Gamble KL, McNeill JKt, Hummer DL (2017) The dynamics of GABA signaling: Revelations from the circadian pacemaker in the suprachiasmatic nucleus. Frontiers in neuroendocrinology 44:35-82, DOI: 10.1016/j.yfrne.2016.11.003.

Bogner W, Gagoski B, Hess AT, Bhat H, Tisdall MD, van der Kouwe AJ, Strasser B, Marjanska M, Trattnig S, Grant E, Rosen B, Andronesi OC (2014) 3D GABA imaging with real-time motion correction, shim update and reacquisition of adiabatic spiral MRSI. Neuroimage 103:290-302, DOI: 10.1016/j.neuroimage.2014.09.032.

Spurny B, Heckova E, Seiger R, Moser P, Klobl M, Vanicek T, Spies M, Bogner W, Lanzenberger R (2019) Automated ROI-Based Labeling for Multi-Voxel Magnetic Resonance Spectroscopy Data Using FreeSurfer. Frontiers in molecular neuroscience 12:28, DOI: 10.3389/fnmol.2019.00028.

# MRS Workshop 2022
## Overcoming the Barriers to Clinical Use
### DISCONNECT 2 RECONNECT
22-24 August 2022 @ EPFL, Lausanne, Switzerland

78

Poster no. 44 (online poster)

Measuring brain lactate and other metabolites at 3T using an enhanced MRS with macromolecule suppression

Xi Chen, Samantha N. Smith, Dost Ongur

*McLean Hospital; Harvard Medical School, Belmont, MA, United States*

Although there were a few studies with important findings of in vivo brain lactate level in schizophrenia (1-3), the measurement of lactate with the routine short-TE MRS techniques is subject to low reliability and rates of usable data even at 7 T. A CRLB criteria of 15 – 20% is widely accepted as a criterion for usable data for all metabolites in proton MRS; for lactate investigators have typically loosened the CRLB criteria to 30% even at 7 T (1-3).

We recently developed a sequence we term HOPE (Half-intensity with macrOmolecule-suPprEssion), an improved short-TE proton MRS technique with macromolecule (MM) suppression. The mechanism of HOPE is demonstrated in the Figure 2: unlike immediately applying 90º pulse after inversion ON in SPECIAL, a delay is inserted. With a well-adjusted delay time, the MM resonance is fully recovered to longitudinal magnetization, while metabolite peaks, which have much longer T1 relaxation time, only recover halfway. Therefore the MM signal is mostly subtracted out in the difference spectrum, while metabolite peaks remain with approximately half intensity. Unlike T2 based methods, this T1 based MM suppression strategy does not extend TE and bring in more J modulations. The main cost is SNR reduction.

Using HOPE, lactate can be measured with an CRLB of 13 ± 3% compared to 26 ± 12% with regular MRS in our pilot data acquired at 3 T from 5 healthy volunteers (Fig. 1). This in vivo brain lactate measurement can be extended not only to 3 T, but also to brain regions with increased challenges such as centrum semiovale (CSO) and DLPFC (Fig 3). A comparison with other sequences on lactate measurement was shown in Table 1. We are applying this method to study the brain lactate change in schizophrenia.


Fig 1 Sequence mechanism of HOPE


Fig 2 HOPE MRS compared to SPECIAL

References:
(1) Wijtenburg et al. Frontiers in psychiatry 2021;12:656459
(2) Rowland et al. Transl Psychiatry 2016;6(11):e967
(3) Wang et al. JAMA psychiatry 2019;76(3):314-323

| | semi-LASER | PRESS | SPECIAL | HOPE |
|---|---|---|---|---|
| TE | 28 ms | 30 ms | 8 ms | 8 ms |
| sample size | 21 | 14 | 10 | 10 |
| CRLB | 27±15% | 41±8% | 26±12% | 13±2% |
| SD% | 34.4% | 38.7% | 22.0% | 15.6% |

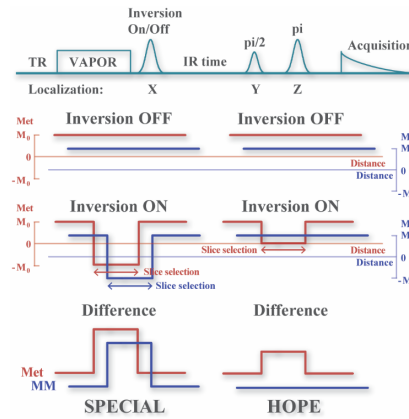Table 1 Comparing CRLB and group SD% of ACC lactate measurement with difference sequences on 3T


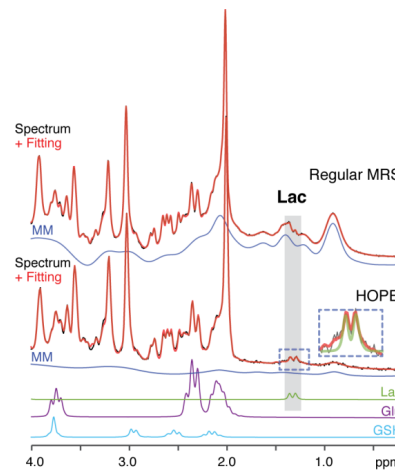Fig 3 HOPE and SPECIAL of CSO and DLPFC with lactate quantification

# MRS Workshop 2022
## Overcoming the Barriers to Clinical Use
### DISCONNECT 2 RECONNECT
22-24 August 2022 @ EPFL, Lausanne, Switzerland

79

Poster no. 45 (online poster)

## Establishing Reproducibility of Global Lactate Measurements in Healthy Subjects at 3T

Ryan Armbruster[1], Neil Wilson[1], Mark Elliott[1], Ravi Prakash Reddy Nanga[1], Ravinder Reddy[1]
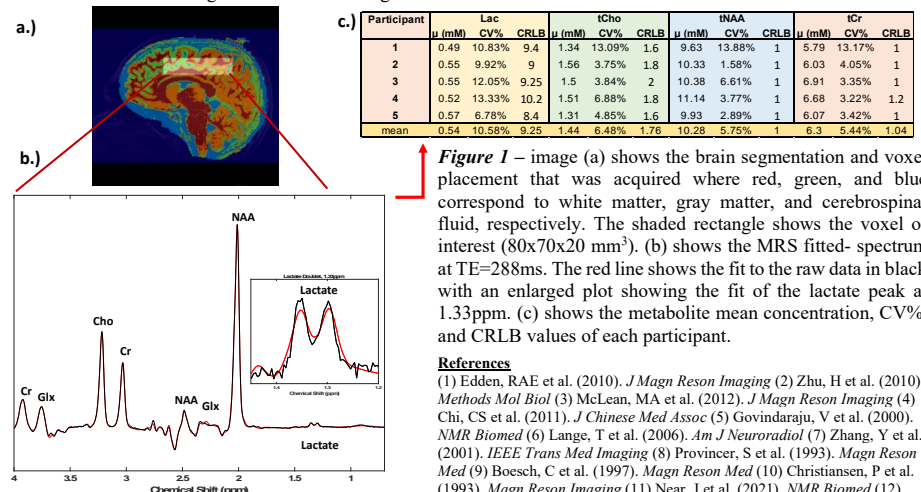
CAMIPM, Department of Radiology, University of Pennsylvania, Philadelphia, Pennsylvania, USA.

**Purpose** - Under oxidative stress glucose metabolism becomes less efficient due to anaerobic conditions which results in lactate production. Some pathologies that cause oxidative stress and thus a lactate increase are acute hypoxia, ischemic injury, brain tumors, and mitochondrial diseases.[1–4] Due to its low concentration (~1mM)[5,6] and overlap with large macromolecules (MM) and lipid signals, short echo times with small voxels cannot detect or resolve the lactate peak, especially in healthy volunteers at 3T. Using a semi-LASER acquisition, long echo, and large voxel we quantify a global lactate concentration in healthy human brain.

**Methods** - Five healthy subjects between the ages of 21-37 were scanned five times each on separate days using a 3T whole body MRI (Prisma, Siemens Healthcare, Erlangen, Germany) and a 64-channel receive array head coil. Structural images were obtained with an MP-RAGE and brain segmentation was performed using FSL[7] (Figure 1a). The MRS acquisition used a semi-laser TR=3s, TE=288ms, BW=2k, and Avg = 256. VAPOR was used with a BW of 70Hz (1 measurement) and OVS was enabled. Total acquisition time was 13m32s. LCModel[8] was used for fitting. Basis-sets were created including the pulse timings of the sequence to optimize fitting. Furthermore, to improve spectral fitting of NAA, PCr, and Cr the $CH_3$ and $CH_2$ peaks were fit separately.[5,6,9] Metabolites of interest are lactate (Lac, 1.33ppm), tCho (glycerophosphocholine + phosphocholine, 3.2ppm), tNAA (total N-acetyl-aspartate + N-acetyl-aspartyl glutamate, 2.0ppm), and tCr (phosphocreatine + creatine, 3.0ppm). $T_2$ values were calculated by using a semi-LASER sequence at TE = 144, 180, 216, 252, 288, 324, and 360ms by fitting the decay curve to equation (5) of Christiansen et al., 1993.[10] Absolute concentration was calculated using equation (6) from Near et al., 2022.[11] Mean absolute concentrations ($\mu$), coefficient of variation (CV%), and Cramer-Rao lower bound (CRLB) are reported in *Figure 1c.*

**Results:** $T_2$ values of Lac, tCho, tNAA, and tCr were 209±18.7, 303±5.7, 311±1.4, and 185±1.3 ms, respectively with $R^2$ values between 0.84-0.99. The mean concentration of Lac, tCho, tNAA, and tCr were 0.54±0.03, 1.44±0.11, 10.28±0.57, and 6.30±0.47 mM, respectively. CV% and CRLB's ranged between 5.44-10.58% and 1-9.25.

**Discussion & Conclusion:** $T_2$ and mean concentrations for tCho, tNAA, and tCr are similar to published values which gives us confidence in our lactate $T_2$ and concentration measurements.[6,12–17] The lactate measurement was also similar to a recent publication at 7T of 0.6mM.[12] Our CV% values for Lac, tCho, tNAA, and tCr are more reproducible than what is published in the literature.[10,12,15,17,18] Going forward our aim is to decrease temporal resolution to under 5 minutes and use this as a global lactate screening method to ensure lactate values are not elevated.

a.)



b.)

c.)

| Participant | Lac | | | tCho | | | tNAA | | | tCr | | |
|---|---|---|---|---|---|---|---|---|---|---|---|---|
| | μ (mM) | CV% | CRLB | μ (mM) | CV% | CRLB | μ (mM) | CV% | CRLB | μ (mM) | CV% | CRLB |
| 1 | 0.49 | 10.83% | 9.4 | 1.34 | 13.09% | 1.6 | 9.63 | 13.88% | 1 | 5.79 | 13.17% | 1 |
| 2 | 0.55 | 9.92% | 9 | 1.56 | 3.75% | 1.8 | 10.33 | 1.58% | 1 | 6.03 | 4.05% | 1 |
| 3 | 0.55 | 12.05% | 9.25 | 1.5 | 3.84% | 2 | 10.38 | 6.61% | 1 | 6.91 | 3.35% | 1 |
| 4 | 0.52 | 13.33% | 10.2 | 1.51 | 6.88% | 1.8 | 11.14 | 3.77% | 1 | 6.68 | 3.22% | 1.2 |
| 5 | 0.57 | 6.78% | 8.4 | 1.31 | 4.85% | 1.6 | 9.93 | 2.89% | 1 | 6.07 | 3.42% | 1 |
| mean | 0.54 | 10.58% | 9.25 | 1.44 | 6.48% | 1.76 | 10.28 | 5.75% | 1 | 6.3 | 5.44% | 1.04 |

***Figure 1*** – image (a) shows the brain segmentation and voxel placement that was acquired where red, green, and blue correspond to white matter, gray matter, and cerebrospinal fluid, respectively. The shaded rectangle shows the voxel of interest (80x70x20 mm³). (b) shows the MRS fitted-spectrum at TE=288ms. The red line shows the fit to the raw data in black with an enlarged plot showing the fit of the lactate peak at 1.33ppm. (c) shows the metabolite mean concentration, CV%, and CRLB values of each participant.

**References**
(1) Edden, RAE et al. (2010). *J Magn Reson Imaging* (2) Zhu, H et al. (2010). *Methods Mol Biol* (3) McLean, MA et al. (2012). *J Magn Reson Imaging* (4) Chi, CS et al. (2011). *J Chinese Med Assoc* (5) Govindaraju, V et al. (2000). *NMR Biomed* (6) Lange, T et al. (2006). *Am J Neuroradiol* (7) Zhang, Y et al. (2001). *IEEE Trans Med Imaging* (8) Provincer, S et al. (1993). *Magn Reson Med* (9) Boesch, C et al. (1997). *Magn Reson Med* (10) Christiansen, P et al. (1993). *Magn Reson Imaging* (11) Near, J et al. (2021). *NMR Biomed* (12) Dehghani, M et al. (2020). *Magn Reson Med* (13) Träber, F et al. (2004). *J Magn Reson Imaging* (14) Mlynrik, V et al. (2001). *NMR Biomed* (15) Barker, PB et al. (1993). *NMR Biomed* (16) Frahm, J et al. (1989). *Magn Reson Med* (17) Madan, A et al. (2015). *Magn Reson Med* (18) Schirmer, T & Auer, DP (2000). *NMR Biomed*

# MRS Workshop 2022
## Overcoming the Barriers to Clinical Use
### DISCONNECT 2 RECONNECT
22-24 August 2022 @ EPFL, Lausanne, Switzerland

80

Poster no. 46 (online poster)

**Prefrontal cortex metabolites measured by 7-Tesla proton magnetic resonance spectroscopy distinguish posttraumatic stress disorder and major depression from control with high sensitivity and specificity**

Kelley M. Swanberg[1], Hetty Prinsen[2], Christopher L. Averill[3,4,5,6], Leonardo Campos[1], Abhinav V. Kurada[1], John H. Krystal[3,4], Ismene L. Petrakis[3,4], Lynnette A. Averill[3,4,5,6], Chadi G. Abdallah[3,4,5,6], and Christoph Juchem[1,2,7,8]

[1]Biomedical Engineering, Columbia University School of Engineering and Applied Science, New York, NY, United States; [2]Radiology and Biomedical Imaging, Yale University School of Medicine, New Haven, CT, United States; [3]Clinical Neuroscience Division, Department of Veterans Affairs, National Center for Posttraumatic Stress Disorder, Veterans Affairs Connecticut Healthcare System, West Haven, CT, United States; [4]Psychiatry, Yale University School of Medicine, New Haven, CT, United States; [5]Psychiatry and Behavioral Sciences, Baylor College of Medicine, Houston, TX, United States; [6]US Department of Veterans Affairs Michael E. DeBakey VA Medical Center, Houston, TX, USA; [7]Radiology, Columbia University Medical Center, New York, NY, United States; [8]Neurology, Yale University School of Medicine, New Haven, CT, United States
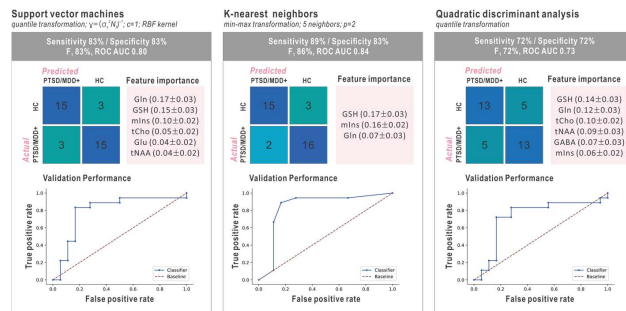
Posttraumatic stress disorder (PTSD) is a psychiatric condition marked by chronic disruptions in mood, cognition, and arousal state following a highly stressful event. PTSD exhibits comorbidity with multiple related illnesses currently treated with overlapping pharmacotherapies, including major depressive disorder (MDD), diagnosed in an estimated 50% of individuals with PTSD [1]. While both PTSD and MDD continue to be diagnosed by symptom-based inventories, proton magnetic resonance spectroscopy (^{1}H MRS) offers a window into their in vivo metabolic signatures and thus potential biomarkers for supporting diagnosis and treatment monitoring. Here we assessed the viability of several supervised classification methods for distinguishing between PTSD and/or MDD from healthy control participants on the basis of ^{1}H-MRS-measured prefrontal cortex metabolites alone.

We measured prefrontal cortex GABA, glutathione, glutamate, glutamine, myoinositol, total N-acetyl aspartate, and total choline concentrations at 7 Tesla in N=38 adult volunteers with and without PTSD and/or MDD (PTSD+ or MDD+ 5F/15M; mean 37±S.D. 13 y.o.; HC 5F/13M, 34±8 y.o.) [2]. Spectra were obtained on a 7-Tesla head-only MR system (Varian Medical Systems, Palo Alto, CA, USA) according to reproducibility-validated acquisition methods [3] and quantified according to empirically tested preprocessing and linear combination modeling procedures [4]. Metabolite concentrations were employed as the sole features in a balanced supervised classification pipeline employing either support vector machines (SVM), K-nearest neighbors (KNN), or quadratic discriminant analysis (QDA). To minimize overfitting, model hyperparameters were tuned on an independent dataset according to leave-one-out cross-validation (LOOCV) accuracies in binary classification of multiple sclerosis phenotypes [5, 6]. Feature selection of hyperparameter-optimized models was performed serially; the feature with the lowest permutation importance was removed until LOOCV accuracy no longer improved.

Sensitivity and specificity of binary classification (PTSD+ or MDD+ vs. HC) on a balanced validation loop (N=18 for each condition) were above 80% for SVM (sensitivity 83%; specificity 83%) and KNN (sensitivity 89%; specificity 83%) and lower for QDA (sensitivity 72%; specificity 72%). Regardless of classifier, glutathione consistently exhibited high permutation importance for distinguishing between PTSD or MDD and control (SVM 0.15±0.03, KNN 0.17±0.03, QDA 0.14±0.03) (Fig. 1).

Taken together, our results demonstrate the relevance of ^{1}H-MRS-measured prefrontal cortex metabolites for identifying individuals with and without posttraumatic stress disorder and/or major depressive disorder and serve as a preliminary step for refining biologically interpretable ^{1}H-MRS-based biomarkers for these and potentially other conditions.



**Figure 1. 7-Tesla ^{1}H-MRS-measured prefrontal metabolites can identify posttraumatic stress disorder (PTSD) or major depressive disorder (MDD) with high sensitivity and specificity even when used directly as the sole features of supervised binary classification models.** Listed below model names are the hyperparameters optimized on an independent data set [4] as described in [5, 6]; shown are confusion matrices and receiver operating characteristic (ROC) curves for held-out validation cases. Note consistent performance and importance of features glutathione (GSH) and glutamine (Gln) regardless of model type. HC: healthy control; AUC: area under the curve; tCho: total choline; tNAA: total N-acetyl aspartate; mIns: myoinositol; Glu: glutamate.

[1] N. K. Rytwinski, M. D. Scur, N. C. Feeny, and E. A. Youngstrom, "The co-occurrence of major depressive disorder among individuals with posttraumatic stress disorder: a meta-analysis," *J Trauma Stress,* vol. 26, no. 3, pp. 299-309, Jun 2013, doi: 10.1002/jts.21814.

[2] K. M. Swanberg, H. Prinsen, C. L. Averill, L. Campos, A. V. Kurada, J. H. Krystal, I. L. Petrakis, L. A. Averill, C. G. Abdallah, and C. Juchem, "Abnormal glutamate metabolism in prefrontal cortex of post-traumatic stress disorder linked to comorbidity with major depression," *Proc Int Soc Magn Reson Med,* no. 3344, 2022.

[3] H. Prinsen, R. A. de Graaf, G. F. Mason, D. Pelletier, and C. Juchem, "Reproducibility measurement of glutathione, GABA, and glutamate: Towards in vivo neurochemical profiling of multiple sclerosis with MR spectroscopy at 7T," *J Magn Reson Imaging,* vol. 45, no. 1, pp. 187-198, Jan 2017, doi: 10.1002/jmri.25356.

[4] K. M. Swanberg, H. Prinsen, K. DeStefano, M. Bailey, A. V. Kurada, D. Pitt, R. K. Fulbright, and C. Juchem, "In vivo evidence of differential frontal cortex metabolic abnormalities in progressive and relapsing-remitting multiple sclerosis," *NMR Biomed,* vol. 34, no. 11, p. e4590, Nov 2021, doi: 10.1002/nbm.4590.

[5] A. V. Kurada, K. M. Swanberg, H. Prinsen, and C. Juchem, "Diagnosis of multiple sclerosis subtype through machine learning analysis of frontal cortex metabolite profiles," *Proc Int Soc Magn Reson Med,* no. 4871, 2019.

[6] K. M. Swanberg, "Optimization of sensitivity to disease-associated cortical metabolic abnormality by evidence-based quantification of in vivo proton magnetic resonance spectroscopy data from 3 Tesla and 7 Tesla," Doctoral dissertation, Columbia University 2022.

# MRS Workshop 2022
## Overcoming the Barriers to Clinical Use
### DISCONNECT 2 RECONNECT
22-24 August 2022 @ EPFL, Lausanne, Switzerland

81

Poster no. 47 (online poster)

Andrea Gropman, M.D.[1] Kuntal Sen, M.D.[1], Kosar Khaksari, Ph.D., [1], Matthew Whitehead, M.D.,[2,3]
[1]Department of Neurogenetics, [2]Neuroradiology, Children's National Hospital, Washington, D.C., U.S.A., and [3]Department of Neuroradiology, Children's Hospital of Philadelphia, Philadelphia, PA, U.S.A.

The urea cycle disorders (UCDs) represent one of the most common groups of inborn errors of metabolism (IEMs), with an estimated incidence of 1 in 35,000. UCDs encompass eight distinct disease entities due to deficiencies of six enzymes as well as two transporters. The most common of these is ornithine transcarbamylase deficiency (OTCD), the only X-linked UCD, with an estimated incidence of 1 in 56,500. Urea cycle-related brain disease on routine T1 and T2 imaging may take on variable neuroimaging manifestations, ranging from apparently normal to abnormal with or without a signature appearance. In the past, we have described the usefulness of multimodal imaging in identifying biomarkers of neuronal injury in UCD patients beyond routine imaging to identify early disease to expedite treatment. Classic OTCD presents in the newborn period with hyperammonemia (HA) characterized by progressive symptoms including irritability, vomiting, difficulty feeding, lethargy, apnea, seizures, and if untreated, coma, multiorgan failure, and death. Symptoms may mimic sepsis. However, not all patients with OTCD present as newborns; partial enzyme defects may present in later childhood with symptoms triggered by metabolic stressors. Recurrent or mild HA after a viral or bacterial infection, surgery, medications (such as steroids, valproate), or trauma is well described in the literature. Patients with partial enzyme defects typically have less dramatic presentations in the form of recurrent vomiting, failure to thrive, protein aversion, cognitive, or attention deficit. Behavioral irregularities, out of proportion to discomfort caused by the illness, are often the sole red flag and present a window of opportunity to diagnose these individuals. Our group has described the utility of multimodal imaging and especially 1H MRS in a research setting, in understanding the long-term effects of HA on the structure and biochemistry of brain. The pathognomonic spectroscopic findings in proximal UCD (OTCD and carbamoyl phosphate synthetase I deficiency) consist of elevated glutamine peak with reduced choline and myoinositol peaks. In arginase deficiency, glutamine is elevated with normal myoinositol and normal or increased choline. We will review clinical cases where the diagnosis was achieved by use of early 1H MRS. The focus will be on scenarios where MRI and 1H MRS are suggestive of or diagnostic for IEM and we suggest it be uniformly part of the clinical radiology routine in children's hospitals in the U.S.A.

Figures:
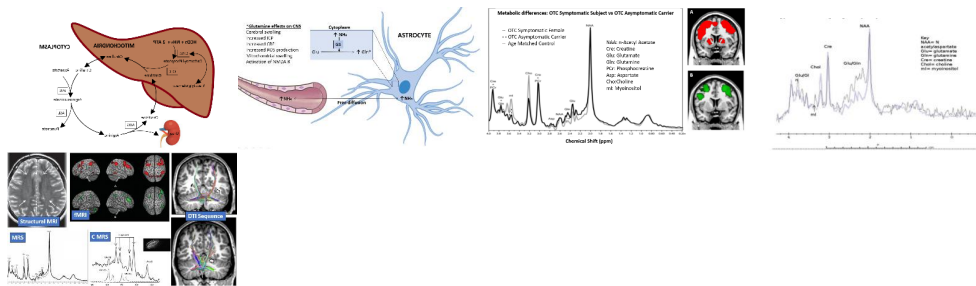
**References**

Lai LM, Gropman AL, Whitehead MT. MR Neuroimaging in Pediatric Inborn Errors of Metabolism. Diagnostics (Basel). 2022 Mar 30;12(4):861. doi: 10.3390/diagnostics12040861. PMID: 35453911; PMCID: PMC9027484.

Sen K, Whitehead M, Castillo Pinto C, Caldovic L, Gropman A. Fifteen years of urea cycle disorders brain research: Looking back, looking forward. Anal Biochem. 2022 Jan 1; 636:114343.

Sen K, Castillo Pinto C, Gropman AL. Expanding Role of Proton Magnetic Resonance Spectroscopy: Timely Diagnosis and Treatment Initiation in Partial Ornithine Transcarbamylase Deficiency. J Pediatr Genet. 2021 Mar;10(1):77-80. doi: 10.1016/j.ab.2021.114343. Epub 2021 Oct 9. PMID: 34637785; PMCID: PMC8671367.

Gropman AL, Fricke ST, Seltzer RR, Hailu A, Adeyemo A, Sawyer A, van Meter J, Gaillard WD, McCarter R, Tuchman M, Batshaw M; Urea Cycle Disorders Consortium. 1H MRS identifies symptomatic and asymptomatic subjects with partial ornithine transcarbamylase deficiency. Mol Genet Metab. 2008 Sep-Oct;95(1-2):21-30. doi: 10.1016/j.ymgme.2008.06.003. Epub 2008 Jul 26. PMID: 18662894; PMCID: PMC3724938.

Gropman AL, Seltzer RR, Yudkoff M, Sawyer A, VanMeter J, Fricke ST. 1H MRS allows brain phenotype differentiation in sisters with late onset ornithine transcarbamylase deficiency (OTCD) and discordant clinical presentations. Mol Genet Metab. 2008 May;94(1):52-60.

MRS Workshop 2022
Overcoming the Barriers to Clinical Use
DISCONNECT 2 RECONNECT
22-24 August 2022 @ EPFL, Lausanne, Switzerland

82

Poster no. 48 (online poster)

### Effect of temporal resolution on fMRS-measured GABA and Glx levels

Duanghathai Pasanta[1,2], David J. White[3], Jason L. He[1], and Talitha Ford[3,4], Nicolaas A. Puts[1,5],

[1]Department of Forensic and Neurodevelopmental Sciences, Sackler Institute for Translational Neurodevelopment, Institute of Psychiatry, Psychology, and Neuroscience, King's College London, [2]Department of Radiologic Technology, Faculty of Associated Medical Sciences, Chiang Mai University, [3]Centre for Human Psychopharmacology & Swinburne Neuroimaging, School of Health Sciences, Swinburne University of Technology, [4]Cognitive Neuroscience Unit, Faculty of Health, Deakin University, [5]MRC Centre for Neurodevelopmental Disorders, King's College London,

### Abstract

Differences in GABA and glutamate function are amongst the most widely accepted theories of autism. Prior work has shown differences in the functional response to faces and objects, associated with differences in social function in ASD. While difference in baseline neurometabolite levels have been shown, differences in neurotransmitter dynamics might be more relevant. However, no study to date has examined the functional dynamics of GABA and glutamate in autism. Here, we performed a pilot fMRS study of social function in neurotypicals in order to examine the GABA and Glx dynamics with the aim to further study altered GABA/Glx/Glu dynamics in autism in the future. We compared GABA and Glutamate + Glutamine (Glx) levels during stimulus viewing quantified using two different approaches; low- and high-temporal resolution analysis (sliding window method). MEGA-PRESS fMRS spectra (TE/TR 68/2000 ms) were acquired from primary visual cortex (3×3×3 cm$^3$). The stimulus paradigm contained 24s social stimuli interleaved with 16s rest blocks, repeated 10 times each (~6.67 mins)(Pitcher et al., 2011). Data were analysed using modified Gannet (Edden et al., 2014) code for both methods. For low-temporal analysis, data were analyzed per functional block (social stimulus viewing; 200 transients) and rest block (256 and 200 transients). For high-temporal analysis, the data were averaged over a window width of 50 transients (~100 s) with 5 transients step size. The results show no change for either GABA or Glx levels in all stimulation periods when compared to rest. However, both GABA and Glx appeared to increase during the last functional block as detected through a changepoint analysis (Lindeløv, 2020). Here we highlight the potential of high-temporal analysis at capturing the neurometabolites responses that are averaged out in block or low-temporal analysis.
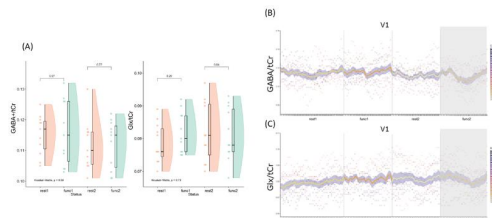
**Figure 1.** (A) Results from low-temporal analysis shows no significant change in GABA+/tCr and Glx/tCr levels in primary visual cortex. Results from high-temporal analysis show effective time course of (B) GABA+/tCr and (C) Glx/tCr in primary visual cortex. Slight decreases of GABA+/tCr and Glx/tCr were detected during the last functional block. FUNC1, FUNC2: participants passively viewed social stimuli; rest1, rest2: participants passively viewed fixation cross.

### References

Edden RAE, Puts NAJ, Harris AD, Barker PB, Evans CJ (2014) Gannet: A batch-processing tool for the quantitative analysis of gamma-aminobutyric acid–edited MR spectroscopy spectra. Journal of Magnetic Resonance Imaging 40:1445–1452.

Lindeløv JK (2020) mcp: An R package for regression with multiple change points.

Pitcher D, Dilks DD, Saxe RR, Triantafyllou C, Kanwisher N (2011) Differential selectivity for dynamic versus static information in face-selective cortical regions. Neuroimage 56:2356–2363.

**MRS Workshop 2022**
Overcoming the Barriers to Clinical Use
DISCONNECT **2** RECONNECT
22-24 August 2022 @ EPFL, Lausanne, Switzerland

83

Poster no. 49 (online poster)

# Exponential Component Analysis and its Application to $^1$H-MRS Data

Ravi Kalyanam, Vince D. Calhoun

## I. INTRODUCTION

This manuscript presents *exponential component analysis* (ECA), a data-driven method to express a time-series signal as a sum of complex exponentials; it is particularly applicable to data generated by resonance phenomenon where physical reasons support such a model. Our research focuses on data-driven methods to analyze $^1$H-MRS data [1].

## II. THEORY

The resonances of biochemicals in a $^1$H-MRS study volume are captured in the acquired *fid*. The relaxation mechanisms of magnetization decay are first-order kinetic equations solutions to which are decaying exponentials, which is why a *fid* is modeled as a sum of decaying exponentials. The embedding of the vector *fid* signal into a (Hankel) structure reveals its rank and can be used to get its low-rank approximation. The use of Hankel to analyze a linear combination of complex exponentials is based on the multivariate generalization of Kronecker's theorem on finite rank Hankel operators [2].

## III. METHODS

The first step in the ECA is to transform a vector signal into a rectangular Hankel form; see below that the anti-diagonals of such a matrix are constant:

$$X = \begin{bmatrix} x_1 & x_2 & \cdots & x_{M+1} \\ x_2 & x_3 & \cdots & x_{M+2} \\ \vdots & \vdots & \vdots & \vdots \\ x_{N-M} & x_{N-M+1} & \cdots & x_N \end{bmatrix}$$

This matrix is then decomposed using SVD to get its rank-one approximation; the resulting matrix is likely not a Hankel, but by separately averaging the elements of each anti-diagonal the Hankel property can be restored. As re-Hankelization may affect the matrix rank, it may need to be minimized again. This basic block of rank minimization and re-Hankelization is repeated until a rank-one Hankel matrix results eventually, and its corresponding signal is an exponential. Our simulation experiments illustrate ECA's ability to denoise and its potency to resolve a single exponential from any input (see Fig 1).

More exponentials can be obtained by repeating the process, each time starting with a Hankel generated from the residuary signal, obtained by subtracting the hitherto resolved ECs from the original signal. This deflationary approach is repeated until desired numbers of components are obtained. In our work, we use square Hankel constructs; the process is pretty much the same even when collectively analyzing multiple signals, in which we start with a mosaic of such Hankels.

## IV. RESULTS

In this section we present results that demonstrate the power of ECA to resolve exponential features from *any* signal. The results illustrating its ability to resolve a noisy realistically composed simulated signal is not presented for brevity.
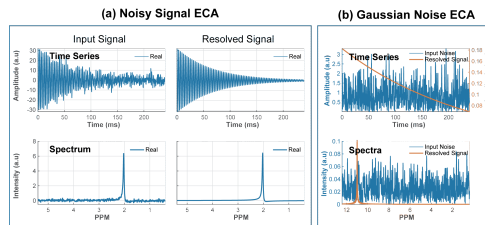


Fig.1: Exponential resolved from noise/noisy signal

Fig. 2 shows how a sum of exponential signals accounts for the residual water peak and help remove confounds from an *in vivo fid*.
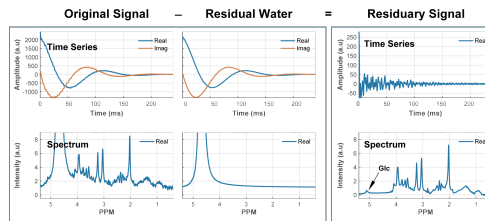


Fig. 2: Application of ECA to remove residual water signal

We observed that some individual exponential components completely capture known singlet peak resonances; likewise few multiplet resonances are accounted by two or more of the resolved exponentials. Whether a resonance is captured by one or more components, a parametric estimate of the resonance can be estimated. These and group ECA results are not presented due to space constraints.

## V. CONCLUSION

ECA reveals exponential basis set underlying a time-series signal and can help resolve signals of interest from confounds and noise from in vivo signals. The parameterization of exponential components can help compare multiple *fid* signals, just as many quantitative analyses allow.

REFERENCES

[1] R. Kalyanam, D. Boutte, K. E. Hutchison, and V. D. Calhoun, "Application of ICA to realistically simulated 1H-MRS data," *Brain Behav,* vol. 5, p. e00345, Jul 2015

[2] S. C. Power, "Finite Rank Multivariable Hankel Forms," *Linear Algebra and Its Applications,* vol. 48, pp. 237-244, 1982.

# MRS Workshop 2022
## Overcoming the Barriers to Clinical Use
### DISCONNECT 2 RECONNECT
22-24 August 2022 @ EPFL, Lausanne, Switzerland

84

Poster no. 50 (online poster)

## Correction of $B_0$ drift in rapid high-resolution MR Spectroscopic Imaging

**Sneha Vaishali Senthil[1,2] , Brenden Kadota[1] , Jamie Near[1,2,3]**

*1.Sunnybrook Research Institute, Toronto, Ontario; 2.McGill University, Montreal, Quebec; 3.Department of Medical Biophysics, University of Toronto, Ontario*

**Introduction:** Magnetic resonance spectroscopic imaging (MRSI) is a powerful imaging tool for evaluating metabolic disruptions and altered neurochemistry in several neurodegenerative disorders, providing quantitative biomarkers that can help track disease progression. Although MRSI has made progress with respect to speed, artefact reduction, spatial resolution, and the quantification of tissue metabolites, the spectral quality remains hampered by patient motion and temporal $B_0$ drift arising from the heating of gradient coils and passive shim elements. This causes the temporal accrual of frequency and phase variations between each repetition thereby causing the misalignment of individual subspectra, spectral line broadening, lineshape distortion and reduced signal to noise ratio (SNR). Different methods have been established to correct for frequency and phase offsets in single voxel spectroscopy. However, drift correction for MRSI is more challenging as the multiple repetitions in an acquisition do not share common k-space points that can be used to estimate and correct for drifts. A Rosette-MRSI acquisition overcomes these shortcomings by capturing the center of k-space during each repetition thus acting as a self-navigator for estimating the frequency and phase drift at each scan. We show how rosette MRSI sampling trajectories offer the possibility to perform frequency and phase drift correction which is otherwise not possible to do in most other commonly used cartesian and non-cartesian sampling trajectories.

**Methods:** A Rosette-MRSI sequence was implemented on a 3T Prisma Siemens MR scanner (Siemens, Germany). Each repetition consisted of a circular trajectory originating at the center of k-space and rotated about the origin during each repetition until full k-space coverage was obtained. Phantom experiments were performed using a GE" Braino" phantom. Rosette MRSI was implemented following a 15-min DTI scan to induce substantial drift. The parameters used were: 320 mm² FOV; 64 x 64 matrix, 101 shots, 8 averages, TR/TE=750/1.6 ms, FA=60°. Data processing and reconstruction were performed using the FID-A toolkit[2]. After performing density compensation, FIDs from the centre of k-space were isolated from each repetition and then, using the first k=0 FID as reference, frequency and phase offsets for each repetition were estimated using time-domain spectral registration, which uses non-linear least-squares minimization to estimate the frequency and phase shift required to optimally align each FID signal to the reference FID. The calculated frequency and phase offsets were applied to the full ADC signals, to achieve frequency and phase drift correction across the whole of k-space.
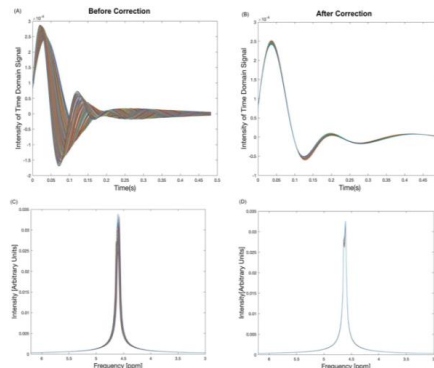


*Figure 1: The FIDS at the center of k-space are plotted for all scans ((A) and (B)) with their corresponding spectra ((C) and (D)) before (left) and after (right) frequency correction using spectral registration.*
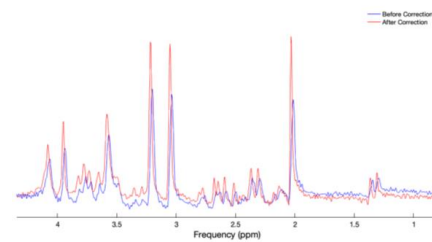
**Results:** The resonant frequency drifted approximately linearly by a total of 4.6Hz and the phase drift ranged from -3° to 4.8° across all scans during the 6-minute scan duration. Spectral registration resulted in a noticeable improvement in the alignment of k=0 FIDs and spectral peaks (Figure 1). Figure 2 shows spectra from a selected ROI, both with and without frequency and phase drift corrections. Future work will involve implementing water suppression and drift correction in *in-vivo* data to capture the additional motion-related frequency and phase variations which are not seen in phantom results.

**Conclusion:** Frequency drift induced by heating of gradient coils and passive shimming can unfavorably affect the processing of acquired MRS data. We developed a rosette-MRSI sequence and demonstrated the use of spectral registration to correct frequency and phase drifts in the acquired data. The results obtained highlight the advantages of self-navigated rosette trajectories for drift correction.



*Figure 2: Drift corrected (blue) and uncorrected (red) MRS spectra plotted after water removal*

**References:** *1. Near J, et al. (2015) Magn Reson Med. 2. Simpson R, et al. (2017) Magn Reson Med. 3. Bagchi S, et al. (1996) IEEE Trans Circuits Syst II Analog Digital Signal Process. 4. Rasche V, et al. (1999) IEEE Trans Med Imaging.*

MRS Workshop 2022
Overcoming the Barriers to Clinical Use
DISCONNECT 2 RECONNECT
22-24 August 2022 @ EPFL, Lausanne, Switzerland

85

# 9   Thanks

We thank you for taking part on **The International Magnetic Resonance Spectroscopy Workshop MRS 2022: "Overcoming the Barriers to Clinical Use"**